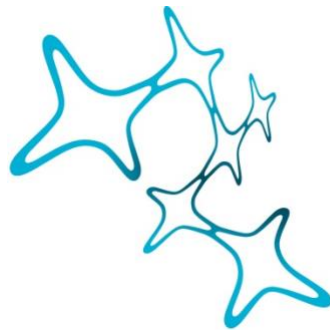# INVESTIGATING THE ROLE AND MODULATION OF MICROGLIA IN FTD-*GRN* USING A HUMAN IPSC-DERIVED PATHOLOGY MODEL

Sophie Robinson

Graduate School of Systemic Neurosciences

LMU Munich

Dissertation der
Graduate School of Systemic Neurosciences der
Ludwig-Maximilians-Universität München

December 2022

Table of Contents

Abbreviations

2D	2-dimensional
3D	3-dimensional
AD	Alzheimer's disease
ADAM	A disintegrin and metalloproteinase
AEP	Asparaginyl endopeptidase
ALS	Amyotrophic lateral sclerosis
APOE	Apoliprotein E
BMP	Bis(monoacylglycero) phosphate
bvFTD	Behavioral variant frontotemporal dementia
C1q	Complement component 1q
C3	Complement component 3
C9orf72	Chromosome 9 open reading frame 72
CBS	Corticobasal syndrome
CD68	Cluster of differentiation 68
CHMPB2B	Charged multivesicular body protein 2B
CNS	Central nervous system
CRISPR	Clustered regularly interspaced short palindromic repeats
crRNA	Clustered regularly interspaced short palindromic repeats ribonucleic acid
CSF	Cerebrospinal fluid
Csf1R	Colony-stimulating factor-1 receptor
CTD	C-terminal domain
CTF	C-terminal fragment
CX3CR1	CX3C motif chemokine receptor 1
DAM	Disease-associated microglia
DKO	Double knockout
DN	Dystrophic neurites
DNA	Deoxyribonucleic acid
DPR	Dipeptide repeat proteins
DSB	Double-stranded break
EWS	Ewing's sarcoma protein
FDG	Fluorodeoxyglucose
FET	Fused in sarcoma, Ewing's sarcoma protein, TATA-binding protein associated factor 2N
FTD	Frontotemporal dementia
FTLD	Frontotemporal lobar degeneration
FUS	Fused in sarcoma
GCI	Glial cytoplasmic inclusions
GRN	Progranulin gene, granulin
GWAS	Genome-wide association study
HDR	Homology-directed repair
hiMGL	Human iMicroglia
hSyn	Human synapsin
IHC	Immunohistochemistry

IL-34	Interleukin 34
IL-6	Interleukin 6
InDel	Insertion or deletion
iPSC	Induced pluripotent stem cell
ITAM	Immunoreceptor tyrosine-based activation motif
kDa	Kilodalton
KO	Knockout
LAMP1	Lysosomal-associated membrane protein 1
LAMP2	Lysosomal-associated membrane protein 2
LGMN	Legumain
LOAD	Late-onset Alzheimer's disease
LOF	Loss-of-function
MAPT	Microtubule-associated protein tau
MEF	Murine embryonic fibroblasts
MGnD	Microglia neurodegenerative diseases
MHC	Major histocompatibility complex
MND	Motor neuron disease
mRNA	Messenger ribonucleic acid
mRNP	Messenger ribonucleoprotein particles
NCI	Neuronal cytoplasmic inclusions
NCL	Neuronal ceroid lipofuscinosis
nfvPPA	Non-fluent variant primary progressive aphasia
NHEJ	Non-homologous end joining
NII	Neuronal intranuclear inclusions
NLS	Nuclear localization sequence
NPC	Neuronal progenitor cells
NTD	N-terminal domain
oAβ	Oligomeric Aβ
OCD	Obsessive compulsive disorder
P2RY12	Purigenic receptor 12
PET	Positron emission tomography
PGRN	Progranulin
PPA	Primary progressive aphasia
PSAP	Prosaposin
PSP	Progressive supranuclear palsy
RNA	Ribonucleic acid
RNA-seq	Ribonucleic acid sequencing
RRM1	RNA recognition motif 1
RRM2	RNA recognition motif 2
sgRNA	Single guide ribonucleic acid
siRNA	Short interfering RNA
sTREM2	Soluble triggering receptor expressed on myeloid cells 2
svPPA	Semantic variant primary progressive aphasia
SYK	Spleen associated tyrosine kinase
TAF14	TATA-binding protein associated factor 2N
TDP-43	43 kDa transactive response deoxyribonucleic acid-binding protein

TFEB   Transcription factor EB
TGF-β Transforming growth factor β
TMEM119   Transmembrane protein 119
TNF   Tumor necrosis factor
tracrRNA   Transactivation clustered regularly interspaced short palindromic repeats
                ribonucleic acid
TREM2   Triggering receptor expressed on myeloid cells 2
TSPO   Translocator protein
UTR   Untranslated region
VCP   Valosin-containing protein

1 Introduction

1.1 Frontotemporal dementia

1.1.1 Frontotemporal dementia

Frontotemporal dementia (FTD) is a clinical term encompassing a group of neurodegenerative diseases characterized by progressive deficits in behavior, executive function, and language (McKhann et al., 2001; Neary et al., 1998). It is the second most common form of early onset dementia, under 65 years. The three major clinical subtypes are behavioral variant FTD (bvFTD) and two forms of primary progressive aphasia (PPA), the non-fluent (nfvPPA) and semantic variant (svPPA). These forms can converge with disease progression (I. R. A. Mackenzie & Neumann, 2016). FTD can also overlap with movement disorders such as motor neuron disease (MND), or amyotrophic lateral sclerosis (ALS), corticobasal syndrome (CBS), and/or progressive supranuclear palsy (PSP) (Lomen-Hoerth, Anderson, & Miller, 2002; Padovani, Agosti, Premi, Bellelli, & Borroni, 2007). A family history is present in 25-50% of cases with autosomal-dominant inheritance in several genes, including the microtubule-associated protein tau (*MAPT*), progranulin (*GRN*), chromosome 9 open reading frame 72 (*C9orf72*), charged multivesicular body protein 2B (*CHMP2B*), and valosin-containing protein (*VCP*) (Rademakers, Neumann, & MacKenzie, 2012).

1.1.2 Frontotemporal lobar degeneration

Frontotemporal lobar degeneration (FTLD) is a pathology describing a heterogeneous group of disorders in which there is selective degeneration of the frontal and temporal lobes as the most prominent and consistent feature. It is the pathology that occurs in FTD-*GRN*. Like other neurodegenerative diseases, the pathology of most cases of FTD consist of abnormal intracellular protein deposits. The major proteins are tau (G. Lee, Leugers, Mol, Transl, & Author, 2012; V. M. Y. Lee, Goedert, & Trojanowski, 2001), 43 kDa transactive response DNA-binding protein (TDP-43) (Arai et al., 2006; Manuela Neumann et al., 2006), the FET protein family (fused in sarcoma (FUS)), Ewing's sarcoma protein (EWS), and TATA-binding protein associated factor 2N (TAF15)) (Manuela Neumann et al., 2011; Manuela Neumann, Rademakers, et al., 2009), and dipeptide repeat proteins (DPR) (M. Neumann & Mackenzie, 2019) (Table 1, Table 2).

FTLD-tau	Pick's disease patient, Pick bodies in temporal cortex		(Manuela Neumann, Tolnay, & Mackenzie, 2009)
FTLD-DPR	DPR-positive neuronal cytoplasmic inclusions (NCI) in cerebellar granular layer		(I. R. A. Mackenzie & Neumann, 2016)
FTLD-FUS	FUS-positive Neuronal intermediate filament inclusion disease (NIFID), round NCI in the hippocampus		(M. Neumann & Mackenzie, 2019)
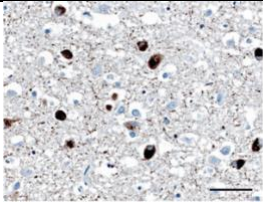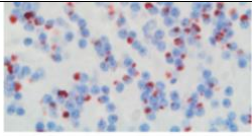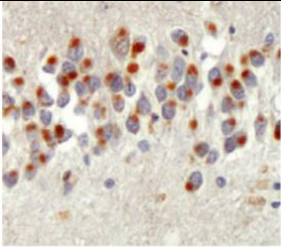
Table 1. Pathologies found in non-TDP-43 FTLD. Copyright permission given in Chapter 6.

1.1.3 TDP-43 structure and function

As this thesis is investigating a model of FTD-*GRN*, I will focus on FTLD-TDP since it is the pathology that is seen in this disease. TDP-43 is a 414 amino acid DNA/RNA-binding protein that is involved in transcription, splicing, mRNA transport and stabilization, and can undergo stress granule formation (Bowden & Dormann, 2016; Ederle & Dormann, 2017; Ratti & Buratti, 2016). It is localized in the nucleus and shuttles between the nucleus and cytoplasm. TDP-43 binds to single stranded DNA (ssDNA) and RNA *in vitro* (Buratti & Baralle, 2001; Takahama, Arai, Kurokawa, & Oyoshi, 2009) and is shown to bind to gene promotors and regulates transcription *in vivo* (Lalmansingh, Urekar, & Reddi, 2011; Ou et al., 1995). It binds to long introns in many pre-mRNAs and regulates splicing (S. C. Ling, Polymenidou, & Cleveland, 2013; Ratti & Buratti, 2016). It also regulates the generation of noncoding RNAs and binds to 3'UTRs of cytosolic mRNAs to control their translation, transport, and stability (Bowden & Dormann, 2016; Ratti & Buratti, 2016). It is expressed in a variety of tissues and ubiquitously expressed (Buratti & Baralle, 2001). The domain organization of TDP-43 consists of an N-terminal domain (NTD), two RNA recognition motifs (RRM1 and RRM2), and a glycine-rich C-terminal domain (CTD) (Figure 1). The NTD is the site of weak nucleotide binding (C. ke Chang et al., 2012; Mompeán, Romano, et al., 2016; Qin, Lim, Wei, & Song, 2014; L. Wang, Kang, Lim, Wei, & Song, 2018). The nuclear localization sequence (NLS) is recognized for active

transport of TDP-43 into the nucleus by Importin-α (Archbold et al., 2018; Nishimura et al., 2010; Pinarbasi et al., 2018; Winton et al., 2008). RRM1 and RRM2 bind to nucleic acids (Kuo, Chiang, Wang, Doudeva, & Yuan, 2014; Lukavsky et al., 2013). The CTD has most of the phosphorylation sites and is required for TDP-43 splicing activity (Ayala et al., 2005; Conicella, Zerze, Mittal, & Fawzi, 2016; Freibaum, Chitta, High, & Taylor, 2010). The subregions of the CTD include two Gly-aromatic-Ser-rich regions and an amyloidogenic core divided into a hydrophobic region and a Q/N-rich region (Mompeán, Chakrabartty, Buratti, & Laurents, 2016). The C-terminal region encodes a glycine-rich low-complexity domain that is called the "prion-like" domain, since it is similar to yeast prion proteins (King, Gitler, & Shorter, 2012). Yeast prion proteins have a distinct prion domain enriched with uncharged polar amino acids and glycine (Alberti, Halfmann, King, Kapila, & Lindquist, 2009; Toombs, McCarty, & Ross, 2010). Aggregated C-terminal fragments of TDP-43 contain a region similar to this and therefore is called prion-like (E. B. Lee, Lee, & Trojanowski, 2011; Manuela Neumann et al., 2006). Deletion of the prion-like domain prevents aggregation *in vitro* and aberrant misfolding events and toxicity in other model systems (Ash et al., 2010; Johnson, McCaffery, Lindquist, & Gitler, 2008).

1.1.4   TDP-43 function and dysfunction

The C-terminal region is known as the amyloidogenic core since it can mediate liquid-liquid phase transition and the formation of solid amyloid-like fibers upon non-physiologically high protein concentrations *in vitro*. Therefore, it is hypothesized that similar mechanisms can give rise to TDP-43 aggregates *in vivo* by being involved in the formation of messenger ribonucleoprotein particles (mRNP), such as stress granules, that could become pathologically altered in FTLD-TDP (Bowden & Dormann, 2016). The cytosolic functions of TDP-43 could be disrupted due to its sequestration into cytosolic aggregates. Examples include disrupted transport and translation of *Map1b* mRNA since it is mislocalized and accumulates in ALS spinal cords (Coyne et al., 2014) and compromised axonal transport of *Nefl* mRNA in *TARDBP* (the gene for TDP-43) A315T or M337V mutated human induced pluripotent stem cell (iPSC) - derived motor neurons (Alami et al., 2014). However, the precise functions of TDP-43 in the brain and mechanisms of disease pathology remain to be determined. In the degenerating brain areas of FTD patients, TDP-43 is severely mislocalized, but it is unclear how it is lost from the nucleus. Loss of nuclear TDP-43 could result in loss of its nuclear functions, including altered mRNA splicing, processing of noncoding RNAs and transcription. There is an association between nuclear TDP-43 depletion and cytoplasmic accumulation of TDP-43. These

disturbances, in addition to the generation of toxic species, could contribute to cell death since TDP-43 functions are essential during brain development and neuronal survival (Iguchi et al., 2013; Kraemer et al., 2010; Sephton et al., 2010; L. S. Wu, Cheng, & Shen, 2012; L. S. Wu et al., 2010). In mouse embryonic stem cells, when TDP-43 is depleted, cryptic exons are retained in mRNAs, which then disrupts their translation and promotes nonsense-mediated decay (J. P. Ling, Pletnikova, Troncoso, & Wong, 2015). In ALS/FTD *post-mortem* tissues, alternative splicing changes, which is the production of variably spliced mRNAs by selecting different combinations of splice sites in the pre-mRNA, have been reported. One example is enhanced TDP-43-associated cryptic exon splicing indicating loss of nuclear TDP-43 functions (J. P. Ling et al., 2015; Xiao et al., 2011; Yang et al., 2014). It has also been found that the C-terminal fragments induce toxicity and cell death in cultured cells, yeast, and transgenic mice (E. B. Lee et al., 2011), which could indicate another detrimental mechanism for neurons. Pathological forms of TDP-43 show ubiquitination, hyperphosphorylation, and N-terminal truncation (Arai et al., 2006; Hasegawa et al., 2008; Manuela Neumann et al., 2006; Manuela Neumann, Tolnay, et al., 2009).

Figure 1. Structure of TDP-43. N-terminal domain (NTD), nuclear localization signal (NLS), RNA-recognition motif 1 (RRM1), and RNA-recognition motif 2 (RRM2). The C-terminal domain is made up of Gly-aromatic-Ser-rich regions (GaroS1 and 2), hydrophobic region (Φ), glutamine-arginine-rich region (Q/N) (Adapted from (François-Moutal et al., 2019)). Copyright permission given in Chapter 6.

1.1.5 TDP-43-associated frontotemporal lobar degeneration

Mutations in *GRN*, *C9orf72*, and *TARDBP* genes are associated with FTLD-TDP. FTLD-TDP presents with degeneration in the frontal and temporal lobes as well as other cortical and subcortical structures, such as the parietal cortex, substantia nigra, basal ganglia, and motor neurons. 50% of cases also present with hippocampal sclerosis (M. Neumann & Mackenzie, 2019). The pathological hallmark lesions are neuronal cytoplasmic inclusions (NCI), neuronal intranuclear inclusions (NII), and dystrophic neurites (DN), as well as glial cytoplasmic inclusions (GCI) in oligodendrocytes (Manuela Neumann et al., 2007) that are immunoreactive for TDP-43, ubiquitin, and p62 (I. R. A. MacKenzie et al., 2010). Inclusions are present in the frontotemporal neocortex and the dentate granule cells of the hippocampus, but also in many subcortical regions (Geser et al., 2009; Josephs, Stroh, Dugger, & Dickson, 2009). The amount

and distribution of TDP-43 pathology in the CNS has a strong correlation with the degree of neurodegeneration (Geser et al., 2009; I. R. MacKenzie et al., 2013). Heterogeneity of morphology, inclusion type, and laminar distribution depends on the clinic-pathological and genetic associations. Inclusion body formations correlate with a large reduction of the physiological nuclear staining of TDP-43 (M. Neumann & Mackenzie, 2019).

There are four pathological subtypes of FTLD-TDP, types A-D (Table 2) (M. Neumann & Mackenzie, 2019). The subtypes are defined by ubiquitin-, TDP-43-, and phospho-TDP-immunohistochemistry (I. R. Mackenzie & Neumann, 2017). Type A is characterized by short, thick DN and compact NCI, abundantly in layer II of the neocortex and lentiform NII in affected cortical regions. Granular NCI are present in the hippocampus, in dentate granule cells. TDP-43-positive GCI are found in the cerebral white mater and affected subcortical regions. Type B is characterized by TDP-43-positive NCI in the cortex with abundant diffuse granular cytoplasmic NCI. TDP-43-positive NCI are also present in lower motor neurons. Type C have long TDP-43-positive DN, which are present in upper cortical layers. NCI are present in the hippocampus. Type D consists of TDP-43-positive lentiform NII and short DN in the neocortex (M. Neumann & Mackenzie, 2019).

Type A	Short neurites, lentiform neuronal intranuclear inclusions (NII), and neuronal cytoplasmic inclusions (NCI)	
Type B	Deep cortical laminae with NCI	
Type C	Long neurites	
Type D	Short neurites and NII	
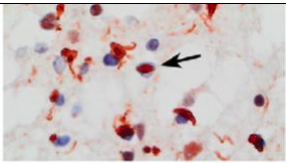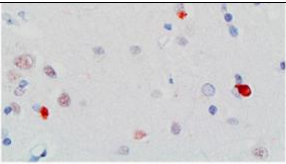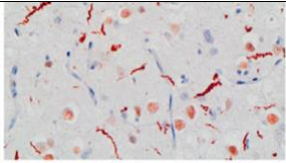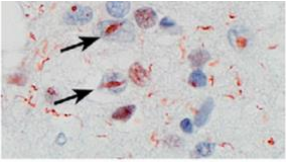
Table 2. FTLD-TDP subtypes A-D (I. R. A. Mackenzie & Neumann, 2016). Copyright permission given in Chapter 6.

1.1.6 *GRN*-associated frontotemporal dementia

Mutations in the progranulin gene (*GRN*) cause up to 20% of familial FTD (Baker et al., 2006; Cruts et al., 2006). There are currently over 100 GRN mutations reported (AD&FTD Mutation Database). These mutations are heterozygous and most of these mutations in null alleles and therefore PGRN haploinsufficiency. The pathology is FTLD-TDP type A with moderate lentiform neuronal intranuclear inclusions (NII) (Mackenzie et al., Acta Neuropathol 2017; Mackenzie et al., Acta Neuropathol 2007; Cairns et al., Am J Pathol 2007). The striatum is most severely affected and there is also hippocampal sclerosis associated with dystrophic neurites (DN). Therefore, the clinical presentation of FTD-*GRN* can be either behavioral variant FTD (bvFTD) or nonfluent variant primary progressive aphasia (nfvPPA), with some degree of parkinsonism (De Muynck & Van Damme, 2011; Woollacott & Rohrer, 2016). The exact mechanism leading to neurodegeneration and TDP-43 aggregation is not known, however there is evidence that a role of lysosomal dysfunction is significant (Paushter, Du, Feng, & Hu, 2018). Homozygous loss-of-function GRN mutations cause a lysosomal storage disease known as neuronal ceroid lipofuscinosis (NCL) (Smith et al., 2012) and FTD-*GRN* patients show some biochemical similarities to those cases, especially in terms of lysosomal dysfunction.

GRN loss-of-function has been investigated in human *in vitro* cultures, C. elegans, zebrafish, and mouse models (Table 3). In human iPSC-derived models, neurons have shown increased sensitivity to cellular stress, as well as decreased nuclear TDP-43, increased insoluble TDP-43, and lysosomal abnormalities such as lipofuscin and lipid accumulation, and impaired processing of prosaposin and reduced lysosomal glucocerebrosidase activity (Almeida et al., 2012; S. Lee & Huang, 2017a; Raitano et al., 2015; Valdez et al., 2017; Valdez, Ysselstein, Young, Zheng, & Krainc, 2020). Human microglia have exhibited lysosomal stress as well (Logan et al., 2021). In C. elegans models, lysosomal abnormalities have been observed (Doyle et al., 2021; Kao et al., 2011). *Danio rerio* models show neuronal abnormalities and neuroinflammation (Campbell et al., 2021; Chitramuthu, Baranowski, Kay, Bateman, & Bennett, 2010; Chitramuthu & Bennett, 2018; Laird et al., 2010; Y. H. Li et al., 2013, 2010; Shankaran et al., 2008; Walsh & Hitchcock, 2017; Zambusi, Pelin Burhan, Di Giaimo, Schmid, & Ninkovic, 2020). In mouse models, astrogliosis and microgliosis is prevalent. There is also lysosomal dysfunction in microglia, lipofuscin accumulation, and increased cytoplasmic and insoluble pTDP-43 (Ahmed et al., 2010; Arrant et al., 2020; Arrant, Filiano, et al., 2019; M. C. Chang et al., 2017; Frew & Nygaard, 2021; Ghoshal, Dearborn, Wozniak, & Cairns, 2012; Götzl et al., 2019, 2018, 2014; M. Huang et al.,

2020; Lui et al., 2016; Nguyen et al., 2018; Petkau et al., 2012; Ward et al., 2014; Wils et al., 2012; Y. Wu et al., 2021; Yin et al., 2010).

Model	Mutation	Phenotype	Reference
Patient iPSC-derived neurons and microglia	GRN^{S116X}	S116X neurons: • Reduced levels of PGRN • Increased sensitivity to ER stress, kinase and staurosporine inhibitors, down-regulation of S6K2 • SORT1 suppression increases extracellular PGRN	(Almeida et al., 2012; S. Lee & Huang, 2017a)
Patient iPSC-derived cortical neurons	$GRN^{IVS1 + 5G>C}$	• Wnt signaling pathway aberrantly activated	(Raitano et al., 2015)
Patient iPSC-derived cortical neurons	$GRN^{c.26C>A, p.A9D het}$	• Decreased nuclear TDP-43 • Increased insoluble TDP-43 • Enlarged electron-dense vesicles • Lipofuscin accumulation • Fingerprinting-like profiles • Granular osmiophilic deposits • Impaired processing of prosaposin to saposin C • Reduced lysosomal glucocerebrosidase activity • Lipid accumulation • Increased insoluble alpha-synuclein	(Valdez et al., 2017, 2020)
iPSC-derived microglia	GRN KO	• Oxidative stress • Lysosomal dysfunction • Endolysosomal membrane damage	(Logan et al., 2021)

Caenorhabditis elegans	*pgrn-1* LOF	• Normal life span • Less progeny by 20% • Few apoptotic bodies but no defects in cell death during development • Altered kinetics of cell death • Faster clearing of apoptotic cells • Lysosomal dysfunction • Defects in autophagic flux	(Doyle et al., 2021; Kao et al., 2011)
Danio rerio	GRN-B LOF	• None • Reduced head size 24hpf	(Chitramuthu et al., 2010; Shankaran et al., 2008)
Danio rerio	GRN-A LOF	• Reduced proliferation and increased apoptosis in hepatocytes • Reduced liver size • Reduced hepatic MET expression • Motor neurons truncated • Early branching • Swimming deficit • Normal touch response • Reduced number of myogenic progenitor cells and impaired muscle growth • Significant delay in neurogenesis • Abnormal neuron development • Spinal motor neurons with shorter axons • Reduced sensory hair cells	(Campbell et al., 2021; Chitramuthu et al., 2010; Chitramuthu & Bennett, 2018; Y. H. Li et al., 2013, 2010; Walsh & Hitchcock, 2017)

		• Retinal abnormalities	
		• Motor behavior changes	
		• Myeloid progenitor differentiation abnormalities	
		• Macrophage abnormalities	
		• Delayed liver regeneration	
Danio rerio	GRN-A and GRN-B LOF	• Motor neurons truncated	(Laird et al., 2010)
Danio rerio	PGRN A9D	• Cytoplasmic missorting of PGRN	(Shankaran et al., 2008)
Danio rerio	PGRN P248L and R432C	• Reduced secretion of PGRN	(Shankaran et al., 2008)
Danio rerio	Grn-deficient	• Pro-inflammatory microglia	(Zambusi et al., 2020)
Mouse	*Grn⁻/⁻*	• No significant neuron loss • Increased microgliosis and astrogliosis • Increased ubiquitin • Increased lipofuscin • Increased cytoplasmic pTDP-43 in IHC • Increased insoluble pTDP-43 from 12 months • Increased proinflammatory and decreased anti-inflammatory cytokines and chemokines • Reduced hippocampal synaptic connectivity • Long-term potentiation impaired • Elevated expression of lysosomal proteins	(Ahmed et al., 2010; Arrant et al., 2020; Arrant, Roth, et al., 2019; M. C. Chang et al., 2017; Ghoshal et al., 2012; Götzl et al., 2019, 2018, 2014; M. Huang et al., 2020; Lui et al., 2016; Petkau et al., 2012; Ward et al., 2014; Wils et al., 2012; Y. Wu et al., 2021; Yin et al., 2010)

		• Accumulation of myelin debris in microglial lysosomes	
		• Reduction in lipid metabolism proteins	
		• Elevated brain levels of extracellular vesicles	
		• Lower β-glucocerebrosidase activity	
		• Impairment of autophagy	
		• Increased complement activation	
		• Enhanced synaptic pruning by microglia	
		• Retinal neuron loss	
Mouse	Grn^{R493X}	• Reduced Grn mRNA levels	(Frew & Nygaard, 2021; Nguyen et al., 2018)
		• Lack detectable progranulin protein	
		• Increased microgliosis	
		• Cytoplasmic TDP-43 accumulation	
		• Reduced synaptic density	
		• Lipofuscinosis	
		• Hyperinflammatory macrophages	
		• Reduced survival	
		• Lysosomal dysfunction	
		• Thalamic neurodegeneration	

Table 3. Overview of observed phenotypes in current *in vivo* and *in vitro* models of FTD-*GRN*.

1.2 Progranulin

1.2.1 Domain composition of progranulin

Progranulin consists of 593 amino acids and has a native molecular weight of ~65 kDa not considering glycosylation (Songsrirote, Li, Ashford, Bateman, & Thomas-Oates, 2010). There are seven full and one half conserved granulin domains connected by linker regions (Figure 2) (Tolkatchev et al., 2008). Each domain consists of ~55 residues with two or four double cysteine motifs and four single cysteine motifs (Hrabal, Chen, James, Bennett, & Ni, 1996; Tolkatchev et al., 2008; Vranken et al., 1999). Progranulin is proteolytically cleaved to release individual granulin peptides. There is evidence that the granulin peptides have functions that are independent of, and sometimes opposed to the full-length precursor protein (Kessenbrock et al., 2008; Salazar et al., 2015; Zhu et al., 2002). For example, progranulin has anti-inflammatory functions while granulin peptides have pro-inflammatory functions (Jian, Konopka, & Liu, 2013; Zhu et al., 2002).
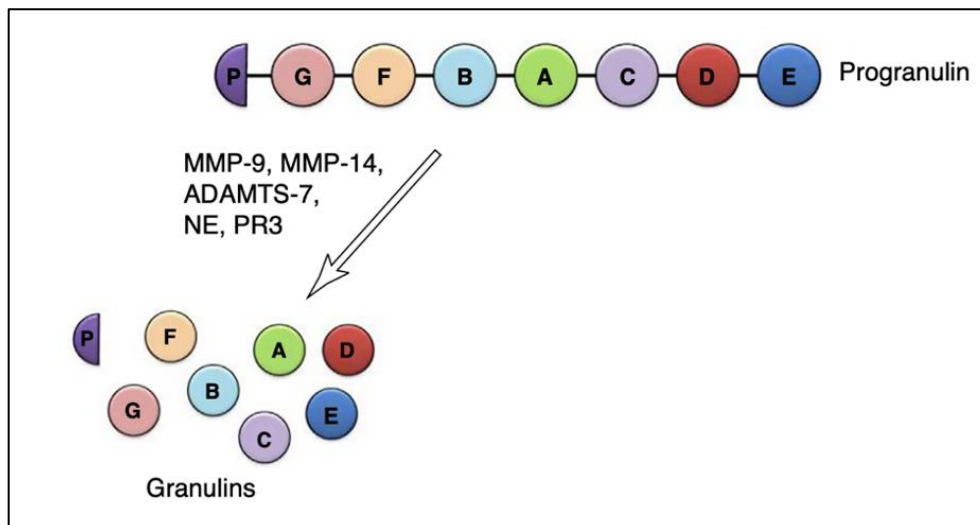
Figure 2. Progranulin domain structure. Each circle represents a granulin domain. PGRN can be proteolytically cleaved by matrix metalloproteinase (MMP)-9, MMP-14, a disintegrin and metalloproteinase with thrombospondin type I motif 7 (ADAMTS-7), neutrophil-secreted elastase (NE), and proteinase (PR)3 (adapted from (Abella et al., 2017)). Copyright permission given in Chapter 6.

1.2.2 Progranulin trafficking to the lysosome

PGRN is translated into the endoplasmic reticulum lumen and then trafficked through the Golgi in secretory vesicles, before being secreted into the extracellular space (Figure 3). Then, it is

either cleaved into granulins (Bai et al., 2009; Butler, Dean, Tam, & Overall, 2008; Kessenbrock et al., 2008; Suh, Choi, Tarassishin, & Lee, 2012; Zhu et al., 2002) or taken up by binding to sortilin (Hu et al., 2010), an endocytic receptor. Sortilin delivers progranulin from the cell surface via endosomes to the lysosome, where it can be cleaved into granulins as well (Capell et al., 2011; Hu et al., 2010). Alternatively, it can also bind to prosaposin (PSAP), a soluble lysosomal protein. When PSAP binds to its own trafficking receptors, it carries PGRN along into the lysosome with it from both the extracellular space as well as the secretory pathway (X. Zhou et al., 2015). PGRN has also been shown to transport PSAP to the lysosome via sortilin (X. Zhou et al., 2017). PGRN colocalizes with LAMP1, additionally supporting its role in the lysosome (Gowrishankar et al., 2015; Hu et al., 2010; Tanaka, Chambers, Matsuwaki, Yamanouchi, & Nishihara, 2014). *GRN*'s promotor contains binding sites for transcription factor EB (TFEB), a transcription factor that is a master regulator of lysosome biogenesis. TFEB overexpression upregulates PGRN expression as well, showing that PGRN is co-regulated with other lysosomal genes (Belcastro et al., 2011; Sardiello et al., 2009; Settembre et al., 2011).

1.2.3   Neuronal ceroid lipofuscinosis – evidence of PGRN function in the lysosome

While mutations causing PGRN haploinsufficiency lead to FTLD, homozygous loss-of-function results in neuronal ceroid lipofuscinosis (NCL), a very rare lysosomal storage disease. NCLs are a family of neurodegenerative diseases with diverse clinical and pathological presentation. Symptoms include motor and cognitive deterioration, retinopathy, and epilepsy. Pathologically, lipofuscin, a lipid and protein aggregate, accumulates in the lysosomes (Kao, McKay, Singh, Brunet, & Huang, 2017). The genetic link between PGRN and NCL strongly implicates a lysosomal function of PGRN, since all NCL genes discovered have a direct or indirect role in regulating lysosomal function. In FTLD-*GRN* patients, NCL-related phenotypes are also reported, for example, an increase in lysosomal storage materials found in cortical neurons and lymphoblasts (Götzl et al., 2014; Ward et al., 2017), supporting the hypothesis that lysosomal dysfunction is a common mechanism in both diseases (Götzl et al., 2014; Valdez et al., 2017; Ward et al., 2017).
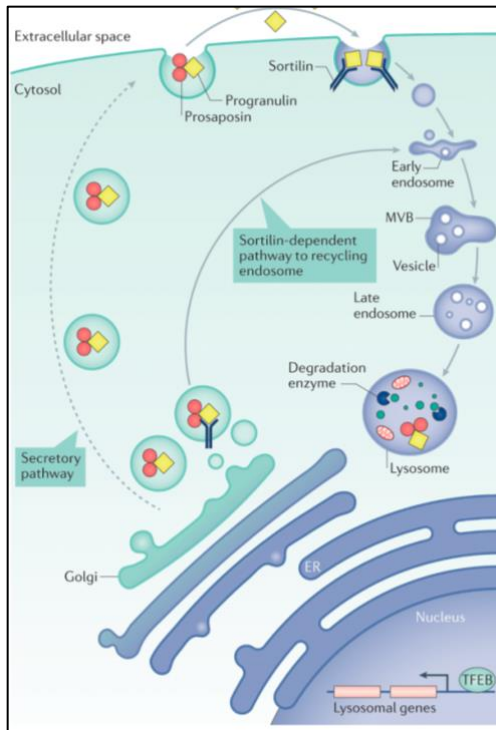
Figure 3. Trafficking of progranulin. Progranulin is in the Golgi apparatus, then secreted through the secretory pathway, which is regulated by the heterodimerization with prosaposin. Once released, it is endocytosed with mediation from sortilin, then reaches the lysosome. It may also reach the lysosome through the multivesicular body, a recycling endosome (adapted from (Kao et al., 2017)). Copyright permission given in Chapter 6.

1.2.4 Progranulin function in microglia

In the brain, PGRN is expressed in astrocytes, neurons, endothelial cells, and oligodendrocyte precursor cells, but has by far the highest expression in microglia (Z. H. Zhang et al., 2014). Therefore, I am interested in why this creates a spatial paradox, as TDP pathology from FTD-*GRN* is mainly seen in neurons. Microglia express and secrete high levels of progranulin, especially when reacting to a trauma or insult. PGRN has been shown to be a chemoattractant for microglia (Pickford et al., 2011). Loss of PGRN in microglia and macrophages causes an increase in phagocytosis and production of pro-inflammatory cytokines, including TNF and IL-6 (Kao et al., 2011; Martens et al., 2012; Yin et al., 2010). Complement genes, such as *C1qa*, *C1qb*, and *C3*, are upregulated in *Grn-/-* mice (Lui et al., 2016), which suggests a role for PGRN in suppressing microglial activation in the aging brain. System-level analysis of the affected genes reveals extensive interactions between lysosomal and innate immunity genes, with complement genes like *C1qa*, *C1qb*, *C1qc*, *C3*, as well as *CD68* and *Trem2* at the center (Lui et

al., 2016). In *Grn*^{-/-} mice, microgliosis, astrogliosis, and obsessive-compulsive-disorder (OCD)-like and disinhibition-like behavior has been reported, such as hyperexcitability like excessive grooming (Lui et al., 2016; Martens et al., 2012; Roberson, 2012; Yin et al., 2010). Aged *Grn*^{-/-} mice have lipofuscin deposits and enlarged lysosomes, which are signatures of NCL (Ahmed et al., 2010; Petkau et al., 2012; Wils et al., 2012). Yin et al., 2010 has shown phosphorylated TDP-43 accumulation in these mice as well. Granular or diffuse cytosolic ubiquitin deposits (Ahmed et al., 2010; Wils et al., 2012; Yin et al., 2010) and p62 aggregation (Tanaka et al., 2014) have also been reported, additionally implicating the endolysosomal system. Microglia have also been shown to have myelin accumulation in the lysosomes in *Grn*^{-/-} mice, indicating impaired lysosomal-mediated clearance of the myelin debris (Y. Wu et al., 2021). FTLD-*GRN* patients show a gradual increase in C1qa and C3 levels in the CSF, as well as microglial infiltration in the frontal cortex (Kao et al., 2017). Thus, I am interested in if the altered lysosomal dysfunction and aberrant microglial activation contributes to the neurodegeneration and neuropathology seen in FTD-*GRN*, and if that is mediated via an unknown cross talk mechanism.

1.2.5   Legumain

It is still unknown how PGRN loss-of-function mutations can lead to FTLD-TDP pathology. However, loss of PGRN instigates pathological processing of TDP-43, and the subsequent cleavage products are deposited in disease-characterizing deposits (Götzl et al., 2018; Root, Merino, Nuckols, Johnson, & Kukar, 2021b). A potential enzyme that can play a role in this mechanism is legumain. Legumain, also known as asparaginyl endopeptidase (AEP), is a caspase-like cysteine protease in the C13 peptidase family. It is autocatalytically activated, involving sequential removal of C- and N- terminal pro-peptides at different pH levels (Figure 4) (Dall & Brandstetter, 2013; Halfon, Patel, Vega, Zurawski, & Zurawski, 1998). It has also been shown that human monocyte-derived dendritic cells have inactive legumain proforms that become activated with lipopolysaccharide when the cells mature (D. N. Li, Matthews, Antoniou, Mazzeo, & Watts, 2003). In legumain-deficient mice, LAMP2-positive membrane structures were found to be enlarged. The aberrant lysosomes merged with late endosomes and accumulated membranous and electron-dense materials. In addition, the processing of lysosomal proteases, cathepsins B, H, and L, from single-chain to two-chain forms was defect (Shirahama-Noda et al., 2003). This shows legumain's significant role in the endosomal/lysosomal degradation system and in the proteolytic activation of cathepsins.

Legumain has also been shown to proteolytically degrade tau in P301S mice (Z. Zhang et al., 2014) and cleave human alpha-synuclein in addition to being highly activated in human Parkinson's disease brains (Z. Zhang et al., 2017), indicating a role in abnormal protein processing in neurodegenerative disease. In FTLD and ALS, TDP-43 is proteolytically cleaved, and two truncated TDP-43 peptides were identified, terminating C-terminal to N291 and N306. These fragments (~35 and 32 kDa) were detected by Western blot in postmortem FTLD brain tissue. *In vitro*, legumain was shown to cleave TDP-43 at these sites (Herskowitz et al., 2012), suggesting that legumain could be the protease responsible for cleaving these fragments. Legumain was also found to process progranulin and liberate granulin-F and increased legumain activity was shown in the degenerating brain regions of individuals with FTLD-TDP-Pgrn (Mohan et al., 2021). I am therefore interested to discover if legumain provides the link between PGRN loss-of-function and pathological TDP-43 processing.
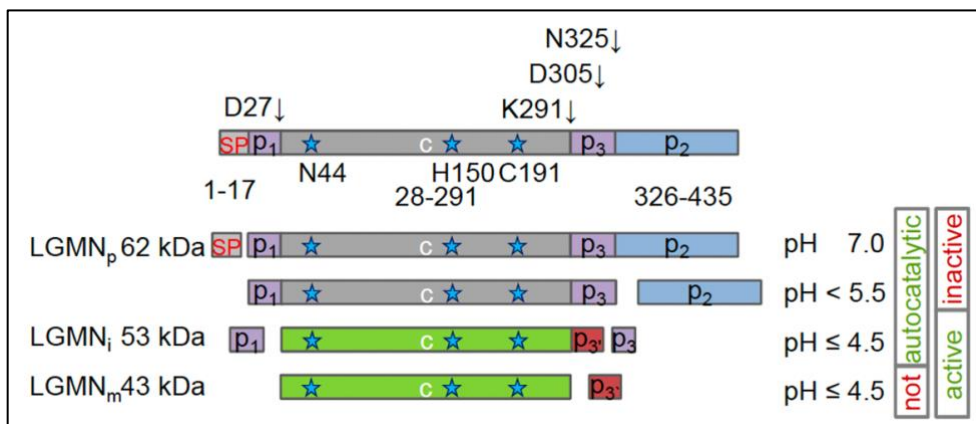
Figure 4. Domain structure and activation of legumain. N- and C-terminal pro-peptides (p1-p3), chain (c), and active centers (stars) are labeled. Proform (LGMN$_p$), intermediate-form (LGMN$_i$), and mature-form (LGMN$_m$) are shown. (adapted from Capell et al., 2022). Copyright permission given in Chapter 6.

1.3   Microglia

1.3.1   Microglia immune function in the brain

Microglia are the innate immune cells of the central nervous system. Progenitor cells are mesoderm-derived myeloid precursors and hematopoietic stem cells that originate from the yolk sac during early embryogenesis. They maintain region-specific densities and there is evidence of temporal and spatial heterogeneity in both the developing and adult brains (Ginhoux et al., 2010). Local tissue-specific factors, like transforming growth factor β (TGF-β), help them acquire

their identity (Butovsky et al., 2014; T'Jonck, Guilliams, & Bonnardel, 2018; Varol, Mildner, & Jung, 2015). Their survival is largely dependent on colony-stimulating factor-1 receptors (Csf1-R) (Greter et al., 2012; Y. Wang et al., 2012), which are binding sites for cytokines like colony-stimulating factor-1 (CSF1) and interleukin 34 (IL-34). The functional states have largely been deduced from their morphology and molecular signatures, including transcriptomes and proteomes.

During development, microglia control the number of neuronal progenitor cells (NPCs) by either actively inducing apoptosis or removing excess and dying NPCs (Ashwell, 1990; Marín-Teva et al., 2004; Sedel, Béchade, Vyas, & Triller, 2004). In this way, they actively shape neuronal circuits. They can also stimulate neurogenesis by supporting maturation, proliferation, and survival of NPCs and neurons (Frost & Schafer, 2016; Ueno et al., 2013). Microglia have been shown to interact with synapses as well, both removing synapses in an activity-dependent manner, and modulating synaptic circuits (Lowery, Tremblay, Hopkins, & Majewska, 2017; Paolicelli et al., 2011; Schafer et al., 2012; Tremblay, Lowery, & Majewska, 2010; Wake, Moorhouse, Miyamoto, & Nabekura, 2013).

In adult brains, microglia constantly surveil the surrounding environment and interact with other cell types (Kettenmann, Kirchhoff, & Verkhratsky, 2013). The cells have a ramified morphology with processes that can extend to encompass areas more than 10-fold the size of their soma (Kettenmann et al., 2013) and phagocytose dead and excess cells. (Sierra et al., 2010). In instances of CNS injury or infection, microglia respond immediately by becoming activated and proliferating, phagocytosing the cellular debris (Davalos et al., 2005; Nimmerjahn, Kirchhoff, & Helmchen, 2005; Stence, Dailey, & Waite, 2001).

1.3.2 TREM2 – a microglia risk gene for dementia

Genome-wide association studies (GWASs) show that microglia express risk genes for several neurodegenerative diseases, including Alzheimer's disease (AD), multiple sclerosis, Parkinson's disease, and frontotemporal dementia, indicating that they play a significant role. A very important example is the gene for triggering receptor of myeloid cells 2 (TREM2) (Borroni et al., 2014; Cuyvers et al., 2014; Guerreiro et al., 2013; Jonsson et al., 2013; Rayaprolu et al., 2013). Rare coding variants, including R47H, R62H, and H157Y, have been discovered that lead to loss-of-function (LOF) of TREM2 and an increased risk for late-onset AD (LOAD) (Bis et al.,

2020; Kleinberger et al., 2017, 2014; Kunkle et al., 2019; Schlepckow et al., 2017; Sims et al., 2017; Song et al., 2017; Thornton et al., 2017; Y. Wang et al., 2015). Other variants in genes expressed by microglia, like ABI3, (Lancaster, 2019; Sims et al., 2017), also increase LOAD risk, indicating that microglial dysfunction may be a major contributor to the disease.

1.3.3   Structure and function of TREM2

TREM2 is a type I, immunoreceptor tyrosine-based activation motif (ITAM)-containing cell surface receptor (Kleinberger et al., 2014; Wunderlich et al., 2013). It is expressed by all cells with myeloid lineage and selectively in microglia in the brain (Hickman et al., 2013). Its ligands include anionic lipids, lipoproteins, and apolipoproteins (Atagi et al., 2015; Bailey, Devaux, & Farzan, 2015; Daws et al., 2003; Y. Wang et al., 2015; Yeh, Wang, Tom, Gonzalez, & Sheng, 2016) and it plays an important role in phagocytosis, including clearance of Aβ peptides (Kleinberger et al., 2014; Xiang et al., 2016). Full-length TREM2 forms a heteromeric complex with DAP12 and activates phospho-SYK signaling downstream (Colonna, 2003). Signaling is terminated through the shedding of the ectodomain by ADAM family proteases, releasing soluble TREM2 (sTREM2) into the extracellular space (Wunderlich et al., 2013). It can be detected in cerebrospinal fluid (CSF), serum, and plasma (Henjum et al., 2016; Heslegrave et al., 2016; Kleinberger et al., 2014; Morenas-Rodríguez et al., 2022; Piccio et al., 2008, 2016; Suárez-Calvet et al., 2016; Suárez‑Calvet et al., 2016). The remaining C-terminal fragment (CTF) is degraded by γ-secretase (Glebov, Wunderlich, Karaca, & Walter, 2016; Wunderlich et al., 2013) (Figure 5).
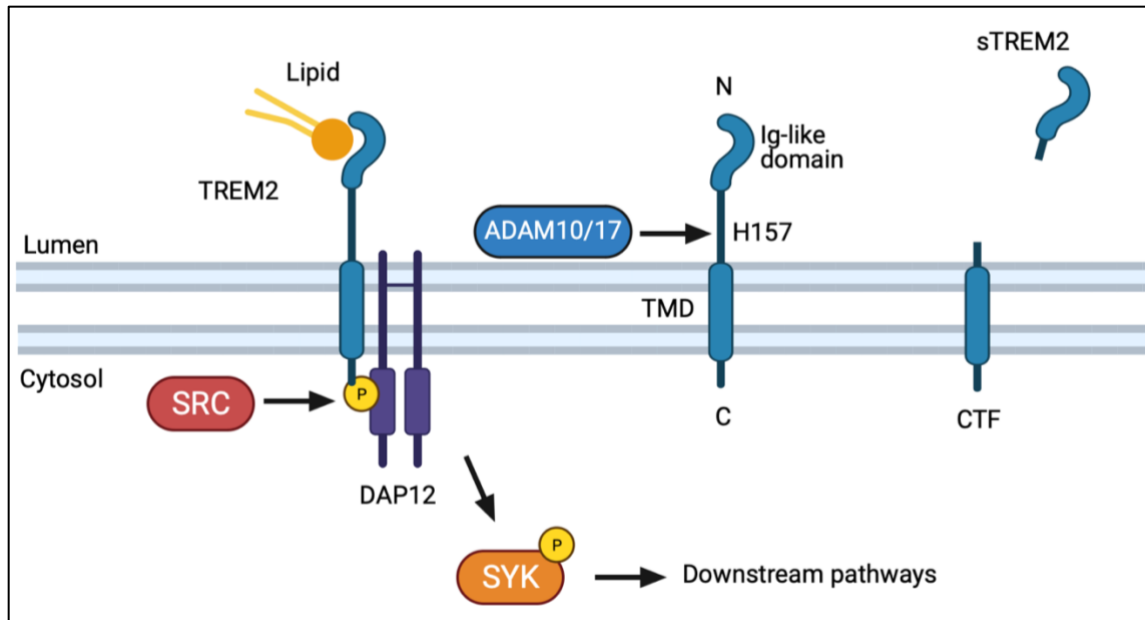
Figure 5. TREM2 signaling pathway (made on Biorender.com). TREM2 is co-expressed with DAP12 on the cell surface. Ligand binding activates the TREM2 signaling pathway, starting with phosphorylation of SYK and leading to downstream pathways. Signaling is terminated through ADAM10/17 protease cleavage, release sTREM2 into the extracellular space.

1.3.4 Disease-associated microglia and the role of TREM2

Currently, microglia state is defined is by transcriptional profiling, for which single-cell RNA sequencing (scRNA-seq) and single-nucleus RNA sequencing (snRNA-seq) have been essential. Differentially expressed specific gene sets are used to define sub-populations that can be overlapping and complex (Keren-Shaul et al., 2017; Mathys et al., 2017, 2019). One subpopulation, known as disease-associated microglia (DAM) or microglia neurodegenerative diseases (MGnD), was first identified in AD mouse models, as distinct from homeostatic microglia (Keren-Shaul et al., 2017; Krasemann et al., 2017). DAM are phenotypically characterized by increased phagocytosis, migration, and chemotaxis, and elevated lipid metabolism. Marker genes of this subpopulation include *TREM2* and *APOE*, with downregulation of homeostatic genes like *P2RY12* and *CX3CR1*. Certain TREM2 LOF mutations lock microglia in a homeostatic state (Keren-Shaul et al., 2017; Krasemann et al., 2017; Nugent et al., 2020) and TREM2 KOs are unable to transition into a DAM state, suggesting a vital, triggering role for TREM2 for this transition. In addition, *TREM2* KO microglia show reduced mTOR signaling and deficiencies in glycolysis, the TCA cycle, and pentose phosphate metabolic pathways (Kleinberger et al., 2017; Ulland et al., 2017). TREM2 LOF mice

have reduced cerebral glucose metabolism, as measured by FDG-microPET (Götzl et al., 2019; Kleinberger et al., 2017). Lack of functional TREM2 is also associated with reduced proliferation and phagocytosis. All this evidence suggests a protective role for the DAM population in neurodegeneration. snRNA-seq analysis has been done on frozen biopsies from individuals with AD pathology. Four subclusters of microglia were detected and one showed a significant overlap with mouse DAM genes, characterized by high expression of major histocompatibility complex (MHC) class II-related genes (Mathys et al., 2019). AD patients who are TREM2-R47H and TREM2-R62H carriers show reduced transcriptional microglial activation compared to control samples, providing further evidence of TREM2's role in regulating microglia state (Keren-Shaul et al., 2017; Nugent et al., 2020; Y. Zhou et al., 2020). TREM2 mutation carriers also show reduced microglial migration and clustering around plaques (Jay et al., 2015; Parhizkar et al., 2019; Ulrich et al., 2014; Y. Wang et al., 2015, 2016) and upregulation of homeostatic markers, like *TMEM119*, *P2RY12*, and *CX3CR1* (Y. Zhou et al., 2020).

1.3.5   Therapeutic TREM2 modulation

There has been recent evidence supporting that TREM2 activation is potentially beneficial in AD. In mouse models, TREM2 has been shown to support plaque compaction and thus reduce plaque-associated neuropathology (Meilandt et al., 2020; Ulrich et al., 2014; Y. Wang et al., 2016). There is also indirect evidence in AD patients that higher levels of TREM2 present in disease are associated with protective effects on disease progression (Ewers et al., 2019; Heslegrave et al., 2016; Kleinberger et al., 2017; Morenas-Rodríguez et al., 2022; Nugent et al., 2020; Piccio et al., 2016; Poliani et al., 2015; Suárez-Calvet et al., 2016; Suárez-calvet et al., 2018; Suárez‑Calvet et al., 2016). It has also been shown using TSPO µPET that microglial activation during aging is significantly reduced by TREM2 LOF mutations (Kleinberger et al., 2017). Due to these findings, therapeutic strategies were developed to modulate microglial function through targeting TREM2 with agonistic antibodies (Cheng et al., 2018; Cignarella et al., 2020; Price et al., 2020; Schlepckow et al., 2020; S. Wang et al., 2020). Both Amgen and Alector have developed antibodies, which appear to have epitopes in the extracellular domain, bind to the stalk region, and activate receptor signaling (Cignarella et al., 2020; Price et al., 2020; S. Wang et al., 2020). They are similar to another antibody developed in house that increases TREM2 on the cell surface of microglia by preventing shedding of the extracellular domain (Schlepckow et al., 2020). These antibodies activate DAP12 phosphorylation and Syk signaling, enhance the survival of microglia under low M-CSF conditions, and increase

expression of proliferation genes. There is also an increase in TREM2 and decrease in P2RY12 expression. Microglia phagocytosis of myelin debris and Aβ was enhanced upon antibody treatment (Cignarella et al., 2020; Schlepckow et al., 2020). Another recent publication describes the effects of a tetravalent TREM2 agonistic antibody (Zhao et al., 2022). The antibody increases TREM2 activation by 100-fold, which resulted in increased microglia phagocytosis of the oligomeric Aβ-lipid (oAβ) complex, migration towards the oAβ, and better microglial survival in vitro. In 5xFAD mice, weekly treatments resulted in reduction of amyloid burden and increased migration and phagocytosis of amyloid plaques by microglia, as well as increased neuronal health, improved cognitive functions, and reduced tau hyperphosphorylation. These studies all point to the benefits of enhancing TREM2 expression in microglia as a potential treatment for AD.

In contrast to TREM2 LOF microglia, microglia in patients with *GRN* mutations and in *Grn* KO mice show an increase in hyperactivation. *Grn* KO mice also have a large increase in TSPO-PET signal and a reduction in FDG-μPET signal (Götzl et al., 2019). In this case, it seemed to me that an increase in DAM signature seems to correlates with neurodegeneration. Therefore, I hypothesized that antagonistic TREM2 antibodies may have therapeutic benefit for FTD by ameliorating the hyperactivation as a potential treatment.

The studies on TREM2 modulation have all been done in mouse models, which are important models to study. However, it is also beneficial to study the effects and mechanisms in a human model. RNA-seq studies of human microglia show limited overlap and more diverse sub-states in comparison to mouse populations. It is also difficult to compare brains from human patients to mouse models of disease, for example end-stage human AD patients to AD mouse models with amyloid but no tau pathology. In addition, there is a lack of cross-species sequence homology and functional homology (Lewcock et al., 2020). In my PhD thesis, I therefore aimed to develop a human model for functional analysis of TREM2.

1.4   Human induced pluripotent stem cells

1.4.1   Induced pluripotent stem cells – a new tool for *in vitro* modeling of disease

In 2006, Takahashi and Yamanaka discovered that adding four exogenous factors, Oct3/4, Sox2, c-Myc, and Klf4, to mouse fibroblasts can reprogram them into cells closely resembling

embryonic stem cells (ESCs) (Takahashi & Yamanaka, 2006). One year later, it was shown that these factors can also reprogram human fibroblasts (Takahashi et al., 2007). These induced pluripotent stem cells (iPSCs) can maintain their pluripotency and divide indefinitely. *In vitro* protocols have been developed that enable the iPSCs to differentiate into various somatic cell types. Currently, iPSCs are being used to investigate neurodegenerative diseases (TCW, 2019), in complement to *in vivo* models, since physiologically relevant brain cell types can be differentiated (McComish & Caldwell, 2018).

1.4.2 iPSC models of neurodegenerative disease

iPSC-derived somatic cell types have been used to model several neurodegenerative diseases (Klimmt, Dannert, & Paquet, 2020). The iPSCs can be either patient-derived or genetically edited. First, relatively basic models were based on 2-dimensional (2D) neuronal monocultures (Birnbaum et al., 2018; Israel et al., 2012; Kondo et al., 2013; Woodruff et al., 2013; Yagi et al., 2011). Recently, 3-dimensional (3D) models have also been developed (Brassard & Lutolf, 2019; Choi et al., 2014; Gonzalez et al., 2018; Park et al., 2018; Raja et al., 2016; Velasco et al., 2019), since there would be more cell-cell interaction, increased extracellular matrix, and a more physiologically relevant environment. This is achieved through either embedding the cells into hydrogels or creating organoids. However, these 3D models also typically contain only neurons. So far, FTD-*GRN* has been investigated in these types of models (Table 3) (Almeida et al., 2012; S. Lee & Huang, 2017b; Logan et al., 2021; Raitano et al., 2015; Valdez et al., 2017, 2020). The lack of other cell types, such as microglia, where PGRN is predominantly expressed, makes it impossible to study the crosstalk between cell types. Therefore, I would like to include the relevant cell types for the disease, including both neurons and microglia, in my model. Existing models were also mostly generated from patient-derived iPSCs. The issue with using patient-derived iPSCs is that when using a healthy donor as a control, it would not be isogenic. One could also edit out the disease-causing mutation from a patient line and use that as a control, however, the genetic background could contain other disease-modifying risk variants and influence the phenotype. Therefore, I would like to genetically introduce mutations using CRISPR/Cas9 into a healthy donor line so that there will be an isogenic control and the phenotype can be securely attributed to the mutation.

1.5 CRISPR/Cas9 as a tool for precise genome editing

The CRISPR/Cas9 system is a recently discovered method that has revolutionized biomedical research. It allows precise and simple genome editing in the form of insertion or exchange of specific DNA sequences at almost any genomic locus. This has led to a new way of studying phenotypes, such as disease pathology, linked to specific genomic sequences (Hsu, Lander, & Zhang, 2014; Knott & Doudna, 2018; Komor, Badran, & Liu, 2017; Wright, Nuñez, & Doudna, 2016).

The CRISPR/Cas9 system was first discovered in bacteria as part of their adaptive immune system against foreign nucleic acids of invading bacteriophages (Barrangou et al., 2007; Brouns et al., 2008). Foreign DNA is cleaved and integrated as spacer sequences in clustered regularly interspaced short palindromic repeats (CRISPR) arrays that have spacers from previous invasions. These are expressed as CRISPR-RNA (crRNA) and bind to transactivation crRNA (tracrRNA) and the Cas9 nuclease. This complex recognizes a repeated attack from the same virus and cuts and degrades the bacteriophage DNA in a targeted way (Deltcheva et al., 2011; Jinek et al., 2012). Since then, it has been discovered that the purified Cas9 nuclease can be used for specific DNA changes *in vitro* and *in vivo* (Cho, Kim, Kim, & Kim, 2013; Cong et al., 2013; Gasiunas, Barrangou, Horvath, & Siksnys, 2012; Jinek et al., 2012, 2013; Mali et al., 2013) by combining it with a single guide RNA (sgRNA). The sgRNA sequence can be customized to target and introduce double stranded breaks (DSBs) into a specific DNA locus. These DSBs are repaired by two major pathways: non-homologous end joining (NHEJ) or homology-directed repair (HDR) (Rouet, Smih, & Jasin, 1994). In the NHEJ pathway, the two DNA ends are fused together and often result in non-specific insertions or deletions (InDel) of between 1-10 basepairs around the cut site (Mali et al., 2013; Paquet et al., 2016). These InDels can cause a frameshift that is useful for creating genetic knockouts by introducing premature stop codons. I used this method to create a GRN KO iPSC line that can be further differentiated into brain cell types.

2 Aim of this Study

Granulin is a gene expressed in microglia and loss of function results in hyperactivation and lysosomal dysfunction, including an increase in the expression and activity of lysosomal proteases. The role of this microglia dysfunction in the pathology is still unclear and we do not understand the spatial paradox of how microglial expressed PGRN/absence of PGRN influences neuronal TDP-43 pathology. We also do not understand the relationship between microglial hyperactivation and lysosomal dysfunction. Since past research has been mostly conducted in mouse models, peripheral cells, and postmortem patient brain tissue, I was interested to set up a human model with disease-relevant cell types hoping that such a model may allow recapitulation of disease pathology.

The first goal of this thesis is generating a human induced pluripotent stem cell (iPSC) derived model recapitulating GRN-related phenotypes. This is done by knocking out *GRN* using CRISPR/Cas9 in iPSCs. These iPSCs are further differentiated into neurons and microglia.

The second goal is investigating the relationship between microglial hyperactivation and lysosomal dysfunction. This is achieved through suppressing hyperactivation of the GRN-/- iPSC-derived microglia with antibodies blocking the TREM2 signaling pathway, which is required to allow microglia to switch from a resting state to a disease associated state.

The third goal is to prove a potential cross talk between microglia and neurons by exploring the relationship between granulin loss of function in microglia and TDP-43 pathology in neurons.

3 Research Articles

3.1 Loss of TREM2 rescues hyperactivation of microglia, but not lysosomal deficits and neurotoxicity in models of progranulin deficiency

Reifschneider A, **Robinson S**, van Lengerich B, Gnörich J, Logan T, Heindl S, Vogt MA, Weidinger E, Riedl L, Wind K, Zatcepin A, Pesämaa I, Haberl S, Nuscher B, Kleinberger G, Klimmt J, Götzl JK, Liesz A, Bürger K, Brendel M, Levin J, Diehl-Schmid J, Suh J, Di Paolo G, Lewcock JW, Monroe KM, Paquet D, Capell A, Haass C. Loss of TREM2 rescues hyperactivation of microglia, but not lysosomal deficits and neurotoxicity in models of progranulin deficiency. EMBO J. 2022 Feb 15;41(4):e109108. doi: 10.15252/embj.2021109108. Epub 2022 Jan 12. PMID: 35019161; PMCID: PMC8844989

Copyright permission given in Chapter 6.

Article

Loss of TREM2 rescues hyperactivation of microglia, but not lysosomal deficits and neurotoxicity in models of progranulin deficiency

Anika Reifschneider[1] (iD), Sophie Robinson[2,3], Bettina van Lengerich[4], Johannes Gnörich[3,5], Todd Logan[4], Steffanie Heindl[2] (iD), Miriam A Vogt[6], Endy Weidinger[7], Lina Riedl[8], Karin Wind[3,5], Artem Zatcepin[3,5] (iD), Ida Pesämaa[3], Sophie Haberl[6], Brigitte Nuscher[1], Gernot Kleinberger[6], Julien Klimmt[2] (iD), Julia K Götzl[1], Arthur Liesz[2,9] (iD), Katharina Bürger[2,3], Matthias Brendel[3,5], Johannes Levin[3,5,7], Janine Diehl-Schmid[7,8], Jung Suh[4], Gilbert Di Paolo[4] (iD), Joseph W Lewcock[4] (iD), Kathryn M Monroe[4,*], Dominik Paquet[2,9,**] (iD), Anja Capell[1,***] (iD) & Christian Haass[1,3,9,****] (iD)

Abstract

Haploinsufficiency of the progranulin (PGRN)-encoding gene (*GRN*) causes frontotemporal lobar degeneration (*GRN*-FTLD) and results in microglial hyperactivation, TREM2 activation, lysosomal dysfunction, and TDP-43 deposition. To understand the contribution of microglial hyperactivation to pathology, we used genetic and pharmacological approaches to suppress TREM2-dependent transition of microglia from a homeostatic to a disease-associated state. *Trem2* deficiency in *Grn* KO mice reduced microglia hyperactivation. To explore antibody-mediated pharmacological modulation of TREM2-dependent microglial states, we identified antagonistic TREM2 antibodies. Treatment of macrophages from *GRN*-FTLD patients with these antibodies led to reduced TREM2 signaling due to its enhanced shedding. Furthermore, TREM2 antibody-treated PGRN-deficient microglia derived from human-induced pluripotent stem cells showed reduced microglial hyperactivation, TREM2 signaling, and phagocytic activity, but lysosomal dysfunction was not rescued. Similarly, lysosomal dysfunction, lipid dysregulation, and glucose hypometabolism of *Grn* KO mice were not rescued by TREM2 ablation. Synaptic loss and neurofilament light-chain (NfL) levels, a biomarker for neurodegeneration, were further elevated in the *Grn/Trem2* KO cerebrospinal fluid (CSF). These findings suggest that TREM2-dependent microglia hyperactivation in

models of *GRN* deficiency does not promote neurotoxicity, but rather neuroprotection.

Introduction

Neurodegenerative diseases are currently incurable and novel therapeutic strategies are desperately required. Besides disease-defining protein deposits (Aguzzi & Haass, 2003), microgliosis is observed in almost all neurodegenerative diseases (Ransohoff, 2016). Microgliosis can be detrimental (Heneka *et al*, 2013; Hong *et al*, 2016a). However, recent findings strongly suggested that certain microglial responses to brain pathology may also be neuroprotective (Deczkowska *et al*, 2020; Lewcock *et al*, 2020). This is based on the identification of variants in genes predominantly or exclusively expressed in microglia within the brain that increase the risk for late-onset Alzheimer's disease (LOAD) and other neurodegenerative

1 Division of Metabolic Biochemistry, Faculty of Medicine, Biomedical Center (BMC), Ludwig-Maximilians-Universität München, Munich, Germany
2 Institute for Stroke and Dementia Research, University Hospital Munich, Ludwig-Maximilians-Universität München, Munich, Germany
3 German Center for Neurodegenerative Diseases (DZNE) Munich, Munich, Germany
4 Denali Therapeutics Inc., South San Francisco, CA, USA
5 Department of Nuclear Medicine, University Hospital, Ludwig-Maximilians-Universität München, Munich, Germany
6 ISAR Bioscience GmbH, Planegg, Germany
7 Department of Neurology, University Hospital, Ludwig-Maximilians-Universität München, Munich, Germany
8 Department of Psychiatry and Psychotherapy, School of Medicine, Technical University of Munich, Munich, Germany
9 Munich Cluster for Systems Neurology (SyNergy), Munich, Germany
   *Corresponding author. Tel: +1 650 4574910; E-mail: monroe@dnli.com
   **Corresponding author. Tel: +49 89 440046123; E-mail: dominik.paquet@med.uni-muenchen.de
   ***Corresponding author. Tel: +49 89 440046534; E-mail: anja.capell@med.uni-muenchen.de
   ****Corresponding author. Tel: +49 89 440046549; E-mail: christian.haass@dzne.de

disorders (Efthymiou & Goate, 2017). Protective microglial functions became particularly evident upon functional investigations of coding variants found within the triggering receptor expressed on myeloid cells 2 (TREM2) gene, which can increase the risk for LOAD and other neurogenerative disorders including frontotemporal dementia-like syndromes (Guerreiro *et al*, 2013; Jonsson *et al*, 2013). These TREM2 variants reduce lipid ligand binding, lipid and energy metabolism, chemotaxis, survival/proliferation, phagocytosis of cellular debris, and potentially other essential microglial functions (Deczkowska *et al*, 2020; Lewcock *et al*, 2020). Moreover, a loss of TREM2 function locks microglia in a dysfunctional homeostatic state (Keren-Shaul *et al*, 2017; Krasemann *et al*, 2017; Mazaheri *et al*, 2017; Nugent *et al*, 2020), in which they are unable to respond to pathological challenges by inducing a disease-associated mRNA signature.

Disease-associated microglia (DAM) respond to amyloid pathology by clustering around amyloid plaques where they exhibit a protective function by encapsulating the protein deposits via a barrier function (Yuan *et al*, 2016) that promotes amyloid plaque compaction (Ulrich *et al*, 2014; Wang *et al*, 2016; Meilandt *et al*, 2020) and reduces *de novo* seeding of amyloid plaques (Parhizkar *et al*, 2019). TREM2 is therefore believed to be a central target for therapeutic modulation of microglial functions (Deczkowska *et al*, 2020; Lewcock *et al*, 2020). A number of agonistic anti-TREM2 antibodies were recently developed (Cheng *et al*, 2018; Cignarella *et al*, 2020; Price *et al*, 2020; Schlepckow *et al*, 2020; Wang *et al*, 2020; Ellwanger *et al*, 2021; Fassler *et al*, 2021), which either enhance cell surface levels of signaling-competent TREM2 by blocking TREM2 shedding and/or crosslinking TREM2 receptors to stimulate downstream signaling via Syk phosphorylation. In preclinical studies, these antibodies boost protective functions of microglia as shown by enhanced amyloid β-peptide and myelin clearance, reduced amyloid plaque load, improved memory in models of amyloidosis, and supported axon regeneration and remyelination in models of demyelinating disorders such as multiple sclerosis (Cheng *et al*, 2018; Cignarella *et al*, 2020; Lewcock *et al*, 2020; Price *et al*, 2020; Schlepckow *et al*, 2020; Wang *et al*, 2020; Bosch-Queralt *et al*, 2021; Ellwanger *et al*, 2021; Fassler *et al*, 2021).

Although increased TREM2 may be protective in AD patients (Ewers *et al*, 2019), in other neurodegenerative diseases, microglia may be overactivated and become dysfunctional (Heneka *et al*, 2013; Hong *et al*, 2016a; Ransohoff, 2016). Therefore, in these contexts, antagonistic TREM2 antibodies may display therapeutic benefit through dampening microglial hyperactivation. A well-described example of a neurodegenerative disorder where microglia are hyperactivated is *GRN*-associated frontotemporal lobar degeneration (*GRN*-FTLD) with TDP-43 (transactive response DNA-binding protein 43 kDa) deposition caused by progranulin (PGRN) deficiency (Baker *et al*, 2006; Cruts *et al*, 2006; Gotzl *et al*, 2019). In models of *GRN*-FTLD-associated haploinsufficiency, hyperactivation of microglia is evident, as demonstrated by an increased disease-associated mRNA signature as well as strongly increased 18-kDa translocator protein positron emission-tomography ((TSPO)-PET) signals in mouse models (Martens *et al*, 2012; Lui *et al*, 2016; Krabbe *et al*, 2017; Gotzl *et al*, 2019; Huang *et al*, 2020; Marschallinger *et al*, 2020; Zhang *et al*, 2020). This is the opposite phenotype of *Trem2* knockout (KO) microglia, which are locked in a homeostatic state (Keren-Shaul *et al*, 2017; Kleinberger *et al*, 2017;

Krasemann *et al*, 2017; Mazaheri *et al*, 2017; Gotzl *et al*, 2019; Nugent *et al*, 2020). Hyperactivation of microglia is also observed in the brain of *GRN*-FTLD patients (Lui *et al*, 2016; Woollacott *et al*, 2018; Gotzl *et al*, 2019). PGRN is a secreted protein, which is also transported to lysosomes (Hu *et al*, 2010; Zhou *et al*, 2015), where it appears to control activity of hydrolases, such as cathepsins and glucocerebrosidase (GCase) (Gotzl *et al*, 2016, 2018; Beel *et al*, 2017; Ward *et al*, 2017; Paushter *et al*, 2018; Arrant *et al*, 2019; Butler *et al*, 2019b; Logan *et al*, 2021). Total loss of PGRN results in a lysosomal storage disorder (Smith *et al*, 2012; Almeida *et al*, 2016). A potential synergistic contribution of lysosomal dysfunction and hyperactivated microglia to the disease pathology and specifically to the deposition of TDP-43 in neurons is likely but currently not understood (Kao *et al*, 2017; Ward *et al*, 2017; Huang *et al*, 2020; Logan *et al*, 2021).

To determine whether hyperactivation of microglia and its pathological consequences in *Grn* KO mice are dependent on aberrant TREM2 signaling, we sought to reduce the microglial activation status by crossing them to *Trem2* KO mice. This reduced the expression of DAM genes, suggesting that negative modulation of TREM2 signaling may be exploited to lower microglial activation in neuroinflammatory disorders. In analogy to the agonistic 4D9 TREM2 antibody developed earlier in our laboratory (Schlepckow *et al*, 2020), we therefore generated monoclonal antibodies with opposite, namely antagonistic, properties. Such antibodies blocked lipid ligand-induced TREM2 signaling, reduced signaling-competent cell surface TREM2 in *GRN*-FTLD patient-derived macrophages, and concomitantly increased shedding of TREM2, which resulted in enhanced release of soluble TREM2 (sTREM2). Therefore, TREM2 antagonist antibodies inhibit receptor function via multiple mechanisms of action. In genetically engineered human-induced pluripotent stem cell-derived (iPSC) microglia-lacking PGRN, the antagonistic antibodies reduced expression of the majority of candidate genes of the DAM signature, however, they failed to restore lysosomal function. Similarly, in *Grn/Trem2* double-knockout (*Double* KO) mice, lysosomal dysfunction was not rescued. Moreover, pathological features such as reduced 2-deoxy-2-[18F]fluoro-d-glucose (FDG) uptake, disturbed lipid metabolism, and abnormal microglial morphology were not ameliorated. Strikingly, synapse loss was exacerbated, and neurofilament light chain (NfL), a sensitive fluid biomarker of neurodegeneration (Meeter *et al*, 2016; Rohrer *et al*, 2016; Preische *et al*, 2019), was also not reduced but unexpectedly increased in the cerebrospinal fluid (CSF). These findings therefore suggest that against common expectations, hyperactivated microglia may retain at least some TREM2-dependent neuroprotective activities.

Results

Trem2 KO dampens hyperactivation of microglia in PGRN-deficient mice

PGRN and TREM2 deficiency results in opposite microglial activation states (Gotzl *et al*, 2019). To determine if reduction in TREM2 signaling can ameliorate hyperactivation of PGRN-deficient microglia, we crossed *Grn* KO mice (Kayasuga *et al*, 2007) to *Trem2* KO mice (Turnbull *et al*, 2006) and performed TSPO-PET imaging using

established protocols (Liu *et al*, 2015; Kleinberger *et al*, 2017). TSPO-PET imaging in mice is rather specific for microglial activation, as plexin treatment and ablation of TREM2, both of which reduce microglia numbers, strongly reduce the TSPO signal (Xiang *et al*, 2021). In line with our earlier findings (Gotzl *et al*, 2019), we confirmed a strong increase in the TSPO-PET signal in the brains of *Grn* KO mice when compared to WT ($P < 0.01$) (Figs 1A and B, and EV5A). We also confirmed reduced TSPO expression in the brain of *Trem2* KO mice ($P < 0.03$) (Figs 1A and B, and EV5A), consistent with our initial findings in TREM2 loss-of-function models (Kleinberger *et al*, 2017; Gotzl *et al*, 2019). Consistent with the above-described goal to dampen hyperactivation of microglia, investigation of *Double* KO mice (Figs 1A and B, and EV5A) indicated a balanced TSPO expression without a significant difference when compared to WT ($P = 0.945$) and a reduction in TSPO expression relative to *Grn* KO mice ($P < 0.05$) (Figs 1A and B, and EV5A).

These findings suggest that DAM gene expression patterns as observed in *Grn* KO mice may be partially rescued in *Double* KO mice. To test this, we isolated microglia from adult mouse brains. Microglial mRNA of all three mouse lines was analyzed using a customized nCounter panel (NanoString Technologies), which includes 65 genes that previously showed opposite expression levels in *Grn* and *Trem2* KO mice (Mazaheri *et al*, 2017; Gotzl *et al*, 2019). Gene expression levels were normalized against the geometric mean of four housekeeping genes, including *Asb10*, *Cltc*, *Hprt1*, and *Tubb5*. In accordance with our previous findings (Gotzl *et al*, 2019), candidate genes of the DAM signature such as *ApoE*, *Cd22*, *Ly9*, *Clec7a*, *Spp1*, and *Olfr110* were massively upregulated in *Grn* KO microglia while these genes were suppressed in the *Trem2* KO microglia (Fig 2A–E). In the *Double* KO microglia, expression of the DAM signature genes *Olfr110*, *Spp1*, and *Clec7a* is fully rescued to WT expression levels and others, such as *Ly9*, *Cd22*, and *ApoE*, are at least partially reduced compared to the *Grn* KO (Fig 2D and E). These data thus provide direct evidence that in *Double* KO mice, the molecular signature of microglia is shifted away from a DAM state toward a homeostatic state.

Antagonistic TREM2 antibodies decrease cell surface TREM2 and reduce ligand-induced Syk signaling in monocyte-derived patient macrophages

Antagonist TREM2 antibodies were generated by immunizing rodents with human TREM2 extracellular domain (ECD)-Fc fusion protein and performing single B-cell sequencing on peripheral lymphoid tissues. Antibodies that bound specifically to human TREM2 were evaluated for functional impact to TREM2 signaling. Antagonistic antibodies were identified by their ability to block TREM2-dependent lipid ligand-induced activation of p-Syk on HEK293 cells overexpressing TREM2/DAP12 (Fig EV1). Cells were dosed with three different concentrations of liposomes, and antagonistic antibody 1 (Ab1) and antagonistic antibody 2 (Ab2), which were found to block phosphatidylserine (PS)-induced p-Syk activity (Fig EV1A). Both antibodies bind to an epitope in the IgV domain between amino acids 30 and 63 of human TREM2 (Figs 3A and EV1B). These selected antibodies were reformatted onto an effector-less human hIgG1-LALAPG backbone, and demonstrated high affinity for cell surface TREM2 (0.38 nM EC50 Ab1 and 0.18 nM EC50
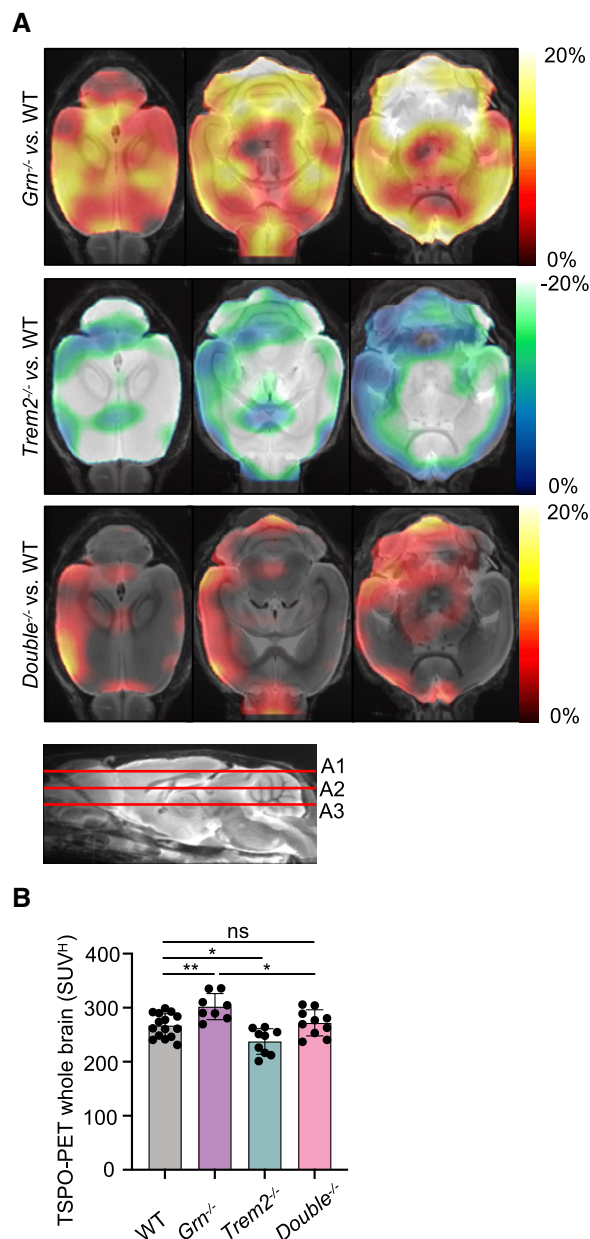
Figure 1. TSPO-PET imaging indicates rescue of microglial hyperactivation in *Double*$^{-/-}$ mice.

A Axial slices as indicated below (A1, A2, and A3) show %-TSPO-PET differences between *Grn*$^{-/-}$, *Trem2*$^{-/-}$, or *Double*$^{-/-}$ mice and WT at the group level. Images adjusted to an MRI template indicate increased microglial activity in the brain of *Grn*$^{-/-}$ mice (hot color scale), compensated microglial activity in the brain of *Double*$^{-/-}$ mice, and decreased microglial activity in the brain of *Trem2*$^{-/-}$ mice (cold color scale), each in contrast against age-matched WT mice.

B Scatter plot illustrates individual mouse TSPO-PET values derived from a whole-brain volume of interest. A total of 8–15 female mice per group at an average age of 11.1 ± 1.6 months (*Grn*$^{-/-}$ (n = 8), *Trem2*$^{-/-}$ (n = 9), *Double*$^{-/-}$ (n = 10), and WT (n = 15)). Data represent mean ± SD. For statistical analysis, one-way ANOVA with Tukey *post hoc* test was used. Statistical significance was set at *$P < 0.05$; **$P < 0.01$; ns, not significant.
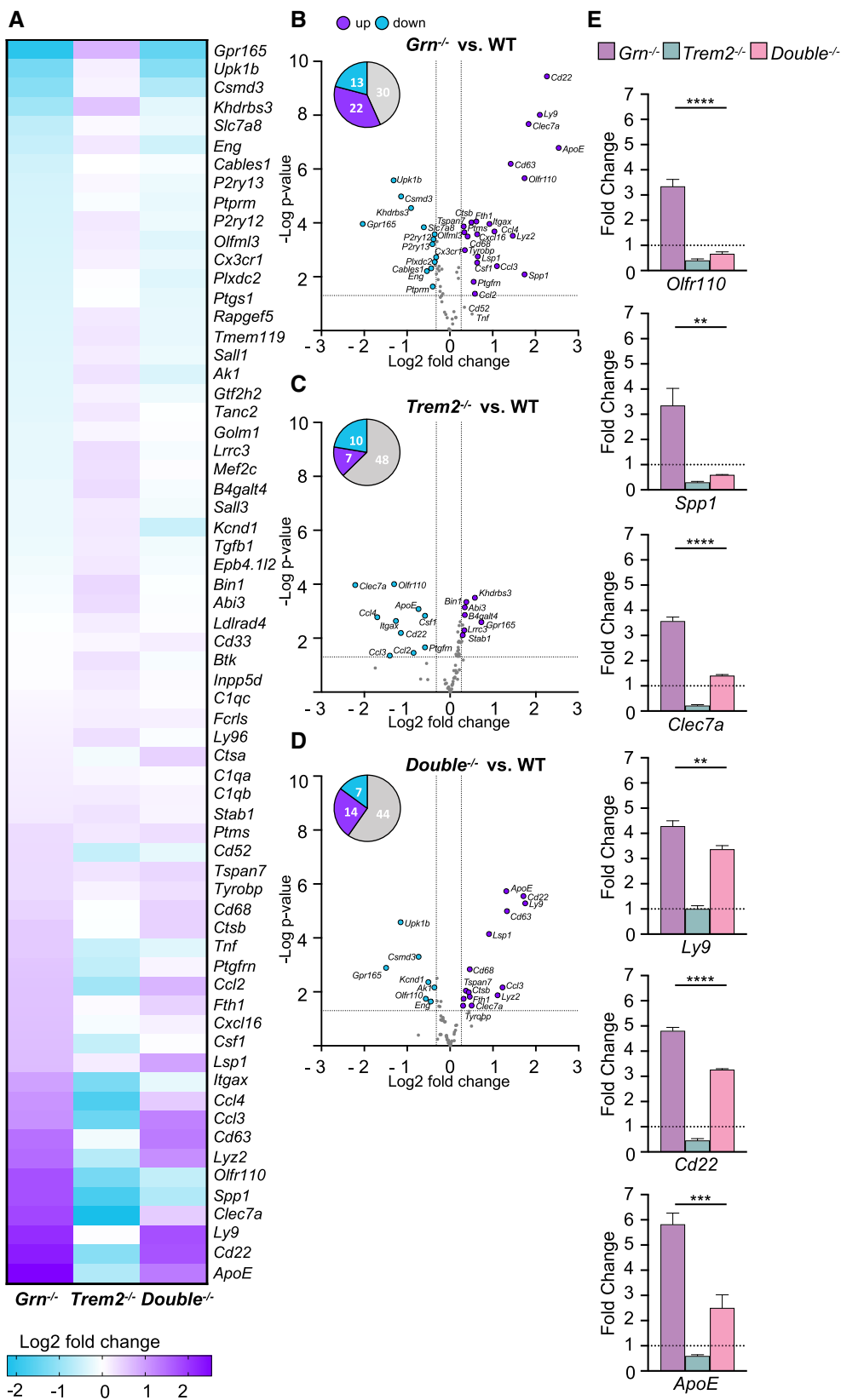
Source data are available online for this figure.

Figure 2.

Figure 2. Loss of TREM2 reduces the DAM signature of *Grn*⁻/⁻ mice.

A Heatmap of 65 DAM-associated gene transcripts analyzed by NanoString in FCRLS- and CD11b-positive *Grn*⁻/⁻ ($n = 6$), *Trem2*⁻/⁻ ($n = 5$), and *Double*⁻/⁻ ($n = 6$) microglia in comparison to WT ($n = 7$) microglia isolated from 6-month-old male mice. The expression-corrected and housekeeping gene normalized RNA counts for each gene and sample were normalized to the mean value of WT followed by a log2 transformation.

B Volcano plot presentation of the differently expressed transcripts in FCRLS- and CD11b-positive *Grn*⁻/⁻ ($n = 6$) in comparison to WT ($n = 6$) microglia isolated from 6-month-old male mice. A total of 35 of 65 analyzed genes are significantly changed more than 20%, with 22 genes upregulated (purple) and 13 genes downregulated (blue).

C Volcano plot presentation of the differently expressed transcripts in FCRLS- and CD11b-positive *Trem2*⁻/⁻ ($n = 5$) in comparison to WT ($n = 6$) microglia isolated from 6-month-old male mice. A total of 17 of 65 analyzed genes are significantly changed more than 20%, with 7 genes upregulated (purple) and 10 genes downregulated (blue).

D Volcano plot presentation of the differently expressed transcripts in FCRLS- and CD11b-positive *Double*⁻/⁻ ($n = 6$) in comparison to WT ($n = 6$) microglia isolated from 6-month-old male mice. A total of 21 of 65 analyzed genes are significantly changed more than 20%, with 14 genes upregulated (purple) and 7 genes downregulated (blue).

E Expression profiles of selected DAM genes, whose mRNA levels are rescued in *Double*⁻/⁻ ($n = 6$) versus *Grn*⁻/⁻ ($n = 6$) microglia. mRNA expression normalized to the mean of the WT cohort. Data represent mean ± SEM.

Data information: For statistical analysis in B–D, the unpaired, two-tailed student's *t*-test was performed, and in E, one-way ANOVA with Dunnett's *post hoc* test was used to compare *Grn*⁻/⁻, *Trem2*⁻/⁻, and *Double*⁻/⁻ microglia. Statistical significance was set at **$P < 0.01$; ***$P < 0.001$; ****$P < 0.0001$.

Source data are available online for this figure.

Ab2 in cell binding) and high affinity to human TREM2 ECD protein binding via surface plasmon resonance (0.21 nM Ab1 and 4.5 nM Ab2) (Fig EV1C–G). Ligand blocking activity was further validated in human monocyte-derived macrophages, which were treated in a dose–response format with antibodies in the presence of PS-containing liposomes to determine the potency of Ab1 and Ab2 to block liposome-induced TREM2-mediated p-Syk signaling (Figs 3B and EV1C).

Next, we tested if antagonistic TREM2 antibodies are capable of reducing TREM2 signaling in *GRN*-FTLD patient-derived macrophages. To do so, we identified four patients with low PGRN plasma levels (Fig 3C) and confirmed heterozygous *GRN* loss-of-function mutation (Fig EV2A and B). We then generated monocyte-derived macrophages from peripheral blood samples of these patients and healthy volunteers. Western blot analysis revealed that macrophages of *GRN* mutation carriers show significantly enhanced levels of mature TREM2 as compared to healthy controls (Fig 3D and E). Although *GRN* mutation carriers express more mature TREM2 than healthy controls, sTREM2 in the conditioned media was not significantly altered (Fig 3D and F). Since evidence exists that shedding of TREM2 terminates cell autonomous signaling in myeloid cells (Kleinberger *et al*, 2014; Schlepckow *et al*, 2017, 2020; Thornton *et al*, 2017), these findings suggest that macrophages from *GRN*-FTLD patients exhibit increased TREM2 signaling, which occurs in conjunction with the microglial hyperactivation phenotype observed *in vitro* and *in vivo* (Gotzl *et al*, 2019).

Macrophages from *GRN*-FTLD patients and healthy controls were then treated with Ab1 and Ab2 for 24 h. TREM2 levels in cell lysates revealed that both antibodies reduced mature TREM2, whereas an isotype control antibody had no effect (Figs 3G and H, and EV2C). The reduction in mature membrane-bound TREM2 was accompanied by an increase in sTREM2 in conditioned media (Fig 3G and I). Thus, in line with the data shown in Figs 3A and B, and EV1A–G, both antibodies reduce signaling-competent mature TREM2 and increase TREM2 shedding. To further demonstrate that TREM2 signaling can be modulated by TREM2 antagonistic antibodies in patient-derived macrophages, we quantified Syk signaling. This demonstrated that both antagonistic antibodies reduce p-Syk in liposome-stimulated macrophages, suggesting that antagonistic TREM2 antibodies may be capable of modulating TREM2 hypersignaling in microglia in a beneficial manner (Fig 3J).

Antagonistic TREM2 antibodies reduce hyperactivation of PGRN-deficient human microglia

To corroborate and extend our findings in human myeloid cells, we aimed to test modulation of TREM2 via the antagonistic antibodies in human-induced pluripotent stem cell (iPSC)-derived microglia (hiMGL). For this purpose, we generated *GRN* KO iPSC by targeting exon 2 using our established CRISPR genome-editing pipeline (Weisheit *et al*, 2020; see methods for details). We deeply phenotyped *GRN* KO iPSC to confirm loss of PGRN protein expression, maintenance of pluripotency, clonality, as well as absence of unintended on- and off-target effects and chromosomal abnormalities (Weisheit *et al*, 2021) (Figs 4A and EV3A–G; Appendix Fig S1). As expected, *GRN* KO hiMGL increased expression of TREM2 (Fig 4B and C) and showed consequently elevated levels of sTREM2 (Fig 4D). PGRN-deficient hiMGL were treated with the antagonistic TREM2 antibodies as described above. Consistent with the antibody mechanism of action, antagonistic antibodies increased secretion of sTREM2 (Fig 4E). In line with this finding, both antagonistic antibodies reduced p-Syk signaling (Fig 4F). Moreover, both antibodies not only reduced the phagocytic activity of WT hiMGL (Fig 4G), but also ameliorated the pathologically increased phagocytic activity of PGRN-deficient hiMGL (Fig 4H), indicating that they dampen the activation state of PGRN-deficient hiMGL. To further extend these findings, we asked if the antagonistic antibodies could also correct the transcriptional signature of hyperactivated hiMGL. Therefore, we used a customized nCounter panel (NanoString Technologies) analyzing gene expression of 82 microglia-related genes and 8 housekeeping genes of WT and PGRN-deficient hiMGL treated with the two antagonistic antibodies or isotype control (Fig 5A). Gene expression levels in each sample were normalized against the geometric mean of five housekeeping genes including *CLTC*, *HPRT1*, *RPL13A*, *TBP* and *PPIA*. DAM genes, such as *APOE*, *SPP1*, *GPNMB*, *CSF1*, *LGALS3*, *CCL3*, *LPL*, *TREM2*, *ITGAX* and *CD68*, were all significantly upregulated in PGRN-deficient hiMGL compared to WT hiMGL (Fig 5A and B). In addition, expression of genes associated with lysosomal dysfunction was also significantly upregulated (*CTSD*, *NPC2*, and *CD68*). Both antagonistic TREM2 antibodies significantly modulated the mRNA signature of PGRN-deficient hiMGL toward a

more homeostatic state (Fig 5A–D). Upregulation of TREM2 in PGRN-deficient hiMGL was completely corrected by treating the cells with either antagonist antibody (Fig 5E). Upregulation of DAM genes was completely (*GPNMB*, *LGALS3*, *SPP1*, *CSF1*, *CCL3*, *LPL*, and *ITGAX*) or at least partially (*APOE* and *CCL2*) rescued, while downregulation of the homeostatic marker *P2RY12* was reversed by antibody treatment (Fig 5E). Thus, TREM2 modulation with antagonistic antibodies ameliorates hyperactivation of microglia.

Reduced TREM2 signaling does not rescue lysosomal dysfunction

Next, we searched for a rescue of lysosomal phenotypes in PGRN-deficient hiMGL. In contrast to the profound rescue of the homeostatic and disease-associated mRNA signatures upon treatment with the two antagonistic antibodies (Fig 5A–E), we did not observe a significant rescue of increased gene expression patterns associated with lysosomal dysfunction upon PGRN deficiency, like *CTSD*, *NPC2*, and *CD68* mRNA expression (Fig 5A–D and F). Antagonistic
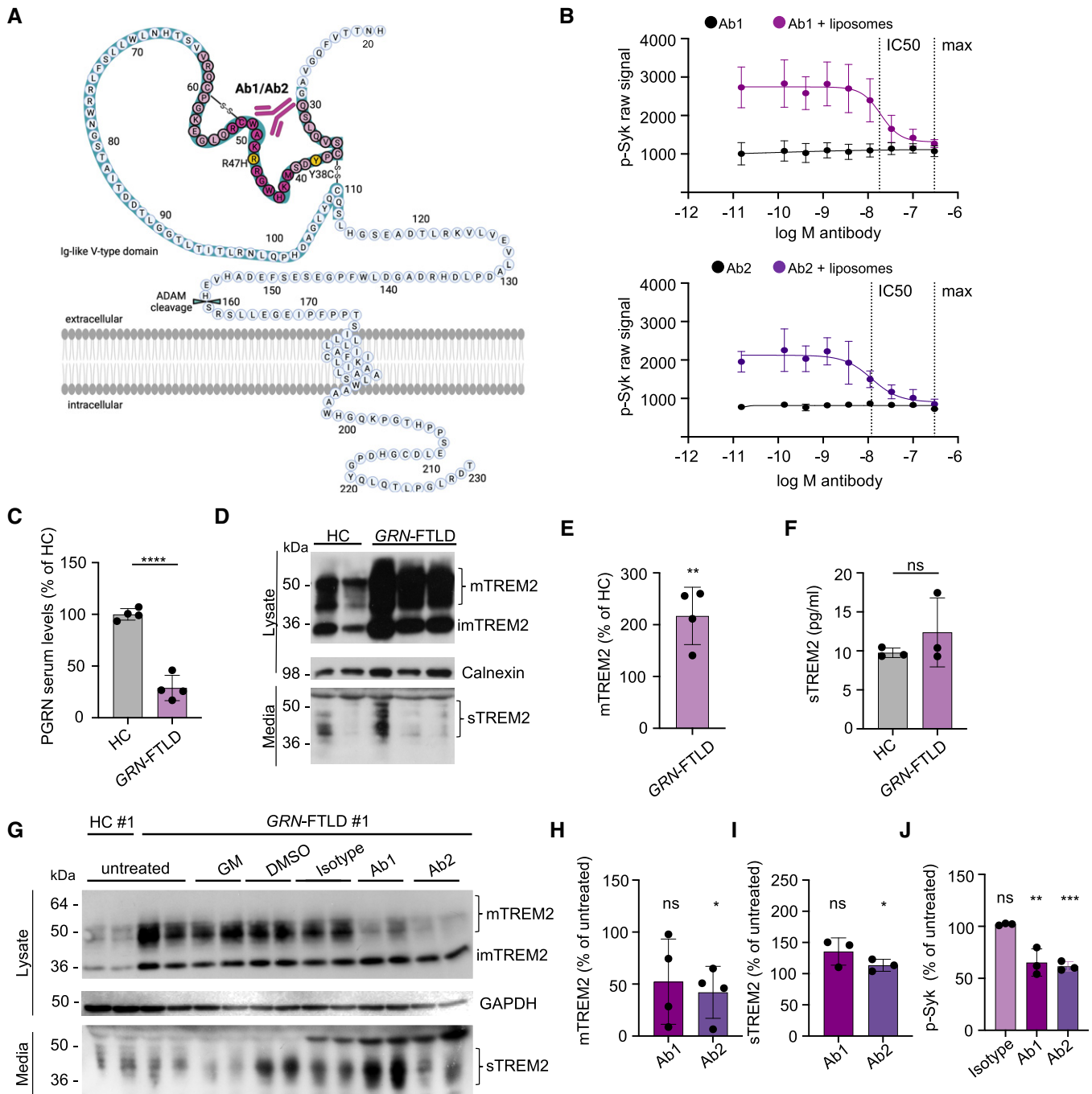

Figure 3.

Figure 3. Human antagonistic TREM2 antibodies rescue elevated membrane-bound TREM2 levels and reduce p-Syk in primary human macrophages isolated from PGRN mutation carriers.

A   Schematic presentation of human TREM2 with the identified binding site of antagonistic antibodies Ab1 and Ab2 (purple) in the Ig-like V-type domain. Light purple indicates the overlapping amino acid sequence of the two peptides, which are bound by Ab1 and Ab2 (see also EV1B). The disease-associated Y38C and R47H mutations are indicated in yellow. Created with BioRender.com.

B   AlphaLISA-mediated quantification of p-Syk in human macrophages with a dose titration treatment of Ab1 and Ab2 with or without liposomes for 5 min. IC50 and maximal inhibition (max) are indicated by a dotted line. Data represent the mean ± SEM (n = 3 independent experiments).

C   ELISA-mediated quantification confirms reduced PGRN serum levels in *GRN* mutation carriers versus healthy controls. PGRN was measured by ELISA in technical triplicates and normalized to serum levels of healthy controls. Data points indicate individual patients (*GRN*-FTLD) and healthy controls (HC).

D   Western blot of TREM2 in lysates and conditioned media of cultured human macrophages isolated from *GRN*-FTLD patients and HC. Mature (mTREM2), immature (imTREM2), and soluble TREM2 (sTREM2) are indicated. Calnexin was used as loading control.

E   Quantification of mTREM2 expression levels in lysates of cultured human macrophages isolated from *GRN*-FTLD patients (data shown in D). mTREM2 levels were normalized to HC (n = 4). Data points indicate individual patients.

F   ELISA-mediated quantification of sTREM2 in conditioned media of human macrophages isolated from *GRN*-FTLD patients and HC (n = 3). sTREM2 could not be measured in conditioned media of human macrophages isolated from patient #3 due to low overall cell yield. Data points indicate individual patients and HC.

G   Western blot of TREM2 in lysates and media of cultured human macrophages isolated from *GRN*-FTLD #1 and HC #1 upon treatment with Ab1 and Ab2. An isotype antibody was used as a negative control. ADAM protease inhibition (GM) does not further increase mTREM2 levels in *GRN*-FTLD patients. Equal amounts of protein were loaded. GAPDH was used as loading control.

H   Quantification of mTREM2 expression normalized to HC (n = 4) (data shown in G). Data points indicate individual patients.

I   ELISA-mediated quantification of sTREM2 in conditioned media of human macrophages isolated from *GRN*-FTLD patients (n = 3). sTREM2 could not be measured in conditioned media of human macrophages isolated from patient #3 due to low overall cell yield. Data points indicate individual patients.

J   AlphaLISA-mediated quantification of p-Syk levels in human macrophages upon treatment with Ab1 and Ab2 with liposomes for 60 min (n = 3). An isotype antibody was used as a negative control. Data points indicate individual patients. Isolated material from patient #3 did not yield enough cells to perform this experiment.

Data information: Data represent mean ± SEM. For statistical analysis of patient samples in comparison to HC, the unpaired, two-tailed student's t-test was performed. Statistical significance was set at *P < 0.05; **P < 0.01; ***P < 0.001; ****P < 0.0001; ns, not significant

Source data are available online for this figure.

antibodies also failed to rescue elevated cathepsin D (CatD) activity in PGRN-deficient hiMGL (Fig 5G).

In total brain lysates of 14-month-old *Grn* KO and *Double* KO mice, CatD single chain (sc) and heavy chain (hc) were both increased without a reduction in *Double* KO mice (Fig 6A–C). Furthermore, the catalytic activity of CatD, which was increased in *Grn* KO mice in an age-dependent manner (Fig 6D and E), was also not rescued by the additional loss of TREM2 (Fig 6E), suggesting that lysosomal dysfunction of *Grn* KO mice cannot be rescued by TREM2 modulation. To further support this, we investigated *Double* KO brains for the accumulation of lipofuscin, an autofluorescent lipopigment, found in *Grn* KO and several lysosomal storage disorders (Gotzl et al, 2014). In line with the failure of the *Double* KO to rescue lysosomal hyperactivity, lipofuscin accumulation was not reduced upon loss of TREM2 in *Grn* KO mice, although remarkably almost no lipofuscin was observed in single *Trem2* KO mice via mechanisms that have yet to be investigated (Fig 6F and G).

Loss of TREM2 does not rescue lysosomal lipid dyshomeostasis in *Grn* KO mice

Previous studies have examined the impact of either *Trem2* or *Grn* deletion on the lipidome of mouse brain. In the case of *Trem2*, no significant lipid changes were observed in *Trem2* KO mouse brain at baseline, although upon cuprizone challenge, a striking accumulation of cholesterol esters and various sphingolipids was revealed (Nugent et al, 2020). In *Grn* KO mice, lipid metabolism is altered (Evers et al, 2017; Marschallinger et al, 2020) and a recent study described an age-independent deficit in levels of the lysosomal lipid bis(monoacylglycerol)phosphate (BMP) that was accompanied by an age-dependent accumulation of the GCase substrate glucosylsphingosine (GlcSph) (Logan et al, 2021). To determine whether

deletion of *Trem2* on the *Grn* KO background has any effect on the composition of the brain lipidome, we performed targeted lipidomic analysis using LCMS on 6-month-old WT, *Grn* KO, *Trem2* KO, and *Double* KO mouse brain homogenates (Fig 7). As previously described (Nugent et al, 2020), the *Trem2* KO showed no significant differences in brain lipid content relative to WT mice (Fig 7B), while the *Grn* KO as well as the *Double* KO showed a significant decrease in several BMP species as well as an increase in GlcSph (Fig 7A, C and E–G), which is consistent with previous data (Logan et al, 2021). Consistent with previous findings (Jian et al, 2016; Arrant et al, 2019; Zhou et al, 2019; Logan et al, 2021) and the increased accumulation of the GCase substrate GlcSph, we found a significant decrease in the GCase activity in *Grn* KO mice and *Double* KO (Fig 7H). Importantly, genetic interaction analysis demonstrated no statistically significant difference in the levels of any analyte in the *Double* KO brain compared to the *Grn* KO alone (Fig 7D). Thus, ablation of TREM2 fails to correct abnormal lysosomal function and lipid metabolism in PGRN-deficient mice.

Enhanced brain pathology in *Double* KO mice suggests a neuroprotective function of hyperactivated microglia

Aged *Grn* KO mice show enhanced synaptic pruning (Lui et al, 2016; Zhang et al, 2020). To investigate if abolishing TREM2 signaling mitigates a neurodegenerative phenotype in 14-month-old *Grn* KO mice, we analyzed the thalamic synaptic density using synaptophysin (SPH) and the vesicular GABA transporter (VGAT) as a marker for presynaptic density (Fig 8A–C). Interestingly, immunohistochemical staining of the thalamic region revealed a reduction in SPH in *Trem2* KO, which was even more robust in *Double* KO mice (Fig 8A and B). Western blot analysis confirmed reduced total SPH levels in *Trem2* KO (Jadhav et al, 2020) and *Double* KO mice (Fig 8D and E). Similarly, immunostainings against VGAT revealed

a further reduction in *Double* KO mice compared to WT, *Grn* KO, and *Trem2* KO (Fig 8A and C).

To obtain additional information on the activation status of *Double* KO microglia, we determined microglial morphology. We extracted morphological features in WT, *Grn* KO, *Trem2* KO, and *Double* KO animals after 3D reconstruction of IBA1+ microglia from confocal *z*-stack images (Fig 8F and G). Microglial cells from *Grn* KO and *Double* KO animals showed a significantly decreased score for "branch volume," "number of branch nodes," and less pronounced for "branch length," as well as a significantly increased score for "sphericity," which is associated with an increased activation state of microglia (Heindl *et al*, 2018). In contrast, the morphological scores for *Trem2* KO animals were comparable to WT. Thus,

although the transcriptional signature of hyperactivated PGRN-deficient microglia is partially rescued by the loss of TREM2, the morphological and immunohistochemical analysis indicates that *Double* KO microglia neither rescue *Grn* KO microglial morphology nor synapse loss.

To further test if reduction in microglial hyperactivation fails to ameliorate secondary neurodegeneration, we analyzed the concentrations of NfL, a fluid biomarker for neuronal damage (Meeter *et al*, 2016; Rohrer *et al*, 2016; Preische *et al*, 2019), in the CSF of 6-month-old (Fig 9A) and 14-month-old mice (Fig 9B). In line with previous findings (Zhang *et al*, 2020), NfL was increased in PGRN-deficient mice, whereas no change was observed in *Trem2* KO animals as compared to WT mice (Fig 9A and B). Surprisingly, we
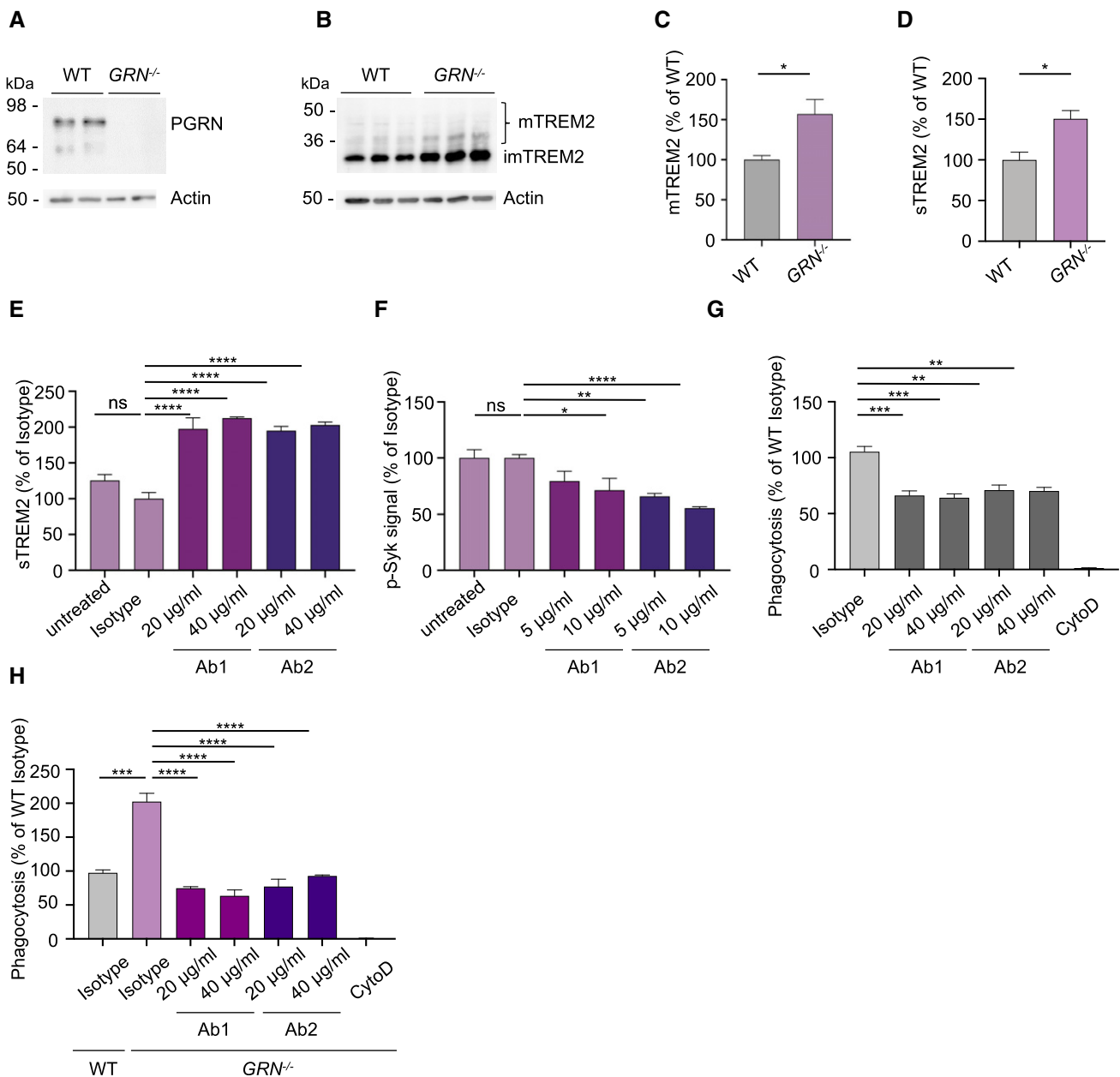

Figure 4.

Figure 4. Antagonistic TREM2 antibodies enhance TREM2 shedding and reduce TREM2-dependent signaling and phagocytosis in PGRN-deficient iPSC-derived human microglia (hiMGL).

A Western blot of PGRN in whole-cell lysates of WT and $GRN^{-/-}$ hiMGL. Actin was used as loading control.
B Western blot of TREM2 in whole-cell lysates of WT and $GRN^{-/-}$ hiMGL. Mature (mTREM) and immature TREM2 (imTREM2) are indicated. Actin was used as loading control.
C Quantification of mTREM2 expression in whole-cell lysates of WT and $GRN^{-/-}$ hiMGL (data shown in B). mTREM2 levels were normalized to WT ($n = 3$, biological replicates).
D ELISA-mediated quantification of sTREM2 in conditioned media of WT and $GRN^{-/-}$ hiMGL ($n = 3$, biological replicates).
E ELISA-mediated quantification of sTREM2 in conditioned media of $GRN^{-/-}$ hiMGL upon treatment with Ab1 and Ab2 (20 µg/ml, 40 µg/ml) ($n = 3$, biological replicates). An isotype antibody (10 µg/ml) was used as a negative control.
F AlphaLISA-mediated quantification of p-Syk levels in $GRN^{-/-}$ hiMGL upon treatment with Ab1 and Ab2 (5 µg/ml, 10 µg/ml) with liposomes (1 mg/ml) for 5 min. ($n = 8$, biological replicates).
G Uptake assay for fluorescent myelin in WT hiMGL. Phagocytosis of myelin significantly decreased upon treatment with TREM2 antagonistic antibodies Ab1 and Ab2 ($n = 4$, biological replicates).
H Uptake assay for fluorescent myelin. $GRN^{-/-}$ hiMGL phagocytose significantly more myelin as compare to WT hiMGL. This is reversed upon treatment with TREM2 antagonistic antibodies Ab1 and Ab2 ($n = 4$, biological replicates).

Data information: Data represent mean ± SEM. For statistical analysis in C and D, the unpaired, two-tailed student's t-test was performed, in E and F, one-way ANOVA with Dunnett's *post hoc* test, and in G and H, one-way ANOVA with Tukey's *post hoc* was used to compare untreated, Ab1, and Ab2 (20 µg/ml and 40µg/ml) conditions to the isotype-treated condition. Statistical significance was set at *$P < 0.05$; **$P < 0.01$; ***$P < 0.001$; ****$P < 0.0001$; and ns, not significant.
Source data are available online for this figure.

found a striking increase in NfL in the 14-month-old *Double* KO mice (Fig 9B), suggesting a protective role of TREM2-dependent microglial hyperactivation in PGRN-deficient mice. To further elucidate which genes and pathological pathways may be affected by eliminating TREM2 in *Grn* KO mice, we isolated mRNA from total brain of all three mouse models after 6 and 14 months of age and searched for changes in mRNA expression using the nCounter Neuropathology panel (NanoString Technologies) (Werner *et al*, 2020). The Neuropathology panel with 770 genes included was specifically designed to analyze neurodegenerative phenotypes in mouse models and allows investigating six fundamental themes of neurodegeneration, namely neurotransmission, neuron–glia interaction, neuroplasticity, cell structure integrity, neuroinflammation, and metabolism. Analysis of total brain mRNA confirmed rescue of the age-dependent *Grn* KO-associated DAM signature in the *Double* KO mice (Fig EV4A–G, Appendix Fig S2A and B) and revealed no significant upregulation of genes associated with neuroinflammation like *Gfap*, *Tnf*, or *Tnfrsf11b* or genes associated with synaptic pruning, such as the complement factors (*C1qc*, *C1qa*, and *C1qb*) compared to WT mice (Fig EV4G). Although differences in the transcriptomic signature of male and female microglia were overserved, as described earlier (Villa *et al*, 2018), rescue of gene expression associated with neuroinflammation and synaptic pruning was evident in both sexes (Fig EV4G, Appendix Fig S3). Pathway analysis in *Grn* KO mice revealed the highest increases in "autophagy," "activated microglia," "angiogenesis," and "disease association" associated clusters with further increase during aging (Fig 9C). These four pathways score very low in *Trem2* KO mice, again confirming opposite effects of the two single-gene deletions. In the 6-month-old and in the 14-month-old cohort, all four pathways score is lower in the *Double* KO than in the single *Grn* KO. Three of these pathways, namely "activated microglia," "angiogenesis," and "disease association," are even downregulated in the 6-month-old *Double* KO cohort compared to WT. However, other pathways like "neuronal cytoskeleton," "tissue integrity," and "transmitter synthesis and storage" and "transmitter response and uptake," are most heavily affected in the 6-month-old *Double* KO, which is consistent with enhanced neuropathological phenotypes.

When looking into individual genes, we found that strikingly, compared to single *Grn* KO and WT mice, only two genes were significantly altered and in fact downregulated more than 20% in the 6-month-old *Double* KO. These include the transcription factor *Npas4* (Neuronal PAS domain protein 4), which regulates activation of genes involved in the excitatory–inhibitory balance and is known to exert neuroprotective activities (Spiegel *et al*, 2014; Fu *et al*, 2020) (Figs 9D and EV4C), and *Grin3b* (Perez-Otano *et al*, 2016), a glutamate receptor subunit (Figs 9D and EV4C). In the 14-month-old cohort *Npas4* expression is not significantly altered in *Double* KO mice compared to WT or *Grn* KO mice, although still reduced in single *Grn* KO mice (Fig 9D). In comparison to single *Grn* KO and WT mice, only four genes were significantly downregulated more than 20% in the *Double* KO mice. Interestingly, three of these, namely *Ninj2*, *Ugt8a*, and *Plnxb3*, are exclusively expressed in oligodendrocytes, suggesting major deficits in myelination in *Double* KO mice (Fig 9E) as recently reported for *Trem2* KO (Wu *et al*, 2021).

Although gene expression analysis of the *Double* KO suggests dampening of the pathological DAM signature, enhanced synaptic loss and increased NfL in CSF of *Double* KO indicate that neurodegeneration of PGRN-deficient mice may not be improved by the additional knockout of TREM2 but instead increased even further. We therefore investigated if the additional loss of TREM2 in PGRN-deficient mice affects deficits in glucose uptake *in vivo*. To determine brain cerebral uptake rates of glucose in *Double* KO *in vivo*, we performed 2-[18F]fluoro-d-glucose PET (FDG-PET). We confirmed a reduced cerebral glucose uptake in *Grn* KO ($P < 0.05$) and *Trem2* KO ($P < 0.0001$) mice compared to WT (Figs 9E and F, and EV5B), as described in previous studies (Kleinberger *et al*, 2017; Gotzl *et al*, 2019). However, we still observed similar decreased glucose uptake in *Double* KO mice when compared to WT ($P < 0.0001$) (Figs 9E and F, and EV5B), revealing a consistently decreased glucose uptake between *Grn* KO, *Trem2* KO, or *Double* KO mice and WT mice. Together, all our findings indicate that reducing hyperactivation of microglia does not ameliorate lysosomal dysfunction of PGRN-deficient mice but may even promote neurodegeneration.
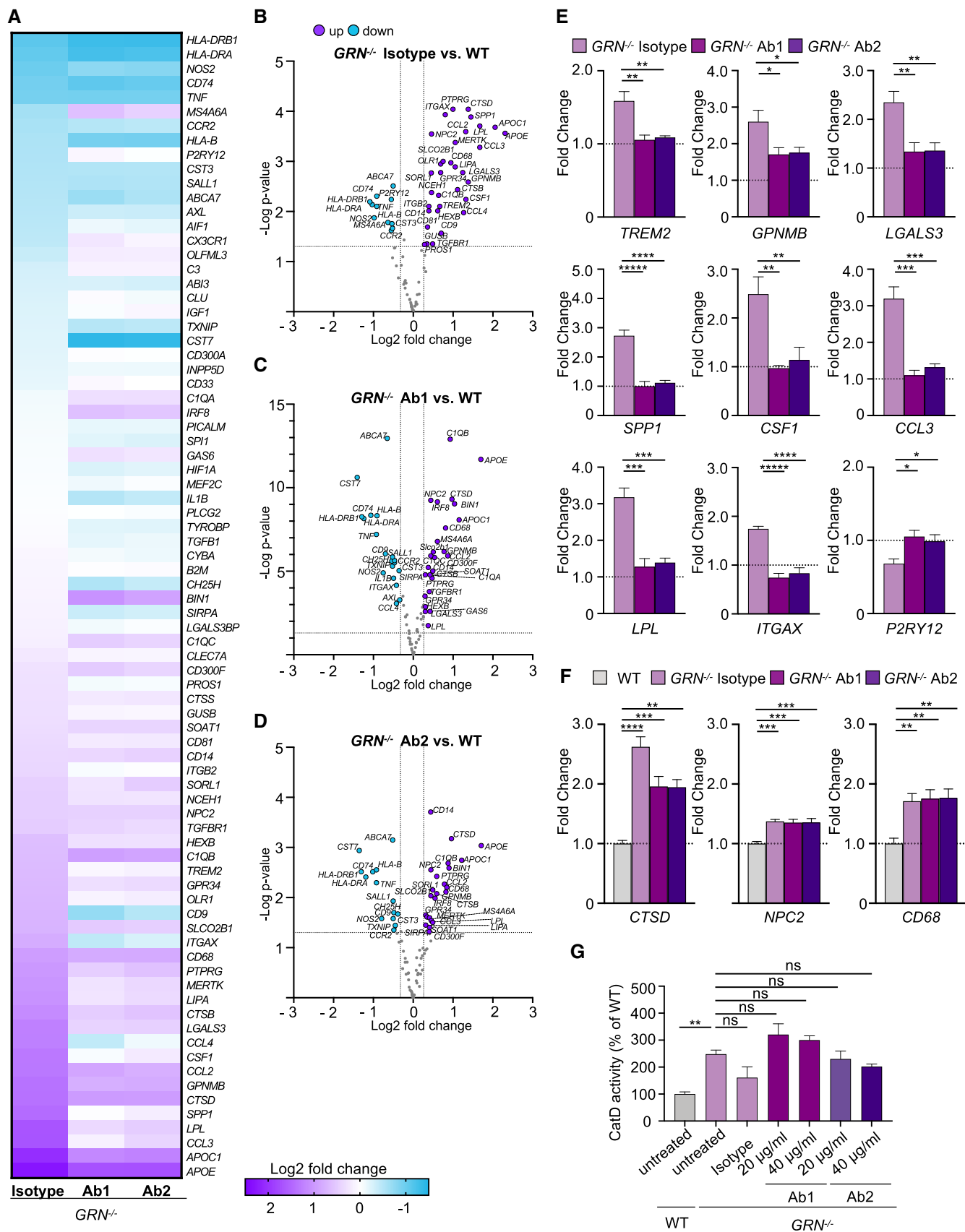
Figure 5.

Figure 5. Antagonistic TREM2 antibodies reduce hyperactivation of PGRN-deficient hiMGL.

A   Expression of all analyzed gene transcripts in $GRN^{-/-}$ hiMGL treated with control isotype antibody, Ab1, or Ab2 in comparison to WT hiMGL. Data show the mean of four individual treatments and NanoString measurements. The mRNA counts for each gene were normalized to the mean value of all WT samples followed by a log2 transformation.

B   Volcano plot presentation of the differently expressed transcripts in $GRN^{-/-}$ hiMGL treated with isotype compared to WT hiMGL. Genes with more than 20% significantly changed expression are marked in purple (upregulated) or blue (downregulated).

C   Volcano plot presentation of the differently expressed transcripts in $GRN^{-/-}$ hiMGL treated with Ab1 comparison to WT hiMGL. Genes with more than 20% significantly changed expression are marked in purple (upregulated) or blue (downregulated).

D   Volcano plot presentation of the differently expressed transcripts in $GRN^{-/-}$ hiMGL treated with Ab2 comparison to WT hiMGL. Genes with more than 20% significantly changed expression are marked in purple (upregulated) or blue (downregulated).

E   Transcript levels of DAM gene transcripts significantly altered in $GRN^{-/-}$ hiMGL, treated with Ab1 or Ab2 in comparison to isotype treatment from the data set in A, and normalized to the mean of the WT hiMGL samples ($n = 4$, biological replicates).

F   Transcript levels of $CTSD$, $NPC2$, and $CD68$ of WT and $GRN^{-/-}$ hiMGL untreated, treated with isotype control, and Ab1 or Ab2 in comparison to WT hiMGL from the data set in A normalized to the mean of the WT hiMGL samples ($n = 4$, biological replicates).

G   Catalytic activity of cathepsin D (CatD) in untreated WT and $GRN^{-/-}$ hiMGL or $GRN^{-/-}$ hiMGL treated with isotype control, Ab1 or Ab2 (20 μg/ml, 40 μg/ml), as measured by a CatD *in vitro* activity assay ($n = 3$, biological replicates).

Data information: Data represent mean ± SEM. For statistical analysis in B–D, the unpaired, two-tailed student's *t*-test was performed, in E, one-way ANOVA with Dunnett's *post hoc* test was used to compare Ab1 and Ab2 (20 μg/ml and 40 μg/ml) conditions to the isotype-treated condition, and in F and G, one-way ANOVA with Dunnett`s *post hoc* test was used to compare Ab1-, Ab2- (20 μg/ml and 40 μg/ml), and isotype-treated condition to WT cells. Statistical significance was set at *$P < 0.05$; **$P < 0.01$; ***$P < 0.001$; ****$P < 0.0001$, *****$P < 0.00001$, and ns, not significant.

Source data are available online for this figure.

Discussion

PGRN and the proteolytically derived granulin peptides may have important lysosomal functions, as exemplified by the identification of homozygous loss-of-function *GRN* mutations, which are causative for NCL (Smith *et al*, 2012). Accumulating evidence suggests that PGRN /granulins directly or indirectly regulate the activity of lysosomal enzymes such as CatD (Beel *et al*, 2017; Valdez *et al*, 2017; Zhou *et al*, 2017; Butler *et al*, 2019a, 2019b; Huang *et al*, 2020), GCase (Jian *et al*, 2016; Arrant *et al*, 2019; Zhou *et al*, 2019), and HexA (Chen *et al*, 2018). The last two enzymes are involved in sphingolipid degradation, a process regulated by the lysosomal phospholipid BMP, which is stabilized by PGRN (Logan *et al*, 2021). PGRN may affect lysosome acidification and thereby lysosomal enzyme activity (Tanaka *et al*, 2017; Logan *et al*, 2021). We and others have shown that PGRN deficiency results in upregulation of several lysosomal enzymes (Gotzl *et al*, 2014, 2018; Klein *et al*, 2017; Huang *et al*, 2020; Root *et al*, 2021). However, it remained unclear if microglial hyperactivation observed in PGRN-deficient microglia contributes to or is a consequence of lysosomal dysfunction. Activated microglia are found in late stages of many neurodegenerative diseases including AD and FTLD, and are believed to be deleterious by promoting synaptic pruning and neuronal cell death (Heneka *et al*, 2013; Hong *et al*, 2016a, 2016b). Specifically, FTLD patients suffering from *GRN* haploinsufficiency show pathological hyperactivation of microglia as measured by TSPO-PET (Martens *et al*, 2012; Gotzl *et al*, 2019; Marschallinger *et al*, 2020; Zhang *et al*, 2020). Similarly, mice lacking PGRN exhibit hyperactivation of microglia as indicated by an enhanced DAM signature including TREM2 and galectin 3, an increased TSPO signal, and increased phagocytic and synaptic pruning activity (Lui *et al*, 2016; Gotzl *et al*, 2019; Zhang *et al*, 2020). We therefore asked if the pathological outcome of PGRN deficiency may be promoted by TREM2-dependent microglial overaction. To address this question, we sought to reduce TREM2-dependent signaling by two independent strategies: genetic loss-of-function and pharmacological inhibition with antagonist antibodies. To achieve the former, we crossed

Trem2 KO mice to the *Grn* KO to generate a *Double* KO model. For the latter approach, we identified TREM2 antagonistic antibodies, which negatively regulate TREM2 by increasing surface receptor shedding and preventing lipid ligand-induced signaling of the co-receptor DAP12. Both approaches successfully dampened several aspects of TREM2-dependent microglial activation. However, although reduction in TREM2 signaling by two independent approaches rescued microglial hyperactivation to some extent, this was not sufficient to ameliorate lysosomal deficits, dysregulation of lysosomal lipids, synapse loss/neurodegeneration, and reduced glucose uptake. These findings demonstrate in this model that microglial hyperactivation is secondary to the primary loss of lysosomal function caused by PGRN deficiency. Surprisingly, inhibition of TREM2 function results in elevated markers for neurodegeneration and synapse loss in *Double* KO animals. Our extensive gene expression analyses do not suggest that the total loss of TREM2 function in *Grn* KO mice causes additional neurotoxicity, for example, by supporting pro-inflammatory microglial responses. Instead, the fact that the additional loss of TREM2 leads to increased brain pathology indicates that TREM2-regulated microglial activation states may not necessarily be deleterious but protective. We suggest that hyperactivated microglia, for example, in *Grn* KO mice, resemble the previously described DAM2 microglia or may develop into them by even further increasing their DAM signature (Keren-Shaul *et al*, 2017). Consistently, fully activated DAM2 microglia were recently described to be particularly protective in a mouse model for amyloidosis and tau pathology (Lee *et al*, 2021). This is very surprising since chronically activated microglia, as observed in PGRN loss-of-function models and mouse models for amyloid and tau pathology, would have been expected to exert significant damage within the brain, for example, by induction of the inflammasome (Heneka *et al*, 2018). However, our findings together with those by Lee *et al* (2021) rather suggest that TREM2-dependent chronic activation is protective, which may have implications for therapeutic attempts employing modulation of TREM2 activity by agonistic antibodies (Deczkowska *et al*, 2020; Lewcock *et al*, 2020). In that regard, the nomenclature used for describing diverse microglial states, namely
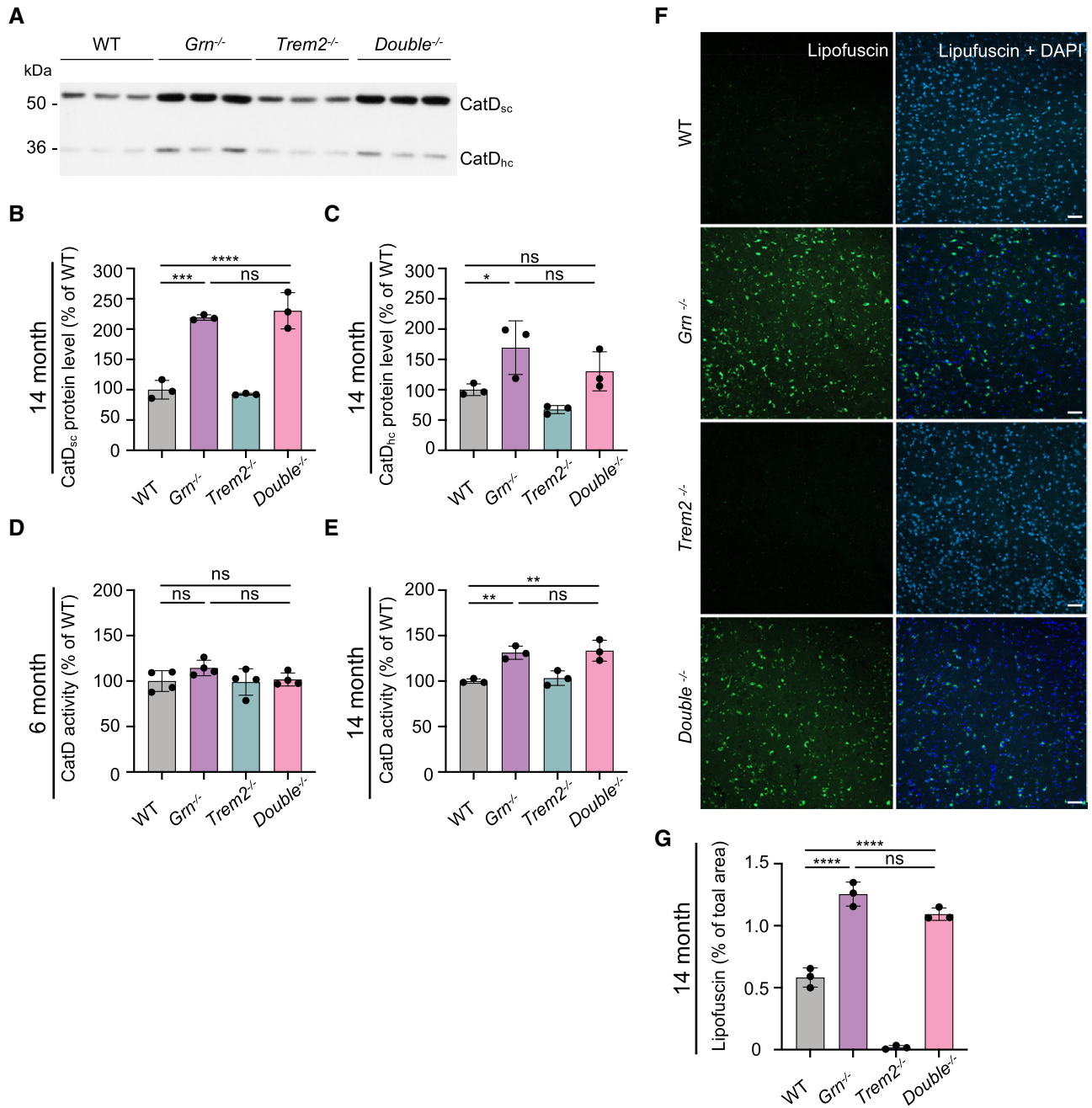
Figure 6. Abolishing TREM2 signaling does not rescue lysosomal dysfunction in *Grn⁻/⁻* mice.

A   Western blot of CatD in total brain lysates from 14-month-old female WT, *Grn⁻/⁻*, *Trem2⁻/⁻*, and *Double⁻/⁻* mice. CatD maturation variants are indicated (sc: single chain; hc: heavy chain; *n* = 3).

B, C   Quantification of CatD variants in A normalized to WT (*n* = 3 per genotype).

D, E   Catalytic activity of CatD in brain lysates from female 6-month-old (*n* = 4 per genotype) (D) or 14-month-old (*n* = 3 per genotype) (E) *Grn⁻/⁻*, *Trem2⁻/⁻*, and *Double⁻/⁻* mice normalized to WT.

F   Immunohistochemical analysis of lipofuscin (green) in coronal brain sections. Representative images of thalamus are shown. Scalebars = 50 μm.

G   Quantification of lipofuscin autofluorescence. Five images per mouse were taken, and means were normalized to WT samples (*n* = 3 per genotype, female).

Data information: Data represent mean ± SEM. For statistical analysis, one-way ANOVA with Tukey's *post hoc* test of *Grn⁻/⁻*, *Trem2⁻/⁻*, and *Double⁻/⁻* was used. Statistical significance was set at *$P < 0.05$; **$P < 0.01$; ***$P < 0.001$; ****$P < 0.0001$, and ns, not significant.

Source data are available online for this figure.
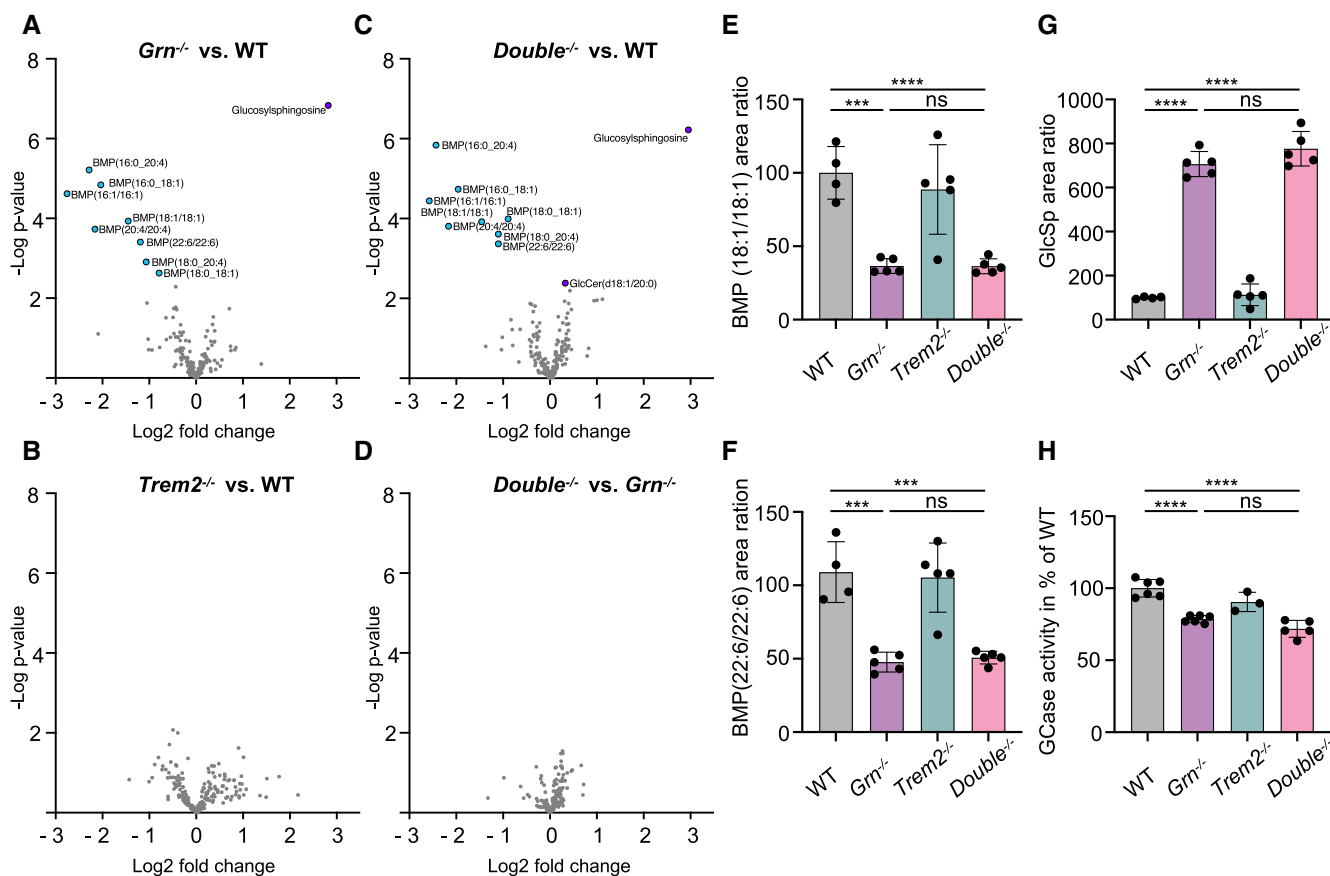
Figure 7. Reduced TREM2 signaling does not rescue dysregulated lipids in *Grn*$^{-/-}$ mice.

A–D Volcano plot presentation of lipids and metabolites upregulated (purple) or downregulated (blue) in total brain homogenates from 6-month-old male *Grn*$^{-/-}$ (A, $n = 5$), *Trem2*$^{-/-}$ (B, $n = 5$), and *Double*$^{-/-}$ (C, $n = 5$) mice in comparison to WT ($n = 4$), and *Double*$^{-/-}$ in comparison to *Grn*$^{-/-}$ mice (D). Counts for each sample were normalized to the mean value of WT followed by a log2 transformation ($n = 4$–5 per genotype). Analyte values were adjusted with an FDR < 10% to exclude type I errors in null hypothesis testing.

E–G Abundance of BMP species and glucosylsphingosine (GlcSph) in total brain of 6-month-old *Grn*$^{-/-}$, *Trem2*$^{-/-}$, *Double*$^{-/-}$, and WT mice ($n = 4$–5 per genotype).

H Glucocerebrosidase (GCase) activity in whole-brain lysates from 6-month-old male *Grn*$^{-/-}$, *Trem2*$^{-/-}$, *Double*$^{-/-}$, and WT mice. The linear increase in fluorescence signal was measured and then normalized to WT mice ($n = 3$–6 per genotype).

Data information: Data represent mean ± SEM. For statistical analysis, one-way ANOVA with Tukey's *post hoc* test of *Grn*$^{-/-}$, *Trem2*$^{-/-}$, and *Double*$^{-/-}$ was used. Statistical significance was set at ***$P < 0.001$; ****$P < 0.0001$, and ns, not significant.
Source data are available online for this figure.

Figure 8. Loss of TREM2 does not prevent synapse loss and activated microglia morphology.

A Immunohistochemical analysis of synaptophysin (SPH, pink) and VGAT (yellow) in coronal brain sections. Representative images of thalamus are shown. Scalebars = 50 μm.

B Quantification of SPH-positive area. Three images per mouse were taken, and means were normalized to WT samples ($n = 3$ per genotype, female).

C Quantification of VGAT-positive area. Three images per mouse were taken, and means were normalized to WT samples ($n = 3$ per genotype, female).

D Western blot of SPH in RIPA lysates from 14-month-old female WT, *Grn*$^{-/-}$, *Trem2*$^{-/-}$, *and Double*$^{-/-}$ mice. Actin was used as loading control.

E Quantification of SPH protein levels in D normalized to WT ($n = 3$).

F Morphological analysis of cortical microglia. Representative maximum-intensity projections of confocal *z*-stack images showing IBA1$^+$ microglial cells of female WT, *Grn*$^{-/-}$, *Trem2*$^{-/-}$, and *Double*$^{-/-}$ mice (scalebar = 50 μm). Arrows point to individual microglia, which are shown as three-dimensional reconstruction, scalebar = 10 μm.

G Morphological differences in cortical microglia from WT, *Grn*$^{-/-}$, *Trem2*$^{-/-}$, and *Double*$^{-/-}$ mice shown by branch volume, sphericity score, branch length, and the number of branch nodes. Statistical analysis of group difference for the morphological scores "Branch volume" (auc = 0.72), "Sphericity score" (auc = 0.82), "Branch length" (auc = 0.69), and "Number of branch nodes" (auc = 0.80) was performed using the Wilcoxon rank-sum test with continuity correction and Bonferroni *post hoc* correction for multiple testing in R (version 4.0.3). Two images per mouse ($n = 3$ per genotype, female) were analyzed, each data point represents one microglia cell. Median and interquartile range are displayed.

Data information: Data represent mean ± SEM. For statistical analysis in B-C and E, one-way ANOVA with Tukey's *post hoc* test of *Grn*$^{-/-}$, *Trem2*$^{-/-}$, and *Double*$^{-/-}$ was used. Statistical significance was set at *$P < 0.05$; **$P < 0.01$; ***$P < 0.001$; ****$P < 0.0001$, and ns, not significant.
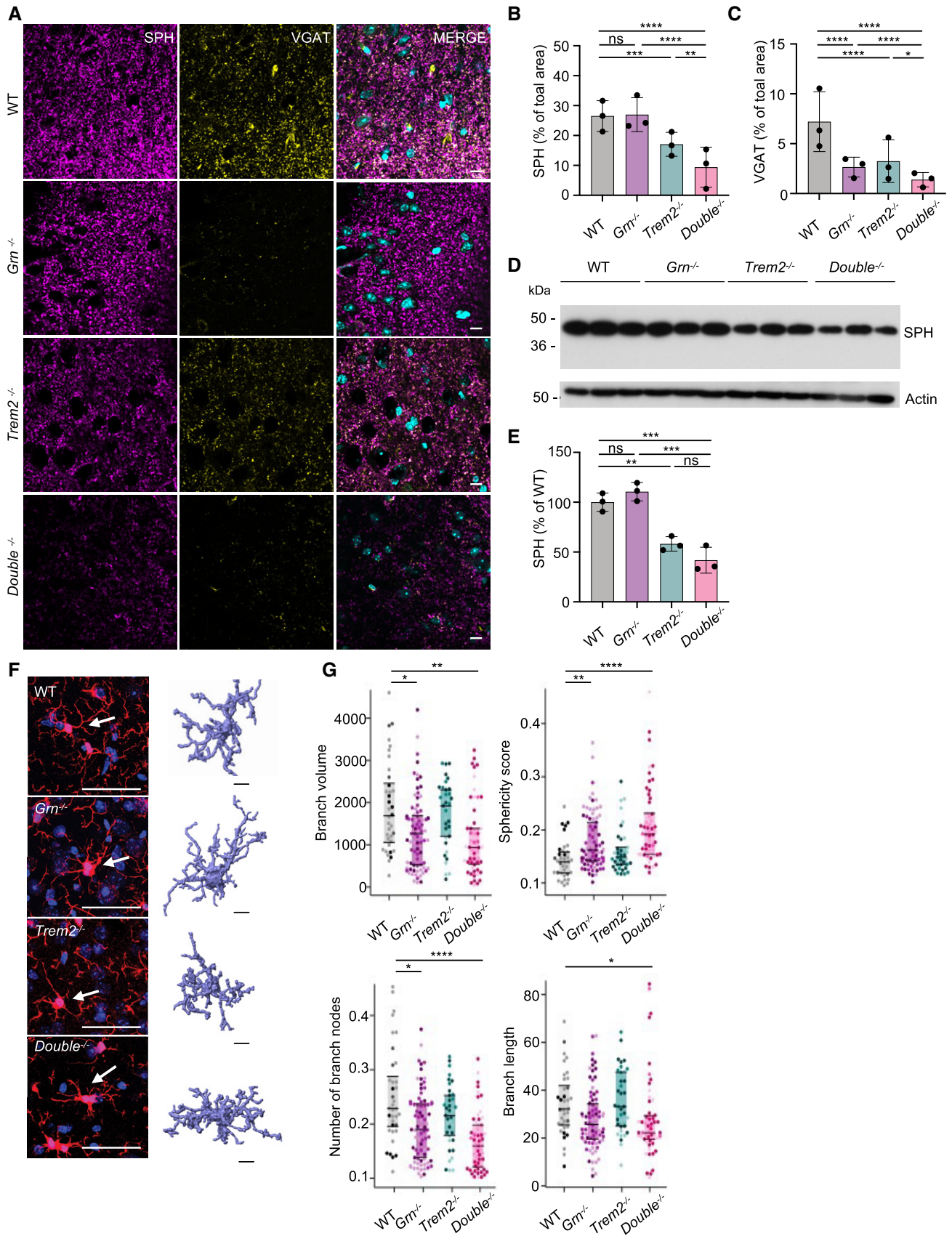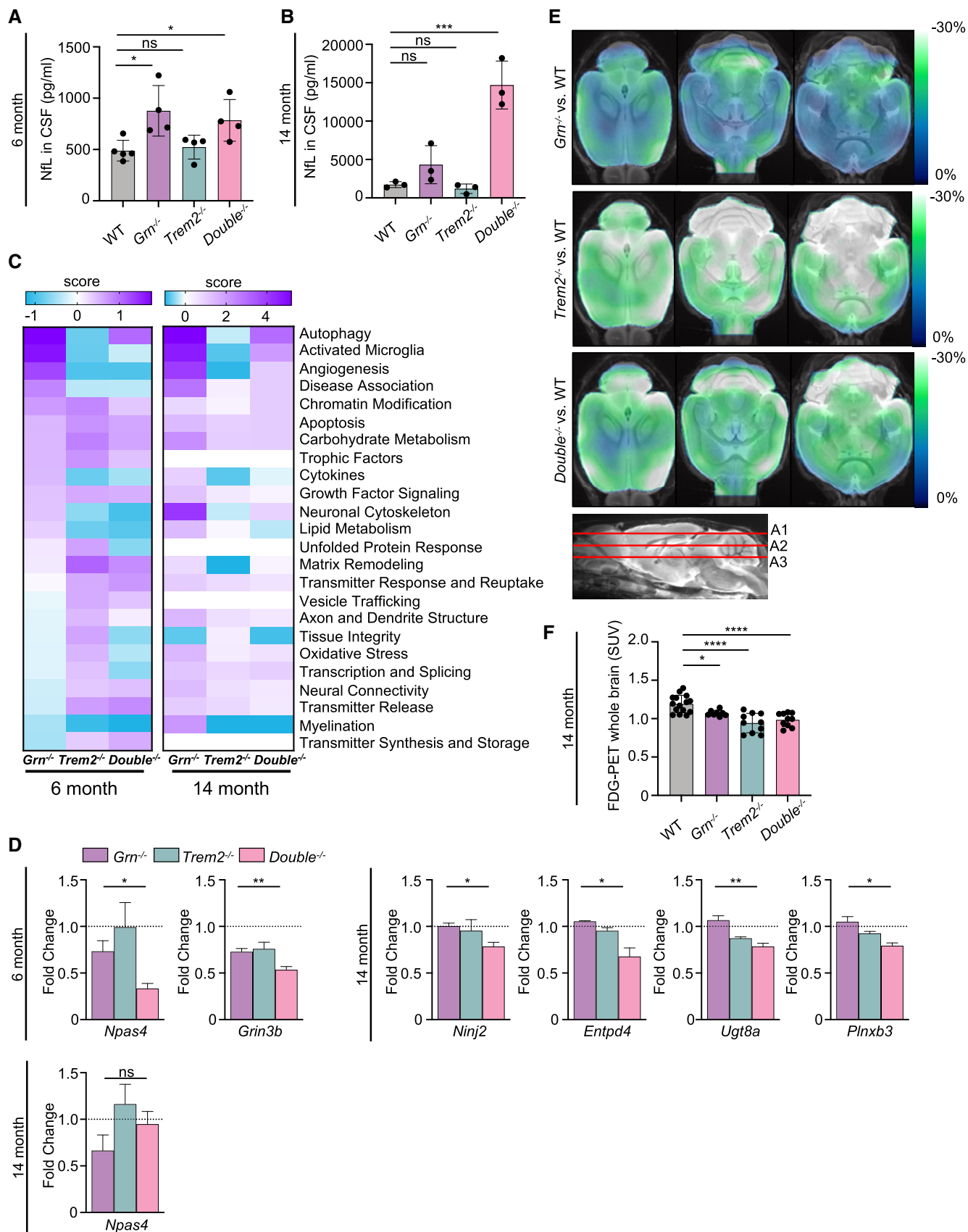Source data are available online for this figure.

Figure 8.

Figure 9.

Figure 9. Hyperactivation of microglia in *Grn*⁻/⁻ mice is not deleterious.

A   Immunoassay-based quantification of neurofilament light-chain (NfL) protein levels in CSF of 6-month-old *Grn*⁻/⁻ (*n* = 4), *Trem2*⁻/⁻ (*n* = 4), *Double*⁻/⁻ (*n* = 4), and WT (*n* = 5) male mice.

B   Immunoassay-based quantification of NfL levels in CSF of 14-month-old *Grn*⁻/⁻, *Trem2*⁻/⁻, *Double*⁻/⁻, and WT female mice (*n* = 3 per genotype).

C   Neuropathology NanoString panel analysis of total brain mRNA expression of 6-month-old and 14-month-old *Grn*⁻/⁻, *Trem2*⁻/⁻, *Double*⁻/⁻, and WT male mice based on NanoString advanced analysis R-script included in the panel (6-month-old mice: *n* = 4, 14-month-old mice: *n* = 3).

D   Transcript levels of all significantly changed genes in *Double*⁻/⁻ versus *Grn*⁻/⁻ brain mRNA of 6-month-old and 14-month-old mice analyzed in C. *Grin3b* were under detection limit in the 14-month-old cohort. Transcript expression is normalized to the mean of the WT cohort.

E   The same cohort of mice scanned for TSPO-PET was additionally scanned for FDG-PET. Axial slices as indicated show %-FDG-PET differences among *Grn*⁻/⁻, *Trem2*⁻/⁻, and *Double*⁻/⁻ (all cold color scales) when compared to WT at the group level. Images were adjusted to an MRI template.

F   Bar graph illustrates individual FDG-PET values derived from a whole-brain volume of interest. Data represent mean ± SD. A total of 8–15 female mice per group at an average age of 10.7 ± 1.5 months (*Grn*⁻/⁻ *n* = 8, *Trem2*⁻/⁻ *n* = 10, *Double*⁻/⁻ *n* = 10, WT *n* = 15) were used.

Data information: Data in A, B, and D represent mean ± SEM. For statistical analysis in A–B, two-way ANOVA with Dunnett's *post hoc* test was used, in D, F, the unpaired, two-tailed student's *t*-test was performed. Statistical significance was set at *$P < 0.05$; **$P < 0.01$; ***$P < 0.001$; ****$P < 0.0001$, and ns, not significant. Source data are available online for this figure.

homeostatic, disease associated, and hyperactivated, may need to be reconsidered. We find these terms misleading, as they indicate that homeostatic microglia are beneficial, whereas disease-associated or -hyperactivated microglia are deleterious. Importantly, the brain environment and pathological context is important for ascribing microglial state and associated functions and requires a deeper understanding beyond transcriptional characterization to elucidate the overall impact to brain function and disease. However, one may describe these fundamentally different states of microglia as "surveilling" versus "responding" microglia to capture activities that occur during normal versus pathological contexts. The term "responding" would implicate that these microglia exert protective effects.

Protective microglial functions are promoted by enhancing TREM2 signaling with agonist TREM2 antibodies (Lewcock *et al*, 2020). All currently described agonistic TREM2 antibodies act via similar mechanisms by inhibiting shedding and directly activating TREM2, and therefore increasing functional receptor on the cell surface (Lewcock *et al*, 2020). Notably, all known agonistic TREM2 antibodies bind to the stalk region close to the cleavage site by ADAM10/17 (Schlepckow *et al*, 2017; Lewcock *et al*, 2020). In contrast, the two antagonistic antibodies described here bind in the IgV-fold between amino acids 30 and 63 (Fig EV1A). Interestingly, this domain of TREM2 harbors a number of AD- and FTLD-associated sequence variants (Colonna & Wang, 2016). The R47H variant increases AD risk and affects TREM2-dependent microglial proliferation, lipid metabolism, and microgliosis. Similarly, the FTLD-associated Y38C variant causes a loss of function by misfolding and retention of TREM2 within the endoplasmic reticulum (Kleinberger *et al*, 2014). Antagonistic antibodies therefore appear to bind at a functionally critical region and may displace natural ligands (e.g., lipids), thus preventing induction of TREM2 signaling, in addition to promoting TREM2 shedding.

Finally, our findings also contribute to addressing the long-standing question of whether microglia can dynamically reverse their activation state in both directions, from homeostatic to DAM and back again. Our findings strongly indicate that even hyperactivated microglia can switch back to homeostatic microglia. The fact that one can influence microglial activation in both directions with TREM2-modulating antibodies is another example for the tremendous dynamics of microglia, and offers the opportunity for therapeutic fine tuning of microglial activity.

Taken together, eliminating TREM2 function and thus reducing hyperactivation by two independent approaches do not rescue lysosomal dysfunction caused by GRN deficiency, but rather exacerbates pathological endpoints characteristic for neurodegeneration, including elevation of CSF NfL and reduced transcription of the neuroprotective transcription factor *Npas*. Thus, despite common assumptions, these results suggest that hyperactivated microglia can retain TREM2-dependent protective functions.

Materials and Methods

Animal experiments and mouse brain tissue

All animal experiments were performed in accordance with German animal welfare law and approved by the government of upper Bavaria. Mice were kept under standard housing conditions including standard pellet food and water provided *ad libitum*. Mice were sacrificed by CO_2 inhalation or deep/lethal anesthesia followed by PBS perfusion. Brain tissue was obtained from male and female of the following mouse strains: C57BL/6J *Grn* (Kayasuga *et al*, 2007) and *Trem2* knockout line (Turnbull *et al*, 2006). To minimize mouse numbers and to reduce variability due to sex differences, both male and female cohorts were used but separately analyzed. PET scans and CSF withdrawal were performed under the animal license: ROB 55.2-2532. Vet_02-18-32.

Isolation, differentiation, and culture of human primary monocytes

Human primary monocytes were isolated from whole blood using Sepmate tubes (StemCell Technologies, #85450) in combination with RosetteSep Human Monocyte Enrichment Cocktail (StemCell Technologies, #15068) according to the manufacturer's protocol. Briefly, fresh blood was collected into EDTA-coated collection tubes and stored at room temperature (RT) until further processing for maximal 6 h. EDTA was added to a final concentration of 1 mM and tubes were mixed by inversion. Fifty μl/ml blood of RosetteSep cocktail was added and samples for incubated for 20 min at RT. Cells were separated on a density gradient using Ficoll-Paque PLUS (ThermoFisher, #11768538). After centrifugation isolated cells were washed with PBS supplemented with 2% FCS. Leftover red blood

cells were lysed using ACK lysing buffer (ThermoFisher, #11509876) for 2 min at RT. Subsequently, cells were washed two times with PBS supplemented with 2% FCS. Cells were counted using Trypan blue as a viability dye and 1×10^6 cells were plated in 10 cm dishes in 10-ml RPMI medium supplemented with 10% FCS, 10% NEAA, 10% L-glutamine, 10% sodium pyruvate, and M-CSF with a final concentration of 50 ng/ml. Forty-eight hours after isolation, 1-ml medium with 500 ng/ml M-CSF was added to the cells. Five days after isolation, cells were washed with PBS and scraped. Cells were counted as described above and plated in either 96-well plates at a density of 5×10^4 cells/well in 100 µl or in 12-well plates at a density of 3×10^5 cells/well in 600 µl RPMI medium supplemented with 10% FCS, 10% NEAA, 10% L-glutamine, 10% sodium pyruvate, and M-CSF with a final concentration of 50 ng/ml.

Generation and maintenance of *GRN* KO iPSC lines

iPSC experiments were performed in accordance with all relevant guidelines and regulations. Female iPSC line A18944 was purchased from ThermoFisher (#A18945). iPSCs were grown in Essential 8 Flex Medium (ThermoFisher, #A2858501) on VTN-coated (Thermo-Fisher, #A14700) cell culture plates at 37°C with 5% CO_2 and split twice a week as small clumps after a 5 min incubation in PBS/EDTA. Prior to electroporation, iPSCs were split to single cells after a 10 min incubation in PBS/EDTA to Geltrex-coated (ThermoFisher, #A1413302) plates and cultured in StemFlex Medium (Thermo-Fisher, #A3349401) containing 10 mM ROCK inhibitor (Selleck-chem S1049) for 2 days. iPSCs were transfected by electroporation as described earlier (Kwart *et al*, 2017) with modifications. Briefly, 2 million cells were harvested with Accutase (ThermoFisher, #A1110501), resuspended in 100 ml cold BTXpress electroporation solution (VWR International GmbH, #732-1285) with 20 mg Cas9 (pSpCas9(BB)-2A-Puro (PX459) V2.0 (gift from Feng Zhang; Addgene plasmid #62988; http://n2t.net/addgene:62988; RRID: Addgene_62988 (Ran *et al*, 2013)) and 5 mg sgRNA cloned into the BsmBI restriction site of the MLM3636 plasmid (gift from Keith Joung, Addgene plasmid #43860; http://n2t.net/addgene:48360; RRID: Addgene_43860). Cells were electroporated with two pulses at 65 mV for 20 ms in a 1 mm cuvette (ThermoFisher, #15437270). After electroporation, cells were transferred to Geltrex-coated 10 cm plates and grown in StemFlex Medium containing 10 mM ROCK inhibitor until visible colonies appeared. Cells expressing Cas9 were selected by 350 ng/ml Puromycin dihydrochloride (VWR International GmbH, #J593) for 3 consecutive days starting 1 day after electroporation (Steyer *et al*, 2018). Single-cell clone colonies were then picked and analyzed by RFLP assay, using NEB enzyme MwoI for the *GRN* KO, and Sanger sequencing as previously described (Kwart *et al*, 2017).

CRISPR/Cas9 genome editing

Design and preparation of editing reagents and quality control of edited iPSCs was performed as described previously (Weisheit *et al*, 2020, 2021). Briefly, we used CRISPOR (http://crispor.tefor.net (Concordet & Haeussler, 2018)) to select guide RNAs and determine putative off-target loci. We chose gRNAs targeting exon 2 of *GRN*, as it is present in most splice isoforms and a frameshift would affect large parts of the coding region. We also ensured presence of nearby stop codons in alternate reading frames in the sequence after the cut

site. Successful knockout was confirmed on mRNA level by qPCR, and on protein level by Western blot using RIPA lysate and ELISA using conditioned media, respectively. For quality control of edited iPSC clones, we checked absence of off-target effects by PCR amplifying and Sanger sequencing the top five hits based on MIT and CFD scores on CRISPOR. We also confirmed absence of on-target effects such as large deletions and loss of heterozygosity using qgPCR and nearby SNP sequencing (Weisheit *et al*, 2021). Finally, we also ensured pluripotency by immunofluorescence staining for typical markers OCT4, NANOG, SSEA4, and TRA160, and chromosomal integrity by molecular karyotyping (LIFE & BRAIN GmbH). One clonal cell line passed the described quality controls and was further differentiated into hiMGL.

Differentiation of human iPSC-derived Microglia (hiMGL)

We differentiated hiMGL from iPSCs as described (Abud *et al*, 2017) with modifications to improve efficiency and yield: When iPSCs were 70–90% confluent, they were split 1:100–200 onto GelTrex-coated six-well plates for the HPC differentiation using EDTA to get around ~20 small colonies per well. Cells were fed with 2 ml of HemA medium (HPC differentiation kit, StemCell Technologies) on day 0 and half-fed with 1 ml on day 2. Media were switched to 2 ml of HemB on day 3 with half-feeds on days 5 and 7 and 1 ml added on top on day 10. On day 12, HPCs were collected as non-adherent cells to either freeze or continue with the microglia differentiation. HPCs were frozen at 1 million cells per ml in BamBanker (FUJIFILM Wako Chemicals). They were then thawed directly onto GelTrex-coated six-well plates with 1 million cells evenly distributed among six wells in 2-ml iMGL media with 25 ng/ml M-CSF, 100 ng/ml IL-34, and 50 ng/ml TGF-β added fresh. One milliliter of media was added every other day. During the microglia differentiation, the cells were split 1:2 every 6–8 days depending on confluency. We did not use CD200 and CX3CL1 for final differentiation, as this did not alter hiMGL gene expression in NanoString analysis. hiMGL were used for experiments on day 16 of the differentiation. A very similar differentiation protocol was published recently (McQuade *et al*, 2018).

Antagonist antibody generation and verification

Antibody generation was carried out by performing single B-cell sequencing on lymphoid tissues from rodents immunized full-length human TREM2 ectodomaine (ECD)-Fc protein (AbCellera Inc.). Antibodies were screened based on binding to human TREM2, and clones of interest were reformatted onto human effectorless human IgG1-LALAPG backbones for material generation and further evaluation of cell-binding potency and functional impact to TREM2 signaling. Antagonists were identified by their ability to block lipid ligand-induced activation of p-Syk on HEK293 cells overexpressing TREM2-DAP12.

Affinity determination and binding kinetics

Human TREM2-binding affinities of anti-TREM2 antibodies were determined by surface plasmon resonance using a Biacore 8K instrument. Biacore Series S CM5 sensor chip was immobilized with a mixture of two monoclonal mouse anti-Fab antibodies (Human Fab capture kit from GE Healthcare) to capture antibodies for binding measurements. In order to measure human TREM2-binding affinities of anti-TREM2 antibodies, serial threefold dilutions of

recombinant human TREM2-ECD protein were injected at a flow rate of 30 µl/min for 300 s followed by 600 s dissociation in HBS-EP$^+$ running buffer (GE, #BR100669). A 1:1 Languir model of simultaneous fitting of k_{on} and k_{off} was used for antigen-binding kinetics analysis.

Epitope mapping of antagonist TREM2 antibodies

Biotinylated polypeptides for human Trem2 IgV domain (Sequences in Fig EV1B) were purchased from Elim Biopharmaceuticals, Inc. N-terminal cysteine was added to peptides to enable maleimide–thiol conjugation of biotin. The lyophilized biotinylated peptides were reconstituted in 20 mM Tris buffer at pH 8.0. Antibody binding to TREM2 IgV domain peptides was detected using a sandwich ELISA. Briefly, a 96-well half-area ELISA plate was coated with streptavidin overnight at 4°C. The following day, biotinylated TREM2 IgV peptides diluted to 1 µM in 1% BSA/PBS were added to the plate and incubated for 1 h. Antibodies diluted to 120 nM in 1% BSA/PBS were then added and incubated for 1 h. Antibodies bound to peptide were detected with anti-Human IgG-HRP secondary antibody diluted in 1% BSA/PBS. Plates were developed with the addition of TMB substrate and stopped by the addition of 2N sulfuric acid. Absorbance at 450 nm was measured on the Synergy Neo2 plate reader (Biotek). A positive signal was identified as an absorbance value above twofold of lower limit of detection (defined as average of blank + threefold SD of blank).

Detection of anti-TREM2 antibody cell binding by flow cytometry

HEK293-overexpressing human TREM2 (HEK293-H6) and HEK293-overexpressing GFP were harvested using 0.05% trypsin and incubated at 37°C for 2 h. All cells were centrifuged and washed in FACS buffer (PBS + 0.5% BSA) twice. Mixed cells were resuspended in FACS buffer at a density of 10^6 cells/ml per cell line. The mixed cell lines were seeded at 100,000 cells per well in a 96-well V-bottom plate and incubated for 20 min at RT. After incubation, the cells were centrifuged and incubated with anti-TREM2 antibodies in a dose titration from 0 to 300 nM for 45 min on ice. After incubation, cells were centrifuged and washed with FACS buffer three times. The cells were then incubated with secondary antibody (Alexa Fluor 647 AffiniPure F(ab')2 fragment goat anti-human IgG (H + L), Jackson ImmunoResearch Laboratories, #109-606-088, 1:800 dilution), for 30 min on ice without exposure to light. After incubation, the cells were washed with FACS buffer three times, resuspended in 100 µl of FACS buffer, and analyzed by flow cytometry (BD FACS-Canto II, San Jose, CA), for which 50,000 events were obtained for each sample. Mean fluorescence intensity (MFI) per cell was calculated by FLowJO software and used for generation of dose–response binding curve.

Antibody treatment

Eight hours after seeding the cells, they were treated with anti-human TREM2 antibodies (Fig EV1C). Antibodies were diluted in RPMI medium and added to the cells with a final concentration of 20 µg/ml. As control for TREM2 shedding, cells were treated with GM6001 (25 µM, Enzo Life Sciences), or DMSO as a vehicle control. hiMGL were seeded in six-well plates with 400,000 cells/well. Eight hours after seeding, antibodies were diluted in iMGL media and added at a concentration of either 20 or 40 µg/ml. Isotype or TREM2 antibodies were added at a concentration of 40 µg/ml and 24 h after antibody treatment, medium and cells were harvested as previously described.

Small animal PET/MRI

All rodent PET procedures followed an established standardized protocol for radiochemistry, acquisition times, and post-processing (Brendel *et al*, 2016; Overhoff *et al*, 2016), which was transferred to a novel PET/MRI system.

All mice were scanned with a 3T Mediso nanoScan PET/MR scanner (Mediso Ltd) with a single-mouse imaging chamber. A 15-min anatomical T1 MR scan was performed at 15 min after [^{18}F]-FDG injection or at 45 min after [^{18}F]-GE180 injection (head receive coil, matrix size 96 × 96 × 22, voxel size 0.24 × 0.24 × 0.80 mm³, repetition time 677 ms, echo time 28.56 ms, and flip angle 90°). PET emission was recorded at 30–60 min p.i. ([^{18}F]-FDG) or at 60–90 min p.i. ([^{18}F]-GE-180). PET list-mode data within 400–600 keV energy window were reconstructed using a 3D iterative algorithm (Tera-Tomo 3D, Mediso Ltd) with the following parameters: matrix size 55 × 62 × 187 mm³, voxel size 0.3 × 0.3 × 0.3 mm³, eight iterations, six subsets. Decay, random, and attenuation correction were applied. The T1 image was used to create a body–air material map for the attenuation correction. We studied PET images of *Grn* KO mice ($n = 8$), *Trem2* KO mice ($n = 10$ or $n = 9$), *Double* KO mice ($n = 10$), and WT mice ($n = 15$), all female at an average age of 10.9 ± 1.6 months or 11.1 ± 1.6 months, as indicated in the figure legends. Normalization of injected activity was performed by the previously validated myocardium correction method (Deussing *et al*, 2018) for [^{18}F]-GE-180 TSPO-PET and by standardized uptake value (SUV) normalization for [^{18}F]-FDG-PET. Groups of *Grn* KO, *Trem2* KO, and *Double* KO mice were compared against WT mice by calculation of %-differences in each cerebral voxel. Finally, [^{18}F]-TSPO-PET and [^{18}F]-FDG-PET values deriving from a whole-brain VOI (Kleinberger *et al*, 2017) were extracted and compared between groups of different genotypes by a one-way ANOVA including Tukey *post hoc* correction.

CSF collection

Mice were fully anesthetized via an intraperitoneal injection of medetomidine (0.5 mg/kg) + midazolam (5 mg/kg) + fentanyl (0.05 mg/kg). CSF was collected as described previously (Lim *et al*, 2018). Briefly, subcutaneous tissue and musculature were removed to expose the meninges overlying the cisterna magna. A glass capillary with a trimmed tip (inner diameter is approximately 0.75 mm) was used to puncture the membrane, and CSF was allowed to flow into the capillary for approximately 10 min. After collection, CSF was centrifuged at 1,000 *g* for 10 min, assessed macroscopically for blood contamination, aliquoted (5 µl) in propylene tubes, snap-frozen in liquid nitrogen, and stored at −80°C until use.

CSF neurofilament light-chain analysis

NfL levels were quantitatively determined in CSF samples using the Simoa NF-light Advantage kit (Quanterix, #103186) following the manufacturer's instructions. CSF samples were diluted 1:10 in sample dilution buffer and mixed with Simoa detector reagent and bead reagent, following an incubation at 30°C for 30 min, shaking

at 800 rpm. Plates were washed with Simoa washing buffer A and SBG reagent from the kit was added. Following a 10 min incubation at 30°C and shaking at 800 rpm, plates were washed twice and sample beads were resuspended in Simoa wash buffer B. NfL concentrations were measured after a 10 min drying at RT using the Simoa DH-1 analyzer (Quanterix).

Gene expression profiling of total brain

Adult mice were perfused transcardially with PBS and dissected brains were snap frozen in liquid nitrogen. Snap frozen brains were mechanically powdered in liquid nitrogen. Total RNA was isolated using the RNeasy Mini kit (Qiagen, #74104) and 60 ng of total RNA per sample was subjected to gene expression profiling using the nCounter® Neuropathology panel from NanoString (NanoString Technologies). Gene expression levels in each sample were normalized against the geometric mean of four housekeeping genes including *Asb10*, *Cltc*, *Hprt1*, and *Tubb5* using the *nSolver Analysis Software*, version 4.0. *Gusb* was excluded because of significant changes in *Grn* KO and *Double* KO mice.

Gene expression profiling of primary microglia

CD11b$^+$ and FCRL$^+$ primary microglia were isolated from adult mouse brain. Mice were perfused transcardially and brains were collected into ice-cold HBSS (ThermoFisher, #14175095). Brain tissue was mechanically dissociated into single-cell suspension using Potter-Elvehjem homogenizers with PTFE Pestle. Microglia cell pellets were resuspended in 70% Percoll and overlayed with equal volumes of 40% Percoll. Microglia were enriched at the interface of 70% (v/v) to 40% (v/v) Percoll after centrifugation (at 18°C, 300*g* for 30 min; slow acceleration and deceleration: 3) (Mazaheri *et al*, 2017). Microglia were collected, filtered through 100 μm cell strainers, and washed with blocking buffer (0.2% BSA in HBSS). Cells were then consecutively stained with FCRLs monoclonal rat antibody (Butovsky *et al*, 2014) (30 min), goat anti-rat APC antibody (Biogegend, # 405407) (20 min), and Cd11b PeCy7 antibody (BD, #553142) (20 min) on ice. Cells were then washed and resuspended in 0.5 ml blocking buffer and subjected to cell sorting. Sorted CD11b$^+$ and FCRL$^+$ cells were pelleted by centrifugation and snap frozen in liquid nitrogen, stored at −80°C until further use. Following total cell lysis in 1:3 diluted RLT buffer (Quiagen, RNeasy Mini Kit), 10,000 cells in 4 μl volume were subjected to gene expression profiling with the nCounter® customized panel from Nano-String (NanoString Technologies). We generated an nCounter panel for analyzing gene expression of 65 microglial activation-related genes including five (*Asb10*, *Cltc*, *Hprt1 Tubb5*, and *Gusb*) housekeeping genes. Gene expression levels in each sample were normalized against the geometric mean of four housekeeping genes using the *nSolver Analysis Software*, version 4.0. *Gusb* was excluded because of significant changes in *Grn* KO and *Double* KO mice.

Gene expression profiling of human hiMGL

hiMGL were seeded into 12-well plates and incubated for 3 h at 37°C (5% CO_2). Thereafter, microglia were treated with TREM2 antagonistic antibodies and isotype control for 24 h. After treatment, cells were collected and RNA was isolated using the E.Z.N.A

HP Total RNA kit (Omega Bio-Tek) according to the manufacturer's instructions. Following isolation, RNA quality was determined using a 4200 TapeStation (Agilent) and gene expression profiling with the nCounter® customized panel from NanoString (NanoString Technologies) was performed. We generated an nCounter panel for analyzing gene expression of 82 microglial-related genes and 8 housekeeping genes. Gene expression levels in each sample were normalized against the geometric mean of five housekeeping genes including *CLTC*, *HPRT1*, *RPL13A*, *TBP*, and *PPIA* using the *nSolver Analysis Software*, version 4.0. *CALR*, *TUBB5*, and *YWAHZ* were excluded because of significant changes in *Grn* KO and WT microglia.

Lipid analysis by liquid chromatography-mass spectrometry (LCMS)

Sample preparation for LCMS

For LCMS sample preparation, 10 mg of brain powder prepared from whole-brain–powered homogenates was mixed with 400 ml of methanol spiked with internal standards and homogenized with a 3 mm tungsten carbide bead (shaken at 25 Hz for 30 s). The methanol fraction was then isolated via centrifugation (20 min at 4°C, 14,000 *g*, followed by transfer of supernatant to a 96-well plate, and 1 h incubation at −20°C followed by an additional 20 min centrifugation (4,000 *g* at 4°C)) and transferred to glass vials for LCMS analysis. For analysis of a GlcCer/GalCer panel, an aliquot of the methanol fraction was dried under N_2 gas and then resuspended in 100 ml of 92.5/5/2.5 CAN/IPA/H2 (MS grade) with 5 mM ammonium formate (MS grade) and 0.5% formic acid (MS grade).

Unless otherwise noted, relative quantification of lipids and metabolites was performed using the Shimadzu Nexera X2 LC system (Shimadzu Scientific Instrument) coupled to Sciex QTRAP 6500+ mass spectrometer (Sciex).

Lipidomic analysis

For each analysis, 5 μl of sample was injected on a BEH C18 1.7 μm, 2.1 × 100 mm column (Waters Corporation), using a flow rate of 0.25 ml/min at 55°C. Mobile phase A consisted of 60:40 acetonitrile/water (v/v); and mobile phase B consisted of 90:10 isopropyl alcohol/acetonitrile (v/v). These buffers were fortified with 10 mM ammonium formate with 0.1% formic acid (positive ionization) or with 10 mM ammonium acetate (negative ionization). The gradient was programmed as follows: 0.0–8.0 min from 45% B to 99% B, 8.0–9.0 min at 99% B, 9.0–9.1 min to 45% B, and 9.1–10.0 min at 45% B. Source settings were as follows: curtain gas at 30 psi; collision gas was set at medium; ion spray voltage at 5,500 V (positive mode) or 4,500 V (negative mode); temperature at 250°C (positive mode) or 600°C (negative mode); ion source gas 1 at 55 psi; and ion source gas 2 at 60 psi. Data acquisition was performed using Analyst 1.6.3 (Sciex) in multiple reaction monitoring mode (MRM). Area ratios of endogenous metabolites and surrogate internal standards were quantified using MultiQuant 3.02 (Sciex).

Protein analysis and Western blotting

Cell pellets obtained from human primary monocytes, cultured hiMGL, or aliquots of powdered frozen brains were lysed in Triton lysis buffer (150 mM NaCl, 50 mM Tris-HCL, pH 7.6, 2 mM EDTA,

1% Triton X-100) supplemented with protease inhibitor (Sigma-Aldrich). Lysates were incubated on ice for 30 min and then centrifuged at 17,000 g for 15 min at 4°C. For sequential biochemical protein extraction of soluble, less soluble, and insoluble proteins, brain powder was lysed in high salt (HS) buffer (0.5 M NaCl, 10 mM Tris-HCL pH 7.5, 5 mM EDTA, 1 mM DTT, 10% sucrose), then RIPA buffer (150 mM NaCl, 20 mM Tris-HCL pH7.4, 1% NP-40, 0.05% Triton X-100, 0.5% sodium-desoxycholate, 2.5 mM EDTA), followed by urea buffer (30 mM Tris-HCL pH 8.5, 7 M urea, 2 M thiourea) as described previously (Gotzl *et al*, 2014). For membrane preparation of hiMG, pellets were resuspended with hypotonic buffer (10 mM Tris, pH 7.4, 1 mM EDTA, pH 8.0, 1 mM EGTA, pH 8.0) and incubated on ice for 30 min, vortexed every 10 min, followed by a freeze–thaw cycle, and centrifuged at 17,000 g for 45 min at 4°C. The supernatants were collected (cytosolic fraction) and the pellet (membrane fraction) resuspended in STEN lysis buffer and incubated on ice for 20 min. Insoluble proteins were pelleted at 17,000 g for 20 min at 4°C and the supernatant (membrane fraction) was collected and used for further analysis. Protein concentrations were determined using the BCA protein assay (Pierce, ThermoFisher). Equal amounts of protein adjusted to lysis buffer were mixed with Laemmli sample buffer supplemented with β-mercaptoethanol. Proteins were separated by SDS-PAGE and transferred onto polyvinylidene difluoride membranes (Immobilon-P, Merck Millipore). Proteins of interest were detected using the following primary antibodies: goat anti-TREM2 (R&D Systems, Inc., #AF1828), rabbit anti-PGRN (ThermoFisher, #40-3400), goat anti-CatD (R&D, #AF1029), mouse anti-SPH (abcam, # ab8049), mouse anti-βActin (Sigma, #A5316), mouse anti-GAPDH (Invitrogen, #AM4300), and rabbit anti-Calnexin (Stressgene, #SPA-860) followed by incubation with horseradish peroxidase-conjugated secondary antibodies and ECL Plus substrate (ThermoFisher, Pierce ECL Plus Western Blotting Substrates). For quantification, images were taken with a Luminescent Image Analyzer LAS-4000 (Fujifilm Life Science, Tokyo, Japan) and evaluated with the Multi GaugeV3.0 software (Fujifilm Life Science, Tokyo, Japan).

ELISA-based quantification of sTREM2 and PGRN

sTREM2 in conditioned media was quantitated using the Meso Scale Discovery Platform as described previously (Schlepckow *et al*, 2020). Briefly, streptavidin-coated small-spot 96-well plates were blocked overnight at 4°C, incubated with 0.125 µg/ml biotinylated polyclonal goat anti-human TREM2 capture antibody (R&D, #BAF1828). After washing, plates were incubated with samples and standards for 2 h at RT. If cells were antibody treated, samples and standards were previously mixed 9:1 with denaturing buffer (200 mM Tris-HCL pH 6.8, 4% (w/v) SDS, 40% (v/v) glycerol, 2% (v/v) β-mercaptoethanol, 50 mM EDTA), and boiled at 95°C for 5 min to dissociate and denature TREM2 antibodies-bound antibodies. Plates were washed before incubation for 1 h at RT with 1 µg/ml mouse anti-human TREM2 antibody (SantaCruz Biotechnology, B-3 SCBT-373828). After washing, plates were incubated with a SULFO-TAG-labeled anti-mouse secondary antibody (MesoScaleDiscovery, R32AC-5) for 1 h at RT. After additional washing steps, 1× Meso Scale Discovery Read buffer was added and the light emission at 620 nm after electrochemical stimulation as measured with a Meso Scale Discovery Sector Imager 2400 reader.

PGRN levels were determined using a previously described protocol (Gotzl *et al*, 2019) using the following antibodies: a biotinylated polyclonal goat anti-human PGRN antibody (R&D, #BAF2420) at 0.2 µg/ml as capture antibody, a mouse anti-human PGRN antibody (R&D, #MAB2420) as detection antibody, and a SULFO-TAG-labeled anti-mouse (MesoScaleDiscovery, #R32AC-5) as secondary antibody.

GRN gene sequencing

All 12 coding exons including intron boundaries of the *GRN gene* were amplified by PCR. For PCR reaction, the Q5 polymerase was used according to the manufacturer's protocol. PCR products were then subjected to Sanger sequencing and sequences were compared to the healthy control sequence. A two base pair deletion in exon 6 was detected using forward primer GGGCCTCATTGACTCCAAG and reverse primer GTGGTGTAAGCGGTACCCTC.

p-Syk AlphaLISA

Phosphorylated SYK (p-Syk) was measured using the AlphaLISA SureFire Ultra p-Syk Assay kit (PerkinElmer, #ALSU-PSYK-A-HV) following the manufacturer's instructions. Briefly, differentiated human macrophages were plated in 100 µl media at a density of 50,000 cells/well. hiMGL were plated in iMGL media at a density of 30,000 cells/well, in 96-well plates, and incubated overnight at 37°C in a cell culture incubator. Plates were then washed three times with HBSS and 50 µl of liposome (1 mg/ml)/antibody (20 µg/ml) mix was added to the cells. Following an incubation at 37°C for 1 h for macrophages, or 5 min for hiMGL, treatment solutions were removed and cells were lysed with 40 µl lysis buffer supplemented with protease inhibitor mix (Sigma) and phosphatase inhibitor (PhosSTOP, Roche) for 30 min at 4°C. Equal volumes of lysate were then subjected to analysis using an EnSpire Multimode Plate Reader (PerkinElmer).

Liposome preparation

POPC/POPS (7:3) liposomes at 10 mg/ml were prepared as follows: 7 mg POPC and 3 mg POPS were dissolved in chloroform followed by thorough evaporation of solvent. The lipid mixture was then resuspended in 1 ml HBSS, and suspensions were extruded using 100 nm polycarbonate membranes (Whatman, #800309) and a LiposoFast extruder device (Sigma-Aldrich) to generate large unilamellar vesicles.

Cathepsin activity assay

hiMGL cell pellets or powdered mouse brain tissue was used for cathepsin D fluorescence-based activity assays (Abnova) as described previously (Gotzl *et al*, 2018). Mouse brain tissue was homogenized using precellys lysing kit (Bertin Instruments, #P000933-LYSK0-A).

GCase activity assay

Brain powder was lysed in GCase lysis buffer (150 mM NaCl, 20 mM Tris-HCl (pH 7.5), 1% Triton X-100, 1 mM EDTA, and

1 mM EGTA) and protein concentrations were determined using the BCA assay. Lysates were adjusted to 2 mg/ml. Lysates were diluted 12.5-fold in GCase activity buffer (100 mM Phosphate Citrate buffer pH 5.2, 0.5% Sodium Taurocholate, 0.25% Triton-X 100) and 4-Methylumbelliferyl β-D-glucopyranoside stock solution (30 mM; Sigma-Aldrich, M3633-1G, stock solution in DMF) was diluted three-fold in the GCase activity buffer. Ninety microliter of the diluted lysates and 10 μl of the diluted 4-Methylumbelliferyl β-D-glucopyranoside were added to a 96-well plate. Plates were incubated for 15 min at 37°C. Signal intensities were measured continuously for 1 h (Ex 365 nm/Em 455 nm).

Phagocytosis assays

Microglial phagocytosis was determined using the IncuCyte S3 Live-Cell Analysis System (Sartorius). hiMGL cells were plated in 96-well plates at 30% confluency. Cells were incubated at 37°C and the confluency (pre-treatment) of each well was determined with the Incu-Cyte S3 3 h after seeding. Thereafter, TREM2 antagonistic antibodies and isotype control were added at 20 and 40 μg/ml. Eighteen hours after antibody treatment, pHrodo-labeled myelin (5 μg/ml) was added to the hiMGL cells and images of fluorescence and phase were captured at 4× in the IncuCyte S3 live cell imager every 15 min. Using IncuCyte 2020B software (Satorius), image masks for phase and fluorescent signal (phagocytosis of pHrodo-labelled myelin) were acquired, and the fluorescent signal was normalized to cell confluency (cell body area), which was measured before the antibody treatment.

pHrodo labeling of myelin

Myelin was labeled with amine reactive pHrodo™ Red succinimidyl ester (ThermoFisher) for 45 min at RT (protected from light). Labeled myelin was washed with PBS and either directly used or stored in aliquots at −80°C.

Immunohistochemistry and image acquisition

Mice were transcardially perfused with PBS and brains were dissected into two hemispheres. One hemisphere was snap frozen and stored at −80°C until further use. The other hemisphere was immersion fixed for 24 h in 4% paraformaldehyde, washed with PBS, and incubated 30% sucrose for 48 h for cryoprotection. After freezing, brains were cut into 50 μm or 100 μm coronal sections using a vibratome (Leica Biosystems), collected in PBS, and stored at 4°C until further use. For visualizing lipofuscin, SPH or VGAT, 50 μm free-floating sections were stained with primary antibodies (mouse anti-VGAT (Synaptic Systems, #131011C3, or rabbit anti-SPH (Abcam, #ab32594)) in 5% donkey serum in PBS overnight at 4°C with slow agitation. After washing, tissue sections were incubated with corresponding secondary antibodies for 3 h at RT. After washing, tissue sections were stained with DAPI for 10 min at RT and mounted onto slides using ProlongTM Gold Antifade reagent (ThermoFisher, #P36961). For morphological analysis of microglia, 100 μm sections were blocked with goat serum blocking buffer (2% goat serum, 0.05% Tween 20 in 0.01 M PBS, pH 7.2–7.4) and stained with anti-IBA1 in primary antibody buffer (1% bovine serum albumin, 0.1% gelatin from cold water fish skin, 0.5% Triton

X-100 in 0.01 M PBS, pH 7.2–7.4) and anti-rabbit IgG-coupled Alexa Flour 555 in secondary antibody buffer (0.05% Tween 20 in 0.01 M PBS, pH 7.2–7.4). After washing, tissue sections were stained with DAPI for 10 min at RT and mounted onto slides using ProlongTM Gold Antifade reagent. Images were acquired using a LSM800 Zeiss confocal microscope and the ZEN 2011 software package (blue edition). For lipofuscin analysis, five images were taken per slide using a 20× objective at 2,048 × 2,048 pixel resolution. For SPH and VGAT analysis, three images were taken per slide using a 20× objective at 2,048 × 2,048 pixel resolution. Total fluorescence above background was quantified using the Fiji software (ImageJ, Version 1.0).

Automated analysis of microglia morphology

For morphological analysis of microglia, two z-stack images per animal (n = 3) were recorded with a 40× objective in a resolution of 1,024 × 1,024 pixels (x–y-pixel size = 0.15598 μm) and a slice distance (z) of 0.4 μm. The raw confocal z-stacks were then analyzed using the Microglia Morphology Quantification Tool (MMQT) for automated analysis of microglial morphology as previously described (Heindl *et al*, 2018). The algorithm was run in MATLAB (Version R2016b). To identify the most discriminating features, a receiver operating characteristic (ROC) analysis was performed in R (version 4.0.3) for calculating the area under the curve (auc) between the groups "WT" and "*Double* KO." Statistical analysis of group difference for the morphological scores, "Branch volume" (auc = 0.72), "Sphericity score" (auc = 0.82), "Branch length" (auc = 0.69), and "Number of branch nodes" (auc = 0.80) was performed using the Wilcoxon rank-sum test with continuity correction and Bonferroni *post hoc* correction for multiple testing in R (version 4.0.3).

Statistical analysis

Data were analyzed using GraphPad Prism 9. If no other test of significance is indicated, for statistical analysis of two groups of samples, the unpaired, two-tailed student's t-test was performed. For comparison of more than two groups, one-way ANOVA and Dunnett's or Tukey's *post hoc* test were used. Statistical significance was set at *$P < 0.05$; **$P < 0.01$; ***$P < 0.001$; and ****$P < 0.0001$.

Data availability

The accession number for the Neuropathology NanoString data reported in this paper is Gene Expression Omnibus GSE181135 http://www.ncbi.nlm.nih.gov/geo/query/acc.cgi?acc = GSE181135 (6-month-old cohort) and GSE185510 http://www.ncbi.nlm.nih.gov/geo/query/acc.cgi?acc = GSE185510 (14-month-old cohort).

Expanded View for this article is available online.

Author contributions

CH, AC, and AR conceived the study and analyzed the results. CH wrote the manuscript with further input from AR, AC, GDP, KMM, JWL, SR, and DP. AR performed and analyzed Western Blots, ELISAs, enzyme activity assays, mRNA isolation, NanoString experiments, and immunofluorescence on all mouse samples. AR isolated and performed all experiments of human-derived macrophages and analyzed hiMGL NanoString data. With supervision of DP, SR generated and validated *GRN* KO hiPSC, differentiated into hiMGL, and performed and analyzed Western Blots, ELISAs, and enzyme activity assays. JK and GK helped to establish hiMGL cell differentiation. KMM and BVL discovered, generated, and validated antagonistic TREM2 antibodies. TL and JS performed lipidomic analysis. MAV and SHa performed NanoString and phagocytosis assays on hiMGL cells. JGn, KW, AZ, and MB conducted, performed, and analyzed PET imaging. SHe performed automated analysis on microglia morphology, with supervision of AL. IP performed CSF isolation. JKG helped to establish mouse lines. JL, KB, JD-S, EW, and LR identified FTLD patients and performed sequencing analysis. BN performed NfL measurements. The synopsis image was created with BioRender.com.

Disclosure statement and competing interests

CH collaborates with Denali Therapeutics, participated on one advisory board meeting of Biogen, and received a speaker honorarium from Novartis and Roche. CH is chief advisor of ISAR Bioscience. KMM, BVL, TL, JS, JWL, and GDP are employees and shareholders of Denali Therapeutics. DP is a scientific advisor of ISAR Bioscience. MB received speaker honoraria from GE healthcare, Roche, and LMI and is an advisor of LMI.

References

Abud EM, Ramirez RN, Martinez ES, Healy LM, Nguyen CHH, Newman SA, Yeromin AV, Scarfone VM, Marsh SE, Fimbres C *et al* (2017) iPSC-derived human microglia-like cells to study neurological diseases. *Neuron* 94: 278–293.e9

Aguzzi A, Haass C (2003) Games played by rogue proteins in prion disorders and Alzheimer's disease. *Science* 302: 814–818

Almeida MR, Macario MC, Ramos L, Baldeiras I, Ribeiro MH, Santana I (2016) Portuguese family with the co-occurrence of frontotemporal lobar degeneration and neuronal ceroid lipofuscinosis phenotypes due to progranulin gene mutation. *Neurobiol Aging* 41: 200 e201–200 e205

Arrant AE, Roth JR, Boyle NR, Kashyap SN, Hoffmann MQ, Murchison CF, Ramos EM, Nana AL, Spina S, Grinberg LT *et al* (2019) Impaired beta-glucocerebrosidase activity and processing in frontotemporal dementia due to progranulin mutations. *Acta Neuropathol Commun* 7: 218

Baker M, Mackenzie IR, Pickering-Brown SM, Gass J, Rademakers R, Lindholm C, Snowden J, Adamson J, Sadovnick AD, Rollinson S *et al* (2006) Mutations in progranulin cause tau-negative frontotemporal dementia linked to chromosome 17. *Nature* 442: 916–919

Beel S, Moisse M, Damme M, De Muynck L, Robberecht W, Van Den Bosch L, Saftig P, Van Damme P (2017) Progranulin functions as a cathepsin D chaperone to stimulate axonal outgrowth in vivo. *Hum Mol Genet* 26: 2850–2863

Bosch-Queralt M, Cantuti-Castelvetri L, Damkou A, Schifferer M, Schlepckow K, Alexopoulos I, Lutjohann D, Klose C, Vaculciakova L, Masuda T *et al* (2021) Diet-dependent regulation of TGFbeta impairs reparative innate immune responses after demyelination. *Nat Metab* 3: 211–227

Brendel M, Probst F, Jaworska A, Overhoff F, Korzhova V, Albert NL, Beck R, Lindner S, Gildehaus F-J, Baumann K *et al* (2016) Glial activation and glucose metabolism in a transgenic amyloid mouse model: a triple-tracer PET study. *J Nucl Med* 57: 954–960

Butler VJ, Cortopassi WA, Argouarch AR, Ivry SL, Craik CS, Jacobson MP, Kao AW (2019a) Progranulin stimulates the in vitro maturation of pro-cathepsin D at acidic pH. *J Mol Biol* 431: 1038–1047

Butler VJ, Cortopassi WA, Gururaj S, Wang AL, Pierce OM, Jacobson MP, Kao AW (2019b) Multi-granulin domain peptides bind to pro-cathepsin D and stimulate its enzymatic activity more effectively than progranulin in vitro. *Biochemistry* 58: 2670–2674

Butovsky O, Jedrychowski MP, Moore CS, Cialic R, Lanser AJ, Gabriely G, Koeglsperger T, Dake B, Wu PM, Doykan CE *et al* (2014) Identification of a unique TGF-beta-dependent molecular and functional signature in microglia. *Nat Neurosci* 17: 131–143

Chen Y, Jian J, Hettinghouse A, Zhao X, Setchell KDR, Sun Y, Liu CJ (2018) Progranulin associates with hexosaminidase A and ameliorates GM2 ganglioside accumulation and lysosomal storage in Tay-Sachs disease. *J Mol Med* 96: 1359–1373

Cheng Q, Danao J, Talreja S, Wen P, Yin J, Sun N, Li C-M, Chui D, Tran D, Koirala S *et al* (2018) TREM2-activating antibodies abrogate the negative pleiotropic effects of the Alzheimer's disease variant Trem 2(R47H) on murine myeloid cell function. *J Biol Chem* 293: 12620–12633

Cignarella F, Filipello F, Bollman B, Cantoni C, Locca A, Mikesell R, Manis M, Ibrahim A, Deng LI, Benitez BA *et al* (2020) TREM2 activation on microglia promotes myelin debris clearance and remyelination in a model of multiple sclerosis. *Acta Neuropathol* 140: 513–534

Colonna M, Wang Y (2016) TREM2 variants: new keys to decipher Alzheimer disease pathogenesis. *Nat Rev Neurosci* 17: 201–207

Concordet JP, Haeussler M (2018) CRISPOR: intuitive guide selection for CRISPR/Cas9 genome editing experiments and screens. *Nucleic Acids Res* 46: W242–W245

Cruts M, Gijselinck I, van der Zee J, Engelborghs S, Wils H, Pirici D, Rademakers R, Vandenberghe R, Dermaut B, Martin J-J *et al* (2006) Null mutations in progranulin cause ubiquitin-positive frontotemporal dementia linked to chromosome 17q21. *Nature* 442: 920–924

Deczkowska A, Weiner A, Amit I (2020) The physiology, pathology, and potential therapeutic applications of the TREM2 signaling pathway. *Cell* 181: 1207–1217

Deussing M, Blume T, Vomacka L, Mahler C, Focke C, Todica A, Unterrainer M, Albert NL, Lindner S, von Ungern-Sternberg B *et al* (2018) Coupling between physiological TSPO expression in brain and myocardium allows stabilization of late-phase cerebral [(18)F]GE180 PET quantification. *NeuroImage* 165: 83–91

Efthymiou AG, Goate AM (2017) Late onset Alzheimer's disease genetics implicates microglial pathways in disease risk. *Mol Neurodegener* 12: 43

Ellwanger DC, Wang S, Brioschi S, Shao Z, Green L, Case R, Yoo D, Weishuhn D, Rathanaswami P, Bradley J *et al* (2021) Prior activation state shapes the microglia response to antihuman TREM2 in a mouse model of Alzheimer's disease. *Proc Natl Acad Sci USA* 118: e2017742118

Evers BM, Rodriguez-Navas C, Tesla RJ, Prange-Kiel J, Wasser CR, Yoo KS, McDonald J, Cenik B, Ravenscroft TA, Plattner F *et al* (2017) Lipidomic and transcriptomic basis of lysosomal dysfunction in progranulin deficiency. *Cell Rep* 20: 2565–2574

Ewers M, Franzmeier N, Suárez-Calvet M, Morenas-Rodriguez E, Caballero MAA, Kleinberger G, Piccio L, Cruchaga C, Deming Y, Dichgans M *et al* (2019) Increased soluble TREM2 in cerebrospinal fluid is associated with reduced cognitive and clinical decline in Alzheimer's disease. *Sci Transl Med* https://doi.org/10.1126/scitranslmed.aav6221

Fassler M, Rappaport MS, Cuno CB, George J (2021) Engagement of TREM2 by a novel monoclonal antibody induces activation of microglia and improves cognitive function in Alzheimer's disease models. *J Neuroinflammation* 18: 19

Fu J, Guo O, Zhen Z, Zhen J (2020) Essential functions of the transcription factor Npas4 in neural circuit development, plasticity, and diseases. *Front Neurosci* 14: 603373

Gotzl JK, Brendel M, Werner G, Parhizkar S, Sebastian Monasor L, Kleinberger G, Colombo AV, Deussing M, Wagner M, Winkelmann J *et al* (2019) Opposite microglial activation stages upon loss of PGRN or TREM2 result in reduced cerebral glucose metabolism. *EMBO Mol Med* 11: 1–15

Gotzl JK, Colombo AV, Fellerer K, Reifschneider A, Werner G, Tahirovic S, Haass C, Capell A (2018) Early lysosomal maturation deficits in microglia triggers enhanced lysosomal activity in other brain cells of progranulin knockout mice. *Mol Neurodegener* 13: 48

Gotzl JK, Lang CM, Haass C, Capell A (2016) Impaired protein degradation in FTLD and related disorders. *Ageing Res Rev* 32: 122–139

Götzl JK, Mori K, Damme M, Fellerer K, Tahirovic S, Kleinberger G, Janssens J, van der Zee J, Lang CM, Kremmer E *et al* (2014) Common pathobiochemical hallmarks of progranulin-associated frontotemporal lobar degeneration and neuronal ceroid lipofuscinosis. *Acta Neuropathol* 127: 845–860

Guerreiro R, Wojtas A, Bras J, Carrasquillo M, Rogaeva E, Majounie E, Cruchaga C, Sassi C, Kauwe JS, Younkin S *et al* (2013) TREM2 variants in Alzheimer's disease. *N Engl J Med* 368: 117–127

Heindl S, Gesierich B, Benakis C, Llovera G, Duering M, Liesz A (2018) Automated morphological analysis of microglia after stroke. *Front Cell Neurosci* 12: 106

Heneka MT, Kummer MP, Stutz A, Delekate A, Schwartz S, Vieira-Saecker A, Griep A, Axt D, Remus A, Tzeng T-C *et al* (2013) NLRP3 is activated in Alzheimer's disease and contributes to pathology in APP/PS1 mice. *Nature* 493: 674–678

Heneka MT, McManus RM, Latz E (2018) Inflammasome signalling in brain function and neurodegenerative disease. *Nat Rev Neurosci* 19: 610–621

Hong S, Beja-Glasser VF, Nfonoyim BM, Frouin A, Li S, Ramakrishnan S, Merry KM, Shi Q, Rosenthal A, Barres BA *et al* (2016a) Complement and microglia mediate early synapse loss in Alzheimer mouse models. *Science* 352: 712–716

Hong S, Dissing-Olesen L, Stevens B (2016b) New insights on the role of microglia in synaptic pruning in health and disease. *Curr Opin Neurobiol* 36: 128–134

Hu F, Padukkavidana T, Vaegter CB, Brady OA, Zheng Y, Mackenzie IR, Feldman HH, Nykjaer A, Strittmatter SM (2010) Sortilin-mediated endocytosis determines levels of the frontotemporal dementia protein, progranulin. *Neuron* 68: 654–667

Huang M, Modeste E, Dammer E, Merino P, Taylor G, Duong DM, Deng Q, Holler CJ, Gearing M, Dickson D *et al* (2020) Network analysis of the progranulin-deficient mouse brain proteome reveals pathogenic mechanisms shared in human frontotemporal dementia caused by GRN mutations. *Acta Neuropathol Commun* 8: 163

Jadhav VS, Lin PBC, Pennington T, Di Prisco GV, Jannu AJ, Xu G, Moutinho M, Zhang J, Atwood BK, Puntambekar SS *et al* (2020) Trem2 Y38C mutation and loss of Trem2 impairs neuronal synapses in adult mice. *Mol Neurodegener* 15: 62

Jian J, Zhao S, Tian Q-Y, Liu H, Zhao Y, Chen W-C, Grunig G, Torres PA, Wang BC, Zeng B *et al* (2016) Association between progranulin and gaucher disease. *EBioMedicine* 11: 127–137

Jonsson T, Stefansson H, Steinberg S, Jonsdottir I, Jonsson PV, Snaedal J, Bjornsson S, Huttenlocher J, Levey AI, Lah JJ *et al* (2013) Variant of TREM2 associated with the risk of Alzheimer's disease. *N Engl J Med* 368: 107–116

Kao AW, McKay A, Singh PP, Brunet A, Huang EJ (2017) Progranulin, lysosomal regulation and neurodegenerative disease. *Nat Rev Neurosci* 18: 325–333

Kayasuga Y, Chiba S, Suzuki M, Kikusui T, Matsuwaki T, Yamanouchi K, Kotaki H, Horai R, Iwakura Y, Nishihara M (2007) Alteration of behavioural phenotype in mice by targeted disruption of the progranulin gene. *Behav Brain Res* 185: 110–118

Keren-Shaul H, Spinrad A, Weiner A, Matcovitch-Natan O, Dvir-Szternfeld R, Ulland TK, David E, Baruch K, Lara-Astaiso D, Toth B *et al* (2017) A Unique microglia type associated with restricting development of Alzheimer's disease. *Cell* 169: 1276–1290.e17

Klein ZA, Takahashi H, Ma M, Stagi M, Zhou M, Lam TT, Strittmatter SM (2017) Loss of TMEM106B ameliorates lysosomal and frontotemporal dementia-related phenotypes in progranulin-deficient mice. *Neuron* 95: 281–296.e6

Kleinberger G, Brendel M, Mracsko E, Wefers B, Groeneweg L, Xiang X, Focke C, Deussing M, Suarez-Calvet M, Mazaheri F *et al* (2017) The FTD-like syndrome causing TREM2 T66M mutation impairs microglia function, brain perfusion, and glucose metabolism. *EMBO J* 36: 1837–1853

Kleinberger G, Yamanishi Y, Suárez-Calvet M, Czirr E, Lohmann E, Cuyvers E, Struyfs H, Pettkus N, Wenninger-Weinzierl A, Mazaheri F *et al* (2014) TREM2 mutations implicated in neurodegeneration impair cell surface transport and phagocytosis. *Sci Transl Med* 6: 243ra286

Krabbe G, Minami SS, Etchegaray JI, Taneja P, Djukic B, Davalos D, Le D, Lo I, Zhan L, Reichert MC *et al* (2017) Microglial NFkappaB-TNFalpha hyperactivation induces obsessive-compulsive behavior in mouse models of progranulin-deficient frontotemporal dementia. *Proc Natl Acad Sci USA* 114: 5029–5034

Krasemann S, Madore C, Cialic R, Baufeld C, Calcagno N, El Fatimy R, Beckers L, O'Loughlin E, Xu Y, Fanek Z *et al* (2017) The TREM2-APOE pathway drives the transcriptional phenotype of dysfunctional microglia in neurodegenerative diseases. *Immunity* 47: 566–581.e9

Kwart D, Paquet D, Teo S, Tessier-Lavigne M (2017) Precise and efficient scarless genome editing in stem cells using CORRECT. Nat Protoc 12: 329–354

Lee SH, Meilandt WJ, Xie L, Gandham VD, Ngu H, Barck KH, Rezzonico MG, Imperio J, Lalehzadeh G, Huntley MA et al (2021) Trem2 restrains the enhancement of tau accumulation and neurodegeneration by beta-amyloid pathology. Neuron 109: 1283–1301 e1286

Lewcock JW, Schlepckow K, Di Paolo G, Tahirovic S, Monroe KM, Haass C (2020) Emerging microglia biology defines novel therapeutic approaches for Alzheimer's disease. Neuron 108: 801–821

Lim NK, Moestrup V, Zhang X, Wang WA, Moller A, Huang FD (2018) An improved method for collection of cerebrospinal fluid from anesthetized mice. J Vis Exp https://doi.org/10.3791/56774

Liu B, Le KX, Park MA, Wang S, Belanger AP, Dubey S, Frost JL, Holton P, Reiser V, Jones PA et al (2015) In vivo detection of age- and disease-related increases in neuroinflammation by 18F-GE180 TSPO MicroPET imaging in wild-type and Alzheimer's transgenic mice. J Neurosci 35: 15716–15730

Logan T, Simon JS, Rana A, Cherf GM, Srivastava A, Davis SS, Yoon Low RL, Chiu C, Fang M, Huang F et al (2021) Rescue of a lysosomal storage disorder caused by BMP deficiency in Grn loss-of-function with a brain penetrant progranulin biologic. Cell 184: 4651–4668.e25

Lui H, Zhang J, Makinson S, Cahill M, Kelley K, Huang H-Y, Shang Y, Oldham M, Martens L, Gao F et al (2016) Progranulin Deficiency Promotes Circuit-Specific Synaptic Pruning By Microglia Via Complement Activation. Cell 165: 921–935

Marschallinger J, Iram T, Zardeneta M, Lee SE, Lehallier B, Haney MS, Pluvinage JV, Mathur V, Hahn O, Morgens DW et al (2020) Lipid-droplet-accumulating microglia represent a dysfunctional and proinflammatory state in the aging brain. Nat Neurosci 23: 194–208

Martens LH, Zhang J, Barmada SJ, Zhou P, Kamiya S, Sun B, Min S-W, Gan LI, Finkbeiner S, Huang EJ et al (2012) Progranulin deficiency promotes neuroinflammation and neuron loss following toxin-induced injury. J Clin Invest 122: 3955–3959

Mazaheri F, Snaidero N, Kleinberger G, Madore C, Daria A, Werner G, Krasemann S, Capell A, Trumbach D, Wurst W et al (2017) TREM2 deficiency impairs chemotaxis and microglial responses to neuronal injury. EMBO Rep 18: 1186–1198

McQuade A, Coburn M, Tu CH, Hasselmann J, Davtyan H, Blurton-Jones M (2018) Development and validation of a simplified method to generate human microglia from pluripotent stem cells. Mol Neurodegener 13: 67

Meeter LH, Dopper EG, Jiskoot LC, Sanchez-Valle R, Graff C, Benussi L, Ghidoni R, Pijnenburg YA, Borroni B, Galimberti D et al (2016) Neurofilament light chain: a biomarker for genetic frontotemporal dementia. Ann Clin Transl Neurol 3: 623–636

Meilandt WJ, Ngu H, Gogineni A, Lalehzadeh G, Lee SH, Srinivasan K, Imperio J, Wu T, Weber M, Kruse AJ et al (2020) Trem2 deletion reduces late-stage amyloid plaque accumulation, elevates the Abeta42:Abeta40 ratio, and exacerbates axonal dystrophy and dendritic spine loss in the PS2APP Alzheimer's mouse model. J Neurosci 40: 1956–1974

Nugent AA, Lin K, van Lengerich B, Lianoglou S, Przybyla L, Davis SS, Llapashtica C, Wang J, Kim DJ, Xia D et al (2020) TREM2 regulates microglial cholesterol metabolism upon chronic phagocytic challenge. Neuron 105: 837–854.e9

Overhoff F, Brendel M, Jaworska A, Korzhova V, Delker A, Probst F, Focke C, Gildehaus F-J, Carlsen J, Baumann K et al (2016) Automated spatial brain normalization and hindbrain white matter reference tissue give improved [(18)F]-Florbetaben PET quantitation in Alzheimer's model mice. Front Neurosci 10: 45

Parhizkar S, Arzberger T, Brendel M, Kleinberger G, Deussing M, Focke C, Nuscher B, Xiong M, Ghasemigharagoz A, Katzmarski N et al (2019) Loss of TREM2 function increases amyloid seeding but reduces plaque-associated ApoE. Nat Neurosci 22: 191–204

Paushter DH, Du H, Feng T, Hu F (2018) The lysosomal function of progranulin, a guardian against neurodegeneration. Acta Neuropathol 136: 1–17

Perez-Otano I, Larsen RS, Wesseling JF (2016) Emerging roles of GluN3-containing NMDA receptors in the CNS. Nat Rev Neurosci 17: 623–635

Preische O, Schultz SA, Apel A, Kuhle J, Kaeser SA, Barro C, Gräber S, Kuder-Buletta E, LaFougere C, Laske C et al (2019) Serum neurofilament dynamics predicts neurodegeneration and clinical progression in presymptomatic Alzheimer's disease. Nat Med 25: 277–283

Price BR, Sudduth TL, Weekman EM, Johnson S, Hawthorne D, Woolums A, Wilcock DM (2020) Therapeutic Trem2 activation ameliorates amyloid-beta deposition and improves cognition in the 5XFAD model of amyloid deposition. J Neuroinflammation 17: 238

Ran FA, Hsu PD, Wright J, Agarwala V, Scott DA, Zhang F (2013) Genome engineering using the CRISPR-Cas9 system. Nat Protoc 8: 2281–2308

Ransohoff RM (2016) How neuroinflammation contributes to neurodegeneration. Science 353: 777–783

Rohrer JD, Woollacott IOC, Dick KM, Brotherhood E, Gordon E, Fellows A, Toombs J, Druyeh R, Cardoso MJ, Ourselin S et al (2016) Serum neurofilament light chain protein is a measure of disease intensity in frontotemporal dementia. Neurology 87: 1329–1336

Root J, Merino P, Nuckols A, Johnson M, Kukar T (2021) Lysosome dysfunction as a cause of neurodegenerative diseases: lessons from frontotemporal dementia and amyotrophic lateral sclerosis. Neurobiol Dis 154: 105360

Schlepckow K, Kleinberger G, Fukumori A, Feederle R, Lichtenthaler SF, Steiner H, Haass C (2017) An Alzheimer-associated TREM2 variant occurs at the ADAM cleavage site and affects shedding and phagocytic function. EMBO Mol Med 9: 1356–1365

Schlepckow K, Monroe KM, Kleinberger G, Cantuti-Castelvetri L, Parhizkar S, Xia D, Willem M, Werner G, Pettkus N, Brunner B et al (2020) Enhancing protective microglial activities with a dual function TREM2 antibody to the stalk region. EMBO Mol Med 12: e11227

Smith K, Damiano J, Franceschetti S, Carpenter S, Canafoglia L, Morbin M, Rossi G, Pareyson D, Mole S, Staropoli J et al (2012) Strikingly different clinicopathological phenotypes determined by progranulin-mutation dosage. Am J Hum Genet 90: 1102–1107

Spiegel I, Mardinly AR, Gabel HW, Bazinet JE, Couch CH, Tzeng CP, Harmin DA, Greenberg ME (2014) Npas4 regulates excitatory-inhibitory balance within neural circuits through cell-type-specific gene programs. Cell 157: 1216–1229

Steyer B, Bu Q, Cory E, Jiang K, Duong S, Sinha D, Steltzer S, Gamm D, Chang Q, Saha K (2018) Scarless genome editing of human pluripotent stem cells via transient puromycin selection. Stem Cell Rep 10: 642–654

Tanaka Y, Suzuki G, Matsuwaki T, Hosokawa M, Serrano G, Beach TG, Yamanouchi K, Hasegawa M, Nishihara M (2017) Progranulin regulates lysosomal function and biogenesis through acidification of lysosomes. Hum Mol Genet 26: 969–988

Thornton P, Sevalle J, Deery MJ, Fraser G, Zhou Y, Stahl S, Franssen EH, Dodd RB, Qamar S, Gomez Perez-Nievas B et al (2017) TREM2 shedding by cleavage at the H157–S158 bond is accelerated for the Alzheimer's disease-associated H157Y variant. EMBO Mol Med 9: 1366–1378

Turnbull IR, Gilfillan S, Cella M, Aoshi T, Miller M, Piccio L, Hernandez M, Colonna M (2006) Cutting edge: TREM-2 attenuates macrophage activation. *J Immunol* 177: 3520 – 3524

Ulrich JD, Finn MB, Wang Y, Shen A, Mahan TE, Jiang H, Stewart FR, Piccio L, Colonna M, Holtzman DM (2014) Altered microglial response to Abeta plaques in APPPS1-21 mice heterozygous for TREM2. *Mol Neurodegener* 9: 20

Valdez C, Wong YC, Schwake M, Bu G, Wszolek ZK, Krainc D (2017) Progranulin-mediated deficiency of cathepsin D results in FTD and NCL-like phenotypes in neurons derived from FTD patients. *Hum Mol Genet* 26: 4861 – 4872

Villa A, Gelosa P, Castiglioni L, Cimino M, Rizzi N, Pepe G, Lolli F, Marcello E, Sironi L, Vegeto E *et al* (2018) Sex-specific features of microglia from adult mice. *Cell Rep* 23: 3501 – 3511

Wang S, Mustafa M, Yuede CM, Salazar SV, Kong P, Long H, Ward M, Siddiqui O, Paul R, Gilfillan S *et al* (2020) Anti-human TREM2 induces microglia proliferation and reduces pathology in an Alzheimer's disease model. *J Exp Med* https://doi.org/10.1084/jem.20200785

Wang Y, Ulland TK, Ulrich JD, Song W, Tzaferis JA, Hole JT, Yuan P, Mahan TE, Shi Y, Gilfillan S *et al* (2016) TREM2-mediated early microglial response limits diffusion and toxicity of amyloid plaques. *J Exp Med* 213: 667 – 675

Ward ME, Chen R, Huang H-Y, Ludwig C, Telpoukhovskaia M, Taubes A, Boudin H, Minami SS, Reichert M, Albrecht P *et al* (2017) Individuals with progranulin haploinsufficiency exhibit features of neuronal ceroid lipofuscinosis. *Sci Transl Med* https://doi.org/10.1126/scitranslmed.aah5642

Weisheit I, Kroeger JA, Malik R, Klimmt J, Crusius D, Dannert A, Dichgans M, Paquet D (2020) Detection of deleterious on-target effects after HDR-mediated CRISPR editing. *Cell Rep* 31: 107689

Weisheit I, Kroeger JA, Malik R, Wefers B, Lichtner P, Wurst W, Dichgans M, Paquet D (2021) Simple and reliable detection of CRISPR-induced on-target effects by qgPCR and SNP genotyping. *Nat Protoc* 16: 1714 – 1739

Werner G, Damme M, Schludi M, Gnorich J, Wind K, Fellerer K, Wefers B, Wurst W, Edbauer D, Brendel M *et al* (2020) Loss of TMEM106B potentiates lysosomal and FTLD-like pathology in progranulin-deficient mice. *EMBO Rep* 21: e50241

Woollacott IOC, Bocchetta M, Sudre CH, Ridha BH, Strand C, Courtney R, Ourselin S, Cardoso MJ, Warren JD, Rossor MN *et al* (2018) Pathological correlates of white matter hyperintensities in a case of progranulin mutation associated frontotemporal dementia. *Neurocase* 24: 166 – 174

Wu Y, Shao W, Todd TW, Tong J, Yue M, Koga S, Castanedes-Casey M, Librero AL, Lee CW, Mackenzie IR *et al* (2021) Microglial lysosome dysfunction contributes to white matter pathology and TDP-43 proteinopathy in GRN-associated FTD. *Cell Rep* 36: 109581

Xiang X, Wind K, Wiedemann T, Blume T, Shi Y, Briel N, Beyer L, Biechele G, Eckenweber F, Zatcepin A *et al* (2021) Microglial activation states drive glucose uptake and FDG-PET alterations in neurodegenerative diseases. *Sci Transl Med* 13: eabe5640

Yuan P, Condello C, Keene CD, Wang Y, Bird TD, Paul SM, Luo W, Colonna M, Baddeley D, Grutzendler J (2016) TREM2 haplodeficiency in mice and humans impairs the microglia barrier function leading to decreased amyloid compaction and severe axonal dystrophy. *Neuron* 92: 252 – 264

Zhang J, Velmeshev D, Hashimoto K, Huang Y-H, Hofmann JW, Shi X, Chen J, Leidal AM, Dishart JG, Cahill MK *et al* (2020) Neurotoxic microglia promote TDP-43 proteinopathy in progranulin deficiency. *Nature* 588: 459 – 465

Zhou X, Paushter DH, Feng T, Pardon CM, Mendoza CS, Hu F (2017) Regulation of cathepsin D activity by the FTLD protein progranulin. *Acta Neuropathol* 134: 151 – 153

Zhou X, Paushter DH, Pagan MD, Kim D, Nunez Santos M, Lieberman RL, Overkleeft HS, Sun Y, Smolka MB, Hu F (2019) Progranulin deficiency leads to reduced glucocerebrosidase activity. *PLoS One* 14: e0212382

Zhou X, Sun L, Bastos de Oliveira F, Qi X, Brown WJ, Smolka MB, Sun Y, Hu F (2015) Prosaposin facilitates sortilin-independent lysosomal trafficking of progranulin. *J Cell Biol* 210: 991 – 1002

Expanded View Figures

A

B

Peptide Sequence	Ab1	Ab2	Isotype
NTTVFQGVAGQSLQVSCPYDSM	-	-	-
QSLQVSCPYDSMKHWGRRKAWCR	+	+	-
MKHWGRRKAWCRQLGEKGPCQRV	+	+	-
QLGEKGPCQRVVSTHNLWLLSF	-	-	-
VSTHNLWLLSFLRRWNGSTAIT	-	-	-
LRRWNGSTAITDDTLGGTLTITL	-	-	-
DDTLGGTLTITLRNLQPHDAGL	-	-	-
RNLQPHDAGLYQCQSLHGSEAD	-	-	-
YQCQSLHGSEADTLRKVLVEVL	-	-	-
TLRKVLVEVLADPLDHRDAGDL	-	-	-
ADPLDHRDAGDLWFPGESESFE	-	-	-
WFPGESESFEDAHVEHSISRSL	-	-	-

C

DC Number	Functional Class	Biacore Affinity (K_D) Human Specific No Mouse XR (nM)	H6 binding EC50 / FOB (200 nM)	Human Macrophage p-Syk IC_{50} (nM)	Human Macrophage pSyk max inhibition in %
Ab1	Antagonist	0.21	0.38 / 22.37	18.0	92
Ab2	Antagonist	4.5	0.18 / 26.28	11.9	98

D

E

F

$K_{on} = 1.4 \times 10^6\ M^{-1}s^{-1}$
$K_{off} = 3.0 \times 10^{-4}\ s^{-1}$
$K_D = 210\ pM$

G

$K_{on} = 1.1 \times 10^6\ M^{-1}s^{-1}$
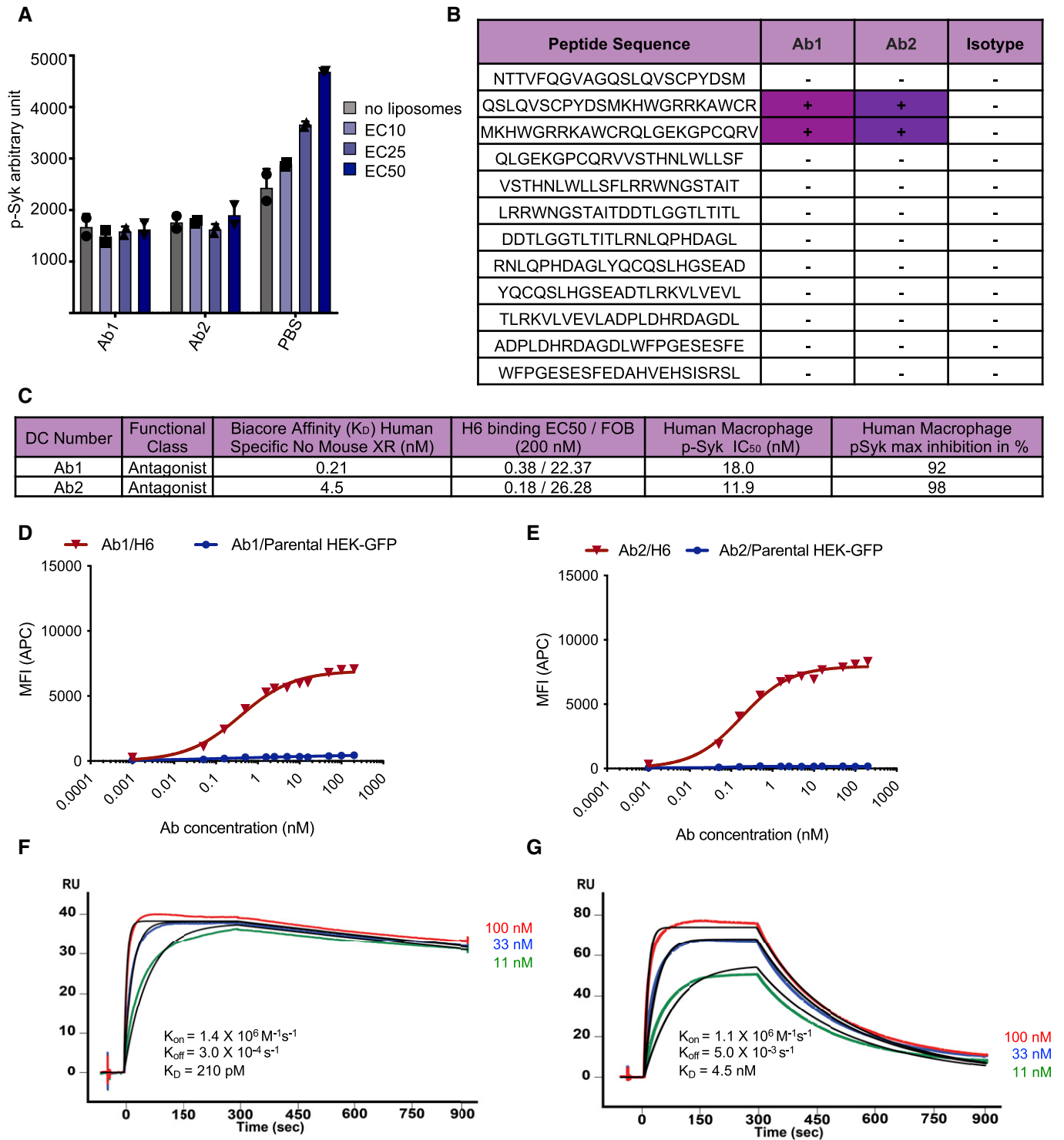$K_{off} = 5.0 \times 10^{-3}\ s^{-1}$
$K_D = 4.5\ nM$

Figure EV1.

**Figure EV1. Generation and characterization of TREM2 antagonistic antibodies.**

A   AlphaLISA quantification of p-Syk levels in HEK293 cells overexpressing TREM2-DAP12 upon treatment with Ab1 or Ab2 with three doses of liposomes (EC10: 0.0189527 mg/ml, EC25: 0.0633607 mg/ml, or EC50: 0.211731 mg/ml). PBS was used as a negative control. Individual data points are shown ($n = 2$ independent experiments).

B   Biochemical binding data of TREM2 IgV peptides to antagonistic antibodies Ab1 and Ab2, as well as isotype control. Positive data represent binding level above a threshold of 2*LLOD (lower limit of detection), from an average of three independent experiments.

C   Table of Ab1 and Ab2 with Biacore binding affinities, cell binding affinities, and liposome signaling (p-Syk) inhibition (EC50 and maximal inhibition) in human macrophage ($n = 3$ independent experiments).

D, E Cell-binding dose–response curves generated by FACS in HEK293 cells overexpressing TREM2/DAP12 versus parental lines shown as mean fluorescence intensity (MFI).

F, G Biacore binding measurements of immobilized antagonist antibody to three concentrations of recombinant hTREM2-ECD.

A

patient #	sex	Age of onset	Clinical diagnosis	*GRN* mutation	PGRN serum levels (in % of HC)
1	f	57	bvFTD	c.759_760del	26,7
2	f	61	dementia (PNFA/SD)	c.328C>T	16,9
3	f	65	bvFTD	c.709-2A>G	46,0
4	f	57	PNFA	c.675-676del	25,7

B

HC #	gender	Age
1	f	59
2	f	53
3	f	64
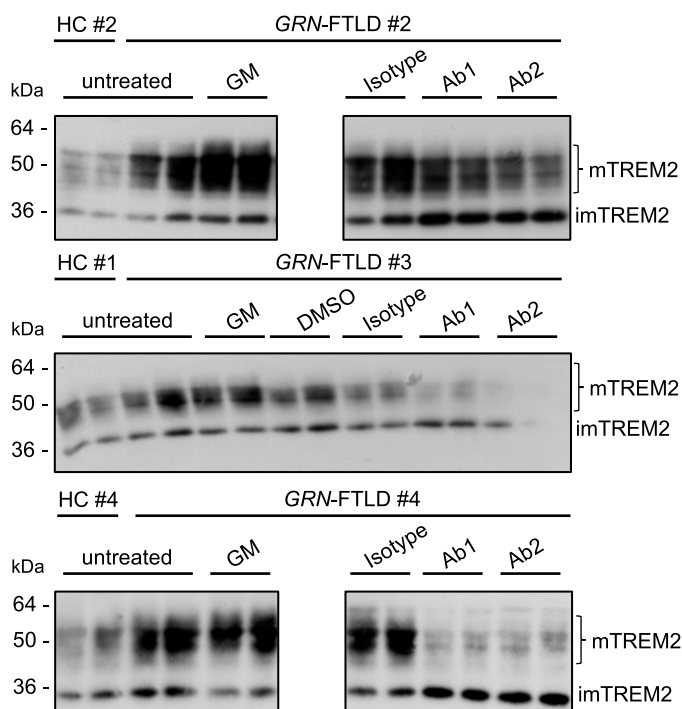
Figure EV2. *GRN*-FTLD patients.

A   Clinical data and mutation status of the four identified *GRN* mutation carriers and healthy controls. Mutation status of patients #1–3 was already confirmed before. The mutation status of patient #4 was detected by sequencing of exons including flanking sequences.

B   Clinical data of healthy controls (HC).

C   Western blot analysis of TREM2 using lysates of cultured human macrophages isolated from *GRN* mutation carriers (patients #2 to #4) (A) and healthy control upon treatment with Ab1 and Ab2. An isotype antibody was used as a negative control. ADAM protease inhibition (GM) does not further increase mTREM2 levels in PGRN mutation carriers. Equal amounts of protein were loaded.

C
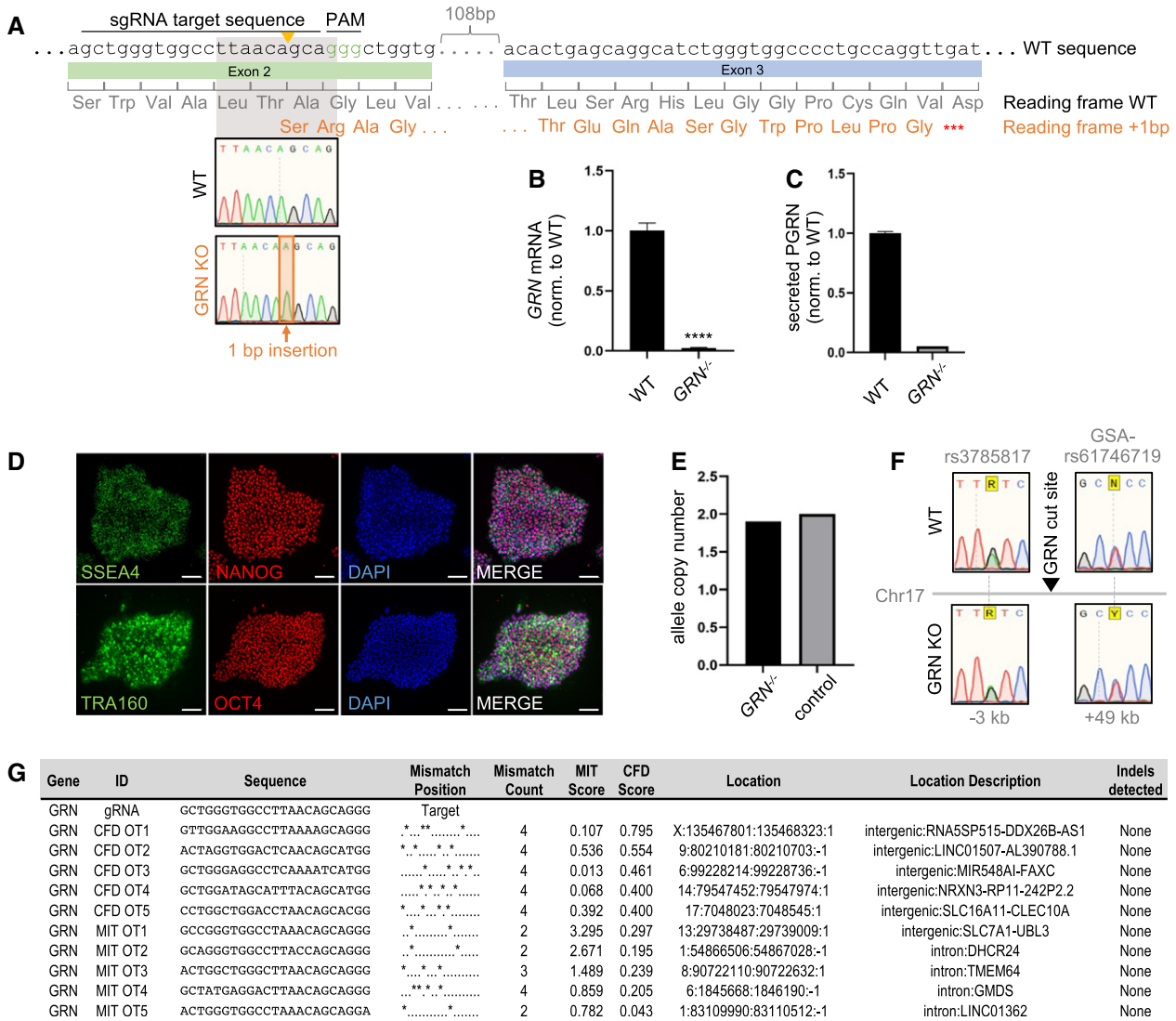
Figure EV3. Generation and characterization of GRN⁻/⁻ iPSC line.

A GRN knockout generation strategy: *GRN* was targeted in exon 2 by a sgRNA (target and PAM sequence indicated), leading to a one base pair insertion in the *GRN*⁻/⁻ line. The resulting frameshift exposes a nearby stop codon.

B *GRN* mRNA transcript levels in WT and *GRN*⁻/⁻ hiMGL normalized to WT, as measured by qPCR (n = 3, biological replicates).

C ELISA-mediated quantification of secreted PGRN in conditioned media of WT and *GRN*⁻/⁻ hiMGL (n = 3, biological replicates).

D Immunofluorescence analysis of pluripotency markers SSEA4, NANOG, TRA160, and OCT 4 with DAPI in *GRN*⁻/⁻ iPSCs. Scalebars = 100 µm.

E, F Analysis of CRISPR-mediated on-target effects by qgPCR quantitation of allele copy number (E) and Sanger sequencing of SNPs near the edited locus in WT and *GRN*⁻/⁻ iPSC lines (F) shows maintenance of both alleles after editing.

G List of top five most similar off-target sites ranked by the CFD and MIT prediction scores, respectively. No off-target editing was detected by Sanger sequencing.

Data information: Data represent the mean ± SD. For statistical analysis, the unpaired, two-tailed student's t-test was performed. Statistical significance was set at ****P < 0.0001, and ns, not significant.

Figure EV4. Differential gene expression in *Grn*$^{-/-}$ and *Trem2*$^{-/-}$ is partially rescued in *Double* KO mice.

A   Volcano plot presentation of the differently expressed transcripts in brains of 6-month-old male *Grn*$^{-/-}$ mice compared to WT brain mRNA (*n* = 4 per genotype). A total of 17 of 752 analyzed genes are significantly changed more than 20%, with 11 genes upregulated (purple) and 6 genes downregulated (blue).

B   Volcano plot presentation of the differently expressed genes in brain mRNA of 6-month-old male *Trem2*$^{-/-}$ mice in comparison to WT brain mRNA (*n* = 4 per genotype). A total of 16 of 752 analyzed genes are significantly changed by more than 20%, with 4 genes upregulated (purple) and 12 genes downregulated (blue).

C   Volcano plot presentation of the differently expressed genes in brain mRNA of 6-month-old male *Double*$^{-/-}$ mice in comparison to WT brain mRNA (*n* = 4 per genotype). A total of 25 of 752 analyzed genes are significantly changed by more than 20%, with 8 genes upregulated (purple) and 17 genes downregulated (blue).

D   Volcano plot presentation of the differently expressed transcripts in brains of 14-month-old male *Grn*$^{-/-}$ mice compared to WT brain mRNA (*n* = 3 per genotype). A total of 49 of 752 analyzed genes are significantly changed more than 20%, with 44 genes upregulated (purple) and 5 genes downregulated (blue).

E   Volcano plot presentation of the differently expressed genes in brain mRNA of 14-month-old male *Trem2*$^{-/-}$ mice in comparison to WT brain mRNA (*n* = 3 per genotype). A total of 7 of 752 analyzed genes are significantly changed by more than 20%, with 7 downregulated (blue).

F   Volcano plot presentation of the differently expressed genes in brain mRNA of 14-month-old male *Double*$^{-/-}$ mice in comparison to WT brain mRNA (*n* = 3 per genotype). A total of 21 of 752 analyzed genes are significantly changed by more than 20%, with 8 genes upregulated (purple) and 13 genes downregulated (blue).

G   Transcript levels of selected significantly rescued genes in *Double*$^{-/-}$ versus *Grn*$^{-/-}$ brain mRNA of 6-month-old (*n* = 4 per genotype) and 14-month-old mice (*n* = 3 per genotype). Transcript expression is normalized to the mean of the WT cohort.

Data information: Data represent mean $\pm$ SEM. For statistical analysis in G, the unpaired, two-tailed student's *t*-test was performed to compare *Grn*$^{-/-}$, *Trem2*$^{-/-}$, and *Double*$^{-/-}$ whole-brain mRNA expression. Statistical significance was set at *P < 0.05; **P < 0.01; ***P < 0.001; ****P < 0.0001, and ns, not significant.
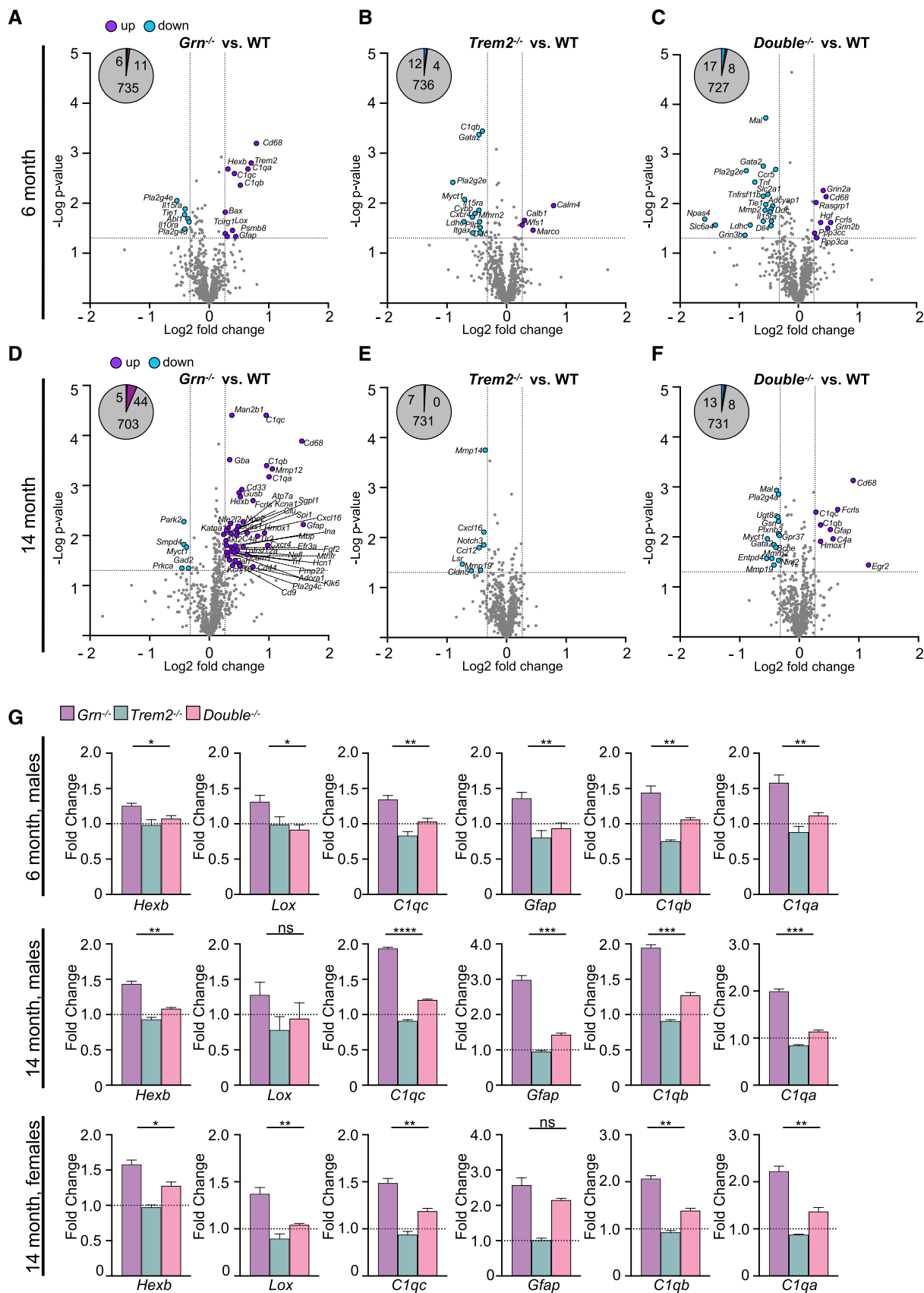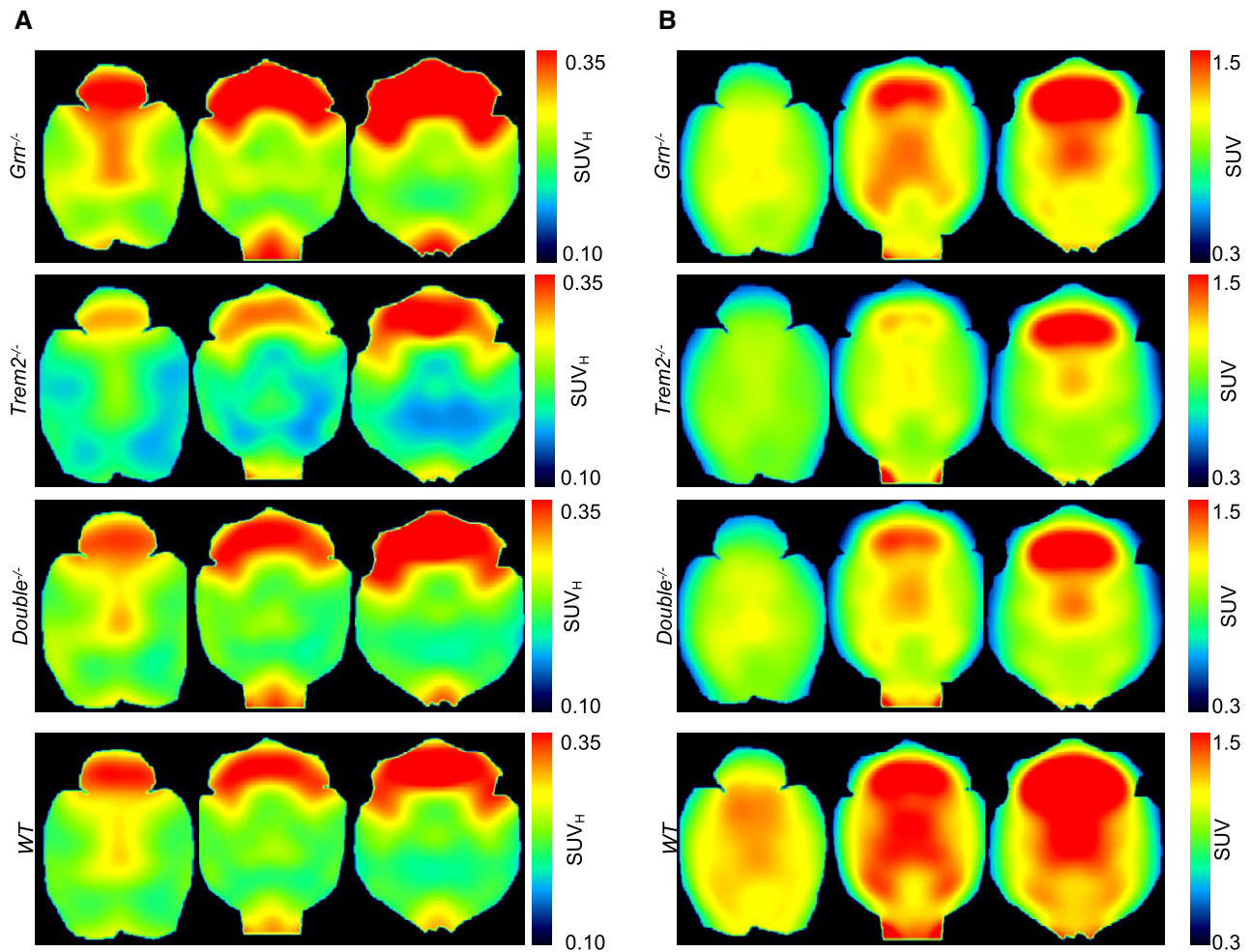
Figure EV4.

Figure EV5. Group-level PET images without MRI template overlay.

Group-averaged axial slices of TSPO-PET (SUV$_H$ scaling) and FDG-PET (SUV scaling) show microglia activity and glucose metabolism in comparison of $Grn^{-/-}$, $Trem2^{-/-}$, $Double^{-/-}$, and WT-type mice. Images represent the raw PET data used for calculation of %-differences in Figs 1A and 9E.

A   TSPO-PET images depict increased microglial activity in $Grn^{-/-}$ mice, reduced microglial activity in $Trem2^{-/-}$ mice, and similar levels of microglial activity in $Double^{-/-}$ and WT mice.

B   FDG-PET images indicate similar reduction in glucose uptake in $Grn^{-/-}$, $Trem2^{-/-}$, and $Double^{-/-}$ in comparison to WT mice.

Table of contents:

Appendix Figure S1 - Molecular karyotyping of *GRN*^{-/-} iPSC line

B allele frequencies (BAF) and Log R ratios are shown for each chromosome in the *GRN*^{-/-} iPSC line. Measured SNPs are indicated by blue dots. BAF values indicate normal zygosities on all chromosomes and Log R ratios confirm absence of detectable deletions or insertions. Overall, the karyotype shows no chromosomal aberrations.

A. Heatmap of significantly changed gene transcripts in whole brain of 6-month-old male *Grn*^{-/-}, *Trem2*^{-/-} and *Double*^{-/-} mice in comparison to WT (n=6 per genotype) detected using the Neuropathology panel by NanoString. Only genes of significantly changed transcript levels in *Grn*^{-/-} in comparison with WT mice are displayed. Changes in expression were only considered if changes are above 20%. mRNA counts for each gene and sample were normalized to the mean value of WT followed by a log2 transformation.

Appendix Figure S2 - Differential gene expression in *Grn*^{-/-} and *Trem2*^{-/-} is partially rescued in *Double* KO mice

A. Heatmap of significantly changed gene transcripts in whole brain of 6-month-old (n=4 per genotype) and 14-month-old (n=3 per genotype) male *Grn*^{-/-}, *Trem2*^{-/-} and *Double*^{-/-} mice in comparison to WT detected using the Neuropathology panel by NanoString. Only genes of significantly changed transcript levels in *Grn*^{-/-} in comparison with WT mice are displayed. mRNA counts for each gene and sample were normalized to the mean value of WT followed by a log2 transformation.

B. Heatmap of significantly changed gene transcripts in whole brain of 6-month-old (n=4 per genotype) and 14-month-old (n=3 per genotype) male *Grn*^{-/-}, *Trem2*^{-/-} and *Double*^{-/-} mice in comparison to WT detected using the Neuropathology panel by NanoString. Only genes of significantly changed transcript levels in *Double*^{-/-} in comparison with WT mice are displayed. mRNA counts for each gene and sample were normalized to the mean value of WT followed by a log2 transformation.

Appendix Figure S3 - Differential gene expression in *Grn*^{-/-} and *Trem2*^{-/-} is partially rescued in *Double* KO mice

A. Heatmap of significantly changed gene transcripts in whole brain of 6-month-old (n=4 per genotype) and 14-month-old (n=3 per genotype) female *Grn*^{-/-}, *Trem2*^{-/-} and *Double*^{-/-} mice in comparison to WT detected using the Neuropathology panel by NanoString. Only genes of significantly changed transcript levels in *Grn*^{-/-} in comparison with WT mice are displayed. mRNA counts for each gene and sample were normalized to the mean value of WT followed by a log2 transformation.
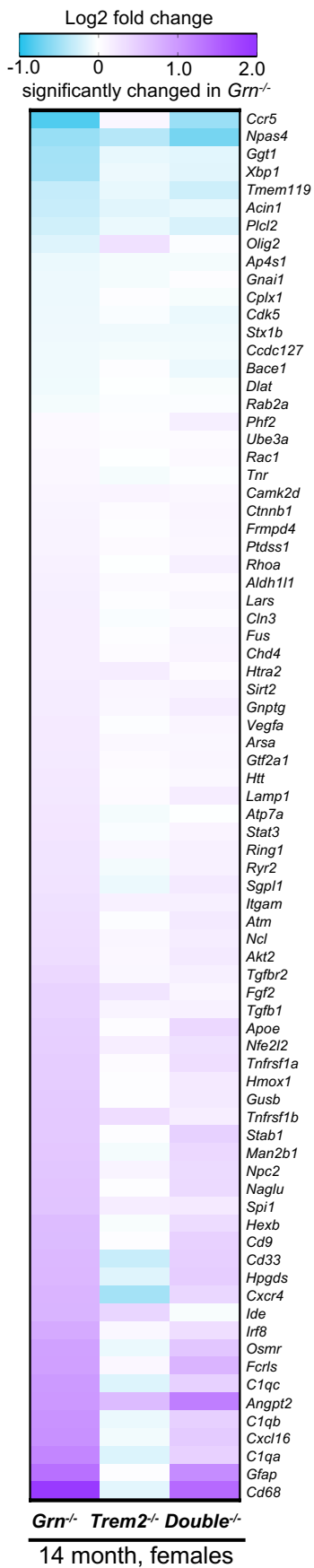
3

Appendix Figure S2, Reifschneider et al.

Appendix Figure S3, Reifschneider et al.
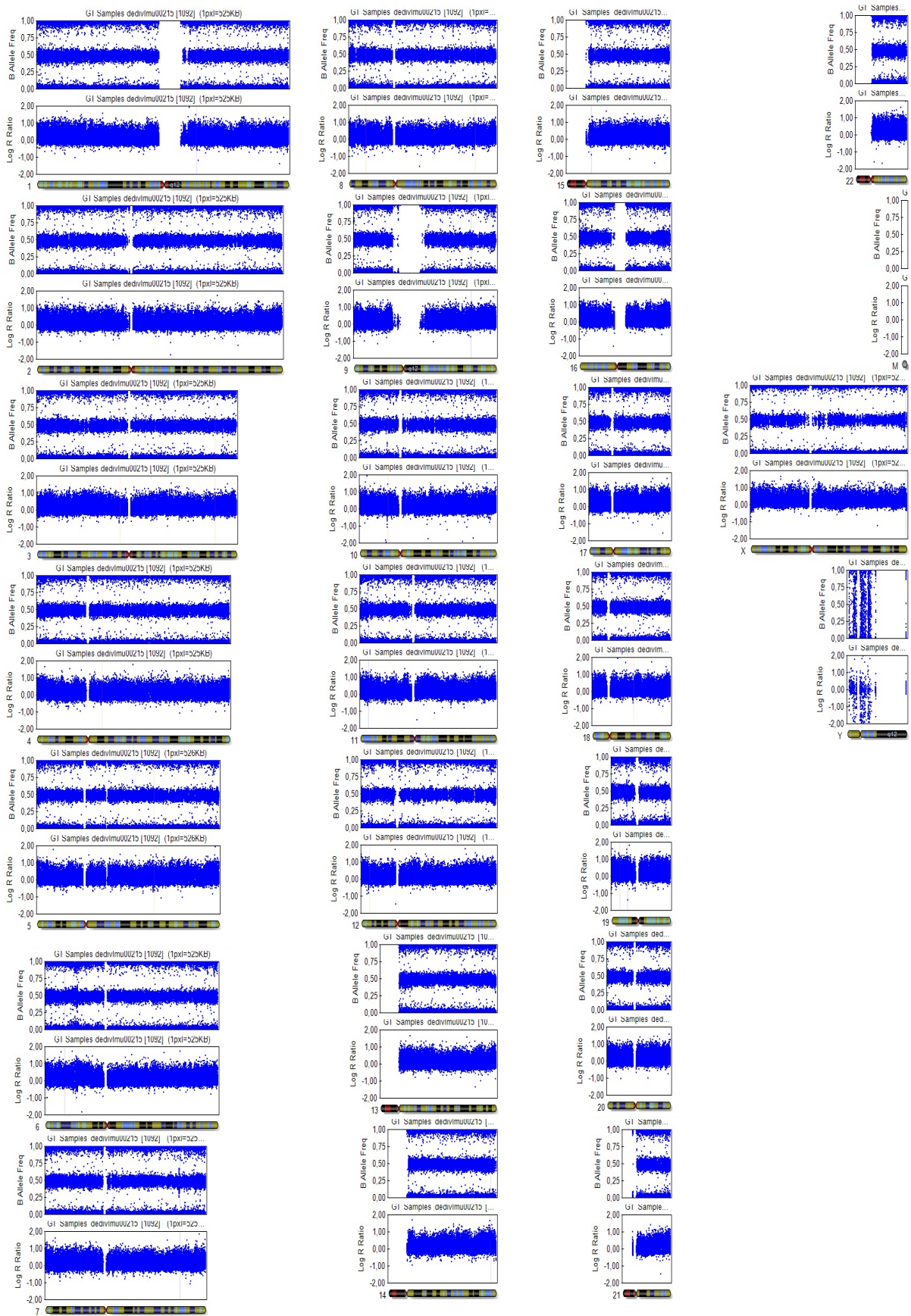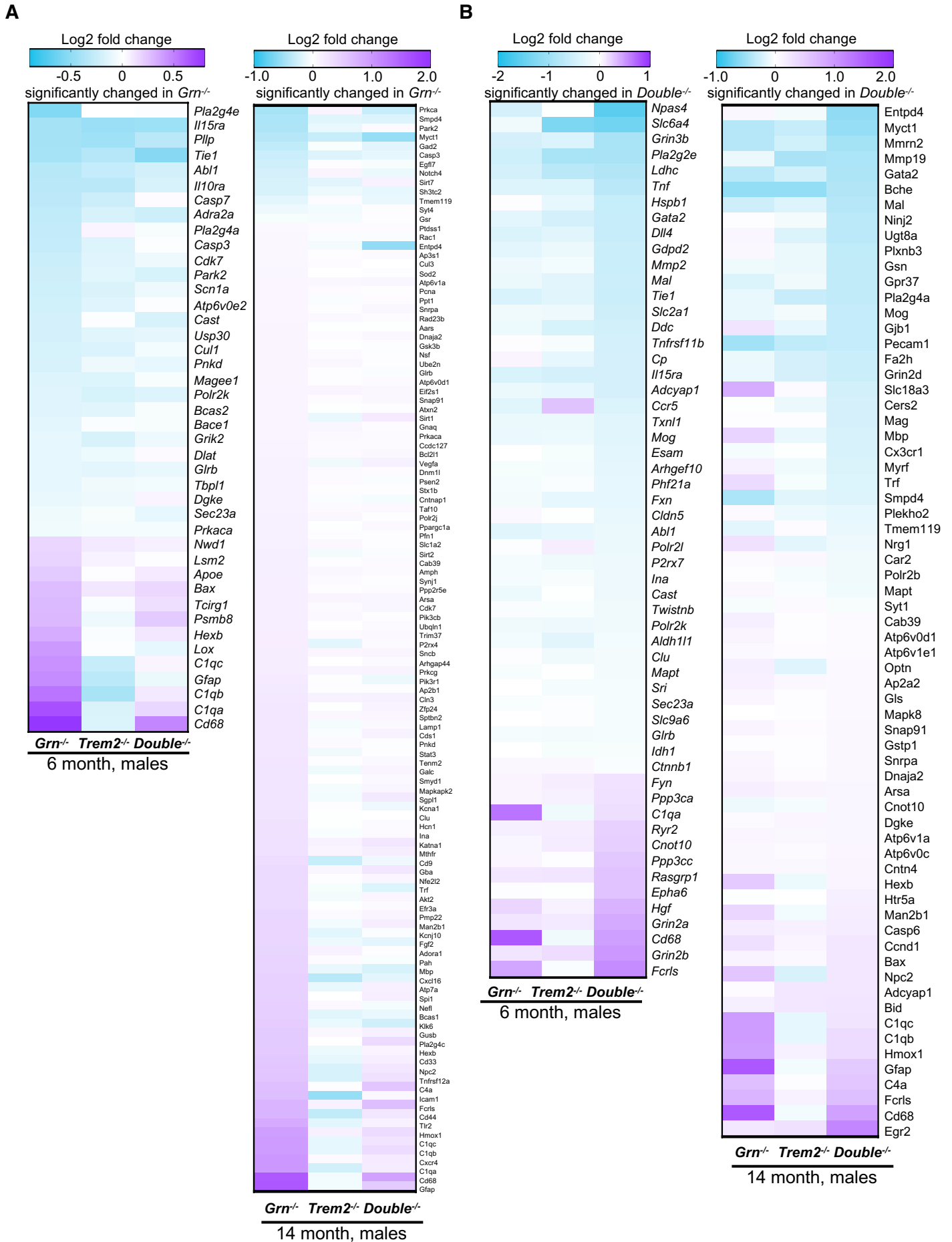
3.2 Enhanced legumain activity links progranulin deficiency to TDP-43 pathology in frontotemporal dementia

Capell A, **Robinson S***, Reich M*, Reifschneider A, Buschmann K, Riemenschneider H, Wauters E, Mühlhofer Q, Werner G, Ahles A, Engelhardt S, Reinheckel T, Edbauer D, Simon MJ, Logan T, Di Paolo G, Van Broeckhoven C, Damme M, Paquet D, Haass C: Enhanced legumain activity links progranulin deficiency to TDP-43 pathology in frontotemporal dementia.

Manuscript in preparation.

Enhanced legumain activity links progranulin deficiency to TDP-43 pathology in frontotemporal dementia

Anja Capell[1+], Sophie Robinson[2,3#], Marvin Reich[2,3#], Anika Reifschneider[1], Katrin Buschmann[1], Henrick Riemenschneider[2], Eline Wauters[4,5], Quirin Mühlhofer[1], Georg Werner[1], Andrea Ahles[6], Stefan Engelhardt[6], Thomas Reinheckel[7], Dieter Edbauer[2,8], Matthew J. Simon[9], Todd Logan[9], Gilbert Di Paolo[9], Christine Van Broeckhoven[4,5], Markus Damme[10], Dominik Paquet[3,8], Christian Haass[1,2,8+]

[1]Biomedical Center (BMC), Division of Metabolic Biochemistry Faculty of Medicine, Ludwig-Maximilians-Universität München, 81377 Munich, Germany

[2]German Center for Neurodegenerative Diseases (DZNE) Munich, 81377 Munich, Germany

[3]Institute for Stroke and Dementia Research (ISD), University Hospital, Ludwig-Maximilians-Universität München, Munich, Germany.

[4]Neurodegenerative Brain Diseases Group, Center for Molecular Neurology, VIB, Antwerp, Belgium.

[5]Department of Biomedical Sciences, University of Antwerp, Antwerp, Belgium.

[6]Institute of Pharmacology and Toxicology, Technical University of Munich, Munich, Germany.

[7]Institute of Molecular Medicine and Cell Research, University of Freiburg, Freiburg, Germany

[8]Munich Cluster for Systems Neurology (SyNergy), Munich, Germany.

[9]Denali Therapeutics Inc., South San Francisco, USA

[10]Institute of Biochemistry, Kiel University, Kiel, Germany.

[#] Contributed equally

[+]Correspondence:

anja.capell@mail03.med.uni-muenchen.de

christian.haass@dzne.de

Loss-of-function mutations in *GRN* are a main genetic cause of frontotemporal lobar degeneration (FTLD) with TDP-43-positive inclusions in neurons and glia but the mechanistic link remains elusive [1-3]. Progranulin (PGRN) is primarily expressed by microglia [4,5] and functions as a secreted growth factor-like protein in the brain [6]. Intracellularly, PGRN is transported to lysosomes, where it is processed into granulin peptides [7-9]. PGRN loss leads to lysosomal dysfunction and hyperactivation of microglia. How PGRN modulates lysosomal function and TDP-43 deposition is largely unknown. We found that PGRN slows maturation and limits proteolytic activity of the lysosomal protease legumain (LGMN). Proteolytic activity of LGMN is strongly elevated in brains of *Grn* knockout (ko) mice, in human induced pluripotent stem cell- (hiPSC) derived ko microglia, and in brains of *GRN*-FTLD patients. Strikingly, increased LGMN activity promoted proteolytic processing of TDP-43 into fragments enriched in inclusions. In a negative feedback loop LGMN proteolytically processes PGRN into granulin peptides which no longer inhibits LGMN activation. Enhanced LGMN activity in *Grn* ko brains is rescued with a brain penetrant progranulin biologic. Our findings reveal a direct link between PGRN and TDP-43 pathology and underscore the central role of PGRN in the regulation of lysosomal activity *via* inhibition of LGMN maturation. Thus, LGMN inhibitors and PGRN replacement strategies may be a novel treatment strategy for FTLD and other neurodegenerative diseases with pronounced TDP-43 co-pathology such as Alzheimer's disease, Lewy Body disorder, and hippocampal sclerosis.

Main

Loss of PGRN causes lysosomal dysfunction with altered cathepsin maturation and initiates pathological processing of TAR DNA binding protein 43 (TDP-43) and subsequent deposition of the cleavage products in disease defining deposits [4,10]. To establish a functional link between PGRN and proteolytic TDP-43 processing, we searched for proteases regulated by PGRN that play key roles in activation of lysosomal hydrolases and could potentially cleave TDP-43. LGMN (asparaginyl endopeptidase, AEP), a caspase-like cysteine protease of the C13 peptidase family emerged as a prime candidate, as it is involved in the proteolytic activation of various

cathepsins [11,12] and, based on *in vitro* experiments, is capable of cleaving TDP-43 [13]. Thus, we investigated LGMN maturation and enzymatic activity in the presence and absence of PGRN. In brains of *Grn* ko mice, LGMN enzymatic activity was significantly increased at all investigated ages (Fig. 1a). This was accompanied by enhanced levels of mature LGMN as monitored by its conversion from the pro-/immature variants to the mature catalytically active variant (Fig. 1b), while mRNA levels were not affected in young mice and only slightly elevated in aged *Grn* ko mice (Fig. 1c). Enhanced expression, maturation and activity of LGMN in the absence of PGRN was further confirmed in mouse embryonic fibroblasts (MEF) obtained from wt and *Grn* ko mice (Fig. 1d–e). Moreover, re-expression of PGRN in *Grn* ko MEF rescued LGMN hyperactivity (Extended Data Fig. 1). Importantly, knockdown of LGMN blunts the increased maturation of cathepsins D, L, and B in the *Grn* ko cells we had reported previously (Fig. 1d–f) [4]. PGRN deficiency is associated with altered maturation of cathepsins D, L and B and these defects are all rescued upon knockdown of LGMN, further supporting a central role of PGRN in modulating LGMN activity (Fig. 1d–f). Thus, these findings suggest that PGRN suppresses LGMN activity and may fine tune lysosomal activation of cathepsins.

Since PGRN is predominantly expressed by microglia within the brain [4,5], while TDP-43 inclusions are mainly found in neurons and less abundant in astroglia, we next investigated cell type-dependent LGMN expression. LGMN and PGRN are both strongly enriched in acutely isolated microglia (Fig. 1g; Extended Data Fig. 2a), which also display the highest LGMN activity (Fig. 1h; Extended Data Fig. 2b). Moreover, microglia show efficient LGMN maturation (Fig. 1g; Extended Data Fig. 2a). In line with the findings shown above, loss of PGRN results in higher LGMN activity in isolated microglia from young and aged mice (Fig. 1g; Extended Data Fig. 2b), while mRNA levels were not elevated (Fig. 1i). Although only very little expression and activity of LGMN was detected within neurons and astrocytes, upon loss of PGRN, the relative increase of the activity in neurons was even stronger than in microglia (Fig. 1h, Extended Data Fig. 2b). Elevated LGMN activity upon PGRN deficiency was also confirmed in cultured primary microglia isolated from wt and *Grn* ko mice (Fig. 1j).

To determine how PGRN regulates LGMN, we investigated whether it directly affects its catalytic activity or interferes with its proteolytic activation. With decreasing pH during its transport to endosomes/lysosomes LGMN is autoproteolytically activated in multiple steps and processed to its final approximately 43 kDa mature form by

1 unknown proteases (Fig. 2a) [14-16]. In lysates of MEF, we detected the proform, the

2 intermediate and the mature variants of LGMN (Fig. 2b). Consistent with a pH-

3 dependent processing of LGMN, in MEF cells LGMN activation is inhibited by blocking

4 the V-type ATPase with bafilomycin A1 (Fig. 2b). Moreover, autocatalytic *in vitro*

5 maturation of the proform to an intermediate variant is facilitated by an acidic pH (Fig.

6 2b). Since we detected more mature LGMN upon PGRN deficiency, we next

7 investigated whether PGRN can influence autocatalytic LGMN maturation [17].

8 Autocatalytic maturation of the recombinant LGMN (rLGMN) proform was monitored

9 at pH 4.0 with and without recombinant PGRN (rPGRN). Proteolytic *in vitro* maturation

10 and enzymatic activation of rLGMN under acidic conditions was significantly slowed in

11 the presence of rPGRN (Fig. 2c–d). Moreover, the presence of rPGRN reduced

12 proteolytic rLGMN activity in a dose-dependent manner with an IC_{50} of 39.28 nM

13 rPGRN (Fig. 2e). However, after full autocatalytic maturation (Fig. 2c), the catalytic

14 activity of rLGMN was identical in the presence and absence of rPGRN (Fig. 2d). While

15 adding PGRN to an *in vitro* activity assay containing activated rLGMN did not affect

16 the catalytic activity of rLGMN (Fig. 2f), activity was reduced when PGRN was added

17 to the rLGMN proform during activation (Fig. 2g). Thus, PGRN does not affect the

18 catalytic activity of LGMN *per se*, but rather slows its autocatalytic maturation.

19 Furthermore, granulin peptides generated from PGRN by elastase digest, neither

20 inhibited *in vitro* maturation nor affected catalytic activity of rLGMN (Fig. 2f–h). Taken

21 together, only full-length PGRN interferes with LGMN activation. Intriguingly, PGRN

22 itself is also a substrate of LGMN as rLGMN efficiently generates granulin peptides *in*

23 *vitro* (Fig. 2i). *In vivo*, granulin peptides are readily detected within purified lysosomes

24 of wt mice (Fig. 2j). In the absence of LGMN, granulin peptides are substantially

25 reduced (Fig. 2j). Hence, LGMN regulates its own maturation by processing of PGRN

26 in a negative feedback loop. However, LGMN is not the only PGRN processing

27 enzyme, since deficiency of cathepsin L also substantially reduces granulin peptides

28 [7,9], while sortilin1, a transport receptor for PGRN [18] does not affect granulin peptide

29 production (Fig. 2j).

30 *GRN* haploinsufficiency is associated with TDP-43 deposition, but the molecular link is

31 unclear [1,2,19]. Since TDP-43 is known to undergo proteolytic processing ([20,21] reviewed

32 in [22]) and contains a number of cleavage sites for LGMN [13] (Fig. 3a), we investigate if

33 the lack of PGRN affects pathological processing of TDP-43 *via* enhanced LGMN

34 activity using a panel of TDP-43 antibodies (Fig. 3a). In lysates derived from MEF we

detected enhanced proteolytic processing of full-length TDP-43 and TDP-43 fragment (TDP-43F) generation in the absence of PGRN, which was fully rescued upon siRNA mediated knockdown of LGMN (Fig. 3b). Moreover, even in the presence of PGRN, reduction of LGMN was sufficient to reduce TDP-43 processing (Fig. 3b). Furthermore, C-terminal fragments (TDP-43CTF) of TDP-43 reminiscent of those observed in FTLD cases [13] are generated in a LGMN dependent manner in the absence of PGRN (Fig. 3b). Full-length TDP-43 and consequently TDP-43F are further truncated by LGMN, because an antibody (CT-abshort) directed to the C-terminal 10 amino acids of TDP-43 detected only smaller TDP-43CTF (Fig. 3b). siRNA-mediated reduction of LGMN prevents C-terminal clipping and TDP-43CTF formation, demonstrating that these processing events are LGMN-dependent (Fig. 3b). Taken together, these findings suggest that the reduction of PGRN results in enhanced LGMN activation, which in turn mediates pathological processing of TDP-43.

Neurons, the cell type primarily presenting TDP-43 pathology in patients, express substantially less PGRN and LGMN and therefore show much less LGMN activity compared to microglia (Fig. 1g–h, Extended Data Fig. 2a–b). We therefore speculated that malfunctional microglia may secrete LGMN, which could be taken up by neurons, where it then mediates pathological TDP-43 processing. In line with that, pathological formation of TDP-43CTF in rat hippocampal neurons accompanied by a reduction of the holoprotein occurs upon neuronal expression of wt LGMN but not a catalytically inactive variant (Fig. 3c, d). To provide evidence that the catalytically inactive LGMN proform can be taken up and activated by neurons, we incubated primary mouse hippocampal neurons with conditioned media from LGMN expressing HeLa cells. Conditioned media contain significant amounts of the inactive, secreted LGMN proform (Fig. 3e). Only secreted wt LGMN is autocatalytically activated upon incubation under acidic conditions and no activity was observed in conditioned media of mutant LGMN or non-transfected HeLa cells (Extended Data Fig. 3a–b). Both, wt and mutant LGMN were taken up and proteolytically processed by neurons but only neurons incubated with wt LGMN show increased catalytic activity (Fig. 3f–g). Moreover, only upon uptake of wt LGMN, substantial pathological processing of TDP-43 is observed, as indicated by the production of the TDP-43CTF (Fig. 3f).

To provide evidence for a pathological link between PGRN reduction, LGMN activation and enhanced TDP-43 processing in humans, we generated a human iPSC line lacking PGRN (Extended Data Fig. 4a–g). Upon differentiation into human iPSC-

derived microglia (hiMG), PGRN deficient (*GRN* ko) hiMG express substantially elevated levels of LGMN accompanied by a significantly enhanced proteolytic activity of LGMN compared to wt hiMG (Fig. 4a–b). In line with our findings in mice, iPSC-derived wt or PGRN deficient human neurons (hiN) show almost no LGMN expression and activity (Fig. 4a–b). Upon co-culture of both cell types, we observe substantially increased TDP-43 processing, which is further elevated when *GRN* ko hiMG are co-cultured with wt hiN (Fig. 4c). This is in line with increased LGMN activity in *GRN* ko hiMG co-cultured with hiN. (Fig. 4d). LGMN-dependent TDP-43 processing is inhibited upon selective neuronal expression of cystatin-7 (Fig. 4c–e, Extended Data Fig. 5a–c). The full rescue of TDP-43 processing upon cystatin-7 expression suggests that LGMN is the TDP-43 processing protease which is enhanced by PGRN deficiency.

Based on our results in human brain cells and mouse models, we assessed LGMN dysregulation in brains of patients suffering from *GRN*-FTLD and observed increased proteolytic activity and maturation of this hydrolase in patient brains relative to controls (Fig. 4f–g). Thus, pathologically increased LGMN activity upon reduction of PGRN expression was observed in mice, MEF, primary murine microglia, human microglia and finally in the brain of FTLD patients with *GRN* haploinsufficiency.

Our findings prompted us to investigate, if the PGRN-LGMN axis could be therapeutically modulated. In this context, the rescue of PGRN deficiency-associated phenotypes *via* a brain penetrant PGRN biologic, referred to as protein transport vehicle (PTV):PGRN, was recently demonstrated [23]. PTV:PGRN exhibits increased brain penetrance in mice due to its ability to bind to transferrin receptor, which facilitates transcytosis across endothelial cells of the blood-brain-barrier. We thus evaluated the ability of PTV:PGRN to modulate brain LGMN activity and maturation 7 and 14 days after single intravenous injection of the biologic at 10 mg/kg into *Grn* ko mice expressing a humanized transferrin receptor (*Grn* ko/ h*TfR* ki mice) (Fig. 5a). PTV:PGRN reduced maturation and activity of LGMN at 14 days post-injection with a trend for a decrease at 7 days (Fig. 5b–c), demonstrating that a novel PGRN replacement strategy reduces pathological activation of a TDP-43 processing enzyme after just a single dose of the biologic.

Taken together, our findings suggest that enhanced LGMN activity in brains of *GRN*-FTLD patients provides a direct link between TDP-43 pathology and *GRN* haploinsufficiency. In various model systems including two independent PGRN deficient mouse lines, MEF, mouse and human microglia and finally in brains of

patients, we consistently found significantly elevated LGMN activity. This indicates that PGRN inhibits LGMN maturation presumably in a chaperone-like manner during trafficking to lysosomes. This inhibitory effect is balanced by LGMN itself, as the hydrolase also processes PGRN into granulin peptides [24], which are not capable of interfering with LGMN maturation. Pathologically enhanced LGMN activity leads to aberrantly increased processing of lysosomal cathepsins, which, consistent with previous findings, may result in dysregulation and malfunction of microglial lysosomes [4,25-27]. While based on our data, direct processing of TDP-43 by LGMN seems likely, a contribution of other proteases activated by LGMN cannot be completely excluded. Our findings support a model where LGMN released by PGRN deficient microglia is taken up by neurons, where it is activated and capable of processing TDP-43, thus resolving the spatial paradox of the differential expression of LGMN and PGRN predominantly in microglia and TDP-43 in neurons. Since TDP-43$_{CTF}$ formation removes the nuclear localization signals of TDP-43, it may allow its cytoplasmic accumulation and aggregation. However, since neuronal LGMN activity also increases upon loss of PGRN (see Fig. 1h), cell autonomous misprocessing of TDP-43 may also contribute to its deposition. If aberrantly elevated LGMN activity also affects complement factor activation [28] remains to be investigated. As *GRN*-FTLD patients also present with co-pathology of additional LGMN substrates, namely tau and α-synuclein, it is conceivable that their accumulation and deposition may also be facilitated by aberrantly enhanced LGMN activity [29-31]. Finally, since TDP-43 pathology and lysosomal dysfunction co-exist in other neurodegenerative diseases such as Alzheimer's disease, Lewy Body dementia and hippocampal sclerosis [32,33] our findings may reveal a disease overarching pathway, which could be modulated by LGMN inhibitors and PGRN replacement strategies.

References

1 Baker, M. *et al.* Mutations in progranulin cause tau-negative frontotemporal dementia linked to chromosome 17. *Nature* **442**, 916-919 (2006).
2 Cruts, M. *et al.* Null mutations in progranulin cause ubiquitin-positive frontotemporal dementia linked to chromosome 17q21. *Nature* **442**, 920-924 (2006).
3 Gass, J. *et al.* Mutations in progranulin are a major cause of ubiquitin-positive frontotemporal lobar degeneration. *Hum Mol Genet* **15**, 2988-3001 (2006).
4 Gotzl, J. K. *et al.* Early lysosomal maturation deficits in microglia triggers enhanced lysosomal activity in other brain cells of progranulin knockout mice. *Mol Neurodegener* **13**, 48 (2018).
5 Lui, H. *et al.* Progranulin Deficiency Promotes Circuit-Specific Synaptic Pruning by Microglia via Complement Activation. *Cell* **165**, 921-935 (2016).

6   He, Z. & Bateman, A. Progranulin (granulin-epithelin precursor, PC-cell-derived growth factor, acrogranin) mediates tissue repair and tumorigenesis. *J Mol Med* **81**, 600-612 (2003).

7   Zhou, X. *et al.* Lysosomal processing of progranulin. *Mol Neurodegener* **12**, 62 (2017).

8   Holler, C. J., Taylor, G., Deng, Q. & Kukar, T. Intracellular Proteolysis of Progranulin Generates Stable, Lysosomal Granulins that Are Haploinsufficient in Patients with Frontotemporal Dementia Caused by GRN Mutations. *eNeuro* **4** (2017).

9   Lee, C. W. *et al.* The lysosomal protein cathepsin L is a progranulin protease. *Mol Neurodegener* **12** (2017).

10   Root, J., Merino, P., Nuckols, A., Johnson, M. & Kukar, T. Lysosome dysfunction as a cause of neurodegenerative diseases: Lessons from frontotemporal dementia and amyotrophic lateral sclerosis. *Neurobiol Dis* **154**, 105360, doi:10.1016/j.nbd.2021.105360 (2021).

11   Shirahama-Noda, K. *et al.* Biosynthetic processing of cathepsins and lysosomal degradation are abolished in asparaginyl endopeptidase-deficient mice. *J Biol Chem* **278**, 33194-33199 (2003).

12   Maehr, R. *et al.* Asparagine endopeptidase is not essential for class II MHC antigen presentation but is required for processing of cathepsin L in mice. *J Immunol* **174**, 7066-7074 (2005).

13   Herskowitz, J. H. *et al.* Asparaginyl endopeptidase cleaves TDP-43 in brain. *Proteomics* **12**, 2455-2463 (2012).

14   Dall, E. & Brandstetter, H. Mechanistic and structural studies on legumain explain its zymogenicity, distinct activation pathways, and regulation. *Proc Natl Acad Sci U S A* **110** (2013).

15   Halfon, S., Patel, S., Vega, F., Zurawski, S. & Zurawski, G. Autocatalytic activation of human legumain at aspartic acid residues. *FEBS Lett* **438**, 114-118 (1998).

16   Li, D. N., Matthews, S. P., Antoniou, A. N., Mazzeo, D. & Watts, C. Multistep autoactivation of asparaginyl endopeptidase in vitro and in vivo. *J Biol Chem* **278**, 38980-38990 (2003).

17   Dall, E. & Brandstetter, H. Structure and function of legumain in health and disease. *Biochimie* **122**, 126-150 (2016).

18   Hu, F. *et al.* Sortilin-mediated endocytosis determines levels of the frontotemporal dementia protein, progranulin. *Neuron* **68**, 654-667 (2010).

19   Mackenzie, I. R. The neuropathology and clinical phenotype of FTD with progranulin mutations. *Acta Neuropathol* **114**, 49-54 (2007).

20   Neumann, M. *et al.* Ubiquitinated TDP-43 in frontotemporal lobar degeneration and amyotrophic lateral sclerosis. *Science* **314**, 130-133 (2006).

21   Igaz, L. M. *et al.* Enrichment of C-terminal fragments in TAR DNA-binding protein-43 cytoplasmic inclusions in brain but not in spinal cord of frontotemporal lobar degeneration and amyotrophic lateral sclerosis. *Am J Pathol* **173**, 182-194 (2008).

22   Buratti, E. TDP-43 post-translational modifications in health and disease. *Expert Opin Ther Targets* **22**, 279-293 (2018).

23   Logan, T. *et al.* Rescue of a lysosomal storage disorder caused by Grn loss of function with a brain penetrant progranulin biologic. *Cell*, doi:10.1016/j.cell.2021.08.002 (2021).

24   Mohan, S. *et al.* Processing of progranulin into granulins involves multiple lysosomal proteases and is affected in frontotemporal lobar degeneration. *Mol Neurodegener* **16**, 51, doi:10.1186/s13024-021-00472-1 (2021).

25   Tanaka, Y. *et al.* Progranulin regulates lysosomal function and biogenesis through acidification of lysosomes. *Hum Mol Genet* **26**, 969-988 (2017).

26   Gotzl, J. K. *et al.* Common pathobiochemical hallmarks of progranulin-associated frontotemporal lobar degeneration and neuronal ceroid lipofuscinosis. *Acta Neuropathol* **127**, 845-860 (2014).

27   Klein, Z. A. *et al.* Loss of TMEM106B Ameliorates Lysosomal and Frontotemporal Dementia-Related Phenotypes in Progranulin-Deficient Mice. *Neuron* **95**, 281-296 e286 (2017).

28   Zhang, J. *et al.* Neurotoxic microglia promote TDP-43 proteinopathy in progranulin deficiency. *Nature* **588**, 459-465 (2020).

29   Hosokawa, M. *et al.* Accumulation of multiple neurodegenerative disease-related proteins in familial frontotemporal lobar degeneration associated with granulin mutation. *Sci Rep* **7**, 1513 (2017).

30   Zhang, Z. *et al.* Cleavage of tau by asparagine endopeptidase mediates the neurofibrillary pathology in Alzheimer's disease. *Nat Med* **20**, 1254-1262 (2014).

31   Zhang, Z. *et al.* Asparagine endopeptidase cleaves alpha-synuclein and mediates pathologic activities in Parkinson's disease. *Nat Struct Mol Biol* **24** (2017).

32   Huang, W. *et al.* TDP-43: From Alzheimer's Disease to Limbic-Predominant Age-Related TDP-43 Encephalopathy. *Front Mol Neurosci* **13** (2020).

33   Cook, C., Zhang, Y. J., Xu, Y. F., Dickson, D. W. & Petrucelli, L. TDP-43 in neurodegenerative disorders. *Expert Opin Biol Ther* **8**, 969-978 (2008).

34   Kametani, F. *et al.* Mass spectrometric analysis of accumulated TDP-43 in amyotrophic lateral sclerosis brains. *Sci Rep* **6** (2016).
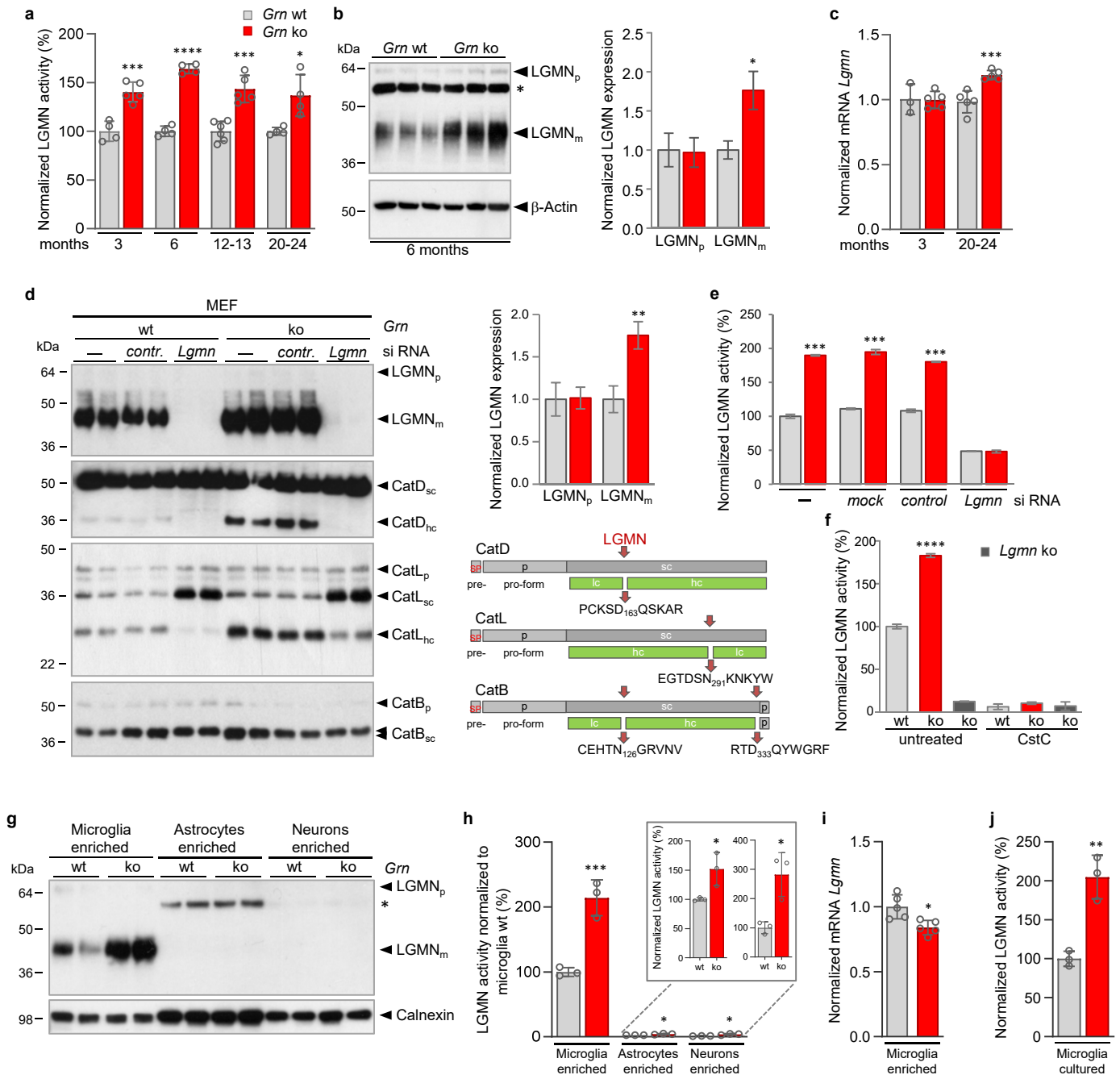
Fig. 1: PGRN deficiency leads to enhanced LGMN maturation and elevated activity accompanied by altered cathepsin processing.

a, *In vitro* LGMN activity of brain homogenate from 3-,6-,12-13-, and 20-24-month-old wild type (wt) and *Grn* knockout (ko) mice (n=4-6 per genotype and age group). **b**, Representative immunoblot for LGMN in total brain homogenate of 6-month-old wt and *Grn* ko mice. Proform (LGMN$_p$), mature form (LGMN$_m$), unspecific band (asterisk) are indicated, β-actin verified equal loading. Quantification of the immunoblot signals normalized to wt (n=3 mice per genotype). **c**, total brain mRNA of 3- and 20-24-month-old mice normalized to wt (n=4-5). **d**, Representative immunoblots of MEF isolated from wt and *Grn* ko mice probed for LGMN, cathepsin D (CatD), cathepsin L (CatL), and cathepsin B (CatB); proform (p), mature (m), single chain (sc), heavy chain (hc) are indicated and cathepsin processing by LGMN is schematically shown. MEF are either non-transfected (-), *control* (*contr.*) or *Lgmn* siRNA transfected. LGMN expression is quantified and normalized to wt. **e**, *In vitro* LGMN activity of non-transfected (-), mock, *control* and *Lgmn* siRNA transfected *Grn* ko MEF normalized to corresponding wt MEF (n=3). **f**, *In vitro* LGMN activity with/without cystatin-3 (2 ng/µl) of wt, *Grn* ko and *Lgmn* ko MEF, normalized to wt (n=3). **g**, Representative immunoblot for LGMN in microglia-, astrocyte- and neuron-enriched brain cell fractions of 4-5-month-old wt and *Grn* ko mice. Proform (LGMN$_p$) and mature form (LGMN$_m$) are indicated, calnexin verified equal loading. **h**, Microglia-, astrocyte- and neuron-enriched fractions from 4-5-month-old *Grn* ko and wt mice analyzed for LGMN activity either normalized to wt microglia or to wt of the respective cell type (insert); n=3 mice per cell type and genotype. **i**, *Lgmn* mRNA of 6-month-old *Grn* ko mice normalized to wt; (n=5). **j**, LGMN *in vitro* activity in lysates of cultured microglia; n=3 mice per genotype.

Data are mean ± s.d. of biologically independent experiments (d,e,f), for all mice replicates individual values are shown; unpaired two-tailed t-test *p<0.5, **p<0.01, ***p<0.001, ****p<0.0001. *P* values and statistical source data are provided.
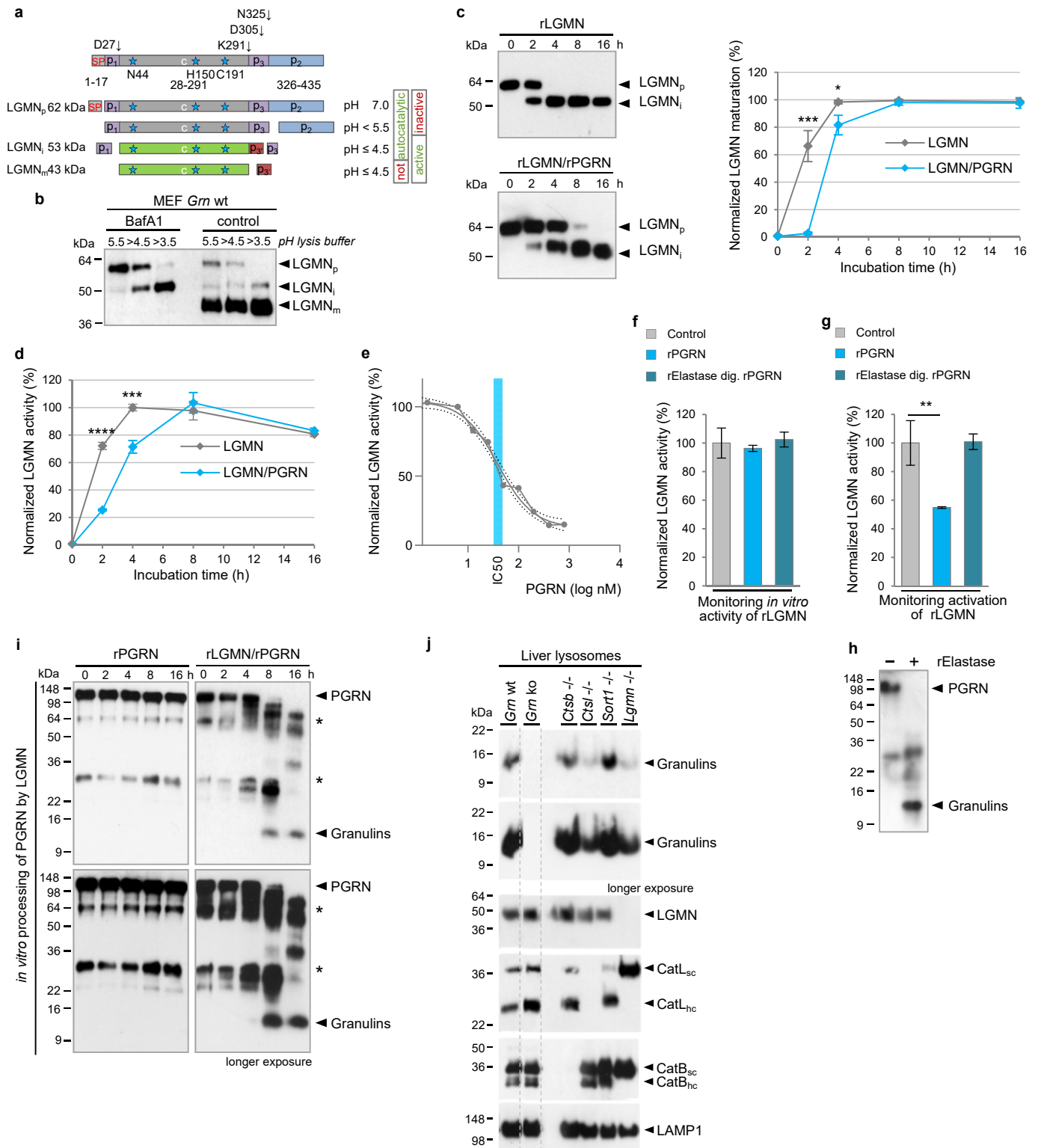
Fig. 2: PGRN modulates LGMN activation and is proteolytically processed by LGMN.

a, Scheme indicating auto- and non-auto-catalytic pH-dependent LGMN maturation. N- and C-terminal pro-peptides (p1-p3) and the chain (c) with the active center residues (stars) are specified. Proform (LGMN$_p$), intermediate- (LGMN$_i$) and mature-form (LGMN$_m$) are indicated. **b**, Bafilomycin (BafA1) inhibits LGMN maturation (left panel), which is partially reconstituted in acidic lysis condition (right panel). **c,d** Immunoblot and activity analysis of *in vitro* maturation of recombinant LGMN (rLGMN) incubated with/without recombinant PGRN (rPGRN) at acidic pH for indicated time points. Quantification of the relative LGMN$_i$ level for each incubation time indicates a significant delay of maturation (**c**) and activity (**d**) in presence of PGRN. **e**, Dose dependent inhibition of LGMN activation during a 2 h preincubation at pH 4.0, followed by activity assays. IC$_{50}$ calculated with non-linear curve fit, 95% confidence interval (CI) are indicated. **f,g**, LGMN activity assays with rPGRN or rElastase digested PGRN added to the assay (**f**) or to the activation step prior to the assay (**g**). **h**, PGRN digest controlled by immunobloting. **i**, Immunoblot analysis of rPGRN turnover and granulin peptide generation by LGMN. **j**, Representative immunoblot of liver lysosome preparation of wt, *Grn*, *Ctsb*, *Ctsl*, *sortilin 1* (*Sort1*), and *Lgmn* ko mice probed for granulins, LGMN, cathepsin L (CatL) and B (CatB), and LAMP1 as loading control.

Data are mean ± s.d. of biologically independent experiments (n=3) (**c,d,e,f,g**); unpaired two-tailed t-test; *p<0.5, **p<0.01, ***p<0.001, ****p<0.0001. *P* values and statistical source data are provided.
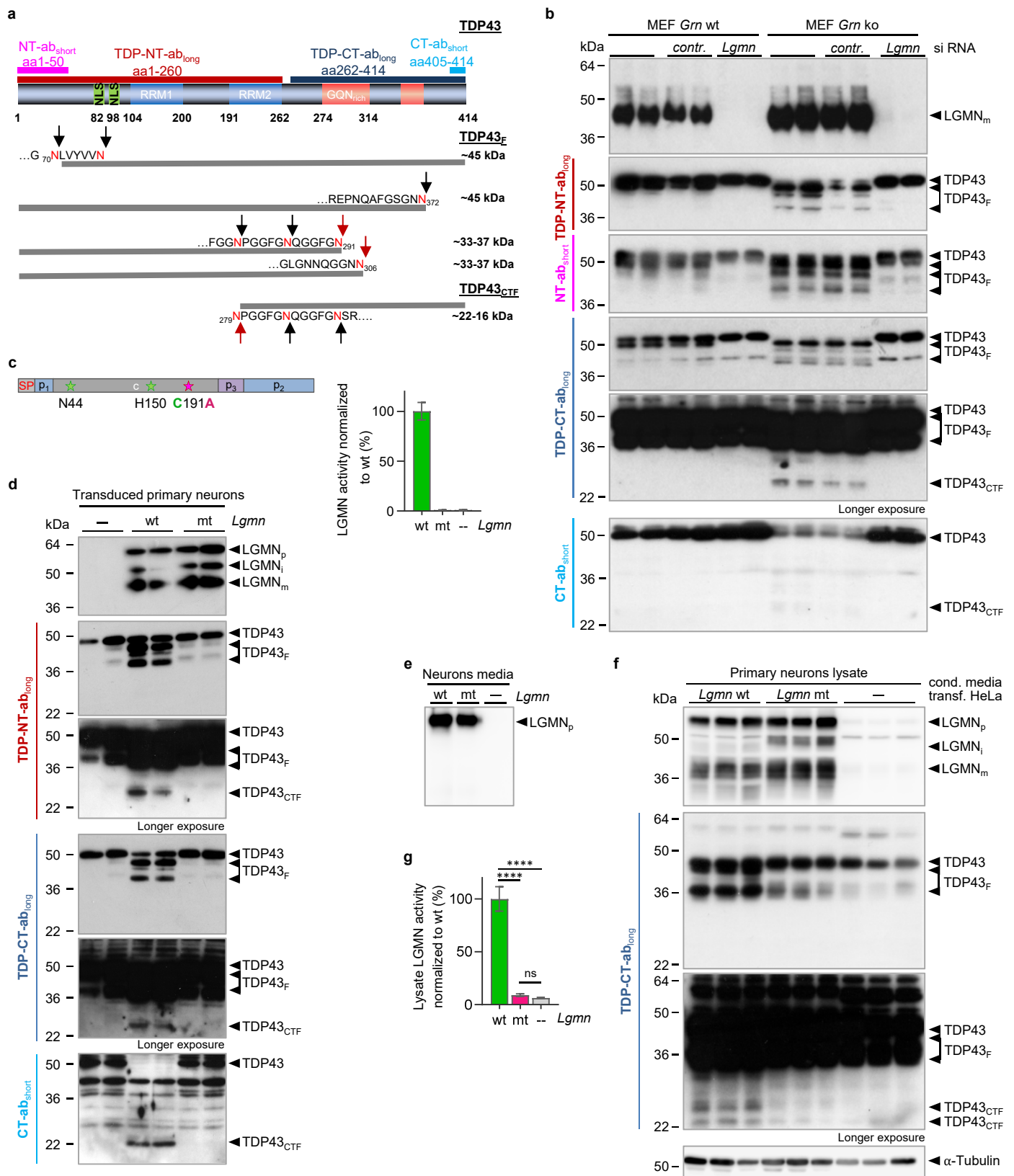
Fig. 3: Enhanced LGMN activity results in accelerated TDP-43 processing.

a, Schematic representation of TDP-43 protein indicates the nuclear localization sequence (NLS, green), the RNA recognition motifs (RRM1/2, blue), the G, Q, N -rich hnRNP-interacting domains (red). N-terminal (NT) and C-terminal (CT) antibodies generated against specified epitopes. Confirmed LGMN cleavage sites and putative fragments are indicated below. Red arrows indicate LGMN cleaved fragments identified in patient material [13,34] **b**, Immunoblot analysis of LGMN and TDP-43, TDP-43 fragments (TDP43$_F$) and C-terminal fragments (TDP43$_{CTF}$) in MEF *Grn* wt and ko with and without *Lgmn* siRNA mediated knockdown. **c**, **d**, Primary cortical rat neurons were transduced with lentiviral vector FUW2 encoding LGMN wt or the proteolytically inactive LGMN C191A variant (mt). LGMN activity in cell lysates confirmed loss of proteolytic activity of the LGMN C191A (**c**). LGMN expression (profom LGMN$_p$, intermediate form LGMN$_i$, mature form LGMN$_m$) and TDP-43 processing are detected by immunoblotting. TDP-43 processing occurs by LGMN wt but not by mt transduction, shown are representative blots of 3 independent experiments (**d**). **e**, **f**, **g**, Primary hippocampal mouse neurons were incubated with 50% of conditioned media of *LGMN* wt, mt or mock transfected HeLa cells. The presence of the LGMN proform is confirmed in culture media (**e**). LGMN uptake by neurons is detected by immunoblot (**f**) and activity assay (**g**). TDP-43 processing analyzed by immunobloting (**f**).

Data are mean ± s.d. of biologically independent experiments (n=3), statistical significance for the activity assay (**g**) was determined by one-way ANOVA and Tukey's post-hoc test; ns, not significant; **** p<0.0001. *P* values and

statistical source data are provided.
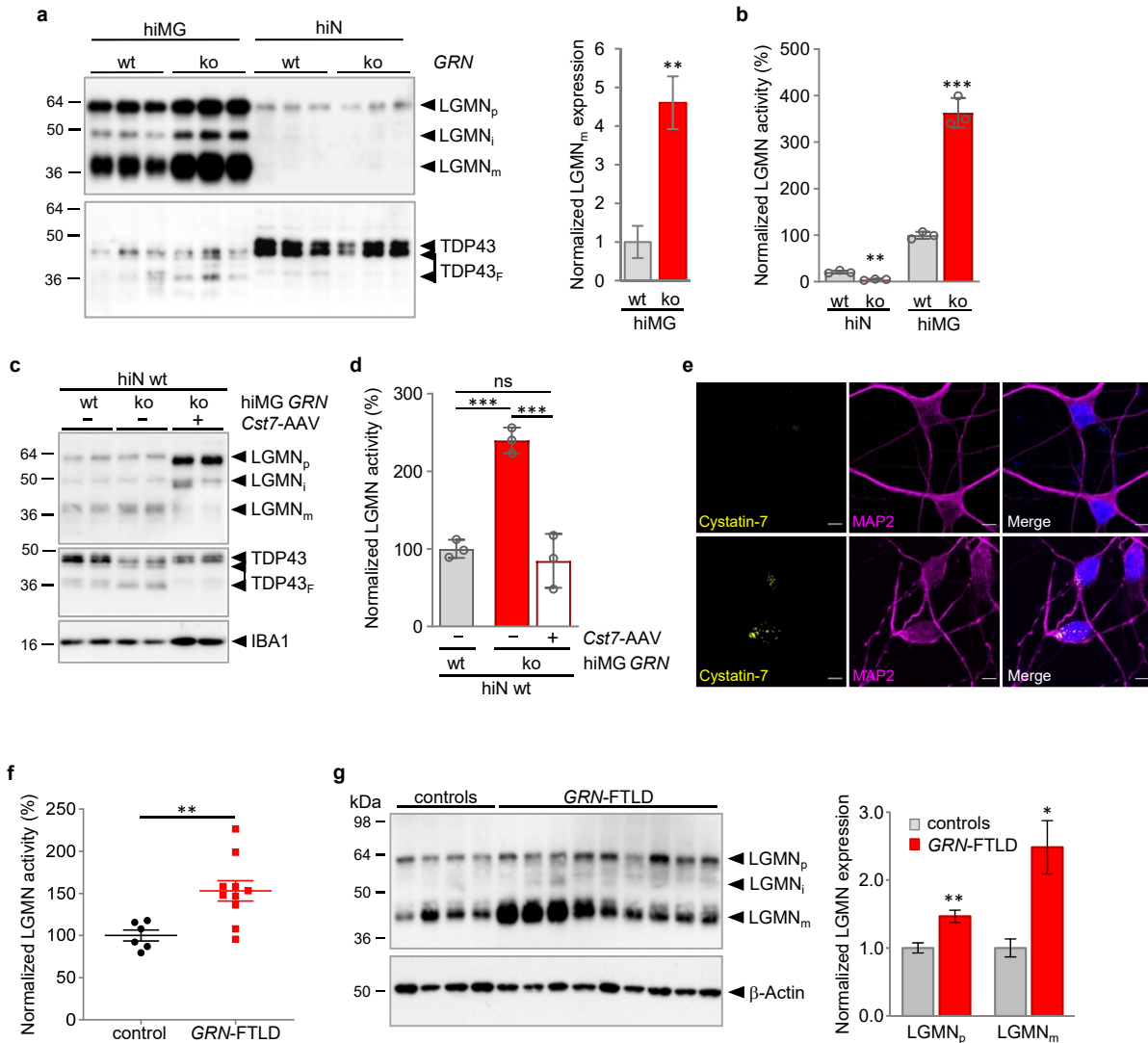
Fig. 4: Elevated LGMN activity in hiPSC-derived microglia and *GRN*-FTLD patients.

a, Representative immunoblot for LGMN of wt and *GRN* deficient (*GRN* ko) hiPSC-derived microglia (hiMG) or neurons (hiN). Proform (LGMN$_p$), intermediate form (LGMN$_i$), and mature form (LGMN$_m$), are indicated. Quantification of the immunoblot shown as mean normalized to wt ± s.d. (n=3). **b**, *In vitro* LGMN activity of lysates from monocultured wt and *GRN* ko hiMG and hiN; mean normalized to wt ± s.d. **c**, **d**, Co-culture of wt hiN with either *GRN* KO or wt hiMG. Immunoblotting (**c**) indicates enhanced LGMN maturation and TDP-43 processing when GRN ko hiMG are co-cultured, AAV-mediated cystatin-7 expression inhibits LGMN maturation and blocks TDP-43 processing. LGMN activity (**d**) normalized to hiN co-cultured with hiMG shown as mean wt ± s.d. (n=3). **e**, Immunohistochemical detection of cystatin-7 (yellow) upon AAV transduction in neurons (MAP2, magenta). Nuclei are stained with DAPI (blue), scale 10 µm. **f**, **g**, LGMN activity (**f**) and expression (**g**) analyzed in brain lysates of frontal cortex from FTLD/*GRN* patients and pathology-negative control cases. LGMN$_p$ and LGMN$_m$ are quantified in the immunoblot and normalized to the signal of the control cases (**g**).

Data are mean ± s.d. of biologically independent experiments (unpaired two-tailed t-test (**a,b,e,f**) or one-way ANOVA and Tukey's post hoc test (**d**); ns, not significant; *p<0.5, **p<0.01, ***p<0.001. *P* values and statistical source data are provided.
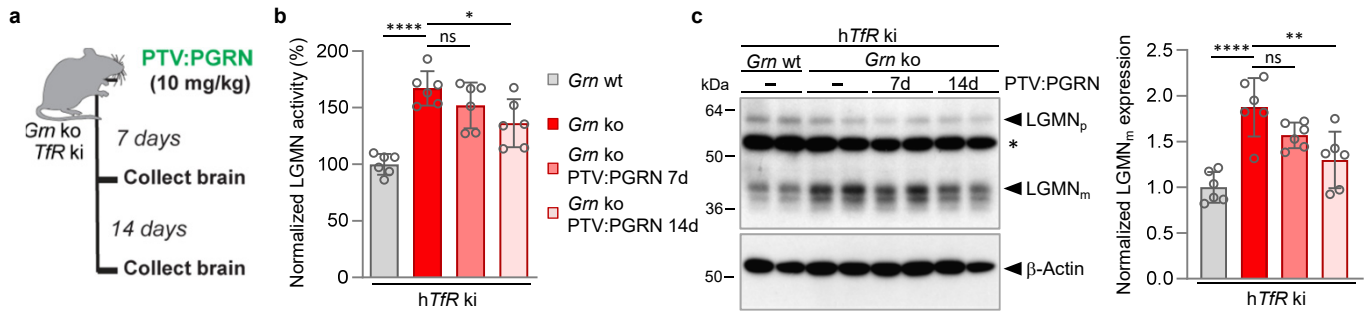
Fig. 5: Rescue of enhanced LGMN maturation and activity by PTV:PGRN in *Grn* ko mice.

a, Schematic of PTV:PGRN single dosing study in *Grn* ko/h*TfR* ki. **b**, LGMN activity of a *Grn* ko/h*TfR* ki mouse model, treated with a single 10 mg/kg *i.v.* dose of PTV:PGRN 7 d and 14 d before analysis. Data indicate the mean normalized to wt h*TfR* ki. (n=6 mice per genotype and treatment, 3-4-month-old). **c**, Representative immunoblot for LGMN in total brain homogenate of wt and *Grn* ko non-treated and treated mice. Proform (LGMN$_p$), mature form (LGMN$_m$), unspecific band (asterisk) are indicated, β-actin verified equal loading. Quantification of LGMN immunoblot signals normalized to wt h*TfR* ki (n=6 mice per genotype and treatment).
Data are mean ± s.d. mice replicates individual values are shown; one-way ANOVA and Tukey's post hoc test; ns, not significant; *p<0.5, **p<0.01, ****p<0.0001. *P* values and statistical source data are provided.

Materials and Methods

Data reporting

No statistical methods were used to predetermine sample size. The investigators were not blinded to allocation during experiments and outcome assessment.

Ethical approval. All the work involving human tissues or mice was carried out in accordance with the Code of Ethics of the World Medical Association (Declaration of Helsinki). The use of human brain material was approved by the local ethic commission of the Ludwig-Maximilian's-University, Munich. All animal experiments were performed in compliance with the national guidelines for animal protection, Germany and with the approval of the regional animal committee (Regierung von Oberbayern) directed by a veterinarian. Mice were kept in small groups under standard housing conditions at constant temperature of 21 ± 2°C, on a 12 h light / 12 h dark cycle, providing standard pellet food and water *ad libitum*. At Denali Therapeutics Inc. all mouse procedures adhered to regulations and protocols approved by Denali Therapeutics Institutional Animal Care and Use Committee. Mice were housed under a 12 h light/ 12 h dark cycle and group housed when possible.

Experimental mouse models

The *Grn* ko mouse line was provided by Dr. M. Nishihara (Department of Veterinary Physiology, The University of Tokyo) [35], backcrossed to the C57BL/6J strain and published before [4,26,36,37]. The second *Grn* ko mouse model and the *Grn* ko/h*TfR*mu/hu ki were previously generated and characterized. *Grn* ko on a C57Bl6/J background were obtained from Jackson Laboratories (JAX strain 013175) [38]. *TfR*mu/hu ki mice (also on a C57Bl6/J background) expressing a chimeric TfR receptor (human TfR apical domain knocked into the mouse receptor) were developed by generating a knock-in of the human apical TfR mouse line using CRISPR, as described previously [39]. Homozygous *TfR*mu/hu male mice were bred to female Grn^{+/−} mice to generate Grn^{−/−} x *TfR*mu/hu mice. *Lgmn* ko [40] , *Ctsl* ko [41], *Ctsb* ko [42], and *Sort1* ko [43] were described before.

Animal ages/sexes for each experiment are indicated in the source data tables.

Mouse handling and tissue collection at Denali Therapeutics

Animal weights were collected at the start and end of the study. Animals were monitored weekly for health/immune issues before and during the study and were excluded from study inclusion if serious concerns were observed. Mice were housed with enrichment and bedding was changed weekly for group housed animals and monthly for single house animals. For study group assignment, littermate animals and when possible – cage-mate animals were assigned to unique experimental groups. Mice received therapeutic treatment via intravenous (IV) tail vein injection (10 mg / kg, ~200 µl total injection volume). At indicated endpoints, animals were anesthetized with tribromoethanol. Following plasma collection, mice were transcardiac perfused with ice-cold PBS. Tissues were then collected, weighed, frozen on dry ice and stored at -80 ºC for subsequent analysis.

Expression and purification of fusion proteins Generation of the transport vehicle (TV) from the effector-less Fc portion of a human IgG1 was previously described [44]. Briefly, the TV was fused N-terminally to the complete native sequence of mature human PGRN, allowing for PGRN to interact with sortilin 1 via its C-terminal region. PTV:PGRN were expressed as knob-in-hole 40 heterodimeric proteins. For PTV:PGRN, Expi293 cells (Thermo Fisher Scientific) were transfected with plasmid DNA encoding the TV Fc polypeptide and PGRN fused to an Fc polypeptide in PEIMax (MW 40,000, Linear, Polysciences). Cultures were harvested 5 days post-transfection. PTV:PGRN were subsequently purified using a series of chromatography steps commonly used for the purification of monoclonal antibodies and Fc-fusion proteins including affinity chromatography and size exclusion chromatography [23].

Mouse brain dissection and brain cell isolation

Mice were sacrificed by CO_2 inhalation or by deep/lethal anesthesia and perfused with ice cold PBS. Brain tissue dissected from adult mice was either snap frozen in liquid nitrogen, mechanically pulverized and stored at -80°C for biochemical analysis or directly subjected to microglia and astrocyte or neuron isolation. Neural cells were acutely isolated from adult mouse brain using MACS Technology (Miltenyi Biotec). Brain tissue was dissociated into a single-cell suspension by enzymatic digestion using the Adult Brain Dissociation Kit P (# 130-107-677, Miltenyi Biotec) and the gentleMACS™ Octo Dissociator (# 614 130-096-427, Miltenyi Biotec) according to manufacturer´s instructions. Microglia and astrocyte isolation was performed from the same mouse brain. Briefly the dissociated cell suspension was applied to a pre-wet

100 µm cell strainer, cells were pelleted at 300 x g, 4°C, 10 min, pellets were washed twice and resuspended in 1 ml 0,5% (w/v) BSA/PBS. CD11b-positive microglia were magnetically labelled with 20 µl anti-CD11b MicroBeads (# 130-049-601, Miltenyi Biotec) and incubated for 20 min in the dark at 4°C with gentle shaking. Cells were washed by adding 1−2 mL of BSA/PBS. The cell pellets were resuspended in 1 ml BSA/PBS and applied together with 1 ml BSA/PBS onto the prepared LS columns (# 130-042-401, Miltenyi Biotec) placed into a QuadroMACS™ Separator (# 130-091-051, Miltenyi Biotec). The columns were washed with 3 × 3 ml BSA/PBS. The flow-through and the first wash containing the unlabeled cells was collected for astrocyte isolation. The columns were removed from the magnetic field, and microglia were flashed out using 5 ml BSA/PBS. To reach a higher purity, the microglia containing eluate was applied onto pre-wetted MS columns (# 130-042-201, Miltenyi Biotec) placed into an OctoMACS™ Separator (# 130-042-108, Miltenyi Biotec), washed 3 x 0.5 ml and eluted with 1 ml BSA/PBS, then immediately stored on ice. For astrocyte isolation the microglia-depleted fraction including the first wash was pelleted and resuspended in 1 ml BSA/PBS, then 10 µL of FcR blocking reagent was added and incubated for 20 min, gentle shaking, in the dark at 4°C, followed by adding 10 µL of anti-ACSA-2 MicroBeads (Anti-ACSA-2 MicroBead Kit, # 130-097-678, Miltenyi Biotec) and an additional incubation for 30 min. Cells were washed and astrocytes were magnetically separated as described for microglia. Neurons were isolated (Adult Neuron Isolation Kit mouse, # 130-126-603, Miltenyi Biotec) according to the manufacturer's instructions including a red blood cell removal and a debris removal step (Adult Brain Dissociation Kit P, # 130-107-677, Miltenyi Biotec). Isolated cells were washed twice with D-PBS (# 14040-133, Thermo Fisher Scientific) to remove BSA, pellets were snap frozen in liquid nitrogen and stored at -80°C until further biochemical analysis.

Mouse embryonic fibroblasts (MEF), HeLa and HEK293T cell culture

All MEF cells were generated as described before [4]. MEF, HeLa, and HEK293T cells were cultured in Dulbecco's modified Eagle's medium (DMEM) with GlutaMAX™-I (# 10566016, Thermo Fisher Scientific) supplemented with 10% (v/v) heat inactivated FBS (# F7524, Sigma-Aldrich), 100 U/ml penicillin, and 100 µg/ml streptomycin (# 15140148, Thermo Fisher Scientific) and if required 1% non-essential amino acids (# 11140050, Thermo Fisher Scientific).

Primary culture of mouse microglia

Microglia were isolated from P11 pups using the MACS Technology (Miltenyi Biotec) as described above. Isolation was carried out under sterile conditions. 60,000 cells were plated in DMEM/F-12, HEPES (# 11594426, Thermo Fisher Scientific) supplemented with 10% (v/v) heat inactivated FBS (# F7524, Sigma-Aldrich), 100 U/ml penicillin, and 100 µg/ml streptomycin (# 15140148, Thermo Fisher Scientific).

Primary mouse neuronal culture

Mouse hippocampal neurons were generated as described previously [45]. In brief, E18 embryos were collected from CO_2-euthanized C57BL/6J wildtype mice. The hippocampi were isolated and dissected in ice-cold dissection buffer (HBSS, 1 mM sodium pyruvate, 10 mM HEPES pH 7.2, all from Thermo Fisher Scientific). Single cell suspension was obtained by pelleting the tissue (300 x g, 3 min, RT) and incubating it for 15 min at 37°C with 0.125% trypsin (# 25200-072, Thermo Fisher Scientific) and 25 U/ml benzonase (# E1014-25KU, Sigma-Aldrich) in DMEM with GlutaMAX™-I. After centrifugation (300 x g, 3 min, RT), tissue was washed in DMEM with GlutaMAX™-I and pelleted again (300 x g, 3 min, RT) before trituration in culture media (neurobasal media, # 21103-049, Thermo Fisher Scientific) with 100 U/ml penicillin, 100 µg/ml streptomycin, 0.5 mM L-glutamine (# 25030-024, Thermo Fisher Scientific) and 1x B-27 supplement (# 17504-044, Thermo Fisher Scientific) with 25 U/ml benzonase and subsequent centrifugation (300 x g, 3 min, RT). The single cells were plated onto poly-D-lysine- (10 µg/ml, # P7280-5MG, Sigma-Aldrich) and laminin- (10 µg/ml, # L2020-1MG, Sigma-Aldrich) coated plates in culture media. On DIV 7, 20% media was added and on DIV 14, cells were used for experiments.

Primary rat neuronal culture

Primary rat neuronal cultures were prepared as follows: Neocortices from E19 rat embryos were dissected in ice-cold dissection media (HBBS, 1% penicillin/streptomycin, 10 mM HEPES pH 7.3, all from Thermo Fisher Scientific) and enzymatically dissociated for 20 min in dissection media (supplemented with 0.25% trypsin, 0.7 mg/ml DNase I). For biochemical experiments, cortical neurons were seeded in 6-well plates (Thermo Fisher Scientific) at a density of 800,000 cells/well and cultured in neurobasal media supplemented with 100 U/ml penicillin, 100 µg/ml streptomycin, 0.5 mM L-glutamine and 1x B-27.

Cloning of *Lgmn*, *Cst3* and *Cst7* constructs and production of adeno-associated virus.

The mouse *Lgmn* cDNA was amplified from MEF cDNA prepared as described for "gene expression analysis", following primers were used:

Lgmn (XhoI) forward 5'-CCCGCTCGAGGCCACCATGACCTGGAGAGTGG-3'

Lgmn (EcoRV) reverse 5'- AGCTTTGATATCTCAGTAGTGACTAAGAC-3'

The amplified *Lgmn* cDNA was subcloned into the XhoI/EcoRV sites of **pcDNA3.1/Zeo(-)**. The *Lgmn* mutation leading to an inactive LGMN C191A variant [16,46] was introduced by site-directed mutagenesis using the QuickChange Site-Directed Mutagenesis Kit (# 200519, Agilent Technologies) according to manufacturer's instruction. The Cys coding base triplet TGT was exchanged to GCT coding for Ala using following primers:

Lgmn(mt)F 5'-GGTGTTCTACATTGAAGCTGCTGAGTCTGGCTCCATGATGAACC-3'

Lgmn(mt)R 5'-GGTTCATCATGGAGCCAGACTCAGCAGCTTCAATGTAGAACACC-3'

For lentiviral expression *Lgmn* (wt) and *Lgmn* (mt) were subcloned into the XhoI/EcoRV sites of the lentiviral expression vector **FUW2** driven by human ubiquitin promoter. Mouse cystatin-3 (# MR225378, OriGene) and cystatin-7 (# MR222507, OriGene) myc-tagged cDNA clones were subcloned into the BamHI/EcoRI sites of pcDNA3 using the following primers:

Cst3 (BamHI) forward 5'-CCCGGATCCCCAACCATGGCCAGCCCGCTGC-3'

Cst7 (BamHI) forward 5'- CCCGGATCCCCAGCCATGCCCTGGTCCTGG -3'

Cst3/7 (EcoRI) reverse 5'- CGGAATTCTTAAACCTTATCGTCGTCATCC -3'

Six hundred three base pairs (603 bp) encoding for cystatin-7 were cloned into the BamHI/EcoRI sites **of pAAV-hSyn-EGFP** (# 50465, Addgene) to receive the plasmid pAAV-hSyn-*Cst7*. To generate double-stranded adeno-associated virus of serotype 9 (AAV9), the plasmid and helper plasmid were transfected into HEK293T cells using polyethylenimine (# 24765, Polysciences). The virus was harvested after 72 h and purified from benzonase-treated cell lysates via an iodixanol density gradient (OptiPrep, Fresenius Kabi Norge). After rebuffering in lactose AAV titers were

determined by real-time PCS on vector genomes using the SYBR Green Master Mix (Roche Molecular Systems).

Lipofectamine 2000 mediated cDNA transfection

For transfection of HeLa and HEK293T cells Lipofectamine 2000 (# 11668030, Thermo Fisher Scientific) was used according to the manufacture's instruction. Briefly, 500 µl of 4 µg/ml plasmid solution in media was mixed with 500 µl DMEM with GlutaMAX™-I containing 20 µl Lipofectamine 2000 and incubated for 20 min at RT before dropwise addition onto HeLa cells at 50-70% confluency. After 6 h, the media was exchanged and after 36 h the media was replaced with 4 ml Opti-MEM® with GlutaMAX™-I media (# 51985-026, Thermo Fisher Scientific). Media and cells were collected 48 h after transfection.

Lentiviral packaging and gene expression

HEK293FT cells of low passage number were seeded into three 10 cm dishes per construct (5×10^6 cells/dish). On the following day, cells were co-transfected with 18.6 µg transfer vector (FUW2_*Lgmn*(wt) or FUW2_*Lgmn*(mt)), 11 µg pSPAX2 and 6.4 µg pVSVG using Lipofectamine 2000 (Thermo Fisher Scientific) in 10% fetal bovine serum/Opti-MEM (Thermo Fisher Scientific). The transfection media was exchanged by plating media supplemented with 13 mg/mL bovine serum albumin (Sigma-Aldrich) on the next day. Lentiviral particles in the cell supernatant were harvested 24 h later by ultracentrifugation (Beckman Coulter; 64,000 x g, 2 h, 4°C). Lentivirus from three 10 cm dishes was resuspended in 120 µl Neurobasal media and stored in aliquots at -80°C for transduction experiments. Primary rat neurons were transduced using 1 µl/well in a 12-well plate. Media and cells were harvested 7 days after transduction.

siRNA Transfection

Lgmn siRNA (# M-044015-01-0005, siGENOME SMART pool, Dharmacon), control siRNA (#D-001210-04-20, siGenome non-targetting pool 4, Dharmacon) and mock reverse transfections were carried out with Lipofectamine™ RNAiMAX (# 13778030, Thermo Fisher Scientific). For each 10 cm dish 3 µl siRNA (20 µM), were diluted in 600 µl Opti-MEM™ (# 31985-062, Thermo Fisher Scientific) before adding 30 µl Lipofectamine™ RNAiMAX and then for complex formation incubated for 15 min at RT. Trypsinized and washed MEF cells were added to reach a final volume of 6 ml culture media without antibiotics and a final siRNA concentration of 10 nM. Next day, media

were exchanged to fresh culture media and 96 h after transfection cells were harvested and pellets were washed in PBS, snap frozen in liquid nitrogen and stored at -80°C.

Human iPSC culture

iPSC experiments were performed in accordance with relevant guidelines and regulations. Female iPSC line A18944 was purchased from Thermo Fisher (# A18945), grown in Essential 8 Flex Medium (# A2858501, Thermo Fisher Scientific) on VTN-coated (# A14700, Thermo Fisher Scientific) cell culture plates with 5% CO_2 at 37°C, and split as small clumps twice a week after a 5 min incubation in PBS/EDTA.

Generation of *GRN* KO iPSCs

Design and preparation of editing reagents and quality control of edited iPSCs was performed as described previously [47,48]. We selected a sgRNA targeting *GRN* exon2, as it is present in most splice isoforms and a frameshift would affect large parts of the coding region. Guide RNAs were electroporated as plasmids together with a Cas9-encoding plasmid. Prior to electroporations, iPSCs were incubated for 10 min in PBS/EDTA, split to single cells on Geltrex-coated (# A1413302, Thermo Fisher Scientific) plates and cultured in StemFlex Medium (# A3349401, Thermo Fisher Scientific) containing 10 mM ROCK inhibitor (# S1049, Selleck Chemicals GmbH) for two days. iPS cells were transfected by electroporation as described earlier [49] with some modifications. Briefly, two million cells were harvested with Accutase, resuspended in 100 ml cold BTXpress electroporation solution (# 732-1285, VWR) with 20 mg Cas9 and 5 mg sgRNA plasmid. Cells were electroporated with 2 pulses at 65 mV for 20 ms in a 1 mm cuvette (# 15437270, Thermo Fisher Scientific). After electroporation, cells were transferred to Geltrex-coated 10 cm plates and grown in StemFlex Medium containing 10 mM ROCK inhibitor until visible colonies appeared. Cells expressing Cas9 were selected in 350 ng/ml puromycin dihydro-chloride (# J593, VWR) for three consecutive days starting one day after electroporation [50]. Single-cell clone colonies then were picked and analyzed by a RFLP assay, using MwoI (# R0573, New England BioLabs GmbH) and Sanger sequencing as previously described [49]. Successful knockout was confirmed on mRNA level by qPCR, and on protein level by immunoblot using RIPA lysate and ELISA using conditioned media, respectively. For quality control of edited iPSC clones, we checked absence of off-target effects by PCR-amplification and sanger sequencing of the top 5 hits based on MIT and CFD scores

on CRISPOR. We also confirmed absence of on-target effects such as large deletions and loss of heterozygosity using qgPCR and nearby SNP sequencing [48]. Finally, we ensured pluripotency by immunofluorescence staining for typical markers OCT4, NANOG, SSEA4 and TRA160, and chromosomal integrity by molecular karyotyping (Supplementary Fig. 1) (Life & Brain Bonn, Germany).

Differentiation of human iPSC-derived Microglia (hiMG)

We differentiated hiMG from iPSCs following the protocol by Abud et al. [51] with modifications to improve yield and efficiency: When iPSCs were 70-90% confluent, we split them 1:100-200 onto GelTrex-coated 6-well plates for the HPC differentiation using EDTA to obtain around ~20 small colonies per well. On day 0 cells were cultured with HemA medium (HPC differentiation kit, StemCell Technologies), followed by half-media exchange on day 2. We switched media to HemB on day 3 with half-media exchange on days 5 and 7 and 50% added on day 10. On day 12 non-adherent HPCs were collected to either freeze or continue with the microglia differentiation. HPCs were frozen at 1 million cells per ml in BamBanker (Wako) and thawed directly onto GelTrex-coated 6-well plates with 1 million cells evenly distributed among 6 wells in 2 ml iMG media with 25 ng/ml M-CSF, 100 ng/ml IL-34, and 50 ng/ml TGFβ added fresh. 1 ml of media was added on top every other day. During the microglia differentiation, the cells were split 1:2 every 6-8 days, depending on confluency. We did do not use CD200 and CX3CL1 as described by McQuade et al. [52]. This did not influence hiMG gene expression, as determined by NanoString analysis [53]. hiMG were used for experiments on day 16 of the differentiation.

Differentiation of human iPSC-derived cortical hiN and co-culture with iMG

iPSC-derived hiN were differentiated as previously published [54]. For cortical neuron maturation, 2 million neuronal precursor cells were seeded on poly-L-ornithine/laminin-coated 6-well plates and maintained in Neurobasal medium (NB) Plus supplemented with B-27 Plus serum-free supplement, and 100 U penicillin per ml and 0.1 mg streptomycin per ml (all Thermo Fisher Scientific). During the first 7 days after plating, cells were treated with 10 μM DAPT (# S2215, Selleckchem) to augment neuronal maturation. 3 days after starting DAPT treatment, 5-Fluorouracil (5-FU) (# F6627-1G, Sigma-Aldrich) was also added for a subsequent 10 days to remove remaining dividing precursors. iN cultured with half media exchange three times per week. One week after

finishing 5-FU treatment, hiMG were added at 300,000 cells per well along with IL-34, M-CSF, and TGFβ (# 200-34, # 200-25, # 100-21, Peprotech) added fresh in the neuron media. The cells were co-cultured for three weeks before being collected for analysis.

Antibodies

Antibodies	Dilution	Source
Rat anti-mouse PGRN, (clone 8H10)	1:50	generated [55]
Rabbit anti-human PGRN	1:1,000	# 40-3400, Thermo Fisher Scientific
Rabbit anti-human PGRN / granulin-peptides	1:1,000	# HPA008763, Atlas Antibodies
Sheep anti-mouse LGMN	1:2,500	# AF2058, R&D Systems
Goat anti-human LGMN	1:1,000	# AF2199, R&D Systems
Goat anti-cathepsin B	1:2,000	# AF1515, R&D Systems
Goat anti-cathepsin D	1:1,000	# sc-6486, Santa Cruz
Goat anti-cathepsin L	1:1,000	# AF965, R&D Systems
Goat anti-cystatin-3	1:1,000	# AF1238, R&D Systems
Rabbit anti-cystatin-7	1:2,500	# 50236, SinoBiological
Mouse anti-tubulin β3 (TUJ)	1:10,000	# 801201, BioLegend
Rabbit anti-IBA1	1:1,000	# GTX100042, GeneTex
Rabbit anti-GFAP	1:5,000	# GA524, DAKO, Agilent
Rabbit anti-TDP-NTlong	1:4,000	# 10782-2-AP, Proteintech
Rabbit anti-TDP-NTshort	1:800	# ARP38941, Aviasy Stemsbiology
Rabbit anti-TDP-CTlong	1:1,000	# 12892-1-AP, Proteintech
Rabbit anti-TDP-CTshort	1:1,000	# TIP-TD-P09, Cosmo Bio
Mouse anti-tubulin α	1:500	# T5168, Sigma-Aldrich
Mouse anti-β-actin	1:5,000	# A 5316, Sigma-Aldrich
Rabbit anti-calnexin	1:5,000	# SPA-860, Stressgene
Mouse anti-TRA-160	1:500	# MAB4360, Millipore
Rabbit anti-OCT4	1:500	# 09-0023, Stemgent
Rabbit anti-NANOG	1:500	# D73G4, Cell Signaling
Mouse anti-SSEA4	1:500	# MC813, Abcam
Chicken anti-MAP2	1:1000	# ab92434, Abcam
Rabbit anti-IBA1	1:500	# PA5-27436, Thermo Fisher Scientific

The following secondary antibodies were used for immunoblots: horseradish peroxidase-conjugated donkey anti-goat IgG (H+L) (Dianova, 1:5,000), donkey anti-sheep IgG goat (Jackson Immuno Research, 1:10,000); 1:10,000), anti-mouse IgG

(Promega, 1:10,000), goat anti-rabbit IgG (Promega, 1:20,000), goat anti-rat IgG + IgM (L+M) (Dianova, 1:5,000) and generated mouse anti-rat IgG2c (1:1,000). For immunofluorescence: goat anti-chicken Alexa 647, donkey anti-rabbit Alexa 568, donkey anti-mouse Alexa 488, (# A32933, # A10042, # A32766, all Invitrogen, Thermo Fisher Scientific).

LGMN *in vitro* activity assay

A fluorescence-based activity assay was used to assess LGMN proteolytic activity of recombinant LGMN, or LGMN activity in lysates and media of the respective cells. Cell pellets or aliquots of powdered brain tissues were homogenized in LGMN-lysis buffer (50 mM sodium citrate pH 5.0, 0.8% NP-40, 1 mM DTT), incubated 15 min (cell lysates) or 20 min (brain lysates) on ice, followed by a 15 min centrifugation at 15,000 x g, 4°C. Protein concentration was determined using the BCA protein assay (Pierce, Thermo Scientific) and indicated amounts of protein in 50 µl LGMN-lysis buffer were pre-incubated in black 96-well plates (FluoroNunc) at 37°C for 10 min, then 50 µl LGMN assay buffer (50 mM sodium citrate pH 5.0, 1 mM EDTA pH 8.0, 1 mM DTT and 200 µM substrate) prewarmed at 37 °C was added. Substrate Z-Ala-Ala-Asn-AMC (# I-1865.0050, BACHEM,) dissolved at 10 mM (100x) in DMSO was prepared and stored in aliquots at -80°C. Cleavage of the quenched fluorescence substrate was continuously measured for 30 min following the increase of the fluorescence signal (excitation, 390 nm; emission, 460 nm) using the Fluoroskan Ascent FL plate reader (Labsystems). The relative enzyme activity was calculated for a period of time with linear substrate turnover.

In vitro activation assays of recombinant LGMN (rLGMN) or of the secreted LGMN (sLGMN) proform

Prior to LGMN activity assays mouse rLGMN (# 2058-CY-010, R&D Systems) or sLGMN proform needs to be autocatalytically activated at acidic pH. 50 ng rLGMN or 25 µl of the collected media of transfected HeLa cells was preincubated in 10 µl or 25 µl acidic activation buffer (100 mM sodium citrate pH 4.0 or 3.5, 1 mM EDTA, 50 mM NaCl) for 4 h or as indicated at 37°C. For the activity assay 40 µl LGMN-lysis buffer was added and LGMN activity was measured as described above. To investigate the inhibitory effect of PGRN on LGMN activity, 200 ng or the indicated amount of human

recombinant PGRN (rPGRN, # 10826-H08H, Sino Biological Inc.) was either added to the activation assay or to the activity assay.

Activity assays of recombinant LGMN treated with recombinant cystatin-3 or cystatin-7

The assay contained 5 nM activated rLGMN and the indicated concentrations of mouse cystatin-3 (# 1238-PI-010, R&D Systems) or cystatin-7 (# 4557-PI-010, R&D Systems). filled up to 50 µl with LGMN-lysis buffer. Further steps of the activity assay are described above. The nonlinear regression curve fit as well as the calculation of top and bottom plateaus and IC_{50} was done in GraphPad Prism using a four-parameter dose-response curve.

Generation of granulin peptides

Elastase generated granulin peptides were obtained by incubation of rPGRN with human neutrophil elastase (# RP-77526, Invitrogen). 50 ng/µl PGRN and 80 ng/µl elastase were incubated in 100 mM sodium citrate pH 6.0 overnight at 37°C, followed by buffer exchange to LGMN activation buffer. Aliquots were stored at -80°C.

Gene expression analysis

For quantitative real time PCR (qRT-PCR) approximately 10-20 mg of powdered mouse brain homogenates were subjected to total RNA preparation using the QIAshredder and RNeasy Mini Kit (Qiagen) according to manufacturer's instructions. 2 µg of RNA was reverse transcribed into cDNA using M-MLV reverse transcriptase (Promega) and oligo(dT) primers (Life Technologies). The following primer sets from Integrated DNA Technologies were used: mouse *Lgmn* Mm.PT.58.5122210 (Exon boundary 10 to 11) and mouse *Gapdh* Mm.PT.39a.1 (Exon boundary 2 to 3). For mouse brain samples, cDNA levels were normalized to *Gapdh* cDNA and relative transcription levels were analyzed using the comparative ΔΔCt method (7500 Software V2.0.5, Applied Biosystems, Life Technologies). The *Lgmn* mRNA level of the microglia-enriched fraction was obtained from a NanoString dataset (Omnibus GSE129709 https://www.ncbi.nlm.nih.gov/geo/query/acc.cgi?acc=GSE129709)[36].

Immunohistochemistry

Cells seeded on 24-well coverslips were fixed for 15 min in 4% paraformaldehyde and washed with PBS, then permeabilized for 15 min at room temperature in (0.1% Triton-X-100 in PBS for co-culture and iPSCs, 0.1% Triton-X-100 and 0.1% saponin in PBS for *Cst7*-transduced hiN) and then washed with PBS again. SuperBlock (# 37515, Thermo Fisher Scientific) was used to block the coverslips for 1 h at RT. Primary antibodies were diluted in SuperBlock added overnight. The coverslips were washed again in PBS and incubated in secondary antibodies (goat anti-chicken 647 1:500, donkey anti-rabbit 568 1:500, donkey anti-mouse 488 1:500, DAPI 1:50000) diluted in SuperBlock for 90 min at RT in the dark. They were washed in PBS again and mounted with Fluoromount G (# 00-4958-02, Thermo Fisher Scientific).

Protein analysis and immunoblotting

Snap frozen cell pellets or powdered brain homogenate were lysed in NP-40 LGMN-lysis buffer (50 mM sodium citrate pH 5.0, 0.8% NP-40, 1 mM DTT), NP-40 STEN-lysis buffer (150 mM NaCl, 50 mM Tris–HCl pH 7.6, 2.5 mM ETDA, 1 % NP40) or RIPA-lysis buffer (150 mM NaCl, 20 mM Tris–HCl pH 7.6, 2.5 mM ETDA, 1% NP-40, 0.1% sodium dodecyl sulfate (SDS), 0.5% sodium-desoxycholate) as indicated. NP-40 STEN- and RIPA-lysis buffer were supplemented with protease inhibitor cocktail (# P8340, Sigma-Aldrich) and phosphatase inhibitor (# 4906845001 PhosStop™, Sigma-Aldrich). Lysates were centrifuged for 20 min, 17,000 x g, 4°C. The protein concentration of the soluble fraction was determined using the BCA protein assay (Pierce, Thermo Fisher Scientific) and equal amount of protein were separated by SDS-PAGE and transferred to polyvinylidene difluoride membranes (Immobilon-P, Merck Millipore). Membranes were blocked for one hour in I-Block™ (# T2015, Thermo Fisher Scientific). Proteins of interest were detected by the indicated primary antibodies followed by horseradish peroxidase-conjugated secondary antibodies detected by ECL Plus (# 32132X3, Pierce™ ECL Plus Western Blotting Substrate, Thermo Fisher Scientific). For the quantitatively analysis, images were taken by a Luminescent Image Analyzer LAS-4000 (Fujifilm Life Science, Tokyo, Japan) and evaluated with the Multi GaugeV3.0 software (Fujifilm Life Science, Tokyo, Japan).

Isolation of liver lysosomes

As described before [56] mice were injected with 4 µl/g bodyweight with 17% (w/v) tyloxapol in 0.9% NaCl four days prior to killing and organ removal. After the removal

of the liver, the liver was homogenized in 5 ml ice-cold 0.25 M sucrose with four strokes at 1,000 rpm in a Potter-Elvehjem homogenizer. The homogenate was subsequently centrifuged for 10 min at 1,000 x g in a tabletop centrifuge, the supernatant was removed and the pellet re-extracted with another 2 ml of 0.25 M sucrose and centrifuged again. The pooled supernatants (postnuclear supernatant; PNS) were used for differential ultracentrifugation: 9 ml of the PNS were centrifuged at 56,000 x g for 7 min (70.1 Ti rotor, Beckmann, Coulter). The supernatant was removed, the pellet (mitochondria / lysosome fraction; ML) homogenized in 8 ml 0.25 M sucrose and centrifuged again at 56,000 x g for 7 min. The final pellet was resuspended in 3 ml of sucrose solution with a density of 1.21 g/ml. This fraction was overlaid with sucrose solutions with a density of 1.15 g/ml (3 ml), 1.14 g/ml (3 ml) and finally 1.06 g/ml to obtain a discontinuous sucrose gradient. The sucrose gradient was centrifuged at 110,000 x g for 150 min in a swinging bucket rotor (SW41 Ti rotor, Beckmann Coulter). Lysosomes were collected from the interphase between the sucrose solution with a density of 1.14 g/ml and 1.06 g/ml.

Statistical analysis

Data are presented as mean ± s.d.. Statistical significance was calculated for comparison of two sample groups by unpaired, two-tailed Student's t-test, and for multiple comparison by one-way ANOVA with Tukey's or Dunnett's post hoc test and indicated as ns, not significant $p > 0.05$; * $p < 0.05$; ** $p < 0.01$; *** $p < 0.001$; **** $p < 0.0001$. All data were analyzed using GraphPad Prism 7 (GraphPad Software Inc.).

Data availability

All data and information are included in the manuscript. Supplementary information and source data are provided with this article. Data are available from corresponding authors upon reasonable request

Methods references

35   Kayasuga, Y. *et al.* Alteration of behavioural phenotype in mice by targeted disruption of the progranulin gene. *Behavioural Brain Research* **185**, 110-118 (2007).
36   Gotzl, J. K. *et al.* Opposite microglial activation stages upon loss of PGRN or TREM2 result in reduced cerebral glucose metabolism. *EMBO Mol Med* **11** (2019).
37   Werner, G. *et al.* Loss of TMEM106B potentiates lysosomal and FTLD-like pathology in progranulin-deficient mice. *EMBO Rep*, e50241 (2020).
38   Yin, F. *et al.* Behavioral deficits and progressive neuropathology in progranulin-deficient mice: a mouse model of frontotemporal dementia. *FASEB J* **24** (2010).

39   Kariolis, M. S. *et al.* Brain delivery of therapeutic proteins using an Fc fragment blood-brain barrier transport vehicle in mice and monkeys. *Sci Transl Med* **12** (2020).

40   Matthews, S. P. *et al.* Distinct protease requirements for antigen presentation in vitro and in vivo. *J Immunol* **184**, 2423-2431 (2010).

41   Roth, W. *et al.* Cathepsin L deficiency as molecular defect of furless: hyperproliferation of keratinocytes and pertubation of hair follicle cycling. *FASEB J* **14**, 2075-2086 (2000).

42   Halangk, W. *et al.* Role of cathepsin B in intracellular trypsinogen activation and the onset of acute pancreatitis. *J Clin Invest* **106**, 773-781 (2000).

43   Jansen, P. *et al.* Roles for the pro-neurotrophin receptor sortilin in neuronal development, aging and brain injury. *Nat Neurosci* **10**, 1449-1457 (2007).

44   Ullman, J. C. *et al.* Brain delivery and activity of a lysosomal enzyme using a blood-brain barrier transport vehicle in mice. *Sci Transl Med* **12** (2020).

45   Seibenhener, M. L. & Wooten, M. W. Isolation and culture of hippocampal neurons from prenatal mice. *J Vis Exp* (2012).

46   Chen, J. M., Rawlings, N. D., Stevens, R. A. & Barrett, A. J. Identification of the active site of legumain links it to caspases, clostripain and gingipains in a new clan of cysteine endopeptidases. *FEBS Lett* **441**, 361-365 (1998).

47   Weisheit, I. *et al.* Detection of Deleterious On-Target Effects after HDR-Mediated CRISPR Editing. *Cell Rep* **31** (2020).

48   Weisheit, I. *et al.* Simple and reliable detection of CRISPR-induced on-target effects by qgPCR and SNP genotyping. *Nat Protoc* **16**, 1714-1739 (2021).

49   Kwart, D., Paquet, D., Teo, S. & Tessier-Lavigne, M. Precise and efficient scarless genome editing in stem cells using CORRECT. *Nat Protoc* **12**, 329-354 (2017).

50   Steyer, B. *et al.* Scarless Genome Editing of Human Pluripotent Stem Cells via Transient Puromycin Selection. *Stem Cell Reports* **10**, 642-654 (2018).

51   Abud, E. M. *et al.* iPSC-Derived Human Microglia-like Cells to Study Neurological Diseases. *Neuron* **94**, 278-293 e279 (2017).

52   McQuade, A. *et al.* Development and validation of a simplified method to generate human microglia from pluripotent stem cells. *Mol Neurodegener* **13**, 67 (2018).

53   Reich, M. *et al.* Alzheimer's Risk Gene TREM2 Determines Functional Properties of New Type of Human iPSC-Derived Microglia. *Front Immunol* **11**, 617860 (2020).

54   Paquet, D. *et al.* Efficient introduction of specific homozygous and heterozygous mutations using CRISPR/Cas9. *Nature* **533**, 125-129 (2016).

55   Wils, H. *et al.* Cellular ageing, increased mortality and FTLD-TDP-associated neuropathology in progranulin knockout mice. *J Pathol* **228**, 67-76 (2012).

56   Markmann, S. *et al.* Quantitative Proteome Analysis of Mouse Liver Lysosomes Provides Evidence for Mannose 6-phosphate-independent Targeting Mechanisms of Acid Hydrolases in Mucolipidosis II. *Mol Cell Proteomics* **16**, 438-450 (2017).

Funding

Author information

These authors contributed equally:

Sophie Robinson and Marvin Reich

Author contributions

AC and CH conceived and designed the study and wrote the manuscript. SR and DP designed, performed and analyzed iPSC experiments. MR, DE, AR performed and analyzed primary neuronal and microglial experiments. KB, cloned LGMN constructs. HR generated lenti virus and performed viral transduction experiments. MR performed and analyzed HeLa conditioned media treated neurons. KB, GW performed experiments with MEF, mice brain and *GRN*-FTLD patient material and recombinant LGMN. MJS, TL, GDP generated, MR analyzed the PTV:PGRN study. QM conducted the cystatins experiments. AA, SE generated and purified the AAV9-Cst7. CVB and EW provided validated FTLD/*GRN* patients brain samples. MD co-initiated the study and performed liver lysosomes isolation on mice provided by AC and TR. All authors commented on the manuscript.

Corresponding authors

Correspondence to Anja Capell or Christian Haass

Ethic Declarations

Conflict of interest

Additional Information

Extended data figures and tables

Supplementary Information

Supplement Figure 1: Molecular karyotyping of GRN ko iPSC line.

Source Data
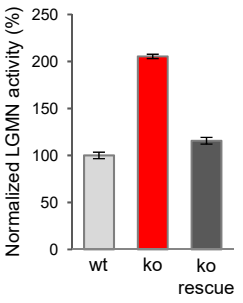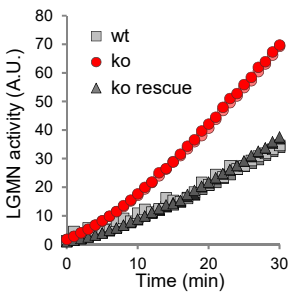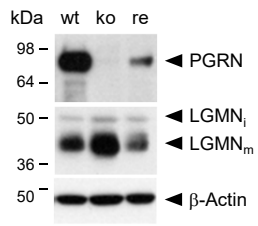
Extended Data Fig. 1: Enhanced LGMN activity of *Grn* ko MEF is rescued upon stable PGRN expression.

Representative immunoblots of MEF wt, *Grn* ko and *Grn* ko stably transfected with a mouse *Grn* cDNA probed for PGRN, LGMN, and β-actin to verify equal loading. LGMN substrate turnover and quantification of LGMN activity normalized to MEF wt of biologically independent duplicates are shown as mean ± s.d.
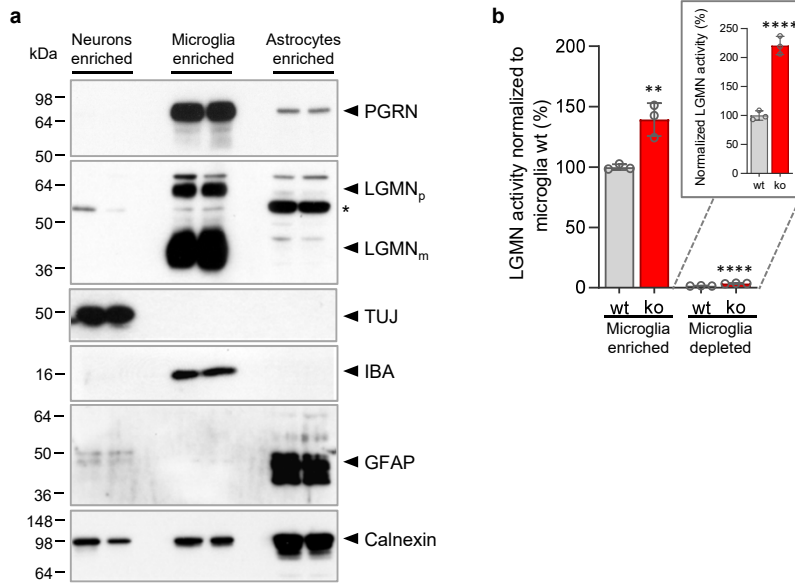
Extended Data Fig. 2: Microglia have the highest PGRN and LGMN expression.

a, Representative immunoblot for PGRN and LGMN in microglia-, astrocyte- and neuron-enriched brain cell fractions isolated of 10-month-old mice. Enrichment of each cell fraction is verified by probing the immunoblot for IBA, GFAP and TUJ. Equal amount of protein was loaded for all cell types, calnexin expression varies between cell types. **b**, Microglia-enriched and -depleted fractions from 10-12-month-old *Grn* ko and wt mice analyzed for LGMN activity either normalized to wt microglia or to wt of the particular cell fraction (insert); n=3 mice per cell type and genotype. Data are mean ± s.d. for mice replicates individual values are shown; unpaired two-tailed t-test, **p<0.01, ****p<0.0001.
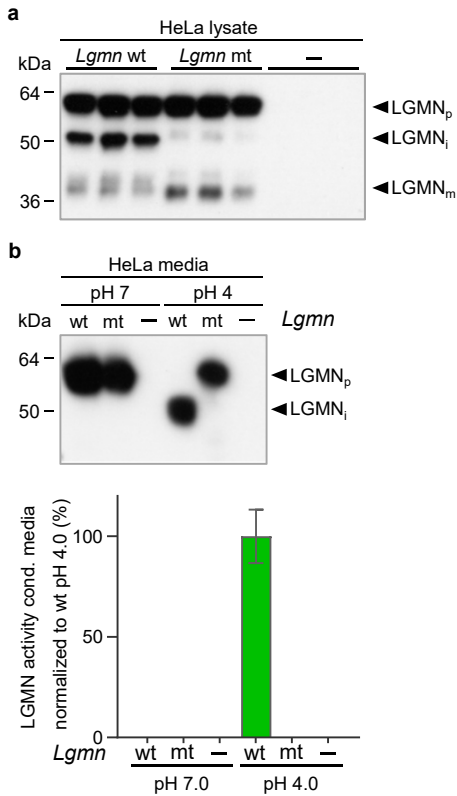
Extended Data Fig. 3: Secreted LGMN proform is autocatalytically processed to an intermediate catalytically active variant.

a, Immunoblot of Lgmn wt or mutant (mt) or empty vector transfected HeLa cell lysates probed for LGMN. Indicated are the LGMN proform (LGMN$_p$), intermediate (LGMN$_i$) and mature (LGMN$_m$) form. **b**, LGMN detected by immunoblotting and LGMN activity assay of conditioned media of transfected HeLa cells incubated at pH 7.0 or pH 4.0.

a, *GRN* knockout strategy: Exon 2 of *GRN* was targeted by a sgRNA (target and PAM sequence shown); a *GRN* ko line was obtained by a one base pair insertion as the resulting frameshift exposes a nearby stop codon. **b**, qPCR of wt and *GRN* ko hiMGL *GRN* mRNA transcript levels normalized to wt (n=3). **c**, ELISA-mediated quantification of secreted PGRN in wt and *GRN* ko hiMGL conditioned media (n=2). **d**, Immunofluorescence analysis of *GRN* ko iPSCs, showing pluripotency markers SSEA4, NANOG, TRA160, and OCT 4 with DAPI. **e**, **f**, Investigating CRISPR-mediated on-target effects using qgPCR quantitation of allele copy number (**e**) and Sanger sequencing of SNPs near the edited locus in wt and *GRN* ko iPSC lines (**f**) showing maintenance of both alleles after editing. **g**, List of top five most similar off-target sites ranked by the CFD and MIT prediction scores, respectively. Sanger sequencing detected no off-target editing. **h**, Immunohistochemical detection of hiMG (IBA1, yellow) and hiN (MAP2, magenta) co-cultured for 3 weeks. Nuclei are stained with DAPI (cyan), scale 100 µm. Data are mean ± s.d. For statistical analysis the unpaired, two-tailed student`s t-test was performed, ****p < 0.0001.

Extended Data Fig. 4: Generation and characterization of *GRN* ko iPSC line

a

b

c
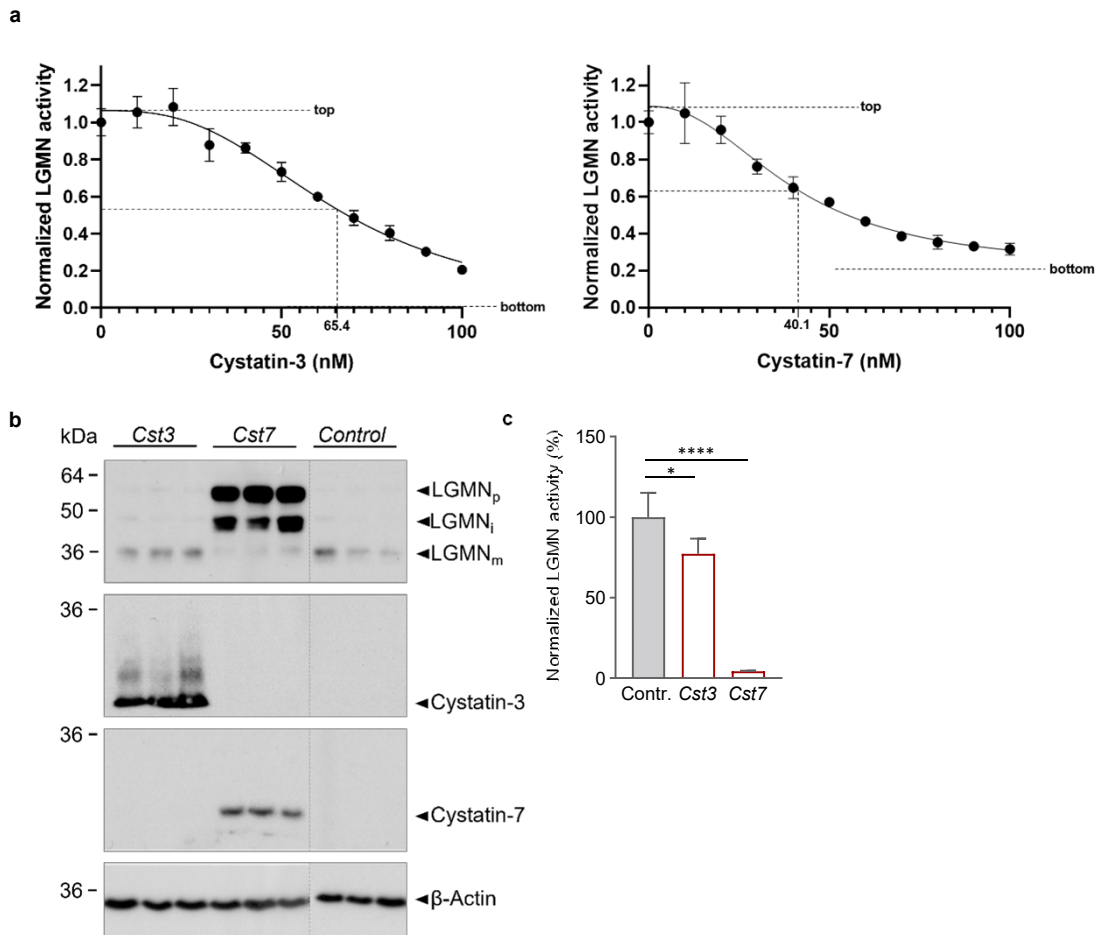
Extended Data Fig. 5: LGMN inhibition by cystatin-3 and cystatin-7

a, Dose-dependent inhibition of recombinant LGMN *via* recombinant cystatin-3 (left) and cystatin-7 (right). The calculated relative IC_{50} of cystatin-3 (65.4 nM) is higher than that of cystatin-7 (40.1 nM), whereas the computed bottom of the curve at higher concentrations is affected conversely. Nonlinear regression (curve fit; variable slope (4 parameters)), top, bottom and IC_{50} are calculated using GraphPad Prism 9. Data points show the mean of three technical replicates ± s.d. normalized to LGMN activity at 0 nM inhibitor. **b**, **c**, HEK 293T cells were transfected with *Cst3*, *Cst7* or pcDNA3 (contr.). Immunobloting (**b**) indicates proform (LGMNp), intermediate form (LGMNi) and mature form (LGMNm) of LGMN, and cystatin-3 and -7 expression. b-Actin was probed to verify equal loading. LGMN maturation (**b**) and activity (**c**) are differentially inhibited by cystatin-3 and cystatin-7. Data are mean ± s.d. of biologically independent experiments normalized to control (n=3). Statistical analysis included one-way ANOVA and Dunnett's multiple comparisons test (c), * p < 0.05, **** p < 0.0001.

Patient ID	Pathological diagnosis	Gender*	Age at death	Mutation	Clinical diagnosis, subtype	Brain region	
P008	FTLD-TDP A	f	69	GRN IVS1+5G>C	FTD, bvFTD	FCx	BA9
P010	FTLD-TDP A	m	63	GRN IVS1+5G>C	FTD, PPA (nfvPPA)	FCx	BA9
P011	FTLD-TDP A	f	75	GRN IVS1+5G>C	FTD, bvFTD	FCx	BA9
P017	FTLD-TDP A	f	72	GRN IVS1+5G>C	FTD, PPA (nfvPPA)	FCx	BA9
P018	FTLD-TDP A	m	74	GRN IVS1+5G>C	Dementia, mixed phenotype	FCx	BA10
P025	FTLD-TDP A	f	72	pAla89Val fs*41	FTD, PPA	FCx	BA10
P035	FTLD-TDP A	f	79	GRN IVS1+5G>C	FTD, bvFTD	FCx	BA9
P036	FTLD-TDP A	m	71	pThr330Ala fs*6	FTD, unspecified	FCx	BA9
P037	FTLD-TDP A	f	67	GRN IVS1+5G>C	FTD, PPA (nfvPPA)	FCx	BA9
P038	FTLD-TDP A	m	60	GRN IVS1+5G>C	FTD, bvFTD	FCx	BA9
C001	Def Control	f	83			FCx	BA10
C002	Def Control	m	63			FCx	BA10
C004	Def Control	m	87			FCx	BA10
C011	Def Control	f	64			FCx	BA10
C012	Def Control	m	79			FCx	BA10
C013	Def Control	m	80			FCx	BA10

* f, female; m, male

VIB Department of molecular Genetics and Antwerp Brain Bank, Institute Born-Bunge: Antwerp, Belgium

Extended Data Table 1: Information on human brain tissue
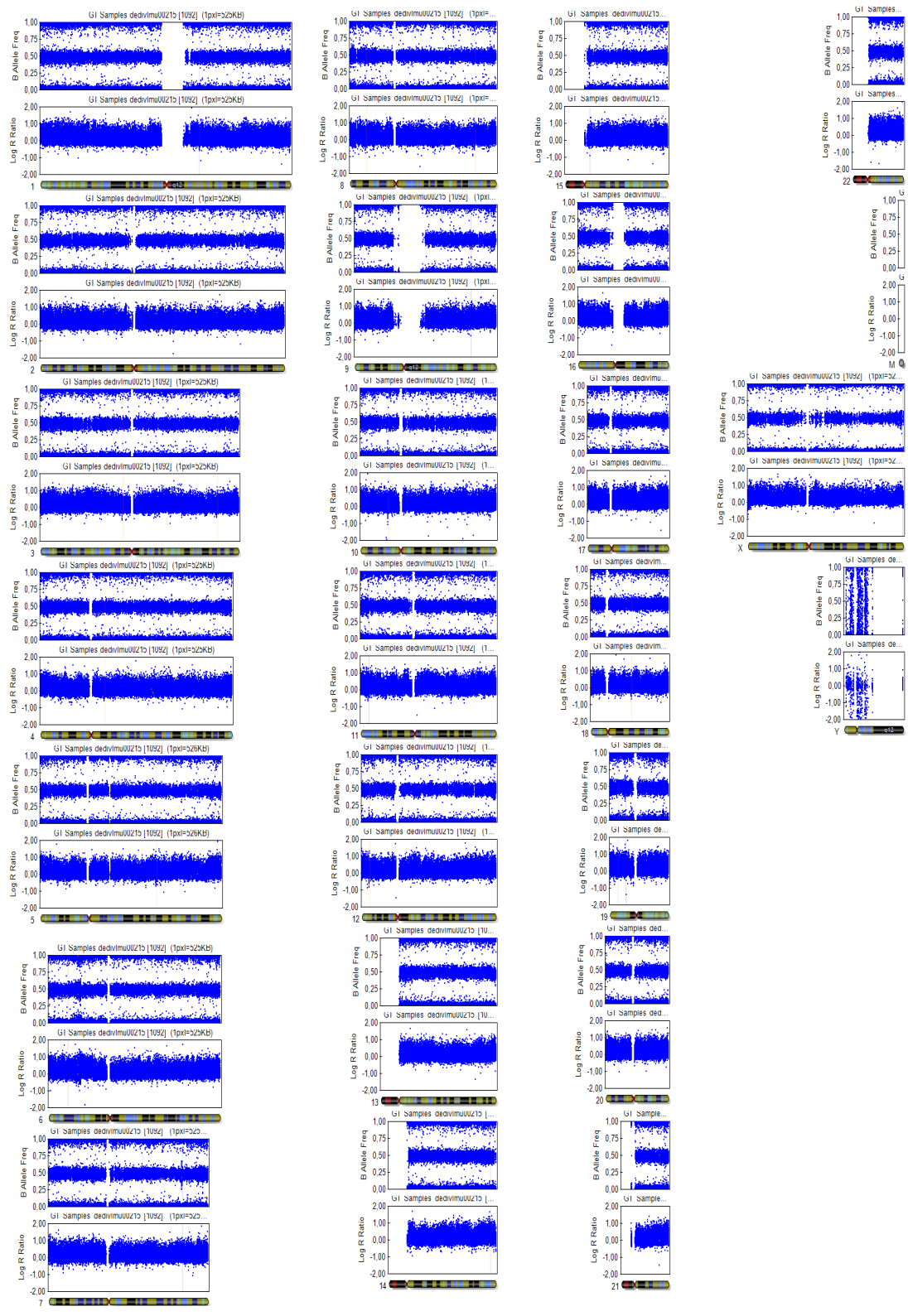
Supplement Figure 1: Molecular karyotyping of GRN ko iPSC line.

B allele frequencies (BAF) and Log R ratios of each chromosome are shown for the GRN ko iPSC line. Blue dots indicate measured SNPs. BAF values show normal zygosities on all chromosomes and Log R ratios confirm absence of detectable deletions or insertions. Overall, the karyotype shows no chromosome aberrations

4 Discussion

4.1 Summary

- PGRN LOF hiMGL have a DAM signature, increased expression of TREM2, TREM2 signaling, myelin phagocytosis, and lysosomal dysfunction
- Treatment of PGRN LOF hiMGL with TREM2 antagonistic antibodies ameliorates the DAM signature, decreases expression of TREM2, TREM2 signaling, and myelin phagocytosis, but fails to rescue the lysosomal dysfunction (Figure 6)
- TREM2/GRN *DKO* mice exhibit synaptic loss and elevated NfL levels and lysosomal dysfunction was not rescued
- LGMN proteolytic activity is strongly upregulated in GRN KO mouse brains, hiMGL, and GRN-FTLD patients and increased LGMN activity enhances TDP-43 processing into fragments enriched in inclusions (Figure 7)

4.2 Hyperactivation of PGRN-deficient microglia is secondary to lysosomal dysfunction

PGRN's critical functions in the lysosome, are illustrated by homozygous loss-of-function mutations that lead to NCL, a lysosomal storage disease (Smith et al., 2012), and by research showing that PGRN deficiency causes an upregulation of lysosomal enzyme expression and activity (Götzl et al., 2018, 2014; W. Huang et al., 2020; Klein et al., 2017; Root, Merino, Nuckols, Johnson, & Kukar, 2021a). FTLD patients with *GRN* haploinsufficiency have neuroinflammation, as measured by TSPO-PET (Götzl et al., 2019; Marschallinger et al., 2020; Martens et al., 2012; J. Zhang et al., 2020), and the microglia have a disease-associated signature (Götzl et al., 2019). It is unknown whether the lysosomal dysfunction contributes to or is a result of microglial hyperactivation and this has also not yet been investigated in a human microglia model. To address this question, I used CRISPR/Cas9 to genetically edit and knock out *GRN* in human iPSCs. I differentiated these cells into human iMicroglia (hiMGL) and characterized their transcriptomic signature, TREM2 expression, phagocytosis phenotype, and lysosomal protease expression and activity, in relation to WT hiMGL (Figure 6). I found that PGRN deficient hiMGL have an increased mRNA expression of disease-associated marker genes, including *APOE*, *SPP1*, and *TREM2*, and a decreased expression of homeostatic genes, including *P2RY12*, *CX3CR1*, and *OLFML3*. They also had a higher expression of TREM2 and

there was increased sTREM2 in conditioned media. Furthermore, there was a higher pSyk signal in the PGRN-deficient microglia, implicating increased TREM2 activation. This indicates that the hiMGL are indeed hyperactivated, with a disease-associated signature. In line with these findings, the PGRN deficient hiMGL phagocytosed more myelin than WT hiMGL. In terms of the lysosomal phenotype, the PGRN deficient hiMGL have a higher expression of lysosomal genes on a transcriptomic level, such as *CD68*, *CTSB*, and *CTSD*, as well as increased cathepsin D activity. This indicates a similar lysosomal dysfunction to what has been previously observed in murine microglia.

To investigate the effects of TREM2-dependent activation on microglial dysfunction, I treated the microglia with two independent antagonistic TREM2 antibodies (Figure 6). I found that treatment with these antibodies decreased the amount of TREM2 on the cellular membrane, increased the amount of sTREM2 shed into the media, and decreased pSyk signaling. Furthermore, antagonistic TREM2 antibody treatment successfully inhibited the increased myelin phagocytosis of PGRN deficient microglia. These results suggest that antagonistic antibodies are inhibiting ligand-binding to TREM2 and decrease TREM2 expression on the cell surface, which all together results in reduced TREM2 signaling. According to the transcriptomic signature of the PGRN deficient hiMGL after treatment, there was a decrease in expression of DAM genes, including *TREM2*, *SPP1*, *CSF1*, and an increase in expression of homeostatic genes, such as *P2RY12*. Together, this indicates that hyperactivation of PGRN deficient microglia was ameliorated. However, looking at the lysosomal phenotype, there was no effect of the treatment on the expression of lysosomal genes, such as *CTSD* and *CD68*, at a transcriptomic level. There was also no rescue of the increased cathepsin D activity. Therefore, the TREM2 inhibition treatment was unable to rescue lysosomal dysfunction caused by PGRN deficiency. To further confirm the DAM phenotype, some additional experiments that could have been done include proliferation assays, migration assays, or morphology analysis. To further explore lysosomal dysfunction, one could additionally look at lysosomal damage or abnormalities, such as Galectin-3 expression, LAMP1 stainings, or measured the lysosomal pH. I could have also looked for buildup of material that could not be digested, like lipid droplets after myelin treatment.
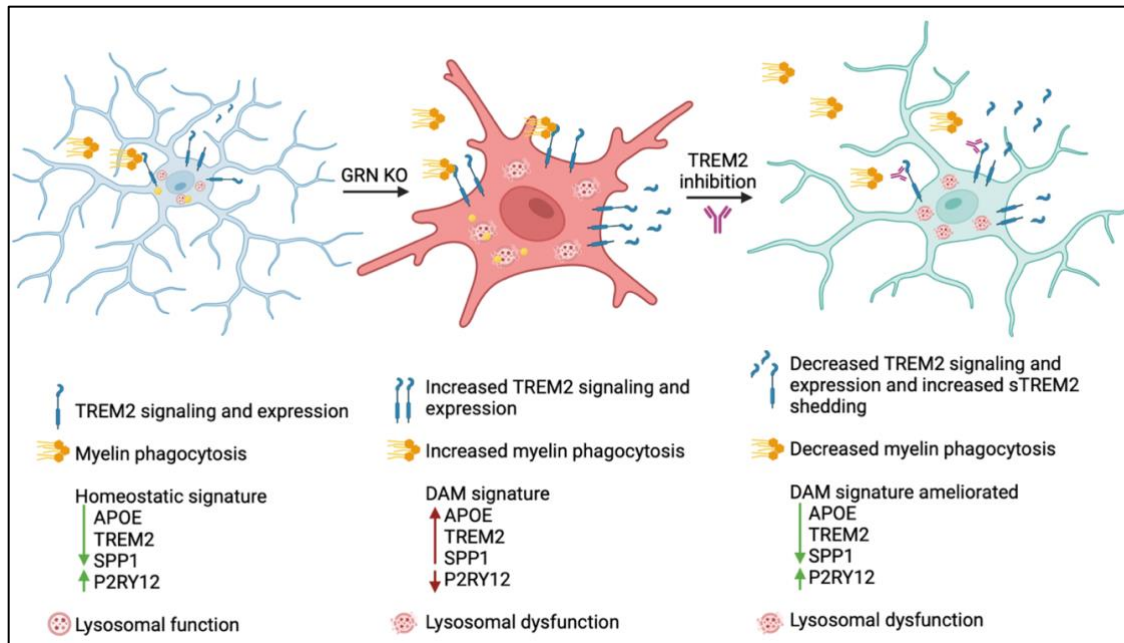
Figure 6. GRN KO hiMGL exhibit increased TREM2 signaling and expression, increased myelin phagocytosis, a DAM signature, and lysosomal dysfunction. Inhibiting TREM2 in GRN KO hiMGL decreases TREM2 signaling and expression, increases TREM2 shedding, decreases myelin phagocytosis, and ameliorates the DAM signature. However, the lysosomal dysfunction is not rescued (created with Biorender.com).

To investigate the TREM2 inhibition effects in another model, we also crossed *Trem2* KO and *Grn* KO mice, to generate a *Double* KO (DKO) model. We found, through TSPO-PET imaging, that there was a rescue of microglial hyperactivation. We also found a reduction of the DAM signature seen in the *Grn* KO mice through transcriptomic analyses. However, the lysosomal abnormalities of increased Cathepsin D expression and activity, and dysregulated lipids, were again not rescued, consistent with my results obtained in hiMGL.

The findings from both the mouse and hiMGL data indicate that the lysosomal dysfunction caused by PGRN deficiency is most likely upstream of the TREM2 signaling activation pathway and could also be independent. This means that the primary phenotype in PGRN deficient microglia is lysosomal dysfunction, which somehow causes the cells to become activated. This activation might somehow be a defensive mechanism. However, hyperactivation can be rescued with TREM2 inhibition, showing that it can be reversed, and microglia can switch back and forth between activation states, even if the lysosomal dysfunction is not rescued. This has implications on future treatments involving modulation of microglial state in neurodegenerative

disease, for example with TREM2 agonists. Since hyperactivation could be a concern for this treatment, it is reassuring to know that the microglia might not be permanently trapped in an activated state.

Also, the relationship between PGRN and TREM2 and their respective pathways is not known. What is known is that PGRN LOF microglia have high expression of TREM2 and that DAM have a high expression of both *TREM2* and *GRN* (Keren-Shaul et al., 2017). Progranulin has been shown to be anti-inflammatory (Tang et al., 2011), so it is possible that it is highly expressed in DAM to regulate an inflammatory phenotype. When it is knocked out, the microglia cannot enter a resting state without external modulation. Another potential explanation is that galectin-3, a marker for lysosomal damage (Jia et al., 2020), has been shown to be upregulated in GRN KO microglia (Logan et al., 2021), and it is also a ligand for TREM2 (Boza-Serrano et al., 2019). This could be how lysosomal dysfunction increases TREM2 expression. However, whether TREM2 and GRN are independent or related remains to be determined.

4.3 TREM2-dependent activation of PGRN LOF microglia is protective for neurons

Activated microglia are found in many neurodegenerative diseases, including AD and FTD, and believed to be detrimental through increased synaptic pruning and promoting cell death (Heneka et al., 2013; Hong, Beja-Glasser, et al., 2016; Hong, Dissing-Olesen, & Stevens, 2016). Microglia in PGRN-deficient mice also show increased phagocytosis and synaptic pruning (Götzl et al., 2019; Lui et al., 2016; J. Zhang et al., 2020). Therefore, we were curious to investigate if hyperactivation in GRN deficient mouse models is also detrimental. In the DKO mice, there was a decrease of synaptic markers, an increase in NfL in the CSF, and a significant effect on neuronal cytoskeleton, tissue integrity, and transmitter response and uptake pathways from transcriptomic analysis, consistent with increased neuropathological phenotypes. There was also reduced expression of the neuroprotective transcription factor, *Npas*. This indicates that TREM2-dependent microglial hyperactivation is not necessarily detrimental, but perhaps even protective. Our initial expectation was that TREM2 antagonistic treatment could be beneficial by alleviating the pathological phenotypes seen in PGRN LOF hiMGL and mice, since previously-seen chronically-activated microglia were shown to be damaging, for example by inducing the inflammasome (Heneka, McManus, & Latz, 2018). However, our results along with (S.-H. Lee et al., 2021) imply that even TREM2-dependent hyperactivation could be protective, and therefore therapeutic modulation with TREM2 agonistic antibodies seem to be

favorable. It also confirms the positive data seen in previously published studies on using TREM2 agonistic antibodies to treat Alzheimer's disease (Cheng et al., 2018; Cignarella et al., 2020; Price et al., 2020; Schlepckow et al., 2020; S. Wang et al., 2020). These antibodies enhance microglia phagocytosis of myelin debris and Aβ (Cignarella et al., 2020; Schlepckow et al., 2020), and improve phagocytosis of and migration towards oAβ as well as microglial survival (Zhao et al., 2022). Treatments in 5xFAD mice resulted in reduction of amyloid burden, better neuronal health, reduced tau hyperphosphorylation, and improved cognitive functions.

4.4   Redefining microglial nomenclature and states

Our study showed how dynamic microglia are in switching between states. A white paper was recently published on the topic of critically defining microglia activation states using better and internationally consistent nomenclature (Paolicelli et al., 2022). They made the point of being careful about defining microglia states using only morphology and marker genes, and that it would be better to use as many factors as possible, including functional assays. I think that it is becoming clearer in the field that the current nomenclature for describing microglial states, for example resting versus hyperactivated, can be misleading. This is because some of them already have positive or negative connotations such as resting microglia being beneficial and hyperactivated microglia being detrimental. Since microglia are immune cells, they are very responsive to their environment, both internal and external. Internal examples include lysosomal dysfunction due to PGRN deficiency, and external examples include cellular debris from degeneration or injury. These responses shape their transcriptional signature and functions, and therefore their effects on neurons and other cell types. Since there is a wide variety of factors and stimuli, there must be a wide variety of states as well (Dolan et al., 2022). I believe that it is difficult to have such rigid definitions and names for each "sub-population" and it must be more of a spectrum or gradient since one "sub-population" can have overlapping phenotypes and marker genes with another. For example, our study showed that the TREM2 antagonistic antibody treated PGRN LOF hiMGL and GRN/TREM2 DKO murine microglia can have an ameliorated activation signature and an upregulated homeostatic signature, but still have lysosomal dysfunction and a neurotoxic effect. Another example is that both interferon-responsive (Aw, Zhang, & Carroll, 2020; Dorman et al., 2022; Roy et al., 2020) and disease-associated microglia (Keren-Shaul et al., 2017) have increased phagocytosis abilities and have higher CD68 expression. However, proinflammatory microglia have been shown to be detrimental and DAM2 have been shown to be protective (S.-H. Lee et al., 2021). More general

terms, such as "homeodynamic" and "responding" microglia for different stimuli can be more appropriate, since these describe the activities performed by microglia in different contexts. It is also important to realize that microglia are very plastic and can transition between reactive states.

## 4.5   Legumain links progranulin deficiency with TDP-43 pathology in FTD

Mutations that result in haploinsufficiency of PGRN lead to frontotemporal dementia with FTLD-TDP pathology. However, the link between PGRN loss of function and TDP-43 pathology is unknown. In *Grn* KO mice, LGMN activity and expression of mature LGMN was found to be increased at all ages from 3 months to 2 years old. *Grn* KO murine embryonic fibroblasts (MEF) also have increased LGMN activity and expression. These results imply that PGRN inhibits the maturation of LGMN. The increased LGMN activity and expression in the MEF cells correlates with enhanced proteolytic TDP-43 processing into fragments seen in pathological inclusions (Herskowitz et al., 2012). When the cells are treated with a *Lgmn* siRNA, effectively knocking down its activity and expression, TDP-43 processing is rescued to WT levels. In primary murine neuron cultures transfected with WT *Lgmn*, TDP-43 processing is also enhanced, to the point where the 25 kDa CTF is seen as well. CTF formation includes removal of the nuclear localization signal of TDP-43, which may lead to its cytoplasmic accumulation and further aggregation. In PGRN deficient hiMGL, I found increased LGMN expression on both the protein and RNA level as well as increased proteolytic activity. However, there was only immature LGMN expressed in WT and GRN KO iNeurons and almost no proteolytic activity. When co-culturing the hiMGL with WT iNeurons, there was increased LGMN expression and activity in the GRN KO hiMGL co-culture, which correlated with increased TDP-43 processing into smaller fragments found in pathological deposits (Figure 7) (Herskowitz et al., 2012). The WT iNeuron and GRN KO hiMGL co-cultures were treated with AAV-Cst7 under a human synapsin (hSyn) promotor, which is specific for neurons (Figure 8). The treatment prevented the elevated levels of mature LGMN and LGMN activity, as well as TDP-43 processing. This implies that the elevated LGMN expression and activity, and the TDP-43 processing in the co-cultures were neuron-specific. Since the iNeurons in all the conditions were WT, the pathology must be a result from the hiMGL genotype in the co-cultures. However, it is still unknown how legumain is transferred from microglia to neurons, either through secretion and uptake, like with exosomes (Guo et al., 2021), or direct contact, like through nanotubes (Chakraborty, Nonaka, Hasegawa, & Zurzolo, 2023; Scheiblich et al., 2021), or if the microglia induce an upregulation of legumain

expression in the neurons. The implied cross talk between the microglia and neurons resolves the spatial paradox of predominant PGRN and LGMN expression in microglia and TDP-43 pathology observed in neurons.

However, this pathologically increased LGMN activity increases abnormal processing of lysosomal cathepsins (Götzl et al., 2018, 2014; Klein et al., 2017; Tanaka et al., 2017), which may result in lysosomal dysfunction. Therefore, other lysosomal proteases cannot be completely excluded. In the future, the mechanism of legumain transfer between microglia and neurons can be further investigated by fluorescently tagging legumain to see if it is traveling from one cell type to another and to see if there is any interaction between legumain and TDP-43. Another option is specific legumain inhibition in microglia and checking the TDP-43 processing in co-cultured neurons.
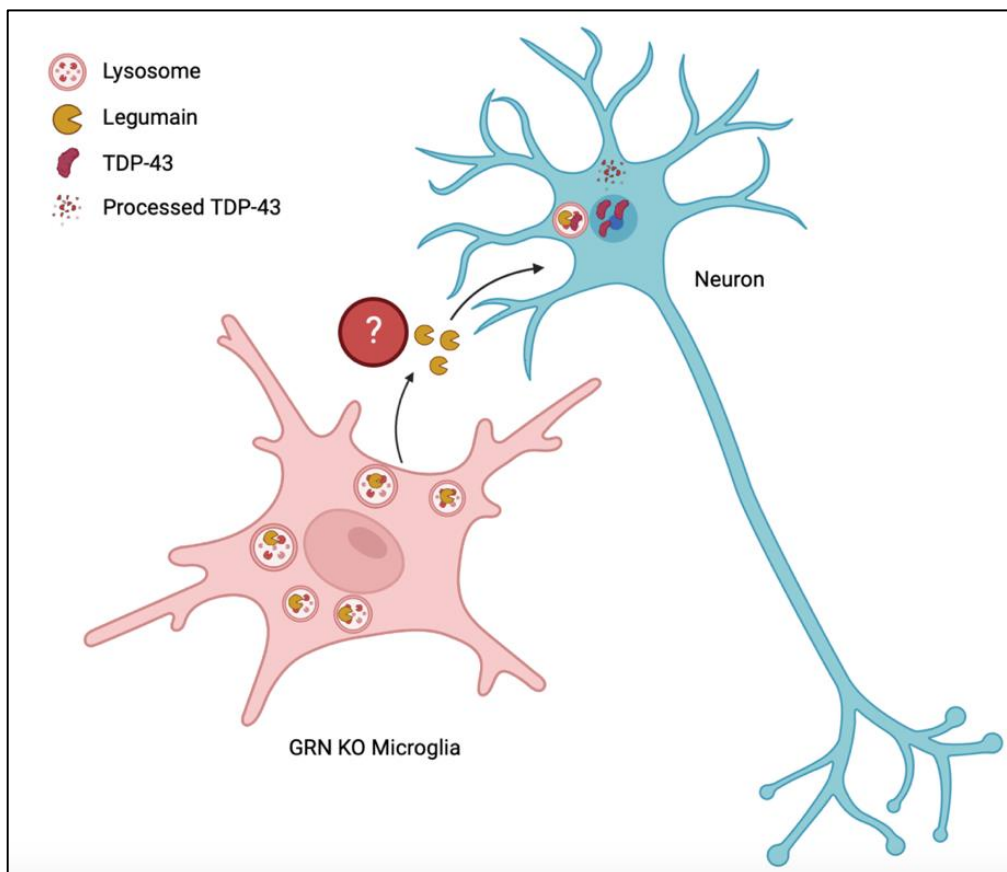
Figure 7. Legumain expression and activity is upregulated in GRN KO microglia. The legumain is transferred to neurons through an unknown mechanism, where it abnormally processes TDP-43. These abnormally processed TDP-43 fragments are a pathological species (created with Biorender.com).
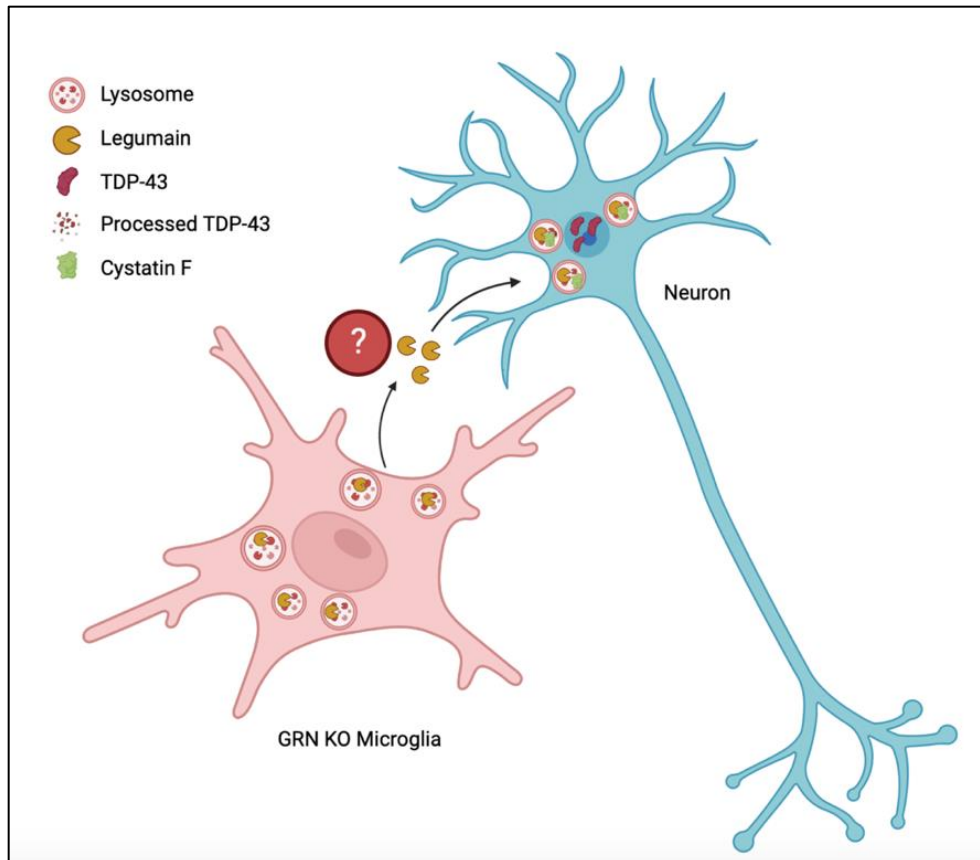
Figure 8. Legumain expression and activity is upregulated in GRN KO microglia. Legumain is transferred to neurons through an unknown mechanism, where it abnormally processes TDP-43. AAV induction of Cystatin F is neuron-specific and the treatment inhibits LGMN activity and prevents TDP-43 processing (created with Biorender.com).

4.6   Consequences for therapeutic treatment of FTD-*GRN*

Our study has implied that treating FTD with TREM2 inhibition would not be beneficial. Not only does it not rescue the lysosomal dysfunction that is seen in the microglia, but it can increase neuropathological phenotypes. Therefore, efforts should be directed at other targets, possibly focusing on the lysosome. One possibility is legumain inhibition. We have shown that inhibiting legumain activity prevents pathological processing of TDP-43. Another possibility that is already being investigated is PGRN replacement therapy (Logan et al., 2021). Logan et al. were able to rescue various phenotypes in PGRN LOF primary murine macrophages and hiMGL including lysosomal dysfunction, endomembrane damage, and oxidative stress. In *Grn* KO mice, they were able to correct levels of glycosylsphingosine and bis(monoacylglycero) phosphate (BMP) and rescue some disease pathology including lipofuscinosis, microgliosis, and neuron damage.

However, since the current PGRN LOF mouse and iPSC-derived models used do not show other aspects of TDP-43 pathology, such as aggregation and mislocalization, it is difficult to investigate possible therapeutics.

4.7   Outlook

The most recent development in iPSC-derived disease modeling is the establishment of the chimeric mouse model. Namely, the transplantation of either human iPSC-derived hiMGL progenitor cells (Abud et al., 2017; Bennett et al., 2018; Claes et al., 2021, 2022; Hasselmann et al., 2019; Mancuso et al., 2019; Mathews et al., 2019; Mcquade et al., 2020; Svoboda et al., 2019) or neuroprogenitor cells (NPCs) (Chen, Kim, & Jiang, 2016; Espuny-Camacho et al., 2017; Najm et al., 2020; Preman et al., 2021) into a mouse brain. The mice used for these experiments need to be immunodeficient (Rag KO or NOD-SCID), so the transplanted cells are not rejected. For the human microglia transplantations, the mice also need to have humanized CSF1 (hCSF1) so human cells can survive. Required cell types are differentiated *in vitro* and then injected into pups, where they further differentiate into either microglia or neurons, respectively. hiMGL transplanted into mice look morphologically heterogeneous, indicating that they are responding to distinct brain regions, potentially reflecting microglia subtypes found in the brain (Abud et al., 2017) since it was previously shown that microglia have region-dependent transcriptional identities (Grabert et al., 2016). Transcriptionally, the transplanted hiMGL in AD mouse models recapitulate a complex expression profile that is characteristic of microglia isolated from human AD-patient tissue (Hasselmann et al., 2019; Mancuso et al., 2019). The cells also have a robust transcriptional response to Aβ-plaques that diverge from and only partially overlap with mouse microglia, revealing novel Aβ response genes that are human specific (Hasselmann et al., 2019; Mancuso et al., 2019). The TREM2 pathway is, however, conserved. Since this model also allows for customization and flexibility in terms of genotypes of both the iPSC-derived cells and mouse, it has been used to study TREM2 KO hiMGL and TREM2 R47H hiMGL in AD mouse models (Claes et al., 2021; Mcquade et al., 2020). Human iNeurons transplanted into the brain of an AD mouse model successfully integrate and express 3R/4R Tau splice isoforms, have abnormal phosphorylation of Tau, conformational Tau changes, and undergo neurodegeneration (Espuny-Camacho et al., 2017). Therefore, this chimeric model has shown success in terms of recapitulating pathological phenotypes of AD in the human iPSC-derived cells (Abud et al., 2017; Claes et al., 2021;

Espuny-Camacho et al., 2017; Hasselmann et al., 2019; Mancuso et al., 2019; Mcquade et al., 2020; Najm et al., 2020; Preman et al., 2021).

As an outlook for my research, I would like to utilize chimeric mouse models to hopefully create a more complete model of FTLD-TDP. Since I have already shown that GRN KO hiMGL can have pathological effects on TDP-43 in neurons, I would like to push this further by using TDP-43 mutant iPSC-derived neurons. The neurons would have a TARDBP M337V mutation, that increases mislocalization and insolubility of TDP-43 (Bilican et al., 2012; Mutihac et al., 2015; Nishimura et al., 2014). I will transplant these NPCs, along with GRN KO hiMGL, into hCSF1 mice (Claes et al., 2022), in hopes of having a model that shows more complete pathology seen in human patients (Figure 9).
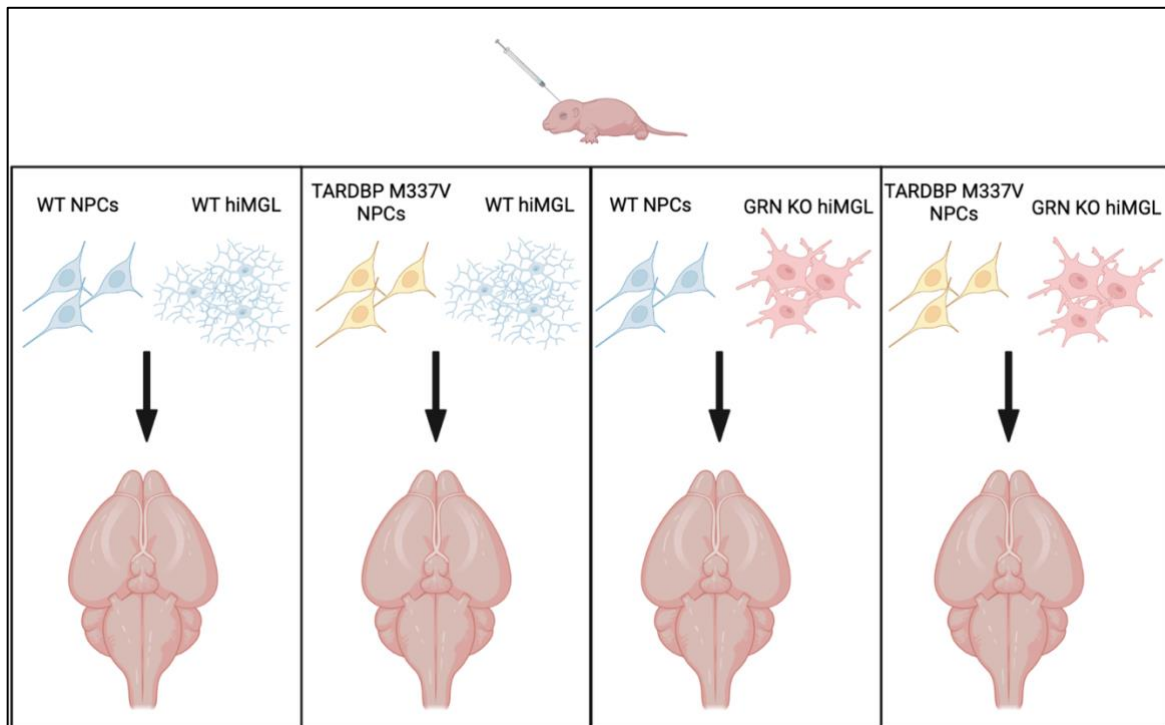
Figure 9. Experimental plan for chimeric mouse model of TDP-43 pathology (made with Biorender.com).

In addition, I will use synergistic modifications by mutating the NLS of *TARDBP* and combining it with the M337V mutation to encourage mislocalization of TDP-43 into the cytoplasm and aggregation. To supplement the 2D co-cultures, I will make 3D brain-tissue-models using these neurons along with WT or PGRN LOF microglia, where the more brain-like environment could also encourage a pathological phenotype.

5 References

Abella, V., Pino, J., Scotece, M., Conde, J., Lago, F., Gonzalez-Gay, M. A., … Gualillo, O. (2017). Progranulin as a biomarker and potential therapeutic agent. *Drug Discovery Today*, *22*(10), 1557–1564. https://doi.org/10.1016/J.DRUDIS.2017.06.006

Abud, E. M., Ramirez, R. N., Martinez, E. S., Healy, L. M., Nguyen, C. H. H., Newman, S. A., … Blurton-Jones, M. (2017). iPSC-Derived Human Microglia-like Cells to Study Neurological Diseases. *Neuron*, *94*(2), 278-293.e9. https://doi.org/10.1016/j.neuron.2017.03.042

Ahmed, Z., Sheng, H., Xu, Y. F., Lin, W. L., Innes, A. E., Gass, J., … Lewis, J. (2010). Accelerated Lipofuscinosis and Ubiquitination in Granulin Knockout Mice Suggest a Role for Progranulin in Successful Aging. *The American Journal of Pathology*, *177*(1), 311–324. https://doi.org/10.2353/AJPATH.2010.090915

Alami, N. H., Smith, R. B., Carrasco, M. A., Williams, L. A., Winborn, C. S., Han, S. S. W., … Taylor, J. P. (2014). Axonal transport of TDP-43 mRNA granules is impaired by ALS-causing mutations. *Neuron*, *81*(3), 536–543. https://doi.org/10.1016/J.NEURON.2013.12.018

Alberti, S., Halfmann, R., King, O., Kapila, A., & Lindquist, S. (2009). A systematic survey identifies prions and illuminates sequence features of prionogenic proteins. *Cell*, *137*(1), 146–158. https://doi.org/10.1016/J.CELL.2009.02.044

Almeida, S., Zhang, Z., Coppola, G., Mao, W., Futai, K., Karydas, A., … Gao, F. B. (2012). Induced Pluripotent Stem Cell Models of Progranulin-Deficient Frontotemporal Dementia Uncover Specific Reversible Neuronal Defects. *Cell Reports*, *2*(4), 789–798. https://doi.org/10.1016/j.celrep.2012.09.007

Arai, T., Hasegawa, M., Akiyama, H., Ikeda, K., Nonaka, T., Mori, H., … Oda, T. (2006). TDP-43 is a component of ubiquitin-positive tau-negative inclusions in frontotemporal lobar degeneration and amyotrophic lateral sclerosis. *Biochemical and Biophysical Research Communications*, *351*(3), 602–611. https://doi.org/10.1016/J.BBRC.2006.10.093

Archbold, H. C., Jackson, K. L., Arora, A., Weskamp, K., Tank, E. M. H., Li, X., … Barmada, S. J. (2018). TDP43 nuclear export and neurodegeneration in models of amyotrophic lateral sclerosis and frontotemporal dementia. *Scientific Reports*, *8*(1). https://doi.org/10.1038/S41598-018-22858-W

Arrant, A. E., Davis, S. E., Vollmer, R. M., Murchison, C. F., Mobley, J. A., Nana, A. L., … Roberson, E. D. (2020). Elevated levels of extracellular vesicles in progranulin-deficient mice and FTD-GRN Patients. *Annals of Clinical and Translational Neurology*, *7*(12), 2433–

2449. https://doi.org/10.1002/ACN3.51242

Arrant, A. E., Filiano, A. J., Patel, A. R., Hoffmann, M. Q., Boyle, N. R., Kashyap, S. N., … Roberson, E. D. (2019). Reduction of microglial progranulin does not exacerbate pathology or behavioral deficits in neuronal progranulin-insufficient mice. *Neurobiology of Disease*, *124*(October 2018), 152–162. https://doi.org/10.1016/j.nbd.2018.11.011

Arrant, A. E., Roth, J. R., Boyle, N. R., Kashyap, S. N., Hoffmann, M. Q., Murchison, C. F., … Roberson, E. D. (2019). Impaired β-glucocerebrosidase activity and processing in frontotemporal dementia due to progranulin mutations. *Acta Neuropathologica Communications*, *7*(1). https://doi.org/10.1186/s40478-019-0872-6

Ash, P. E. A., Zhang, Y. J., Roberts, C. M., Saldi, T., Hutter, H., Buratti, E., … Link, C. D. (2010). Neurotoxic effects of TDP-43 overexpression in C. elegans. *Human Molecular Genetics*, *19*(16), 3206–3218. https://doi.org/10.1093/HMG/DDQ230

Ashwell, K. (1990). Microglia and cell death in the developing mouse cerebellum. *Developmental Brain Research*, *55*(2), 219–230. https://doi.org/10.1016/0165-3806(90)90203-B

Atagi, Y., Liu, C. C., Painter, M. M., Chen, X. F., Verbeeck, C., Zheng, H., … Bu, G. (2015). Apolipoprotein E Is a Ligand for Triggering Receptor Expressed on Myeloid Cells 2 (TREM2). *The Journal of Biological Chemistry*, *290*(43), 26043–26050. https://doi.org/10.1074/JBC.M115.679043

Aw, E., Zhang, Y., & Carroll, M. (2020). Microglial responses to peripheral type 1 interferon. *Journal of Neuroinflammation*, *17*(1), 1–13. https://doi.org/10.1186/S12974-020-02003-Z/FIGURES/5

Ayala, Y. M., Pantano, S., D'Ambrogio, A., Buratti, E., Brindisi, A., Marchetti, C., … Baralle, F. E. (2005). Human, Drosophila, and C.elegans TDP43: nucleic acid binding properties and splicing regulatory function. *Journal of Molecular Biology*, *348*(3), 575–588. https://doi.org/10.1016/J.JMB.2005.02.038

Bai, X.-H., Wang, D.-W., Kong, L., Zhang, Y., Luan, Y., Kobayashi, T., … Liu, C.-J. (2009). ADAMTS-7, a Direct Target of PTHrP, Adversely Regulates Endochondral Bone Growth by Associating with and Inactivating GEP Growth Factor §. *MOLECULAR AND CELLULAR BIOLOGY*, *29*(15), 4201–4219. https://doi.org/10.1128/MCB.00056-09

Bailey, C. C., Devaux, L. B., & Farzan, M. (2015). The Triggering Receptor Expressed on Myeloid Cells 2 Binds Apolipoprotein E. *The Journal of Biological Chemistry*, *290*(43), 26033–26042. https://doi.org/10.1074/JBC.M115.677286

Baker, M., Mackenzie, I. R., Pickering-Brown, S. M., Gass, J., Rademakers, R., Lindholm, C., …

Hutton, M. (2006). Mutations in progranulin cause tau-negative frontotemporal dementia linked to chromosome 17. *Nature*, *442*(7105), 916–919. https://doi.org/10.1038/nature05016

Barrangou, R., Fremaux, C., Deveau, H., Richards, M., Boyaval, P., Moineau, S., … Horvath, P. (2007). CRISPR provides acquired resistance against viruses in prokaryotes. *Science (New York, N.Y.)*, *315*(5819), 1709–1712. https://doi.org/10.1126/SCIENCE.1138140

Belcastro, V., Siciliano, V., Gregoretti, F., Mithbaokar, P., Dharmalingam, G., Berlingieri, S., … Di Bernardo, D. (2011). Transcriptional gene network inference from a massive dataset elucidates transcriptome organization and gene function. *Nucleic Acids Research*, *39*(20), 8677–8688. https://doi.org/10.1093/nar/gkr593

Bennett, F. C., Bennett, M. L., Yaqoob, F., Mulinyawe, S. B., Grant, G. A., Hayden Gephart, M., … Barres, B. A. (2018). A Combination of Ontogeny and CNS Environment Establishes Microglial Identity. *Neuron*, *98*(6), 1170-1183.e8. https://doi.org/10.1016/J.NEURON.2018.05.014

Bilican, B., Serio, A., Barmada, S. J., Nishimura, A. L., Sullivan, G. J., Carrasco, M., … Chandran, S. (2012). Mutant induced pluripotent stem cell lines recapitulate aspects of TDP-43 proteinopathies and reveal cell-specific vulnerability. *Proceedings of the National Academy of Sciences of the United States of America*, *109*(15), 5803–5808. https://doi.org/10.1073/pnas.1202922109

Birnbaum, J. H., Wanner, D., Gietl, A. F., Saake, A., Kündig, T. M., Hock, C., … Tackenberg, C. (2018). Oxidative stress and altered mitochondrial protein expression in the absence of amyloid-β and tau pathology in iPSC-derived neurons from sporadic Alzheimer's disease patients. *Stem Cell Research*, *27*, 121–130. https://doi.org/10.1016/J.SCR.2018.01.019

Bis, J. C., Jian, X., Kunkle, B. W., Chen, Y., Hamilton-Nelson, K. L., Bush, W. S., … Farrer, L. A. (2020). Whole exome sequencing study identifies novel rare and common Alzheimer's-Associated variants involved in immune response and transcriptional regulation. *Molecular Psychiatry*, *25*(8), 1859–1875. https://doi.org/10.1038/S41380-018-0112-7

Borroni, B., Ferrari, F., Galimberti, D., Nacmias, B., Barone, C., Bagnoli, S., … Padovani, A. (2014). Heterozygous TREM2 mutations in frontotemporal dementia. *Neurobiology of Aging*, *35*(4), 934.e7-934.e10. https://doi.org/10.1016/J.NEUROBIOLAGING.2013.09.017

Bowden, H. A., & Dormann, D. (2016). Altered mRNP granule dynamics in FTLD pathogenesis. *Journal of Neurochemistry*, *138*, 112–133. https://doi.org/10.1111/JNC.13601

Boza-Serrano, A., Ruiz, R., Sanchez-Varo, R., García-Revilla, J., Yang, Y., Jimenez-Ferrer, I., … Deierborg, T. (2019). Galectin-3, a novel endogenous TREM2 ligand, detrimentally

regulates inflammatory response in Alzheimer's disease. *Acta Neuropathologica*, *138*(2), 251–273. https://doi.org/10.1007/S00401-019-02013-Z

Brassard, J. A., & Lutolf, M. P. (2019). Engineering Stem Cell Self-organization to Build Better Organoids. *Cell Stem Cell*, *24*(6), 860–876. https://doi.org/10.1016/J.STEM.2019.05.005

Brouns, S. J. J., Jore, M. M., Lundgren, M., Westra, E. R., Slijkhuis, R. J. H., Snijders, A. P. L., … Van Der Oost, J. (2008). Small CRISPR RNAs guide antiviral defense in prokaryotes. *Science*, *321*(5891), 960–964. https://doi.org/10.1126/science.1159689

Buratti, E., & Baralle, F. E. (2001). Characterization and functional implications of the RNA binding properties of nuclear factor TDP-43, a novel splicing regulator of CFTR exon 9. *The Journal of Biological Chemistry*, *276*(39), 36337–36343. https://doi.org/10.1074/JBC.M104236200

Butler, G. S., Dean, R. A., Tam, E. M., & Overall, C. M. (2008). Pharmacoproteomics of a Metalloproteinase Hydroxamate Inhibitor in Breast Cancer Cells: Dynamics of Membrane Type 1 Matrix Metalloproteinase-Mediated Membrane Protein Shedding. *Molecular and Cellular Biology*, *28*(15), 4896–4914. https://doi.org/10.1128/mcb.01775-07

Butovsky, O., Jedrychowski, M. P., Moore, C. S., Cialic, R., Lanser, A. J., Gabriely, G., … Weiner, H. L. (2014). Identification of a unique TGF-β-dependent molecular and functional signature in microglia. *Nature Neuroscience*, *17*(1), 131–143. https://doi.org/10.1038/nn.3599

Campbell, C. A., Fursova, O., Cheng, X., Snella, E., McCune, A., Li, L., … Espín-Palazón, R. (2021). A zebrafish model of granulin deficiency reveals essential roles in myeloid cell differentiation. *Blood Advances*, *5*(3), 796–811. https://doi.org/10.1182/BLOODADVANCES.2020003096

Capell, A., Liebscher, S., Fellerer, K., Brouwers, N., Willem, M., Lammich, S., … Haass, C. (2011). Rescue of progranulin deficiency associated with frontotemporal lobar degeneration by alkalizing reagents and inhibition of vacuolar ATPase. *Journal of Neuroscience*, *31*(5), 1885–1894. https://doi.org/10.1523/JNEUROSCI.5757-10.2011

Chakraborty, R., Nonaka, T., Hasegawa, M., & Zurzolo, C. (2023). Tunnelling nanotubes between neuronal and microglial cells allow bi-directional transfer of α-Synuclein and mitochondria. *Cell Death & Disease*, *14*(5). https://doi.org/10.1038/S41419-023-05835-8

Chang, C. ke, Wu, T. H., Wu, C. Y., Chiang, M. hui, Toh, E. K. W., Hsu, Y. C., … Huang, J. J. T. (2012). The N-terminus of TDP-43 promotes its oligomerization and enhances DNA binding affinity. *Biochemical and Biophysical Research Communications*, *425*(2), 219–224. https://doi.org/10.1016/J.BBRC.2012.07.071

Chang, M. C., Srinivasan, K., Friedman, B. A., Suto, E., Modrusan, Z., Lee, W. P., … Sheng, M. (2017). Progranulin deficiency causes impairment of autophagy and TDP-43 accumulation. *Journal of Experimental Medicine*, *214*(9), 2611–2628. https://doi.org/10.1084/JEM.20160999

Chen, C., Kim, W. Y., & Jiang, P. (2016). Humanized neuronal chimeric mouse brain generated by neonatally engrafted human iPSC-derived primitive neural progenitor cells. *JCI Insight*, *1*(19). https://doi.org/10.1172/JCI.INSIGHT.88632

Cheng, Q., Danao, J., Talreja, S., Wen, P., Yin, J., Sun, N., … Sambashivan, S. (2018). TREM2-activating antibodies abrogate the negative pleiotropic effects of the Alzheimer's disease variant Trem2R47H on murine myeloid cell function. *Journal of Biological Chemistry*, *293*(32), 12620–12633. https://doi.org/10.1074/jbc.RA118.001848

Chitramuthu, B. P., Baranowski, D. C., Kay, D. G., Bateman, A., & Bennett, H. P. J. (2010). Progranulin modulates zebrafish motoneuron development in vivo and rescues truncation defects associated with knockdown of Survival motor neuron 1. *Molecular Neurodegeneration*, *5*(1), 1–13. https://doi.org/10.1186/1750-1326-5-41/FIGURES/9

Chitramuthu, B. P., & Bennett, H. P. J. (2018). Application of zebrafish and knockdown technology to define progranulin neuronal function. *Methods in Molecular Biology*, *1806*, 207–231. https://doi.org/10.1007/978-1-4939-8559-3_15/COVER

Cho, S. W., Kim, S., Kim, J. M., & Kim, J. S. (2013). Targeted genome engineering in human cells with the Cas9 RNA-guided endonuclease. *Nature Biotechnology*, *31*(3), 230–232. https://doi.org/10.1038/nbt.2507

Choi, S. H., Kim, Y. H., Hebisch, M., Sliwinski, C., Lee, S., D'Avanzo, C., … Kim, D. Y. (2014). A three-dimensional human neural cell culture model of Alzheimer's disease. *Nature 2014 515:7526*, *515*(7526), 274–278. https://doi.org/10.1038/NATURE13800

Cignarella, F., Filipello, F., Bollman, B., Cantoni, C., Locca, A., Mikesell, R., … Piccio, L. (2020). TREM2 activation on microglia promotes myelin debris clearance and remyelination in a model of multiple sclerosis. *Acta Neuropathologica*, *140*(4), 513–534. https://doi.org/10.1007/s00401-020-02193-z

Claes, C., Danhash, E. P., Hasselmann, J., Chadarevian, J. P., Shabestari, S. K., England, W. E., … Blurton-Jones, M. (2021). Plaque-associated human microglia accumulate lipid droplets in a chimeric model of Alzheimer's disease. *Molecular Neurodegeneration*, *16*(1). https://doi.org/10.1186/s13024-021-00473-0

Claes, C., England, W. E., Danhash, E. P., Kiani Shabestari, S., Jairaman, A., Chadarevian, J. P., … Davtyan, H. (2022). The P522R protective variant of PLCG2 promotes the

expression of antigen presentation genes by human microglia in an Alzheimer's disease mouse model. *Alzheimer's & Dementia*. https://doi.org/10.1002/ALZ.12577

Colonna, M. (2003). TREMs in the immune system and beyond. *Nature Reviews Immunology 2003 3:6*, *3*(6), 445–453. https://doi.org/10.1038/NRI1106

Cong, L., Ran, F. A., Cox, D., Lin, S., Barretto, R., Habib, N., … Zhang, F. (2013). Multiplex genome engineering using CRISPR/Cas systems. *Science*, *339*(6121), 819–823. https://doi.org/10.1126/science.1231143

Conicella, A. E., Zerze, G. H., Mittal, J., & Fawzi, N. L. (2016). ALS Mutations Disrupt Phase Separation Mediated by α-Helical Structure in the TDP-43 Low-Complexity C-Terminal Domain. *Structure*, *24*(9), 1537–1549. https://doi.org/10.1016/J.STR.2016.07.007

Coyne, A. N., Siddegowda, B. B., Estes, P. S., Johannesmeyer, J., Kovalik, T., Daniel, S. G., … Zarnescu, D. C. (2014). Futsch/MAP1B mRNA Is a Translational Target of TDP-43 and Is Neuroprotective in a Drosophila Model of Amyotrophic Lateral Sclerosis. *Journal of Neuroscience*, *34*(48), 15962–15974. https://doi.org/10.1523/JNEUROSCI.2526-14.2014

Cruts, M., Gijselinck, I., Van Der Zee, J., Engelborghs, S., Wils, H., Pirici, D., … Van Broeckhoven, C. (2006). Null mutations in progranulin cause ubiquitin-positive frontotemporal dementia linked to chromosome 17q21. *Nature*, *442*(7105), 920–924. https://doi.org/10.1038/nature05017

Cuyvers, E., Bettens, K., Philtjens, S., Van Langenhove, T., Gijselinck, I., van der Zee, J., … Sleegers, K. (2014). Investigating the role of rare heterozygous TREM2 variants in Alzheimer's disease and frontotemporal dementia. *Neurobiology of Aging*, *35*(3), 726.e11-726.e19. https://doi.org/10.1016/J.NEUROBIOLAGING.2013.09.009

Dall, E., & Brandstetter, H. (2013). Mechanistic and structural studies on legumain explain its zymogenicity, distinct activation pathways, and regulation. *Proceedings of the National Academy of Sciences of the United States of America*, *110*(27), 10940–10945. https://doi.org/10.1073/pnas.1300686110

Davalos, D., Grutzendler, J., Yang, G., Kim, J. V., Zuo, Y., Jung, S., … Gan, W. B. (2005). ATP mediates rapid microglial response to local brain injury in vivo. *Nature Neuroscience 2005 8:6*, *8*(6), 752–758. https://doi.org/10.1038/NN1472

Daws, M. R., Sullam, P. M., Niemi, E. C., Chen, T. T., Tchao, N. K., & Seaman, W. E. (2003). Pattern recognition by TREM-2: binding of anionic ligands. *Journal of Immunology (Baltimore, Md. : 1950)*, *171*(2), 594–599. https://doi.org/10.4049/JIMMUNOL.171.2.594

De Muynck, L., & Van Damme, P. (2011). Cellular effects of progranulin in health and disease. *Journal of Molecular Neuroscience*, *45*(3), 549–560. https://doi.org/10.1007/S12031-011-

9553-Z/FIGURES/2

Deltcheva, E., Chylinski, K., Sharma, C. M., Gonzales, K., Chao, Y., Pirzada, Z. A., … Charpentier, E. (2011). CRISPR RNA maturation by trans-encoded small RNA and host factor RNase III. *Nature*, *471*(7340), 602–607. https://doi.org/10.1038/nature09886

Dolan, M.-J., Therrien, M., Jereb, S., Kamath, T., Atkeson, T., Marsh, S. E., … Stevens, B. (2022). A resource for generating and manipulating human microglial states in vitro. *BioRxiv*.

Dorman, L. C., Nguyen, P. T., Escoubas, C. C., Vainchtein, I. D., Xiao, Y., Lidsky, P. V, … Molofsky, A. V. (2022). A type I interferon response defines a conserved microglial state required for effective neuronal phagocytosis. *BioRxiv : The Preprint Server for Biology*. https://doi.org/10.1101/2021.04.29.441889

Doyle, J. J., Maios, C., Vrancx, C., Duhaime, S., Chitramuthu, B., Bennett, H. P. J., … Parker, J. A. (2021). Chemical and genetic rescue of in vivo progranulin-deficient lysosomal and autophagic defects. *Proceedings of the National Academy of Sciences of the United States of America*, *118*(25). https://doi.org/10.1073/PNAS.2022115118/-/DCSUPPLEMENTAL

Ederle, H., & Dormann, D. (2017). TDP-43 and FUS en route from the nucleus to the cytoplasm. *FEBS Letters*, *591*(11), 1489–1507. https://doi.org/10.1002/1873-3468.12646

Espuny-Camacho, I., Arranz, A. M., Fiers, M., Snellinx, A., Ando, K., Munck, S., … De Strooper, B. (2017). Hallmarks of Alzheimer's Disease in Stem-Cell-Derived Human Neurons Transplanted into Mouse Brain. *Neuron*, *93*(5), 1066-1081.e8. https://doi.org/10.1016/j.neuron.2017.02.001

Ewers, M., Franzmeier, N., Suárez-Calvet, M., Morenas-Rodriguez, E., Caballero, M. A. A., Kleinberger, G., … Haass, C. (2019). Increased soluble TREM2 in cerebrospinal fluid is associated with reduced cognitive and clinical decline in Alzheimer's disease. *Science Translational Medicine*, *11*(507). https://doi.org/10.1126/scitranslmed.aav6221

François-Moutal, L., Perez-Miller, S., Scott, D. D., Miranda, V. G., Mollasalehi, N., & Khanna, M. (2019). Structural Insights Into TDP-43 and Effects of Post-translational Modifications. *Frontiers in Molecular Neuroscience*, *12*. https://doi.org/10.3389/FNMOL.2019.00301

Freibaum, B. D., Chitta, R. K., High, A. A., & Taylor, J. P. (2010). Global analysis of TDP-43 interacting proteins reveals strong association with RNA splicing and translation machinery. *Journal of Proteome Research*, *9*(2), 1104–1120. https://doi.org/10.1021/PR901076Y/SUPPL_FILE/PR901076Y_SI_004.PDF

Frew, J., & Nygaard, H. B. (2021). Neuropathological and behavioral characterization of aged Grn R493X progranulin-deficient frontotemporal dementia knockin mice. *Acta*

Neuropathologica Communications, *9*(1). https://doi.org/10.1186/S40478-021-01158-X

Frost, J. L., & Schafer, D. P. (2016). Microglia: Architects of the Developing Nervous System. *Trends in Cell Biology*, *26*(8), 587–597. https://doi.org/10.1016/J.TCB.2016.02.006

Gasiunas, G., Barrangou, R., Horvath, P., & Siksnys, V. (2012). Cas9-crRNA ribonucleoprotein complex mediates specific DNA cleavage for adaptive immunity in bacteria. *Proceedings of the National Academy of Sciences of the United States of America*, *109*(39). https://doi.org/10.1073/pnas.1208507109

Geser, F., Martinez-Lage, M., Robinson, J., Uryu, K., Neumann, M., Brandmeir, N. J., … Trojanowski, J. Q. (2009). Clinical and Pathological Continuum of Multisystem TDP-43 Proteinopathies. *Archives of Neurology*, *66*(2), 180. https://doi.org/10.1001/ARCHNEUROL.2008.558

Ghoshal, N., Dearborn, J. T., Wozniak, D. F., & Cairns, N. J. (2012). Core features of frontotemporal dementia recapitulated in progranulin knockout mice. *Neurobiology of Disease*, *45*(1), 395–408. https://doi.org/10.1016/J.NBD.2011.08.029

Ginhoux, F., Greter, M., Leboeuf, M., Nandi, S., See, P., Gokhan, S., … Merad, M. (2010). Fate mapping analysis reveals that adult microglia derive from primitive macrophages. *Science (New York, N.Y.)*, *330*(6005), 841–845. https://doi.org/10.1126/SCIENCE.1194637

Glebov, K., Wunderlich, P., Karaca, I., & Walter, J. (2016). Functional involvement of γ-secretase in signaling of the triggering receptor expressed on myeloid cells-2 (TREM2). *Journal of Neuroinflammation*, *13*(1). https://doi.org/10.1186/S12974-016-0479-9

Gonzalez, C., Armijo, E., Bravo-Alegria, J., Becerra-Calixto, A., Mays, C. E., & Soto, C. (2018). Modeling amyloid beta and tau pathology in human cerebral organoids. *Molecular Psychiatry 2018 23:12*, *23*(12), 2363–2374. https://doi.org/10.1038/S41380-018-0229-8

Götzl, J. K., Brendel, M., Werner, G., Parhizkar, S., Sebastian Monasor, L., Kleinberger, G., … Haass, C. (2019). Opposite microglial activation stages upon loss of PGRN or TREM 2 result in reduced cerebral glucose metabolism . *EMBO Molecular Medicine*, *11*(6). https://doi.org/10.15252/emmm.201809711

Götzl, J. K., Colombo, A. V., Fellerer, K., Reifschneider, A., Werner, G., Tahirovic, S., … Capell, A. (2018). Early lysosomal maturation deficits in microglia triggers enhanced lysosomal activity in other brain cells of progranulin knockout mice. *Molecular Neurodegeneration*, *13*(1). https://doi.org/10.1186/s13024-018-0281-5

Götzl, J. K., Mori, K., Damme, M., Fellerer, K., Tahirovic, S., Kleinberger, G., … Capell, A. (2014). Common pathobiochemical hallmarks of progranulin-associated frontotemporal lobar degeneration and neuronal ceroid lipofuscinosis. *Acta Neuropathologica*, *127*(6),

845–860. https://doi.org/10.1007/s00401-014-1262-6

Gowrishankar, S., Yuan, P., Wu, Y., Schrag, M., Paradise, S., Grutzendler, J., … Ferguson, S. M. (2015). Massive accumulation of luminal protease-deficient axonal lysosomes at Alzheimer's disease amyloid plaques. *Proceedings of the National Academy of Sciences of the United States of America*, *112*(28), E3699–E3708. https://doi.org/10.1073/PNAS.1510329112

Grabert, K., Michoel, T., Karavolos, M. H., Clohisey, S., Kenneth Baillie, J., Stevens, M. P., … McColl, B. W. (2016). Microglial brain region−dependent diversity and selective regional sensitivities to aging. *Nature Neuroscience 2016 19:3*, *19*(3), 504–516. https://doi.org/10.1038/NN.4222

Greter, M., Helft, J., Chow, A., Hashimoto, D., Mortha, A., Agudo-Cantero, J., … Merad, M. (2012). GM-CSF Controls Nonlymphoid Tissue Dendritic Cell Homeostasis but Is Dispensable for the Differentiation of Inflammatory Dendritic Cells. *Immunity*, *36*(6), 1031–1046. https://doi.org/10.1016/J.IMMUNI.2012.03.027

Guerreiro, R., Wojtas, A., Bras, J., Carrasquillo, M., Rogaeva, E., Majounie, E., … Hardy, J. (2013). TREM2 Variants in Alzheimer's Disease . *New England Journal of Medicine*, *368*(2), 117–127. https://doi.org/10.1056/NEJMOA1211851/SUPPL_FILE/NEJMOA1211851_DISCLOSURES.PDF

Guo, M., Hao, Y., Feng, Y., Li, H., Mao, Y., Dong, Q., & Cui, M. (2021). Microglial Exosomes in Neurodegenerative Disease. *Frontiers in Molecular Neuroscience*, *14*. https://doi.org/10.3389/FNMOL.2021.630808

Halfon, S., Patel, S., Vega, F., Zurawski, S., & Zurawski, G. (1998). Autocatalytic activation of human legumain at aspartic acid residues. *FEBS Letters*, *438*(1–2), 114–118. https://doi.org/10.1016/S0014-5793(98)01281-2

Hasegawa, M., Arai, T., Nonaka, T., Kametani, F., Yoshida, M., Hashizume, Y., … Akiyama, H. (2008). Phosphorylated TDP-43 in frontotemporal lobar degeneration and amyotrophic lateral sclerosis. *Annals of Neurology*, *64*(1), 60–70. https://doi.org/10.1002/ANA.21425

Hasselmann, J., Coburn, M. A., England, W., Figueroa Velez, D. X., Kiani Shabestari, S., Tu, C. H., … Blurton-Jones, M. (2019). Development of a Chimeric Model to Study and Manipulate Human Microglia In Vivo. *Neuron*, *103*(6), 1016-1033.e10. https://doi.org/10.1016/j.neuron.2019.07.002

Heneka, M. T., Kummer, M. P., Stutz, A., Delekate, A., Schwartz, S., Vieira-Saecker, A., … Golenbock, D. T. (2013). NLRP3 is activated in Alzheimer's disease and contributes to

pathology in APP/PS1 mice. *Nature*, *493*(7434), 674–678.
https://doi.org/10.1038/nature11729

Heneka, M. T., McManus, R. M., & Latz, E. (2018, October 1). Inflammasome signalling in brain
function and neurodegenerative disease. *Nature Reviews Neuroscience*. Nature Publishing
Group. https://doi.org/10.1038/s41583-018-0055-7

Henjum, K., Almdahl, I. S., Årskog, V., Minthon, L., Hansson, O., Fladby, T., & Nilsson, L. N. G.
(2016). Cerebrospinal fluid soluble TREM2 in aging and Alzheimer's disease. *Alzheimer's
Research & Therapy*, *8*(1). https://doi.org/10.1186/S13195-016-0182-1

Herskowitz, J. H., Gozal, Y. M., Duong, D. M., Dammer, E. B., Gearing, M., Ye, K., … Seyfried,
N. T. (2012). Asparaginyl endopeptidase cleaves TDP-43 in brain. *Proteomics*, *12*(15–16),
2455–2463. https://doi.org/10.1002/pmic.201200006

Heslegrave, A., Heywood, W., Paterson, R., Magdalinou, N., Svensson, J., Johansson, P., …
Zetterberg, H. (2016). Increased cerebrospinal fluid soluble TREM2 concentration in
Alzheimer's disease. *Molecular Neurodegeneration*, *11*(1). https://doi.org/10.1186/S13024-
016-0071-X

Hickman, S. E., Kingery, N. D., Ohsumi, T. K., Borowsky, M. L., Wang, L. C., Means, T. K., & El
Khoury, J. (2013). The microglial sensome revealed by direct RNA sequencing. *Nature
Neuroscience 2013 16:12*, *16*(12), 1896–1905. https://doi.org/10.1038/NN.3554

Hong, S., Beja-Glasser, V. F., Nfonoyim, B. M., Frouin, A., Li, S., Ramakrishnan, S., … Stevens,
B. (2016). Complement and Microglia Mediate Early Synapse Loss in Alzheimer Mouse
Models. *Science*, *352*(6286), 716. https://doi.org/10.1126/SCIENCE.AAD8373

Hong, S., Dissing-Olesen, L., & Stevens, B. (2016, February 1). New insights on the role of
microglia in synaptic pruning in health and disease. *Current Opinion in Neurobiology*.
Elsevier Ltd. https://doi.org/10.1016/j.conb.2015.12.004

Hrabal, R., Chen, Z., James, S., Bennett, H. P. J., & Ni, F. (1996). The hairpin stack fold, a
novel protein architecture for a new family of protein growth factors. *Nature Structural
Biology*, *3*(9), 747–751. https://doi.org/10.1038/NSB0996-747

Hsu, P. D., Lander, E. S., & Zhang, F. (2014, June 5). Development and applications of
CRISPR-Cas9 for genome engineering. *Cell*. Elsevier B.V.
https://doi.org/10.1016/j.cell.2014.05.010

Hu, F., Padukkavidana, T., Vægter, C. B., Brady, O. A., Zheng, Y., Mackenzie, I. R., …
Strittmatter, S. M. (2010). Sortilin-mediated endocytosis determines levels of the
frontotemporal dementia protein, progranulin. *Neuron*, *68*(4), 654–667.
https://doi.org/10.1016/j.neuron.2010.09.034

Huang, M., Modeste, E., Dammer, E., Merino, P., Taylor, G., Duong, D. M., … Kukar, T. (2020). Network analysis of the progranulin-deficient mouse brain proteome reveals pathogenic mechanisms shared in human frontotemporal dementia caused by GRN mutations. *Acta Neuropathologica Communications*, *8*(1), 163. https://doi.org/10.1186/s40478-020-01037-x

Huang, W., Zhou, Y., Tu, L., Ba, Z., Huang, J., Huang, N., & Luo, Y. (2020, February 28). TDP-43: From Alzheimer's Disease to Limbic-Predominant Age-Related TDP-43 Encephalopathy. *Frontiers in Molecular Neuroscience*. Frontiers Media S.A. https://doi.org/10.3389/fnmol.2020.00026

Iguchi, Y., Katsuno, M., Niwa, J. I., Takagi, S., Ishigaki, S., Ikenaka, K., … Sobue, G. (2013). Loss of TDP-43 causes age-dependent progressive motor neuron degeneration. *Brain : A Journal of Neurology*, *136*(Pt 5), 1371–1382. https://doi.org/10.1093/BRAIN/AWT029

Israel, M. A., Yuan, S. H., Bardy, C., Reyna, S. M., Mu, Y., Herrera, C., … Goldstein, L. S. B. (2012). Probing sporadic and familial Alzheimer's disease using induced pluripotent stem cells. *Nature 2012 482:7384*, *482*(7384), 216–220. https://doi.org/10.1038/NATURE10821

Jay, T. R., Miller, C. M., Cheng, P. J., Graham, L. C., Bemiller, S., Broihier, M. L., … Lamb, B. T. (2015). TREM2 deficiency eliminates TREM2+ inflammatory macrophages and ameliorates pathology in Alzheimer's disease mouse models. *The Journal of Experimental Medicine*, *212*(3), 287–295. https://doi.org/10.1084/JEM.20142322

Jia, J., Claude-Taupin, A., Gu, Y., Choi, S. W., Peters, R., Bissa, B., … Deretic, V. (2020). Galectin-3 Coordinates a Cellular System for Lysosomal Repair and Removal. *Developmental Cell*, *52*(1), 69-87.e8. https://doi.org/10.1016/J.DEVCEL.2019.10.025

Jian, J., Konopka, J., & Liu, C. (2013). Insights into the role of progranulin in immunity, infection, and inflammation. *Journal of Leukocyte Biology*, *93*(2), 199–208. https://doi.org/10.1189/JLB.0812429

Jinek, M., Chylinski, K., Fonfara, I., Hauer, M., Doudna, J. A., & Charpentier, E. (2012). A programmable dual-RNA-guided DNA endonuclease in adaptive bacterial immunity. *Science*, *337*(6096), 816–821. https://doi.org/10.1126/SCIENCE.1225829/SUPPL_FILE/JINEK.SM.PDF

Jinek, M., East, A., Cheng, A., Lin, S., Ma, E., & Doudna, J. (2013). RNA-programmed genome editing in human cells. *ELife*, *2*(2). https://doi.org/10.7554/ELIFE.00471

Johnson, B. S., McCaffery, J. M., Lindquist, S., & Gitler, A. D. (2008). A yeast TDP-43 proteinopathy model: Exploring the molecular determinants of TDP-43 aggregation and cellular toxicity. *Proceedings of the National Academy of Sciences of the United States of America*, *105*(17), 6439–6444. https://doi.org/10.1073/PNAS.0802082105

Jonsson, T., Stefansson, H., Steinberg, S., Jonsdottir, I., Jonsson, P. V., Snaedal, J., … Stefansson, K. (2013). Variant of TREM2 Associated with the Risk of Alzheimer's Disease . *New England Journal of Medicine*, *368*(2), 107–116. https://doi.org/10.1056/nejmoa1211103

Josephs, K. A., Stroh, A., Dugger, B., & Dickson, D. W. (2009). Evaluation of subcortical pathology and clinical correlations in FTLD-U subtypes. *Acta Neuropathologica*, *118*(3), 349–358. https://doi.org/10.1007/S00401-009-0547-7/FIGURES/8

Kao, A. W., Eisenhut, R. J., Martens, L. H., Nakamura, A., Huang, A., Bagley, J. A., … Kenyon, C. (2011). A neurodegenerative disease mutation that accelerates the clearance of apoptotic cells. *Proceedings of the National Academy of Sciences of the United States of America*, *108*(11), 4441–4446. https://doi.org/10.1073/PNAS.1100650108/-/DCSUPPLEMENTAL

Kao, A. W., McKay, A., Singh, P. P., Brunet, A., & Huang, E. J. (2017). Progranulin, lysosomal regulation and neurodegenerative disease. *Nature Reviews Neuroscience*, *18*(6), 325–333. https://doi.org/10.1038/nrn.2017.36

Keren-Shaul, H., Spinrad, A., Weiner, A., Matcovitch-Natan, O., Dvir-Szternfeld, R., Ulland, T. K., … Amit, I. (2017). A Unique Microglia Type Associated with Restricting Development of Alzheimer's Disease. *Cell*, *169*(7), 1276-1290.e17. https://doi.org/10.1016/j.cell.2017.05.018

Kessenbrock, K., Fröhlich, L., Sixt, M., Lämmermann, T., Pfister, H., Bateman, A., … Jenne, D. E. (2008). Proteinase 3 and neutrophil elastase enhance inflammation in mice by inactivating antiinflammatory progranulin. *Journal of Clinical Investigation*. https://doi.org/10.1172/JCI34694

Kettenmann, H., Kirchhoff, F., & Verkhratsky, A. (2013). Microglia: new roles for the synaptic stripper. *Neuron*, *77*(1), 10–18. https://doi.org/10.1016/J.NEURON.2012.12.023

King, O. D., Gitler, A. D., & Shorter, J. (2012). The tip of the iceberg: RNA-binding proteins with prion-like domains in neurodegenerative disease. *Brain Research*, *1462*, 61. https://doi.org/10.1016/J.BRAINRES.2012.01.016

Klein, Z. A., Takahashi, H., Ma, M., Stagi, M., Zhou, M., Lam, T. K. T., & Strittmatter, S. M. (2017). Loss of TMEM106B Ameliorates Lysosomal and Frontotemporal Dementia-Related Phenotypes in Progranulin-Deficient Mice. *Neuron*, *95*(2), 281-296.e6. https://doi.org/10.1016/j.neuron.2017.06.026

Kleinberger, G., Brendel, M., Mracsko, E., Wefers, B., Groeneweg, L., Xiang, X., … Haass, C. (2017). The FTD -like syndrome causing TREM 2 T66M mutation impairs microglia

function, brain perfusion, and glucose metabolism . *The EMBO Journal*, *36*(13), 1837–1853. https://doi.org/10.15252/embj.201796516

Kleinberger, G., Yamanishi, Y., Suárez-Calvet, M., Czirr, E., Lohmann, E., Cuyvers, E., … Haass, C. (2014). TREM2 mutations implicated in neurodegeneration impair cell surface transport and phagocytosis. *Science Translational Medicine*, *6*(243). https://doi.org/10.1126/scitranslmed.3009093

Klimmt, J., Dannert, A., & Paquet, D. (2020). ScienceDirect Neurodegeneration in a dish : advancing human stem- cell-based models of Alzheimer ' s disease. *Current Opinion in Neurobiology*, *61*, 96–104. https://doi.org/10.1016/j.conb.2020.01.008

Knott, G. J., & Doudna, J. A. (2018). CRISPR-Cas guides the future of genetic engineering. *Science (New York, N.Y.)*, *361*(6405), 866. https://doi.org/10.1126/SCIENCE.AAT5011

Komor, A. C., Badran, A. H., & Liu, D. R. (2017, January 12). CRISPR-Based Technologies for the Manipulation of Eukaryotic Genomes. *Cell*. Cell Press. https://doi.org/10.1016/j.cell.2016.10.044

Kondo, T., Asai, M., Tsukita, K., Kutoku, Y., Ohsawa, Y., Sunada, Y., … Inoue, H. (2013). Modeling Alzheimer's disease with iPSCs reveals stress phenotypes associated with intracellular Aβ and differential drug responsiveness. *Cell Stem Cell*, *12*(4), 487–496. https://doi.org/10.1016/J.STEM.2013.01.009

Kraemer, B. C., Schuck, T., Wheeler, J. M., Robinson, L. C., Trojanowski, J. Q., Lee, V. M. Y., & Schellenberg, G. D. (2010). Loss of Murine TDP-43 disrupts motor function and plays an essential role in embryogenesis. *Acta Neuropathologica*, *119*(4), 409–419. https://doi.org/10.1007/S00401-010-0659-0/FIGURES/5

Krasemann, S., Madore, C., Cialic, R., Baufeld, C., Calcagno, N., El Fatimy, R., … Butovsky, O. (2017). The TREM2-APOE Pathway Drives the Transcriptional Phenotype of Dysfunctional Microglia in Neurodegenerative Diseases. *Immunity*, *47*(3), 566-581.e9. https://doi.org/10.1016/j.immuni.2017.08.008

Kunkle, B. W., Grenier-Boley, B., Sims, R., Bis, J. C., Damotte, V., Naj, A. C., … Pericak-Vance, M. A. (2019). Genetic meta-analysis of diagnosed Alzheimer's disease identifies new risk loci and implicates Aβ, tau, immunity and lipid processing. *Nature Genetics*, *51*(3), 414–430. https://doi.org/10.1038/s41588-019-0358-2

Kuo, P. H., Chiang, C. H., Wang, Y. T., Doudeva, L. G., & Yuan, H. S. (2014). The crystal structure of TDP-43 RRM1-DNA complex reveals the specific recognition for UG- and TG-rich nucleic acids. *Nucleic Acids Research*, *42*(7), 4712. https://doi.org/10.1093/NAR/GKT1407

Laird, A. S., van Hoecke, A., De Muynck, L., Timmers, M., van den Bosch, L., Van Damme, P., & Robberecht, W. (2010). Progranulin is neurotrophic in vivo and protects against a mutant TDP-43 induced axonopathy. *PloS One*, *5*(10). https://doi.org/10.1371/JOURNAL.PONE.0013368

Lalmansingh, A. S., Urekar, C. J., & Reddi, P. P. (2011). TDP-43 is a transcriptional repressor: the testis-specific mouse acrv1 gene is a TDP-43 target in vivo. *The Journal of Biological Chemistry*, *286*(13), 10970–10982. https://doi.org/10.1074/JBC.M110.166587

Lancaster, T. M. (2019). Associations between rare microglia-linked Alzheimer's disease risk variants and subcortical brain volumes in young individuals. *Alzheimer's & Dementia : Diagnosis, Assessment & Disease Monitoring*, *11*, 368. https://doi.org/10.1016/J.DADM.2019.03.005

Lee, E. B., Lee, V. M. Y., & Trojanowski, J. Q. (2011). Gains or losses: molecular mechanisms of TDP43-mediated neurodegeneration. *Nature Reviews Neuroscience 2011 13:1*, *13*(1), 38–50. https://doi.org/10.1038/NRN3121

Lee, G., Leugers, C. J., Mol, P., Transl, B., & Author, S. (2012). Tau and Tauopathies NIH Public Access Author Manuscript. *Prog Mol Biol Transl Sci*, *107*, 263–293. https://doi.org/10.1016/B978-0-12-385883-2.00004-7

Lee, S.-H., Meilandt, W. J., Xie, L., Gandham, V. D., Ngu, H., Barck, K. H., … Hansen, D. V. (2021). Trem2 restrains the enhancement of tau accumulation and neurodegeneration by β-amyloid pathology. *Neuron*, 1–19. https://doi.org/10.1016/j.neuron.2021.02.010

Lee, S., & Huang, E. J. (2017a). Modeling ALS and FTD with iPSC-derived neurons. *Brain Research*, *1656*, 88–97. https://doi.org/10.1016/j.brainres.2015.10.003

Lee, S., & Huang, E. J. (2017b, February 1). Modeling ALS and FTD with iPSC-derived neurons. *Brain Research*. Elsevier B.V. https://doi.org/10.1016/j.brainres.2015.10.003

Lee, V. M. Y., Goedert, M., & Trojanowski, J. Q. (2001). Neurodegenerative tauopathies. *Annual Review of Neuroscience*, *24*, 1121–1159. https://doi.org/10.1146/ANNUREV.NEURO.24.1.1121

Lewcock, J. W., Schlepckow, K., Di Paolo, G., Tahirovic, S., Monroe, K. M., & Haass, C. (2020, December 9). Emerging Microglia Biology Defines Novel Therapeutic Approaches for Alzheimer's Disease. *Neuron*. Cell Press. https://doi.org/10.1016/j.neuron.2020.09.029

Li, D. N., Matthews, S. P., Antoniou, A. N., Mazzeo, D., & Watts, C. (2003). Multistep autoactivation of asparaginyl endopeptidase in vitro and in vivo. *Journal of Biological Chemistry*, *278*(40), 38980–38990. https://doi.org/10.1074/jbc.M305930200

Li, Y. H., Chen, H. Y., Li, Y. W., Wu, S. Y., Wangta-Liu, Lin, G. H., … Wu, J. L. (2013).

Progranulin regulates zebrafish muscle growth and regeneration through maintaining the pool of myogenic progenitor cells. *Scientific Reports 2013 3:1*, *3*(1), 1–8. https://doi.org/10.1038/SREP01176

Li, Y. H., Chen, M. H. C., Gong, H. Y., Hu, S. Y., Li, Y. W., Lin, G. H., … Wu, J. L. (2010). Progranulin A-mediated MET Signaling Is Essential for Liver Morphogenesis in Zebrafish. *Journal of Biological Chemistry*, *285*(52), 41001–41009. https://doi.org/10.1074/JBC.M110.138743

Ling, J. P., Pletnikova, O., Troncoso, J. C., & Wong, P. C. (2015). TDP-43 repression of nonconserved cryptic exons is compromised in ALS-FTD. *Science*, *349*(6248), 650–655. https://doi.org/10.1126/science.aab0983

Ling, S. C., Polymenidou, M., & Cleveland, D. W. (2013). Converging mechanisms in ALS and FTD: disrupted RNA and protein homeostasis. *Neuron*, *79*(3), 416–438. https://doi.org/10.1016/J.NEURON.2013.07.033

Logan, T., Simon, M. J., Rana, A., Cherf, G. M., Srivastava, A., Davis, S. S., … Di Paolo, G. (2021). Rescue of a lysosomal storage disorder caused by Grn loss of function with a brain penetrant progranulin biologic. *Cell*, *184*(18), 4651-4668.e25. https://doi.org/10.1016/J.CELL.2021.08.002

Lomen-Hoerth, C., Anderson, T., & Miller, B. (2002). The overlap of amyotrophic lateral sclerosis and frontotemporal dementia. *Neurology*, *59*(7), 1077–1079. https://doi.org/10.1212/WNL.59.7.1077

Lowery, R. L., Tremblay, M. E., Hopkins, B. E., & Majewska, A. K. (2017). The microglial fractalkine receptor is not required for activity-dependent plasticity in the mouse visual system. *Glia*, *65*(11), 1744–1761. https://doi.org/10.1002/GLIA.23192

Lui, H., Zhang, J., Makinson, S. R., Cahill, M. K., Kelley, K. W., Huang, H. Y., … Huang, E. J. (2016). Progranulin Deficiency Promotes Circuit-Specific Synaptic Pruning by Microglia via Complement Activation. *Cell*, *165*(4), 921–935. https://doi.org/10.1016/j.cell.2016.04.001

Lukavsky, P. J., Daujotyte, D., Tollervey, J. R., Ule, J., Stuani, C., Buratti, E., … Allain, F. H. T. (2013). Molecular basis of UG-rich RNA recognition by the human splicing factor TDP-43. *Nature Structural & Molecular Biology 2013 20:12*, *20*(12), 1443–1449. https://doi.org/10.1038/NSMB.2698

Mackenzie, I. R. A., & Neumann, M. (2016, August 1). Molecular neuropathology of frontotemporal dementia: insights into disease mechanisms from postmortem studies. *Journal of Neurochemistry*. Blackwell Publishing Ltd. https://doi.org/10.1111/jnc.13588

MacKenzie, I. R. A., Neumann, M., Bigio, E. H., Cairns, N. J., Alafuzoff, I., Kril, J., … Mann, D.

M. A. (2010). Nomenclature and nosology for neuropathologic subtypes of frontotemporal lobar degeneration: an update. *Acta Neuropathologica*, *119*(1), 1–4. https://doi.org/10.1007/S00401-009-0612-2

MacKenzie, I. R., Arzberger, T., Kremmer, E., Troost, D., Lorenzl, S., Mori, K., … Neumann, M. (2013). Dipeptide repeat protein pathology in C9ORF72 mutation cases: Clinico-pathological correlations. *Acta Neuropathologica*, *126*(6), 859–879. https://doi.org/10.1007/S00401-013-1181-Y/TABLES/4

Mackenzie, I. R., & Neumann, M. (2017). Reappraisal of TDP-43 pathology in FTLD-U subtypes. *Acta Neuropathologica*, *134*(1), 79–96. https://doi.org/10.1007/S00401-017-1716-8/TABLES/7

Mali, P., Yang, L., Esvelt, K. M., Aach, J., Guell, M., DiCarlo, J. E., … Church, G. M. (2013). RNA-guided human genome engineering via Cas9. *Science*, *339*(6121), 823–826. https://doi.org/10.1126/science.1232033

Mancuso, R., Van Den Daele, J., Fattorelli, N., Wolfs, L., Balusu, S., Burton, O., … De Strooper, B. (2019). Stem-cell-derived human microglia transplanted in mouse brain to study human disease. *Nature Neuroscience 2019 22:12*, *22*(12), 2111–2116. https://doi.org/10.1038/S41593-019-0525-X

Marín-Teva, J. L., Dusart, I., Colin, C., Gervais, A., Van Rooijen, N., & Mallat, M. (2004). Microglia Promote the Death of Developing Purkinje Cells. *Neuron*, *41*(4), 535–547. https://doi.org/10.1016/S0896-6273(04)00069-8

Marschallinger, J., Iram, T., Zardeneta, M., Lee, S. E., Lehallier, B., Haney, M. S., … Wyss-Coray, T. (2020). Lipid-droplet-accumulating microglia represent a dysfunctional and proinflammatory state in the aging brain. *Nature Neuroscience*, *23*(2), 194–208. https://doi.org/10.1038/s41593-019-0566-1

Martens, L. H., Zhang, J., Barmada, S. J., Zhou, P., Kamiya, S., Sun, B., … Farese, R. V. (2012). Progranulin deficiency promotes neuroinflammation and neuron loss following toxin-induced injury. *Journal of Clinical Investigation*, *122*(11), 3955–3959. https://doi.org/10.1172/JCI63113

Mathews, S., Branch Woods, A., Katano, I., Makarov, E., Thomas, M. B., Gendelman, H. E., … Gorantla, S. (2019). Human Interleukin-34 facilitates microglia-like cell differentiation and persistent HIV-1 infection in humanized mice. *Molecular Neurodegeneration*, *14*(1). https://doi.org/10.1186/S13024-019-0311-Y

Mathys, H., Adaikkan, C., Gao, F., Young, J. Z., Manet, E., Hemberg, M., … Tsai, L. H. (2017). Temporal Tracking of Microglia Activation in Neurodegeneration at Single-Cell Resolution.

Cell Reports, *21*(2), 366–380. https://doi.org/10.1016/J.CELREP.2017.09.039

Mathys, H., Davila-Velderrain, J., Peng, Z., Gao, F., Mohammadi, S., Young, J. Z., … Tsai, L. H. (2019). Single-cell transcriptomic analysis of Alzheimer's disease. *Nature 2019 570:7761*, *570*(7761), 332–337. https://doi.org/10.1038/S41586-019-1195-2

McComish, S. F., & Caldwell, M. A. (2018, July 5). Generation of defined neural populations from pluripotent stem cells. *Philosophical Transactions of the Royal Society B: Biological Sciences*. Royal Society Publishing. https://doi.org/10.1098/rstb.2017.0214

McKhann, G. M., Albert, M. S., Grossman, M., Miller, B., Dickson, D., & Trojanowski, J. Q. (2001). Clinical and pathological diagnosis of frontotemporal dementia: report of the Work Group on Frontotemporal Dementia and Pick's Disease. *Archives of Neurology*, *58*(11), 1803–1809. https://doi.org/10.1001/ARCHNEUR.58.11.1803

Mcquade, A., Kang, Y. J., Hasselmann, J., Jairaman, A., Sotelo, A., Coburn, M., … Cahalan, M. (2020). Gene expression and functional deficits underlie TREM2-knockout microglia responses in human models of Alzheimer's disease. *Nature Communications*, 1–17. https://doi.org/10.1038/s41467-020-19227-5

Meilandt, W. J., Ngu, H., Gogineni, A., Lalehzadeh, G., Lee, S. H., Srinivasan, K., … Hansen, X. D. V. (2020). Trem2 Deletion Reduces Late-Stage Amyloid Plaque Accumulation, Elevates the Aβ42:Aβ40 Ratio, and Exacerbates Axonal Dystrophy and Dendritic Spine Loss in the PS2APP Alzheimer's Mouse Model. *The Journal of Neuroscience : The Official Journal of the Society for Neuroscience*, *40*(9), 1956–1974. https://doi.org/10.1523/JNEUROSCI.1871-19.2019

Mohan, S., Sampognaro, P. J., Argouarch, A. R., Maynard, J. C., Welch, M., Patwardhan, A., … Kao, A. W. (2021). Processing of progranulin into granulins involves multiple lysosomal proteases and is affected in frontotemporal lobar degeneration. *Molecular Neurodegeneration*, *16*(1). https://doi.org/10.1186/s13024-021-00472-1

Mompeán, M., Chakrabartty, A., Buratti, E., & Laurents, D. V. (2016). Electrostatic Repulsion Governs TDP-43 C-terminal Domain Aggregation. *PLoS Biology*, *14*(4). https://doi.org/10.1371/JOURNAL.PBIO.1002447

Mompeán, M., Romano, V., Pantoja-Uceda, D., Stuani, C., Baralle, F. E., Buratti, E., & Laurents, D. V. (2016). The TDP-43 N-terminal domain structure at high resolution. *The FEBS Journal*, *283*(7), 1242–1260. https://doi.org/10.1111/FEBS.13651

Morenas-Rodríguez, E., Li, Y., Nuscher, B., Franzmeier, N., Xiong, C., Suárez-Calvet, M., … Xu, X. (2022). Soluble TREM2 in CSF and its association with other biomarkers and cognition in autosomal-dominant Alzheimer's disease: a longitudinal observational study.

The Lancet Neurology, *21*(4), 329–341. https://doi.org/10.1016/S1474-4422(22)00027-8

Mutihac, R., Alegre-Abarrategui, J., Gordon, D., Farrimond, L., Yamasaki-Mann, M., Talbot, K., & Wade-Martins, R. (2015). TARDBP pathogenic mutations increase cytoplasmic translocation of TDP-43 and cause reduction of endoplasmic reticulum Ca2+ signaling in motor neurons. *Neurobiology of Disease*, *75*, 64–77. https://doi.org/10.1016/j.nbd.2014.12.010

Najm, R., Zalocusky, K. A., Zilberter, M., Yoon, S. Y., Hao, Y., Koutsodendris, N., … Huang, Y. (2020). In Vivo Chimeric Alzheimer's Disease Modeling of Apolipoprotein E4 Toxicity in Human Neurons. *Cell Reports*, *32*(4). https://doi.org/10.1016/J.CELREP.2020.107962

Neary, D., Snowden, J. S., Gustafson, L., Passant, U., Stuss, D., Black, S., … Benson, D. F. (1998). Frontotemporal lobar degeneration: a consensus on clinical diagnostic criteria. *Neurology*, *51*(6), 1546–1554. https://doi.org/10.1212/WNL.51.6.1546

Neumann, M., & Mackenzie, I. R. A. (2019, February 1). Review: Neuropathology of non-tau frontotemporal lobar degeneration. *Neuropathology and Applied Neurobiology*. Blackwell Publishing Ltd. https://doi.org/10.1111/nan.12526

Neumann, Manuela, Bentmann, E., Dormann, D., Jawaid, A., Dejesus-Hernandez, M., Ansorge, O., … MacKenzie, I. R. A. (2011). FET proteins TAF15 and EWS are selective markers that distinguish FTLD with FUS pathology from amyotrophic lateral sclerosis with FUS mutations. *Brain : A Journal of Neurology*, *134*(Pt 9), 2595–2609. https://doi.org/10.1093/BRAIN/AWR201

Neumann, Manuela, Kwong, L. K., Truax, A. C., Vanmassenhove, B., Kretzschmar, H. A., Van Deerlin, V. M., … Lee, V. M. Y. (2007). TDP-43-positive white matter pathology in frontotemporal lobar degeneration with ubiquitin-positive inclusions. *Journal of Neuropathology and Experimental Neurology*, *66*(3), 177–183. https://doi.org/10.1097/01.JNEN.0000248554.45456.58

Neumann, Manuela, Rademakers, R., Roeber, S., Baker, M., Kretzschmar, H. A., & MacKenzie, I. R. A. (2009). A new subtype of frontotemporal lobar degeneration with FUS pathology. *Brain*, *132*(11), 2922. https://doi.org/10.1093/BRAIN/AWP214

Neumann, Manuela, Sampathu, D. M., Kwong, L. K., Truax, A. C., Micsenyi, M. C., Chou, T. T., … Lee, V. M. Y. (2006). Ubiquitinated TDP-43 in frontotemporal lobar degeneration and amyotrophic lateral sclerosis. *Science (New York, N.Y.)*, *314*(5796), 130–133. https://doi.org/10.1126/SCIENCE.1134108

Neumann, Manuela, Tolnay, M., & Mackenzie, I. R. A. (2009, December). The molecular basis of frontotemporal dementia. *Expert Reviews in Molecular Medicine*.

https://doi.org/10.1017/S1462399409001136

Nguyen, A. D., Nguyen, T. A., Zhang, J., Devireddy, S., Zhou, P., Karydas, A. M., … Farese, R. V. (2018). Murine knockin model for progranulin-deficient frontotemporal dementia with nonsense-mediated mRNA decay. *Proceedings of the National Academy of Sciences of the United States of America*, *115*(12), E2849–E2858. https://doi.org/10.1073/PNAS.1722344115

Nimmerjahn, A., Kirchhoff, F., & Helmchen, F. (2005). Neuroscience: Resting microglial cells are highly dynamic surveillants of brain parenchyma in vivo. *Science*, *308*(5726), 1314–1318. https://doi.org/10.1126/SCIENCE.1110647/SUPPL_FILE/1110647S9.MOV

Nishimura, A. L., Shum, C., Scotter, E. L., Abdelgany, A., Sardone, V., Wright, J., … Shaw, C. E. (2014). Allele-specific knockdown of ALS-associated mutant TDP-43 in neural stem cells derived from induced pluripotent stem cells. *PLoS ONE*, *9*(3). https://doi.org/10.1371/journal.pone.0091269

Nishimura, A. L., Upunski, V., Troakes, C., Kathe, C., Fratta, P., Howell, M., … Rogelj, B. (2010). Nuclear import impairment causes cytoplasmic trans-activation response DNA-binding protein accumulation and is associated with frontotemporal lobar degeneration. *Brain : A Journal of Neurology*, *133*(Pt 6), 1763–1771. https://doi.org/10.1093/BRAIN/AWQ111

Nugent, A. A., Lin, K., van Lengerich, B., Lianoglou, S., Przybyla, L., Davis, S. S., … Di Paolo, G. (2020). TREM2 Regulates Microglial Cholesterol Metabolism upon Chronic Phagocytic Challenge. *Neuron*, *105*(5), 837-854.e9. https://doi.org/10.1016/j.neuron.2019.12.007

Ou, S.-H. I., Wu, F., Harrich, D., Leo´, L., Garci´a, L. F., Garci´a-Marti´nez, G., … Gaynor, R. B. (1995). Cloning and characterization of a novel cellular protein, TDP-43, that binds to human immunodeficiency virus type 1 TAR DNA sequence motifs. *Journal of Virology*, *69*(6), 3584. https://doi.org/10.1128/JVI.69.6.3584-3596.1995

Padovani, A., Agosti, C., Premi, E., Bellelli, G., & Borroni, B. (2007). Extrapyramidal symptoms in Frontotemporal Dementia: Prevalence and clinical correlations. *Neuroscience Letters*, *422*(1), 39–42. https://doi.org/10.1016/J.NEULET.2007.05.049

Paolicelli, R. C., Bolasco, G., Pagani, F., Maggi, L., Scianni, M., Panzanelli, P., … Gross, C. T. (2011). Synaptic pruning by microglia is necessary for normal brain development. *Science (New York, N.Y.)*, *333*(6048), 1456–1458. https://doi.org/10.1126/SCIENCE.1202529

Paolicelli, R. C., Sierra, A., Stevens, B., Tremblay, M. E., Aguzzi, A., Ajami, B., … Wyss-Coray, T. (2022). Microglia states and nomenclature: A field at its crossroads. *Neuron*, *110*(21), 3458–3483. https://doi.org/10.1016/J.NEURON.2022.10.020

Paquet, D., Kwart, D., Chen, A., Sproul, A., Jacob, S., Teo, S., … Tessier-Lavigne, M. (2016). Efficient introduction of specific homozygous and heterozygous mutations using CRISPR/Cas9. *Nature*, *533*(7601), 125–129. https://doi.org/10.1038/nature17664

Parhizkar, S., Arzberger, T., Brendel, M., Kleinberger, G., Deussing, M., Focke, C., … Haass, C. (2019). Loss of TREM2 function increases amyloid seeding but reduces plaque-associated ApoE. *Nature Neuroscience*, *22*(2), 191–204. https://doi.org/10.1038/s41593-018-0296-9

Park, J., Wetzel, I., Marriott, I., Dréau, D., D'Avanzo, C., Kim, D. Y., … Cho, H. (2018). A 3D human triculture system modeling neurodegeneration and neuroinflammation in Alzheimer's disease. *Nature Neuroscience 2018 21:7*, *21*(7), 941–951. https://doi.org/10.1038/S41593-018-0175-4

Paushter, D. H., Du, H., Feng, T., & Hu, F. (2018, July 1). The lysosomal function of progranulin, a guardian against neurodegeneration. *Acta Neuropathologica*. Springer Verlag. https://doi.org/10.1007/s00401-018-1861-8

Petkau, T. L., Neal, S. J., Milnerwood, A., Mew, A., Hill, A. M., Orban, P., … Leavitt, B. R. (2012). Synaptic dysfunction in progranulin-deficient mice. *Neurobiology of Disease*, *45*(2), 711–722. https://doi.org/10.1016/J.NBD.2011.10.016

Piccio, L., Buonsanti, C., Cella, M., Tassi, I., Schmidt, R. E., Fenoglio, C., … Cross, A. H. (2008). Identification of soluble TREM-2 in the cerebrospinal fluid and its association with multiple sclerosis and CNS inflammation. *Brain : A Journal of Neurology*, *131*(Pt 11), 3081–3091. https://doi.org/10.1093/BRAIN/AWN217

Piccio, L., Deming, Y., Del-Águila, J. L., Ghezzi, L., Holtzman, D. M., Fagan, A. M., … Cruchaga, C. (2016). Cerebrospinal fluid soluble TREM2 is higher in Alzheimer disease and associated with mutation status. *Acta Neuropathologica*, *131*(6), 925–933. https://doi.org/10.1007/S00401-016-1533-5/TABLES/2

Pickford, F., Marcus, J., Miguel Camargo, L., Xiao, Q., Graham, D., Mo, J.-R., … Hutton, M. (2011). Molecular Pathogenesis of Genetic and Inherited Diseases Progranulin Is a Chemoattractant for Microglia and Stimulates Their Endocytic Activity. *Am J Pathol*, *178*, 284–295. https://doi.org/10.1016/j.ajpath.2010.11.002

Pinarbasi, E. S., Cağatay, T., Fung, H. Y. J., Li, Y. C., Chook, Y. M., & Thomas, P. J. (2018). Active nuclear import and passive nuclear export are the primary determinants of TDP-43 localization. *Scientific Reports 2018 8:1*, *8*(1), 1–16. https://doi.org/10.1038/s41598-018-25008-4

Poliani, P. L., Wang, Y., Fontana, E., Robinette, M. L., Yamanishi, Y., Gilfillan, S., & Colonna, M. (2015). TREM2 sustains microglial expansion during aging and response to

demyelination. *The Journal of Clinical Investigation*, *125*(5), 2161–2170.
https://doi.org/10.1172/JCI77983

Preman, P., Tcw, J., Calafate, S., Snellinx, A., Alfonso-Triguero, M., Corthout, N., … Arranz, A.
M. (2021). Human iPSC-derived astrocytes transplanted into the mouse brain undergo
morphological changes in response to amyloid-β plaques. *Molecular Neurodegeneration*,
16(1). https://doi.org/10.1186/S13024-021-00487-8

Price, B. R., Sudduth, T. L., Weekman, E. M., Johnson, S., Hawthorne, D., Woolums, A., &
Wilcock, D. M. (2020). Therapeutic Trem2 activation ameliorates amyloid-beta deposition
and improves cognition in the 5XFAD model of amyloid deposition. *Journal of
Neuroinflammation*, *17*(1). https://doi.org/10.1186/s12974-020-01915-0

Qin, H., Lim, L. Z., Wei, Y., & Song, J. (2014). TDP-43 N terminus encodes a novel ubiquitin-like
fold and its unfolded form in equilibrium that can be shifted by binding to ssDNA.
Proceedings of the National Academy of Sciences of the United States of America,
111(52), 18619–18624. https://doi.org/10.1073/PNAS.1413994112

Rademakers, R., Neumann, M., & MacKenzie, I. R. (2012). Advances in understanding the
molecular basis of frontotemporal dementia. *Nature Reviews. Neurology*, *8*(8), 423–434.
https://doi.org/10.1038/NRNEUROL.2012.117

Raitano, S., Ordovàs, L., De Muynck, L., Guo, W., Espuny-Camacho, I., Geraerts, M., …
Verfaillie, C. M. (2015). Restoration of progranulin expression rescues cortical neuron
generation in an induced pluripotent stem cell model of frontotemporal dementia. *Stem Cell
Reports*, *4*(1), 16–24. https://doi.org/10.1016/j.stemcr.2014.12.001

Raja, W. K., Mungenast, A. E., Lin, Y. T., Ko, T., Abdurrob, F., Seo, J., & Tsai, L. H. (2016).
Self-Organizing 3D Human Neural Tissue Derived from Induced Pluripotent Stem Cells
Recapitulate Alzheimer's Disease Phenotypes. *PLOS ONE*, *11*(9), e0161969.
https://doi.org/10.1371/JOURNAL.PONE.0161969

Ratti, A., & Buratti, E. (2016). Physiological functions and pathobiology of TDP-43 and FUS/TLS
proteins. *Journal of Neurochemistry*, *138 Suppl 1*, 95–111.
https://doi.org/10.1111/JNC.13625

Rayaprolu, S., Mullen, B., Baker, M., Lynch, T., Finger, E., Seeley, W. W., … Ross, O. A.
(2013). TREM2 in neurodegeneration: evidence for association of the p.R47H variant with
frontotemporal dementia and Parkinson's disease. *Molecular Neurodegeneration*, *8*(1).
https://doi.org/10.1186/1750-1326-8-19

Roberson, E. D. (2012). Mouse models of frontotemporal dementia. *Annals of Neurology*, *72*(6),
837–849. https://doi.org/10.1002/ANA.23722

Root, J., Merino, P., Nuckols, A., Johnson, M., & Kukar, T. (2021a). Lysosome dysfunction as a cause of neurodegenerative diseases: Lessons from frontotemporal dementia and amyotrophic lateral sclerosis. *Neurobiology of Disease*, *154*, 105360. https://doi.org/10.1016/j.nbd.2021.105360

Root, J., Merino, P., Nuckols, A., Johnson, M., & Kukar, T. (2021b, July 1). Lysosome dysfunction as a cause of neurodegenerative diseases: Lessons from frontotemporal dementia and amyotrophic lateral sclerosis. *Neurobiology of Disease*. Academic Press Inc. https://doi.org/10.1016/j.nbd.2021.105360

Rouet, P., Smih, F., & Jasin, M. (1994). Introduction of double-strand breaks into the genome of mouse cells by expression of a rare-cutting endonuclease. *Molecular and Cellular Biology*, *14*(12), 8096. https://doi.org/10.1128/MCB.14.12.8096

Roy, E. R., Wang, B., Wan, Y. W., Chiu, G., Cole, A., Yin, Z., … Cao, W. (2020). Type I interferon response drives neuroinflammation and synapse loss in Alzheimer disease. *The Journal of Clinical Investigation*, *130*(4), 1912–1930. https://doi.org/10.1172/JCI133737

Salazar, D. A., Butler, V. J., Argouarch, A. R., Hsu, T.-Y., Mason, A., Nakamura, A., … Kao, W. (2015). Neurobiology of Disease The Progranulin Cleavage Products, Granulins, Exacerbate TDP-43 Toxicity and Increase TDP-43 Levels. https://doi.org/10.1523/JNEUROSCI.4808-14.2015

Sardiello, M., Palmieri, M., Ronza, A. Di, Medina, D. L., Valenza, M., Gennarino, V. A., … Ballabio, A. (2009). A gene network regulating lysosomal biogenesis and function. *Science*, *325*(5939), 473–477. https://doi.org/10.1126/SCIENCE.1174447/SUPPL_FILE/SARDIELLO-SOM.PDF

Schafer, D. P., Lehrman, E. K., Kautzman, A. G., Koyama, R., Mardinly, A. R., Yamasaki, R., … Stevens, B. (2012). Microglia sculpt postnatal neural circuits in an activity and complement-dependent manner. *Neuron*, *74*(4), 691–705. https://doi.org/10.1016/J.NEURON.2012.03.026

Scheiblich, H., Dansokho, C., Mercan, D., Schmidt, S. V., Bousset, L., Wischhof, L., … Heneka, M. T. (2021). Microglia jointly degrade fibrillar alpha-synuclein cargo by distribution through tunneling nanotubes. *Cell*, *184*(20), 5089-5106.e21. https://doi.org/10.1016/J.CELL.2021.09.007

Schlepckow, K., Kleinberger, G., Fukumori, A., Feederle, R., Lichtenthaler, S. F., Steiner, H., & Haass, C. (2017). An Alzheimer-associated TREM2 variant occurs at the ADAM cleavage site and affects shedding and phagocytic function . *EMBO Molecular Medicine, 9*(10), 1356–1365. https://doi.org/10.15252/emmm.201707672

Schlepckow, K., Monroe, K. M., Kleinberger, G., Cantuti-Castelvetri, L., Parhizkar, S., Xia, D., … Haass, C. (2020). Enhancing protective microglial activities with a dual function TREM2 antibody to the stalk region. *EMBO Molecular Medicine*, e11227. https://doi.org/10.15252/emmm.201911227

Sedel, F., Béchade, C., Vyas, S., & Triller, A. (2004). Macrophage-derived tumor necrosis factor alpha, an early developmental signal for motoneuron death. *The Journal of Neuroscience : The Official Journal of the Society for Neuroscience*, *24*(9), 2236–2246. https://doi.org/10.1523/JNEUROSCI.4464-03.2004

Sephton, C. F., Good, S. K., Atkin, S., Dewey, C. M., Mayer, P., Herz, J., & Yu, G. (2010). TDP-43 is a developmentally regulated protein essential for early embryonic development. *The Journal of Biological Chemistry*, *285*(9), 6826–6834. https://doi.org/10.1074/JBC.M109.061846

Settembre, C., Malta, C. Di, Polito, V. A., Arencibia, M. G., Vetrini, F., Erdin, S., … Ballabio, A. (2011). TFEB Links Autophagy to Lysosomal Biogenesis. *Science*, *332*(6036), 1429–1433. https://doi.org/10.1126/science.1204592

Shankaran, S. S., Capell, A., Hruscha, A. T., Fellerer, K., Neumann, M., Schmid, B., & Haass, C. (2008). Missense Mutations in the Progranulin Gene Linked to Frontotemporal Lobar Degeneration with Ubiquitin-immunoreactive Inclusions Reduce Progranulin Production and Secretion. *Journal of Biological Chemistry*, *283*(3), 1744–1753. https://doi.org/10.1074/JBC.M705115200

Shirahama-Noda, K., Yamamoto, A., Sugihara, K., Hashimoto, N., Asano, M., Nishimura, M., & Hara-Nishimura, I. (2003). Biosynthetic processing of cathepsins and lysosomal degradation are abolished in asparaginyl endopeptidase-deficient mice. *Journal of Biological Chemistry*, *278*(35), 33194–33199. https://doi.org/10.1074/jbc.M302742200

Sierra, A., Encinas, J. M., Deudero, J. J. P., Chancey, J. H., Enikolopov, G., Overstreet-Wadiche, L. S., … Maletic-Savatic, M. (2010). Microglia shape adult hippocampal neurogenesis through apoptosis-coupled phagocytosis. *Cell Stem Cell*, *7*(4), 483–495. https://doi.org/10.1016/J.STEM.2010.08.014

Sims, R., Van Der Lee, S. J., Naj, A. C., Bellenguez, C., Badarinarayan, N., Jakobsdottir, J., … Schellenberg, G. D. (2017). Rare coding variants in PLCG2, ABI3, and TREM2 implicate microglial-mediated innate immunity in Alzheimer's disease. *Nature Genetics 2017 49:9*, *49*(9), 1373–1384. https://doi.org/10.1038/NG.3916

Smith, K. R., Damiano, J., Franceschetti, S., Carpenter, S., Canafoglia, L., Morbin, M., … Berkovic, S. F. (2012). Strikingly different clinicopathological phenotypes determined by

progranulin-mutation dosage. *American Journal of Human Genetics*, *90*(6), 1102–1107. https://doi.org/10.1016/J.AJHG.2012.04.021

Song, W., Hooli, B., Mullin, K., Jin, S. C., Cella, M., Ulland, T. K., … Colonna, M. (2017). Alzheimer's disease-associated TREM2 variants exhibit either decreased or increased ligand-dependent activation. *Alzheimer's & Dementia : The Journal of the Alzheimer's Association*, *13*(4), 381. https://doi.org/10.1016/J.JALZ.2016.07.004

Songsrirote, K., Li, Z., Ashford, D., Bateman, A., & Thomas-Oates, J. (2010). Development and application of mass spectrometric methods for the analysis of progranulin N-glycosylation. *Journal of Proteomics*, *73*(8), 1479–1490. https://doi.org/10.1016/J.JPROT.2010.02.013

Stence, N., Dailey, M. E., & Waite, M. (2001). Confocal imaging of microglial cell dynamics in hippocampal slice cultures. *Glia*, *33*(3), 256–266. https://doi.org/10.1006/meth.1999.0775

Suárez-Calvet, M., Caballero, M. Á. A., Kleinberger, G., Bateman, R. J., Fagan, A. M., Morris, J. C., … Haass, C. (2016). Early changes in CSF sTREM2 in dominantly inherited Alzheimer's disease occur after amyloid deposition and neuronal injury. *Science Translational Medicine*, *8*(369). https://doi.org/10.1126/SCITRANSLMED.AAG1767

Suárez-calvet, M., Capell, A., Ángel, M., Caballero, A., Morenas-, E., Fellerer, K., … Haass, C. (2018). CSF progranulin increases in the course of Alzheimer ' s disease and is associated with sTREM 2 , neurodegeneration and cognitive decline, 1–21. https://doi.org/10.15252/emmm.201809712

Suárez-Calvet, M., Kleinberger, G., Araque Caballero, M. Á., Brendel, M., Rominger, A., Alcolea, D., … Haass, C. (2016). sTREM2 cerebrospinal fluid levels are a potential biomarker for microglia activity in early-stage Alzheimer's disease and associate with neuronal injury markers. *EMBO Molecular Medicine*, *8*(5), 466–476. https://doi.org/10.15252/EMMM.201506123

Suh, H. S., Choi, N., Tarassishin, L., & Lee, S. C. (2012). Regulation of progranulin expression in human microglia and proteolysis of progranulin by matrix metalloproteinase-12 (MMP-12). *PloS One*, *7*(4). https://doi.org/10.1371/JOURNAL.PONE.0035115

Svoboda, D. S., Barrasa, M. I., Shu, J., Rietjens, R., Zhang, S., Mitalipova, M., … Jaenisch, R. (2019). Human iPSC-derived microglia assume a primary microglia-like state after transplantation into the neonatal mouse brain. *Proceedings of the National Academy of Sciences*, 201913541. https://doi.org/10.1073/pnas.1913541116

T'Jonck, W., Guilliams, M., & Bonnardel, J. (2018). Niche signals and transcription factors involved in tissue-resident macrophage development. *Cellular Immunology*, *330*, 43–53. https://doi.org/10.1016/J.CELLIMM.2018.02.005

Takahama, K., Arai, S., Kurokawa, R., & Oyoshi, T. (2009). Identification of DNA binding specificity for TLS. *Nucleic Acids Symposium Series (2004)*, (53), 247–248. https://doi.org/10.1093/NASS/NRP124

Takahashi, K., Tanabe, K., Ohnuki, M., Narita, M., Ichisaka, T., Tomoda, K., & Yamanaka, S. (2007). Induction of Pluripotent Stem Cells from Adult Human Fibroblasts by Defined Factors. *Cell*, *131*(5), 861–872. https://doi.org/10.1016/j.cell.2007.11.019

Takahashi, K., & Yamanaka, S. (2006). Induction of Pluripotent Stem Cells from Mouse Embryonic and Adult Fibroblast Cultures by Defined Factors. *Cell*, *126*(4), 663–676. https://doi.org/10.1016/j.cell.2006.07.024

Tanaka, Y., Chambers, J. K., Matsuwaki, T., Yamanouchi, K., & Nishihara, M. (2014). Possible involvement of lysosomal dysfunction in pathological changes of the brain in aged progranulin-deficient mice. https://doi.org/10.1186/s40478-014-0078-x

Tanaka, Y., Suzuki, G., Matsuwaki, T., Hosokawa, M., Serrano, G., Beach, T. G., … Nishihara, M. (2017). Progranulin regulates lysosomal function and biogenesis through acidification of lysosomes. *Human Molecular Genetics*, *26*(5), 969–988. https://doi.org/10.1093/hmg/ddx011

Tang, W., Lu, Y., Tian, Q. Y., Zhang, Y., Guo, F. J., Liu, G. Y., … Liu, C. J. (2011). The growth factor progranulin binds to TNF receptors and is therapeutic against inflammatory arthritis in mice. *Science (New York, N.Y.)*, *332*(6028), 478–484. https://doi.org/10.1126/SCIENCE.1199214

TCW, J. (2019, April 23). Human iPSC application in Alzheimer's disease and Tau-related neurodegenerative diseases. *Neuroscience Letters*. Elsevier Ireland Ltd. https://doi.org/10.1016/j.neulet.2019.01.043

Thornton, P., Sevalle, J., Deery, M. J., Fraser, G., Zhou, Y., Ståhl, S., … Crowther, D. C. (2017). TREM 2 shedding by cleavage at the H157-S158 bond is accelerated for the Alzheimer's disease-associated H157Y variant . *EMBO Molecular Medicine*, *9*(10), 1366–1378. https://doi.org/10.15252/emmm.201707673

Tolkatchev, D., Malik, S., Vinogradova, A., Wang, P., Chen, Z., Xu, P., … Ni, A. F. (2008). Structure dissection of human progranulin identifies well-folded granulin/epithelin modules with unique functional activities. *Protein Science*, *17*(4), 711–724. https://doi.org/10.1110/PS.073295308

Toombs, J. A., McCarty, B. R., & Ross, E. D. (2010). Compositional determinants of prion formation in yeast. *Molecular and Cellular Biology*, *30*(1), 319–332. https://doi.org/10.1128/MCB.01140-09

Tremblay, M. Ě., Lowery, R. L., & Majewska, A. K. (2010). Microglial Interactions with Synapses Are Modulated by Visual Experience. *PLOS Biology*, *8*(11), e1000527. https://doi.org/10.1371/JOURNAL.PBIO.1000527

Ueno, M., Fujita, Y., Tanaka, T., Nakamura, Y., Kikuta, J., Ishii, M., & Yamashita, T. (2013). Layer V cortical neurons require microglial support for survival during postnatal development. *Nature Neuroscience 2013 16:5*, *16*(5), 543–551. https://doi.org/10.1038/NN.3358

Ulland, T. K., Song, W. M., Huang, S. C. C., Ulrich, J. D., Sergushichev, A., Beatty, W. L., … Colonna, M. (2017). TREM2 Maintains Microglial Metabolic Fitness in Alzheimer's Disease. *Cell*, *170*(4), 649-663.e13. https://doi.org/10.1016/J.CELL.2017.07.023

Ulrich, J. D., Finn, M. B., Wang, Y., Shen, A., Mahan, T. E., Jiang, H., … Holtzman, D. M. (2014). Altered microglial response to Aβ plaques in APPPS1-21 mice heterozygous for TREM2. *Molecular Neurodegeneration*, *9*(1). https://doi.org/10.1186/1750-1326-9-20

Valdez, C., Wong, Y. C., Schwake, M., Bu, G., Wszolek, Z. K., & Krainc, D. (2017). Progranulin-mediated deficiency of cathepsin D results in FTD and NCL-like phenotypes in neurons derived from FTD patients. *Human Molecular Genetics*, *26*(24), 4861–4872. https://doi.org/10.1093/hmg/ddx364

Valdez, C., Ysselstein, D., Young, T. J., Zheng, J., & Krainc, D. (2020). Progranulin mutations result in impaired processing of prosaposin and reduced glucocerebrosidase activity. *Human Molecular Genetics*, *29*(5), 716–726. https://doi.org/10.1093/hmg/ddz229

Varol, C., Mildner, A., & Jung, S. (2015). Macrophages: development and tissue specialization. *Annual Review of Immunology*, *33*, 643–675. https://doi.org/10.1146/ANNUREV-IMMUNOL-032414-112220

Velasco, S., Kedaigle, A. J., Simmons, S. K., Nash, A., Rocha, M., Quadrato, G., … Arlotta, P. (2019). Individual brain organoids reproducibly form cell diversity of the human cerebral cortex. *Nature 2019 570:7762*, *570*(7762), 523–527. https://doi.org/10.1038/S41586-019-1289-X

Vranken, W. F., Chen, Z. G., Xu, P., James, S., Bennett, H. P. J., & Ni, F. (1999). A 30-residue fragment of the carp granulin-1 protein folds into a stack of two β-hairpins similar to that found in the native protein. *The Journal of Peptide Research*, *53*(5), 590–597. https://doi.org/10.1034/J.1399-3011.1999.00048.X

Wake, H., Moorhouse, A. J., Miyamoto, A., & Nabekura, J. (2013). Microglia: actively surveying and shaping neuronal circuit structure and function. *Trends in Neurosciences*, *36*(4), 209–217. https://doi.org/10.1016/J.TINS.2012.11.007

Walsh, C. E., & Hitchcock, P. F. (2017). Progranulin regulates neurogenesis in the developing vertebrate retina. *Developmental Neurobiology*, *77*(9), 1114–1129. https://doi.org/10.1002/DNEU.22499

Wang, L., Kang, J., Lim, L., Wei, Y., & Song, J. (2018). TDP-43 NTD can be induced while CTD is significantly enhanced by ssDNA to undergo liquid-liquid phase separation. *Biochemical and Biophysical Research Communications*, *499*(2), 189–195. https://doi.org/10.1016/J.BBRC.2018.03.121

Wang, S., Mustafa, M., Yuede, C. M., Salazar, S. V., Kong, P., Long, H., … Colonna, M. (2020). Anti-human TREM2 induces microglia proliferation and reduces pathology in an Alzheimer's disease model. *Journal of Experimental Medicine*, *217*(9). https://doi.org/10.1084/jem.20200785

Wang, Y., Cella, M., Mallinson, K., Ulrich, J. D., Young, K. L., Robinette, M. L., … Colonna, M. (2015). TREM2 lipid sensing sustains the microglial response in an Alzheimer's disease model. *Cell*, *160*(6), 1061–1071. https://doi.org/10.1016/J.CELL.2015.01.049

Wang, Y., Szretter, K. J., Vermi, W., Gilfillan, S., Rossini, C., Cella, M., … Colonna, M. (2012). IL-34 is a tissue-restricted ligand of CSF1R required for the development of Langerhans cells and microglia. *Nature Immunology 2012 13:8*, *13*(8), 753–760. https://doi.org/10.1038/NI.2360

Wang, Y., Ulland, T. K., Ulrich, J. D., Song, W., Tzaferis, J. A., Hole, J. T., … Colonna, M. (2016). TREM2-mediated early microglial response limits diffusion and toxicity of amyloid plaques. *Journal of Experimental Medicine*, *213*(5), 667–675. https://doi.org/10.1084/jem.20151948

Ward, M. E., Chen, R., Huang, H. Y., Ludwig, C., Telpoukhovskaia, M., Taubes, A., … Green, A. J. (2017). Individuals with progranulin haploinsufficiency exhibit features of neuronal ceroid lipofuscinosis. *Science Translational Medicine*, *9*(385). https://doi.org/10.1126/SCITRANSLMED.AAH5642

Ward, M. E., Taubes, A., Chen, R., Miller, B. L., Sephton, C. F., Gelfand, J. M., … Gan, L. (2014). Early retinal neurodegeneration and impaired Ran-mediated nuclear import of TDP-43 in progranulin-deficient FTLD. *The Journal of Experimental Medicine*, *211*(10), 1937–1945. https://doi.org/10.1084/JEM.20140214

Wils, H., Kleinberger, G., Pereson, S., Janssens, J., Capell, A., Van Dam, D., … Kumar-Singh, S. (2012). Cellular ageing, increased mortality and FTLD-TDP-associated neuropathology in progranulin knockout mice. *The Journal of Pathology*, *228*(1), 67–76. https://doi.org/10.1002/PATH.4043

Winton, M. J., Igaz, L. M., Wong, M. M., Kwong, L. K., Trojanowski, J. Q., & Lee, V. M. Y. (2008). Disturbance of nuclear and cytoplasmic TAR DNA-binding protein (TDP-43) induces disease-like redistribution, sequestration, and aggregate formation. *Journal of Biological Chemistry*, *283*(19), 13302–13309. https://doi.org/10.1074/jbc.M800342200

Woodruff, G., Young, J. E., Martinez, F. J., Buen, F., Gore, A., Kinaga, J., … Goldstein, L. S. B. (2013). The presenilin-1 ΔE9 mutation results in reduced γ-secretase activity, but not total loss of PS1 function, in isogenic human stem cells. *Cell Reports*, *5*(4), 974–985. https://doi.org/10.1016/J.CELREP.2013.10.018

Woollacott, I. O. C., & Rohrer, J. D. (2016). The clinical spectrum of sporadic and familial forms of frontotemporal dementia. *Journal of Neurochemistry*, *138 Suppl 1*, 6–31. https://doi.org/10.1111/JNC.13654

Wright, A. V., Nuñez, J. K., & Doudna, J. A. (2016, January 14). Biology and Applications of CRISPR Systems: Harnessing Nature's Toolbox for Genome Engineering. *Cell*. Cell Press. https://doi.org/10.1016/j.cell.2015.12.035

Wu, L. S., Cheng, W. C., & Shen, C. K. J. (2012). Targeted depletion of TDP-43 expression in the spinal cord motor neurons leads to the development of amyotrophic lateral sclerosis-like phenotypes in mice. *The Journal of Biological Chemistry*, *287*(33), 27335–27344. https://doi.org/10.1074/JBC.M112.359000

Wu, L. S., Cheng, W., Hou, S. C., Yan, Y. T., Jiang, S. T., & Shen, C. K. J. (2010). TDP-43, a neuro-pathosignature factor, is essential for early mouse embryogenesis. *Genesis*, *48*(1), 56–62. https://doi.org/10.1002/DVG.20584

Wu, Y., Shao, W., Todd, T. W., Tong, J., Yue, M., Koga, S., … Prudencio, M. (2021). Microglial lysosome dysfunction contributes to white matter pathology and TDP-43 proteinopathy in GRN-associated FTD. *Cell Reports*, *36*(8). https://doi.org/10.1016/j.celrep.2021.109581

Wunderlich, P., Glebov, K., Kemmerling, N., Tien, N. T., Neumann, H., & Walter, J. (2013). Sequential proteolytic processing of the triggering receptor expressed on myeloid cells-2 (TREM2) protein by ectodomain shedding and γ-secretase-dependent intramembranous cleavage. *The Journal of Biological Chemistry*, *288*(46), 33027–33036. https://doi.org/10.1074/JBC.M113.517540

Xiang, X., Werner, G., Bohrmann, B., Liesz, A., Mazaheri, F., Capell, A., … Haass, C. (2016). TREM2 deficiency reduces the efficacy of immunotherapeutic amyloid clearance. *EMBO Molecular Medicine*, *8*(9), 992–1004. https://doi.org/10.15252/EMMM.201606370

Xiao, S., Sanelli, T., Dib, S., Sheps, D., Findlater, J., Bilbao, J., … Robertson, J. (2011). RNA targets of TDP-43 identified by UV-CLIP are deregulated in ALS. *Molecular and Cellular*

Neurosciences, *47*(3), 167–180. https://doi.org/10.1016/J.MCN.2011.02.013

Yagi, T., Ito, D., Okada, Y., Akamatsu, W., Nihei, Y., Yoshizaki, T., … Suzuki, N. (2011). Modeling familial Alzheimer's disease with induced pluripotent stem cells. *Human Molecular Genetics*, *20*(23), 4530–4539. https://doi.org/10.1093/HMG/DDR394

Yang, C., Wang, H., Qiao, T., Yang, B., Aliaga, L., Qiu, L., … Xu, Z. (2014). Partial loss of TDP-43 function causes phenotypes of amyotrophic lateral sclerosis. *Proceedings of the National Academy of Sciences of the United States of America*, *111*(12). https://doi.org/10.1073/PNAS.1322641111/-/DCSUPPLEMENTAL/SAPP.PDF

Yeh, F. L., Wang, Y., Tom, I., Gonzalez, L. C., & Sheng, M. (2016). TREM2 Binds to Apolipoproteins, Including APOE and CLU/APOJ, and Thereby Facilitates Uptake of Amyloid-Beta by Microglia. *Neuron*, *91*(2), 328–340. https://doi.org/10.1016/J.NEURON.2016.06.015

Yin, F., Banerjee, R., Thomas, B., Zhou, P., Qian, L., Jia, T., … Ding, A. (2010). Exaggerated inflammation, impaired host defense, and neuropathology in progranulin-deficient mice. *The Journal of Experimental Medicine*, *207*(1), 117–128. https://doi.org/10.1084/jem.20091568

Zambusi, A., Pelin Burhan, Ö., Di Giaimo, R., Schmid, B., & Ninkovic, J. (2020). Granulins Regulate Aging Kinetics in the Adult Zebrafish Telencephalon. *Cells*, *9*(2). https://doi.org/10.3390/CELLS9020350

Zhang, J., Velmeshev, D., Hashimoto, K., Huang, Y. H., Hofmann, J. W., Shi, X., … Huang, E. J. (2020). Neurotoxic microglia promote TDP-43 proteinopathy in progranulin deficiency. *Nature*, *588*(7838), 459–465. https://doi.org/10.1038/s41586-020-2709-7

Zhang, Z. H., Jhaveri, D. J., Marshall, V. M., Bauer, D. C., Edson, J., Narayanan, R. K., … Zhao, Q. Y. (2014). A Comparative Study of Techniques for Differential Expression Analysis on RNA-Seq Data. *PLOS ONE*, *9*(8), e103207. https://doi.org/10.1371/JOURNAL.PONE.0103207

Zhang, Z., Kang, S. S., Liu, X., Ahn, E. H., Zhang, Z., He, L., … Ye, K. (2017). Asparagine endopeptidase cleaves α-synuclein and mediates pathologic activities in Parkinson's disease. *Nature Structural and Molecular Biology*, *24*(8), 632–642. https://doi.org/10.1038/nsmb.3433

Zhang, Z., Song, M., Liu, X., Kang, S. S., Kwon, I. S., Duong, D. M., … Ye, K. (2014). Cleavage of tau by asparagine endopeptidase mediates the neurofibrillary pathology in Alzheimer's disease. *Nature Medicine*, *20*(11), 1254–1262. https://doi.org/10.1038/nm.3700

Zhao, P., Xu, Y., Jiang, L. L., Fan, X., Li, L., Li, X., … An, Z. (2022). A tetravalent TREM2

agonistic antibody reduced amyloid pathology in a mouse model of Alzheimer's disease. *Science Translational Medicine*, *14*(661), eabq0095. https://doi.org/10.1126/SCITRANSLMED.ABQ0095

Zhou, X., Paushter, D. H., Feng, T., Sun, L., Reinheckel, T., & Hu, F. (2017). Lysosomal processing of progranulin. *Molecular Neurodegeneration*, *12*(1). https://doi.org/10.1186/s13024-017-0205-9

Zhou, X., Sun, L., de Oliveira, F. B., Qi, X., Brown, W. J., Smolka, M. B., … Hu, F. (2015). Prosaposin facilitates sortilin-independent lysosomal trafficking of progranulin. *Journal of Cell Biology*, *210*(6), 991–1002. https://doi.org/10.1083/jcb.201502029

Zhou, Y., Song, W. M., Andhey, P. S., Swain, A., Levy, T., Miller, K. R., … Colonna, M. (2020). Human and mouse single-nucleus transcriptomics reveal TREM2-dependent and TREM2-independent cellular responses in Alzheimer's disease. *Nature Medicine 2020 26:1*, *26*(1), 131–142. https://doi.org/10.1038/S41591-019-0695-9

Zhu, J., Nathan, C., Jin, W., Sim, D., Ashcroft, G. S., Wahl, S. M., … Ding, A. (2002). Conversion of Proepithelin to Epithelins: Roles of SLPI and Elastase in Host Defense and Wound Repair ist that coordinate the phasing of otherwise incompati-ble actions by diverse host cells in a wound Secretory leukocyte protease inhibitor (SLPI) is a pro-tein named for its presence in epithelial secretions and its ability to inhibit neutrophil elastase and cathepsin G. *Cell*, *111*, 867–878.

6 Copyright information

7 Curriculum Vitae

SOPHIE ROBINSON

EDUCATION

Graduate School of Systemic Neurosciences, Ludwig-Maximilians-Universität München   **Munich, DE**
- *2018 – present:* Fast-Track PhD student, Neuroscience

Carnegie Mellon University   **Pittsburgh, PA**
- *2012-2016:* B.S. Psychology and Biological Sciences with University Honors // GPA: 3.71/4.00
- *Honors*: Order of Omega, Dietrich College Dean's List with Honors and with High Honors

PROFESSIONAL EXPERIENCE

PhD Student, German Center for Neurodegenerative Diseases (DZNE), Dr. Christian Haass   **Munich, DE**
- *September 2019 – present*

PhD Student, Institute for Stroke and Dementia Research (ISD), Dr. Dominik Paquet   **Munich, DE**
- *September 2019 – present*

Clinical Operations Intern, Roche Genentech   **South San Francisco, CA**
- *June 2017 – June 2018*

Research Assistant, Stanford School of Medicine, Dr. Ronald Levy   **Stanford, CA**
- *June 2016 – June 2017*

Research Assistant, Carnegie Mellon University   **Pittsburgh, PA**
- *August 2015 – May 2016,* Dr. Brooke Feeney, The Relationships Lab, Department of Psychology
- *August 2014 – May 2015,* Dr. Alison Barth, Department of Biological Sciences
- *October 2013 – May 2014,* Dr. J. David Creswell, Department of Psychology

Teaching Assistant, Carnegie Mellon University, Department of Psychology   **Pittsburgh, PA**
- *August 2015 – December 2015,* Dr. Kenneth Kotovsky, Introduction to Psychology
- *August 2015 – December 2015,* Dr. Marlene Behrmann, Biological Foundations of Behavior

Research Assistant, Yale School of Medicine, Dr. Stephen Strittmatter   **New Haven, CT**
- *June 2015 – August 2015*
- *June 2014 – August 2014*
- *June 2013 – August 2013*

Research Assistant, Yale School of Medicine, Dr. Jun Lu   **New Haven, CT**
- *June 2012 – August 2012*

Research Assistant, Stanford School of Medicine, Dr. Tony Wyss-Coray   **Stanford, CA**
- *June 2011 – August 2011*
- *June 2010 – August 2010*

8 List of Publications

Gottschlich A, Thomas M, Grünmeier R, Lesch S, Rohrbacher L, Igl V, Briukhovetska D, Benmebarek MR, Vick B, Dede S, Müller K, Xu T, Dhoqina D, Märkl F, **Robinson S**, Sendelhofert A, Schulz H, Umut O, Kavaka V, Tsiverioti CA, Carlini E, Nandi S, Strzalkowski T, Lorenzini T, Stock S, Jie Müller P, Dörr J, Seifert M, Cadilha BL, Brabenec R, Röder N, Rataj F, Nüesch M, Modemann F, Wellbrock J, Fiedler W, Kellner C, Beltrán E, Herold T, Paquet D, Jeremias I, von Baumgarten L, Endres S, Subklewe M, Marr C, Kobold S: Single-cell transcriptomic atlas-guided development of CAR-T cells for the treatment of acute myeloid leukemia. Nat. Biotechnol. 2023 Mar 13. PMID: 36914885

Reifschneider A, **Robinson S**, van Lengerich B, Gnörich J, Logan T, Heindl S, Vogt MA, Weidinger E, Riedl L, Wind K, Zatcepin A, Pesämaa I, Haberl S, Nuscher B, Kleinberger G, Klimmt J, Götzl JK, Liesz A, Bürger K, Brendel M, Levin J, Diehl-Schmid J, Suh J, Di Paolo G, Lewcock JW, Monroe KM*, Paquet D*, Capell A*, Haass C*: Loss of TREM2 rescues hyperactivation of microglia, but not lysosomal deficits and neurotoxicity in models of progranulin deficiency. EMBO J. 2022 Feb 15. PMID: 35019161

Sallets A, **Robinson S**, Kardosh A, and Levy R: Enhancing immunotherapy of STING agonist for lymphoma in preclinical models. Blood Adv. 2018 Sep 11. PMID: 30194137

Salazar SV, Gallardo C, Kaufman AC, Herber CS, Haas LT, **Robinson S**, Manson JC, Lee MK, Strittmatter SM: Conditional deletion of Prnp rescues behavioral and synaptic deficits after disease onset in transgenic Alzheimer's mice. J Neurosci. 2017 Aug 21. PMID: 28842420

Kaufman AC, Salazar SV, Haas LT, Yang J, Kostylev MA, Jeng AT, **Robinson SA**, Gunther EC, van Dyck CH, Nygaard HB, Strittmatter SM: Fyn inhibition rescues established memory and synapse loss in Alzheimer mice. Ann Neurol. 2015 Mar 21. PMID: 25707991

9   Affidavit

Eidesstattliche Versicherung/Affidavit

<u>Sophie Robinson</u> (Studierende/Student)

Hiermit versichere ich an Eides statt, das ich die vorliegende Dissertation "Investigating the role and modulation of microglia in FTD-*GRN* using a human iPSC-derived pathology model" selbstständig angefertigt habe, mich außer der angegebenen keiner weiteren Hilfsmittel bedient und alle Erkenntnisse, die aus dem Schrifttum ganz oder annähernd übernommen sind, als solche kenntlich gemacht und nach ihrer Herkunft unter Bezeichnung der Fundstelle einzeln nachgewiesen habe.

I hereby confirm that the dissertation "Investigating the role and modulation of microglia in FTD-*GRN* using a human iPSC-derived pathology model" is the result of my own work and that I have only used sources or materials listed and specified in the dissertation.

München/Munich, 29.11.2022   Sophie Robinson

                                                                 _____

10 Declaration of Author Contributions

Loss of TREM2 rescues hyperactivation of microglia, but not lysosomal deficits and neurotoxicity in models of progranulin deficiency.
Reifschneider A, **Robinson S**, van Lengerich B, Gnörich J, Logan T, Heindl S, Vogt MA, Weidinger E, Riedl L, Wind K, Zatcepin A, Pesämaa I, Haberl S, Nuscher B, Kleinberger G, Klimmt J, Götzl JK, Liesz A, Bürger K, Brendel M, Levin J, Diehl-Schmid J, Suh J, Di Paolo G, Lewcock JW, Monroe KM, Paquet D, Capell A, Haass C.
EMBO J. 41(4):e109108. doi: 10.15252/embj.2021109108.

CH, AC, and AR conceived the study and analyzed the results. CH wrote the manuscript with further input from AR, AC, GDP, KMM, JWL, SR, and DP. AR performed and analyzed Western Blots, ELISAs, enzyme activity assays, mRNA isolation, NanoString experiments, and immunofluorescence on all mouse samples. AR isolated and performed all experiments of human-derived macrophages and analyzed hiMGL NanoString data. With supervision of DP, SR generated and validated GRN KO hiPSC, differentiated into hiMGL, and performed and analyzed Western Blots, ELISAs, and enzyme activity assays. JK and GK helped to establish hiMGL cell differentiation. KMM and BVL discovered, generated, and validated antagonistic TREM2 antibodies. TL and JS performed lipidomic analysis. MAV and SHa performed NanoString and phagocytosis assays on hiMGL cells. JGn, KW, AZ, and MB conducted, performed, and analyzed PET imaging. SHe performed automated analysis on microglia morphology, with supervision of AL. IP performed CSF isolation. JKG helped to establish mouse lines. JL, KB, JD-S, EW, and LR identified FTLD patients and performed sequencing analysis. BN performed NfL measurements. The synopsis image was created with BioRender.com.

My contribution to this paper in detail:

I edited iPSCs using CRISPR/Cas9 to generate the GRN KO iPSC line. I performed various quality controls to end up with a final cell line. I differentiated the iPSCs into microglia and performed various experiments including cell lysis, Western blot analysis and ELISAs for protein expression, an alphaLISA for phosphorylation, and enzyme activity assays. I further interpreted this data, created figures, and commented on the manuscript. I generated labeled myelin and collaborated with ISAR Biosciences for the myelin phagocytosis assay as well as for the Nanostring data. Figures 4, 5, and EV3 comprise my contribution to this publication.

Enhanced legumain activity links progranulin deficiency to TDP-43 pathology in frontotemporal dementia
Capell, A., **Robinson, S.***, Reich, M.*, Reifschneider, A., Buschmann, K., Riemenschneider, H., Wauters, E., Mühlhofer, Q., Werner, G., Ahles, A., Engelhardt, S., Reinheckel, T., Edbauer, D., Simon, M., Logan, T., Di Paolo, G., Van Broeckhoven, C., Damme, M., Paquet, D., Haass, C.
Manuscript in preparation

AC and CH conceived and designed the study and wrote the manuscript. SR and DP designed, performed and analyzed iPSC experiments. MR, DE, AR performed and analyzed primary neuronal and microglial experiments. KB, cloned LGMN constructs. HR generated lenti virus and performed viral transduction experiments. MR performed and analyzed HeLa conditioned media treated neurons. KB, GW performed experiments with MEF, mice brain and GRN-FTLD patient material and recombinant LGMN. MJS, TL, GDP generated, MR analyzed the PTV:PGRN study. QM conducted the cystatins experiments. AA, SE generated and purified the AAV9-Cst7. CVB and EW provided validated FTLD/GRN patients brain samples. MD co-initiated the study and performed liver lysosomes isolation on mice provided by AC and TR. All authors commented on the manuscript.

My contribution to this paper in detail:

I edited iPSCs using CRISPR/Cas9 to generate the GRN KO iPSC line. I performed various quality controls to end up with a final cell line. I differentiated the iPSCs into microglia and neurons and created monocultures and co-cultures of both cell types. I performed various experiments including cell lysis and Western blot for protein expression, RNA extraction and qPCRs for RNA expression, and enzyme activity assays. I also performed an AAV transduction on the neurons. I further interpreted this data, created figures, and commented on the manuscript. Figures 4A-E comprise my contribution to this publication.

Herewith, I confirm the contributions of Sophie Robinson to the articles.

Signatures:

_____
Sophie Robinsion

_____   _____   _____   _____
 Christian Haass   Dominik Paquet   Anika Reifschneider,   Anja Capell,
 Supervisor   Supervisor   First author   First author

Date/Place: <u>29.11.2022, Munich</u>

11 Acknowledgements

First and foremost, I would like to thank my mentors and thesis advisors, Christian and Dominik. I am grateful for all the guidance, knowledge, example, and scientific discussion so freely and enthusiastically given, as well as for the opportunity to pursue such amazing projects, and attend scientific meetings, both small and large, and collaborate with so many people in the field from both academia and industry. You have really given me such a unique and valuable experience that I have learned and grown so much from. I would also like to thank Anja for the supervision and guidance, always helping me with any questions inside and outside the lab, as well as the support given in general during my PhD.

I would like to thank my TAC members, Martin and Florence, for giving such great guidance and encouragement. I always looked forward to the stimulating and engaging scientific discussions we had at the TAC meetings. I would also like to thank my examiners, Soyon and Eddie, for their support and feedback on my thesis.

I am grateful to my collaborators at ISAR Bioscience, especially Gernot, Miriam, and Sophie, and at Denali Therapeutics, especially Bettina, Kate, Todd, Joe, Matt, and Gil, for their scientific contributions and support, and exciting and educational discussions during our meetings. I would also like to thank the entire CSD for providing such an educational and fun environment to work in.

I would like to thank Judith, Julien, Carolina, Dennis, Angelika, Liliana, Merle, Isabel, and Joey for making the lab such a great atmosphere, which was much needed and a huge relief from the stress, for always providing scientific, personal, and organizational support, and for all the fun inside and outside of the lab. The breaks, beer gardens, picnics, hikes, movie nights, dinners, brunches, island trips, parties, and so much more were all amazing. You are all inspiringly talented and hard-working and are such wonderful and caring friends through the ups and downs inside and outside of the PhD. I really could not have made it without you guys. I am also grateful to Jenny, Vanessa, and Nathalie for the organizational support and Sam, Melanie, and Lisa for their scientific contributions and help for my projects overall.

I would like to thank Ida, Lis, Maria, Astrid, Matteo, Iñaki, and Marvin for being incredible pillars of support and sources of comfort during the last several years, from small breaks in the kitchen to much needed ice cream outings, walks around campus, dinners, hikes, ski trips, and video calls. We had so much fun inside and outside the lab, with beer festivals, dinners, movies, retreats, Overcooked games, as well as invaluable scientific discussion and support. I would also like to thank Anika, Quirin, Georg, Kai, Chris, Estrella, Katrin, Brigitte, Claudia, Ramona, Michael, Sven, Alice, Heike, Kati, and Bettina for help in the lab, for the scientific discussions and guidance in lab meetings, and for being such a great group to work with. I am grateful to Nicole and Sabine for all the organizational support and keeping the lab going, nothing would be possible without you.

I am so grateful to my GSN friends for being an amazing support system right from the beginning when we all moved to Munich. I would especially like to thank Berni, Danielle, Alessio, Clara, Leonie, Ioanna, and Sam. Individually, I am grateful for all the roommate shenanigans, Kennedy's trips, study sessions, beer festivals, dinners, brunches, retreats, parties, hikes, ski trips, camping trips, barbecues, Isar trips, lake trips, movie nights (as well as GBBO, Ted Lasso, or whatever other show we're watching), Slovenia (and Croatia), Freiburg,

Nürnberg, Tuscany, birthdays, Secret Santas, Christmas markets, and so so much more. Every time we're together, no matter how much stress is going on during the PhD or in life, I can always count on dying from laughter... or eating… or hiking. We've grown so much together since we first moved here and you all inspire me in so many ways and mean so much to me. Thank you for everything. I would also like to thank Adrien, Anne-Laure, and Eric for making Munich feeling more like home, you have done so much and I will always be grateful.

I would like to thank my friends from back home, especially Vivian, Kevin, Nick, Roy, Eugene, Tanya, Allyn, Danielle, Maggie, and Taryn. Even though we live a continent and ocean apart, it always feels like nothing has changed whenever I go back home. Thank you for always being willing to do special activities together, for visiting me here, and for going on amazing trips together. Thank you also for the video calls and phone calls that are always so much fun, such a huge comfort, and transport me back home for a little bit. I am happy we were able to remain so close, despite the time and distance, and I am so grateful to have you in my life. Last, but definitely not least, I would like to thank my family. You have all inspired and guided me in various ways throughout my life that brought me here. Mom and Dad, thank you for unconditionally rooting for me, for all the lessons you have taught me throughout my life, and the guidance and advice you have given, especially during my PhD. I am sorry for missing so many things by living so far away, but I appreciate everything you have done for me. I could not have made it without you.